CHARACTERISATION OF HYPOGENE COVELLITE ASSEMBLAGES AT THE CHUQUICAMATA PORPHYRY COPPER DEPOSIT, CHILE, SECTION 4500N

by

Meghan H. Lewis

Submitted in partial fulfilment of the requirements
for the degree of Master of Science

at

Dalhousie University
Halifax, Nova Scotia
December, 1996

TABLE OF CONTENTS

	Page
Table of contents	iv
List of Figures	vi
List of Tables	vii
Abstract	xi
Acknowledgements	xii
Chapter 1 Introduction	
1.1 General Statement	1
1.2 What is a Porphyry Copper Deposit?	1
1.3 The Nature of the Problem	3
1.4 Chuquicamata Porphyry Copper and Associated Deposits	3
1.4.1 Local Geology	4
1.4.2 Previous Work on Sulphide Mineral Assemblages at Chuquicamata	6
1.4.3 Present Geological Models	10
1.5 Objectives	11
1.6 Methodology	13
1.6.1 Sulphide Petrology	13
1.6.2 Sulphur Isotope Thermometry	14
1.7 Organisation of the Thesis	15
Chapter 2 The Cu-Fe-S and Related Systems	
2.1 General Statement	16
2.2 Mineralogical Associations in the Binary Cu-S System	16
2.3 Mineralogical Associations in the Ternary Cu-Fe-S System	19
2.4 Covellite Crystal Chemistry	24
2.5 Experimental Studies with Covellite	24
2.6 Related Systems: Zn-Fe-S and Cu-As(-Sb)-S	28
2.7 Highlights Relevant to this Study	30
Chapter 3 Minerals and Mineral Assemblages at Chuquicamata	
3.1 Definition of Relevant Terms	32
3.2 Main Ore Minerals: Textural Occurrence, Properties and Chemistry	32
3.2.1 Covellite	38
3.2.2 Anilite	43
3.2.3 Digenite	43
3.2.4 Enargite	47
3.2.5 Bornite	49
3.2.6 Chalcopyrite	51
3.2.7 Sphalerite	52
3.2.8 Pyrite	53

3.2.9 Molybdenite 55
3.2.10 Wolframite 56
3.2.11 Colusite 57
3.2.12 Idaite 59
3.3 Mineral Groupings/ Assemblages 60
3.3.1 Covellite (-Digenite) Assemblages 65
3.3.2 Digenite (-Bornite) Assemblages 74
3.3.3 Chalcopyrite Assemblages 78
3.3.4 Sphalerite Assemblages 88
3.3.5 Molybdenite Assemblages 91
3.3.6 Other Pyrite Assemblages 94
3.4 Distribution of Assemblages 95
3.4.1 Assemblages Characteristic of Quartz-sericite Alteration 95
3.4.2 Assemblages Characteristic of Potassic Alteration 97
3.4.3 Assemblages Charactersitic of Quartz-sericite Overprinting Potassic Alteration 98
3.5 Paragenetic Sequence of Assemblages 100
3.6 Hypogene vs Supergene Covellite 107

Chapter 4 Temperature Limits on Assemblages from Experimental Work on Cu-Fe-S Phases
4.1 Introduction 109
4.2 Assemblages in the Cu-Fe-S System 109
4.3 Other Assemblages 114
4.4 Summary 115

Chapter 5 Sulphur Isotope Study
5.1 Sulphur Isotope theory and Mechanisms of Fractionation 118
5.2 Method of Analysis 120
5.3 Purpose 121
5.4 Results for the Present Study 123
5.5 Sulphate - Sulphide Equilibria 124
5.6 Summary 134

Chapter 6 Conclusions and Recommendations
6.1 Conclusions 135
6.2 Recommendations 136

Appendix A Electron Microprobe Analyses 138
Appendix B X-ray Diffraction Analyses 164
Appendix C Hand Sample Descriptions, 4500N Section 203

References 217

LIST OF FIGURES

Chapter 1 Page

Figure 1.1. Concentric alteration zoning in a typical porphyry copper deposit. 5

Figure 1.2. Index map locating Chuquicamata with respect to its Latitude and Longitude. 8

Figure 1.3. Simplified plan view of the Chuquicamata open pit. 9

Figure 1.4. Cross-section 4500N through the deposit. 12

Chapter 2

Figure 2.1. Phase relations of condensed phases in the central portion of the copper-sulphur system. 18

Figure 2.2. Minerals reported within the Cu-Fe-S system. 22

Figure 2.3 a. Schematic phase relations in the central portion of the Cu-Fe-S system at 400°C, and b. at 300°C (after Craig and Scott, 1979). 26

Figure 2.4. Structure of covellite, CuS. 27

Chapter 3

Figure 3.1. Cu vs Fe plot of covellites from Chuquicamata. 41

Figure 3.2. Cu-Fe-S diagram showing fields of covellite and blue-remaining covellite from Chuquicamata. 42

Figure 3.3. Cu vs Fe plot showing Fe content of digenites from Chuquicamata. 45

Figure 3.4. Cu-Fe-S plot showing digenites from Chuquicamata. 46

Figure 3.5. Zn vs Cu plot showing variation in sphalerite compositions from Chuquicamata. 54

Figure 3.6 Sample cu205. DDH 2967, 514.90m. Reflected light photograph of a euhedral pyrite grain surrounded by massive digenite-covellite. 66

Figure 3.7 a. Sample cu192. DDH 2967, 325.93m. Reflected light photograph of fine-grained sub-rounded thin-lamellar grains of covellite disseminated in vein sulphate. 70

Figure 3.7 b. Sample cu214. DDH 2967, 211.60m. Reflected light photograph of typical sample of supergene ore. 71

Figure 3.8. Sample cu204. DDH 2967, 513.05m. Reflected light photograph of pyrite grains with spaces infilled by curved tabular wolframite. 72

Figure 3.9 a. Sample cu441. DDH 2242, 145.32m. Reflected light photograph of a sample of fault gouge. 75

Figure 3.9 b. Sample cu467. DDH 2242, 261.27m. Reflected light photograph of massive vein digenite with rims of colusite. 76

Figure 3.10 a. Sample cu476. DDH 2242, 288.10m. Reflected light photograph of bornite and digenite in an exsolution relationship. 79

Figure 3.10 b. Sample cu491. DDH 2234, 306.79m. Reflected light photograph of bornite and digenite in a replacement relationship. 80

Figure 3.11. Sample cu450. DDH 2242, 161.98m. Reflected light photograph of semi-massive covellite + idaite. 85

Figure 3.12 a. Sample cu455. DDH 2242, 193.86m. Reflected light photograph of covellite replacing chalcopyrite. 86

Figure 3.12 b. Sample cu494. DDH 2234, 219.84m. Reflected light photograph of metastable assemblage covellite + chalcopyrite. 87

Figure 3.13. Sample cu507. DDH 2234, 113.65m. Reflected light photograph of possible supergene sphalerite. 92

Figure 3.14. Sample cu433. DDH 2242, 56.45m. Plane light photograph of a cut section of drill core through a 'blue vein'. 93

Figure 3.15. Chuquicamata cross-section 4500N, with alteration zones. 102

Figure 3.16. Distribution of covellite-digenite assemblages in section 4500N. 103

Figure 3.17. Distribution of sphalerite assemblages in section 4500N. 104

Figure 3.18. Distribution of chalcopyrite assemblages in section 4500N. 105

Figure 3.19. Inferred (ore) mineral paragenesis for section 4500N. 106

Chapter 4

Figure 4.1. Cu-Fe-S system at 300^{0}C isotherm. 111

Figure 4.2. Estimated temperatures of mineralisation for assemblages in section 4500N. 116

Chapter 5

Figure 5.1. Schematic diagram of a basic mass spectrometer. 122

Figure 5.2. Plot of sulphate and sulphide δ^{34}S permil values vs delta (Δ) values of coexisting sulphate-sulphide pairs from Chuquicamata nd El Salvador. 128

Figure 5.3. Estimate of δ^{34}S value for total sulphur for the Chuquicamata system 130

Figure 5.4 a. Stability fields of sulphur phases in a pH-log f_{O2} diagram at 250^{0}C, and b. δ^{34}S values of sulphides and sulphates at 250^{0}C. 132

Figure 5.5. Mole fractions of aqueous sulphur species relative to total sulphur content plotted on a ph-log f_{O2} diagram. 133

LIST OF TABLES

Chapter 2 Page

Table 1. Minerals and phases of the Cu-S system. 20

Table 2. Minerals and phases of the Cu-Fe-S system. 21

Chapter 3

Table 3. Chuquicamata, Section 4500N. 34

Table 4. Chemical composition of hypogene covellite from Chuquicamata. 39

Table 5. Chemical composition of blaubleibender covellite from Chuquicamata. 40

Table 6. Chemical composition of digenite from Chuquicamata. 47

Table 7. Chemical composition of enargite from Chuquicamata. 48

Table 8. Chemical composition of bornite from Chuquicamata. 50

Table 9. Analyses of possible anomalous bornites from Chuquicamata. 50

Table 10. Chemical composition of chalcopyrite from Chuquicamata. 51

Table 11. Chemical composition of sphalerite from Chuquicamata. 53

Table 12. Chemical composition of pyrite from Chuquicamata. 55

Table 13. Chemical composition of colusite from Chuquicamata. 58

Table 14. Chemical composition of idaite from Chuquicamata. 60

Table 15. Distribution of ore minerals in section 4500N. 61

Chapter 4

Table 16. Summary of invariant points for the condensed Cu-Fe-s system. 112

Chapter 5

Table 17. Sulphur isotope results as $\delta^{34}S$ values for sulphides and sulphates from Chuquicamata. 125

Table 18. Regression analysis for sulphide-sulphate data points from Chuquicamata. 127

ABSTRACT

Covellite (CuS) has traditionally been described as a mineral formed by supergene oxidation processes, although its occurrence as a hypogene mineral is well documented. However, it may be difficult to distinguish hypogene covellite from that of supergene origin without consideration of associated minerals and geologic setting. Also, the mineralogical relationships surrounding covellite in the Cu-Fe-S system are poorly constrained with respect to temperature, particularly above 250°C.

This thesis was planned as a first step towards the characterisation of covellite, attempting to develop practical criteria for the differentiation of hypogene from supergene covellite in the Chuquicamata porphyry copper deposit, Chile. Approximately 120 samples of ore were collected from 3 drillholes that intersect the major alteration zones (e.g. potassic, quartz-sericitic, chloritic), within the 4500N coordinate section, recommended by mine staff to be representative of the deposit. The petrology and mineralogy of the samples were studied using reflected light microscopy, x-ray diffraction, and the electron microprobe.

Both supergene and hypogene covellite are prominent ore minerals in the studied section of Chuquicamata. This study indicates that hypogene and supergene covellite differ both texturally (in habit and mineral assemblages), and compositionally with respect to minor constituents (specifically iron content).

Hypogene covellites from Chuquicamata contain significant Fe, which varies systematically from 0 to < 5 weight %, and appears to indicate crystallisation along the covellite-idaite tie line. The Fe content of hypogene covellite has not been adequately documented before. In contrast, supergene covellite in the studied samples rarely deviates from the stoichiometric composition CuS.

The hypogene sulphide assemblages were studied in the context of experimentally-determined sulphide phase equilibria to pose constraints on temperatures of ore deposition. Assemblages from within the potassic zone of alteration in the 4500N section at Chuquicamata can be constrained to a temperature range of approximately 400 to 600°C, although they may have been as low as 300°C. The conspicuous occurrence in the potassic alteration zone of the non-equilibrium assemblage chalcopyrite-covellite in the proportion ca. 2:9 may suggest rapid unmixing of idaite when pyrite failed to nucleate. Assemblages from the quartz-sericite zone suggest crystallization temperatures between 300 and 435°C (based on covellite-digenite assemblages). Late-stage hydrothermal polymetallic veins probably formed above 275-320°C.

Sulphur isotopic compositions of coexisting sulphides and sulphates (mainly anhydrite) from Chuquicamata were determined to complement the petrologic study. Coexisting sulphur-bearing minerals indicate temperatures of equilibration between 300 and 375°C for samples from the quartz-sericite alteration zone. Isotopic temperatures are therefore in agreement with temperatures of mineralisation inferred from sulphide phase equilibria.

ACKNOWLEDGEMENTS

I must first and foremost thank Dr. Marcos Zentilli for his direction of this research, for his support throughout the project, and for the candy he brought back from Chile. I must also thank the members of my supervisory committee, M. Graves, of Cuesta Research Ltd., and Dr. P. Reynolds. Dr. M. Zentilli and Milton Graves are thanked for collection of field data. Mr. Graves' substantial experience in matters relating to ore mineralogy and economic geology proved to be a most valuable resource throughout the duration of this thesis. Critical discussions with, and suggestions by, all three members of my committee improved the thesis greatly. Dr. P. Reynolds was especially helpful with the isotopic data and its interpretation.

Dr. A. Anderson, of St. Francis Xavier University, and Dr. B. Clarke suggested constructive and worthwhile improvements to the final version.

Thanks must also be extended to A.M. Grist for a myriad of technical and friendly supports, and for being a fount of knowledge, to A.M. Grist and C.C. Walls for their lessons in various software programs, to G. Brown for his expertise in producing incredibly perfect polished sections, to A. Arnott for the sharing of her excellent petrographic descriptions of samples from Chuquicamata, to R. MacKay for his supervision on the electron microprobe and his aid in interpretation of the data, to D. Fox for valuable contributions ranging from scientific consultations to photographic services, to D. Lindsay for scientific discussions and his aid in sampling, to J. Rojas de la Rivera, of Codelco Chuquicamata, for help in selecting sample intervals, and to K. Taylor for suggestions and help with XRD and isotopic data.

Finally, I would like to thank Darlene Van de Rijt and especially Norma Keeping for all of their support in the office and their invaluable sense of humour.

CHAPTER 1: INTRODUCTION

1.1 General Statement

In broad terms, the primary objective of this project is to aid in providing limits to the temperature, pressure, and chemical character of the fluids responsible for ore deposition in the Chuquicamata porphyry copper deposit, through study of the sulphide petrology. In particular, the focus is on the covellite-bearing ore mineral assemblages, both supergene and hypogene, which have not previously been detailed.

1.2 What is a Porphyry Copper Deposit?

There are many types of porphyry system, characterised on the basis of metal content, hydrothermal alteration patterns and tectonic settings, but they all possess three main features: (1) sulphides of Fe, Cu, Mo, Zn, and locally native Au, are disseminated in veins and stringers forming stockworks; (2) the mineralisation is spatially and genetically related to intrusive bodies, of which at least one has a distinct porphyritic texture; and (3) large volumes of rock are affected by hydrothermal alteration/ mineralisation (Lowell and Guilbert 1970). Porphyry copper deposits tend to be low-grade (ca. 1% Cu), large-tonnage deposits (>100 * 10^6 tonnes) (Clark 1993).

Porphyry systems generally occur at convergent plate margins and in rift-related settings (Sillitoe 1972). The Andean deposits, including Chuquicamata and the well-studied El Salvador deposit, are examples of convergent margin porphyries above subduction zones at continental margins. The evolution of porphyry copper systems is strictly associated with the magmatic events related to the plate boundaries, but the origin and source of the metals are debated by many authors (summarised in Pirajno 1992).

As mentioned above, hydrothermal alteration and sulphide mineralisation are essential in the formation of porphyry deposits. Magmatic waters are first exsolved from the crystallizing porphyry intrusion. The early magmatic-hydrothermal solutions form at temperatures between 750 to 450^{0}C, at depths between 1 and 5 km below the surface. The fluids are exsolved over a period of time, and they circulate through both the cooling intrusive and the adjacent wall-rocks. These later magmatic waters generally mix with convective fluids (some of meteoric origin); the

later hydrothermal solutions have temperatures from 450 to 250°C and form at depths between 1 and < 0.5 km. The alteration- mineralisation patterns of porphyry systems depend on the nature of the fluids and the compositions of the intrusives and the wall-rocks.

Several models have been described in the last 25 years for the dominant patterns of alteration and mineralisation associated with porphyry deposits (Meyer and Hemley 1967; Gustafson and Hunt 1975). The most widely accepted model is that of Lowell and Guilbert (1970), which postulates concentric zones of alteration assemblages around a high-temperature core. The earliest alteration is a result of the effects of alkali metasomatism (usually potassic) within the intrusive porphyry body. Figure 1.1 depicts the zonal patterns related to a quartz-monzonite porphyry system. The potassic core gives way to diffuse propylitic alteration; this zone is characterised by disseminated and veinlet-type sulphide mineralisation. The later hydrothermal alteration zones form more or less concentric zones about the potassic core, overprinting the early metasomatic effects and causing a redistribution of the sulphide mineralisation (Guilbert 1986); the phyllic, or quartz-sericite, zone surrounds and overlaps the potassic zone. Mineralisation consists of pyrite (up to 30% by volume in disseminations and veinlets; Pirajno 1992), chalcopyrite, bornite, molybdenite, and rare Au (Hollister 1978). Many variations of, and departures from, this model exist in natural systems, but it is accepted as a *generalised* model of alteration for porphyry systems.

The mineralisation formed during the stages described above is the hypogene mineralisation, formed from ascending, hot ore fluids. Many of the largest porphyry deposits (Cu and Au) have been significantly enriched as a result of chemical weathering, through a process referred to as supergene enrichment (Garrels,1954). The supergene enrichment of disseminated Cu deposits depends on the association of copper sulphides with pyrite and other iron-bearing sulphides, such as chalcopyrite and bornite. The oxidation of these Fe sulphides (by the addition of H_2O in the presence of O_2) creates a localized acid environment (Faure 1991). As a result, Cu^{2+} remains in solution and is transported down to the water table, where it is reduced to Cu^{+} and comes in contact with hypogene sulphides in the unweathered zone. The solution now has a large Cu^{+}/Fe^{2+} ratio; when pyrite is exposed to this solution, equilibrium is reestablished by the (simultaneous) precipitation of Cu and dissolution of Fe (i.e., pyrite is replaced by a copper-rich

mineral such as chalcocite, Cu_2S, or covellite, CuS). In other words, rock below the water table becomes significantly enriched in Cu, where the Cu is derived from copper-bearing sulphide minerals above the water table (Garrels 1954). Supergene processes occur at 20-50^{0}C, significantly lower temperatures than hypogene processes.

1.3 The Nature of the Problem

One of the first problems to be addressed deals with the basics of sulphide petrology, namely an effort to recognize high- to low-temperature equilibrium mineral assemblages. Although mining of the deeper hypogene sulphides started in Chuquicamata about 60 years ago, little has been published in the scientific literature on their distribution, mineral associations, and chemical make-up.

Another problem to be investigated was the apparent misinterpretation of covellite assemblages. Because until the 1960's the mine exploited the near-surface, weathered part of the Chuquicamata ore system, it was assumed that covellite (CuS) occurred only as a supergene mineral in the Chuquicamata deposit (Lopez 1939), and until 1992 covellite was used by mine staff as an indicator mineral to characterize supergene ore in the course of mapping. Although it is now recognised that covellite occurs in both supergene and hypogene assemblages at Chuquicamata (Zentilli et al. 1994), there continues to be a practical problem distinguishing hypogene covellite assemblages from those of supergene origin, both in hand specimen and under the microscope.

1.4 Chuquicamata Porphyry Copper and Associated Deposits

The Chuquicamata porphyry copper deposit has long been described as a world-class mineral deposit (Cook 1978). The deposit contains over 45 million tonnes of copper metal, and the open pit is about 3.5 km in length, 1.5 km wide, and has been excavated to over 700 m (Clark 1993). Over 150 mineral species and groups occur there, several of which are unique to Chuquicamata.

The Chuquicamata deposit is a major representative of a number of porphyry copper deposits of Eocene-Oligocene age in the Central Andes, most of which occur in a longitudinal association with the Domeyko Fault System, a shear system that extends over 2000 km. These

porphyry copper systems are genetically linked to calc-alkaline magmatism in response to subduction of oceanic crust under the continental margin of South America (Sillitoe 1986). Chuquicamata (centred at ca. Lat.22°16.5'S / Long.68°54'W) is located in the Atacama desert, about 3000 m.a.s.l. and 240 km NE of the port of Antofagasta. The mine is 16 km north of the town of Calama, listed in *The Guiness Book of World Records* as the driest spot on Earth. Because many of the abundant copper-bearing mineral species are readily soluble, the high copper grades in the upper zones of the deposit are partly a result of the extreme aridity of the region. Figure 1.2 is an index map marking the location of Chuquicamata. The deposit itself occurs in the Chuquicamata Plutonic Complex, an elongate granodioritic porphyry complex composed of three subdivisions, the Este, Oeste, and Banco porphyries, distinguishable on the basis of textural variations. To the west, the deposit and the Chuquicamata porphyries are separated from the unmineralised Fortuna granodiorite by the West Fissure, a major fault structure (Zentilli et al. 1995).

1.4.1 Local Geology

Mineralisation discussed in this thesis is confined to the various phases of the granodioritic- monzogranitic Chuqui porphyry, namely the Este, Banco, and Oeste porphyries; contacts between the three units are generally difficult to define (Zentilli et al 1995). Figure 1.3 shows the geology of the deposit and the unmineralised rocks adjacent to it. To the east, the Chuqui porphyry complex intrudes Mesozoic metasediments and Paleozoic igneous and metamorphic rocks (Alvarez and Flores 1985). The Elena Granodiorite is locally in contact with the Este porphyry on the East side of the deposit, but the contact relationships are ambiguous: it is not clear whether Elena is a textural variation of the Chuqui porphyry, related to its emplacement and cooling pattern (Ambrus 1979), or whether the Elena granodiorite is an entirely separate (Paleozoic?) unit (Aracena 1981). To the west, mineralisation is truncated by the West Fissure, a north to north-east trending fault zone that is a major branch of the regional Domeyko Fault System (Lindsay et al. 1995). West of the fault lies the Fortuna Granodiorite, a generally unaltered, in places weakly mineralised, porphyritic hornblende granodiorite. Several authors have suggested (e.g., Ambrus 1979; Sillitoe 1973) that the Fortuna granodiorite is the unmineralised precursor of the Chuqui porphyry, perhaps even an underlying intrusive having undergone uplift

Figure 1.1. Schematic drawing of the Lowell-Guilbert model of alteration-mineralisation zonal patterns related to a quartz-monzonite porphyry system. Alteration: K, potassic; A, argillic; QSP, phyllic (quartz-sericite pyrite); P, propylitic; CSE, chlorite-sericite-epidote +/- magnetite; QSC, quartz-sericite-chlorite +/- K-feldspar (after Lowell and Guilbert 1970). The Chuquicamata of today is a result of a later quartz-sericite stage (T_1) overprinting the earlier potassic stage (T_0) after considerable exhumation of the system (as hypothesized by Zentilli et al 1994), giving a lower-temperature core surrounded by a zone of high-temperature alteration-mineralisation assemblages at the level of present-day erosion.

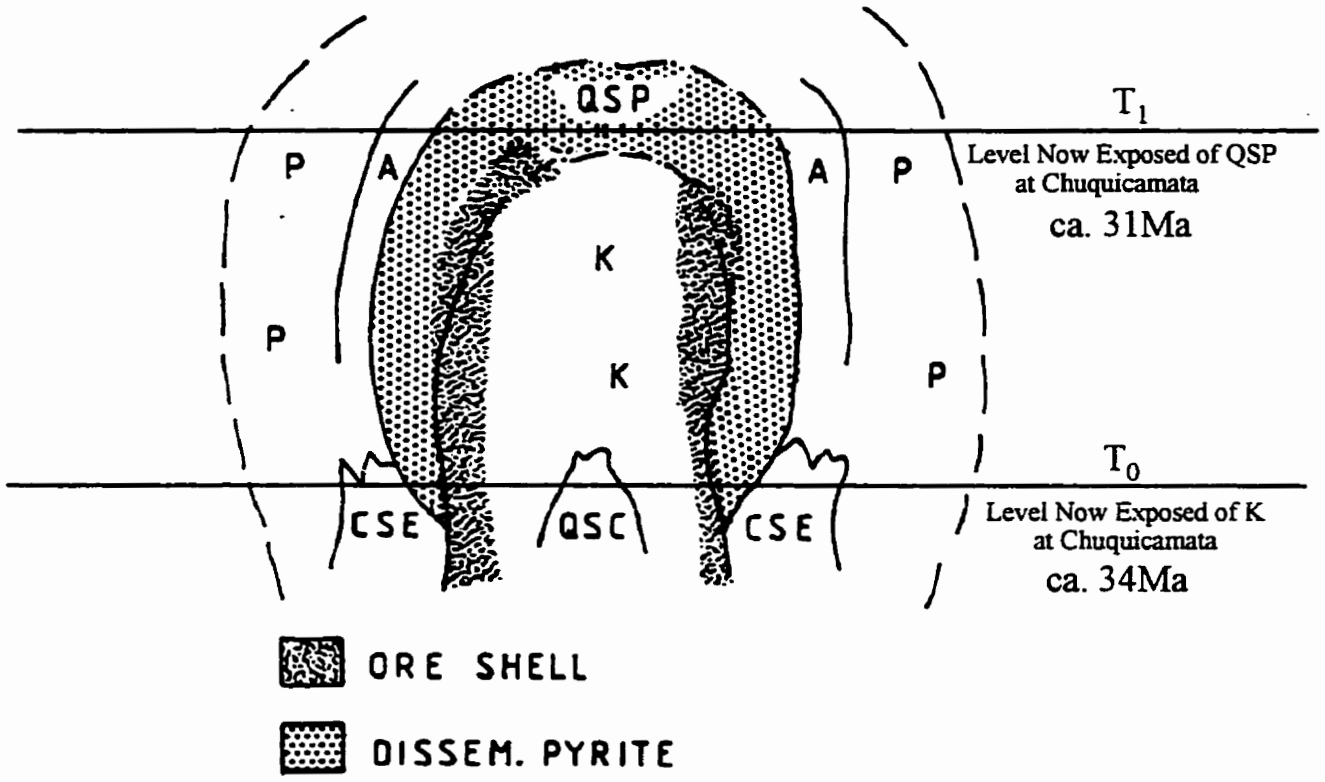

and exhumation (Sillitoe 1973). However, a recent study at Dalhousie University by Arnott et al. (1996), using the aluminum in hornblende (based on the work of Hammarstrom and Zen 1986), shows that the Fortuna granodiorite was probably formed at too shallow a depth to be the root of the Chuqui porphyries. Regional structural mapping (e.g., Reutter et al. 1993) suggests the possibility of significant strike-slip displacement across the West Fissure (possibly resulting in the displacement from 5 to 35 km of a large portion of the altered and mineralised zone).

The leaching, oxidation, and secondary enrichment common to many porphyry systems (section 1.2) played an important role in the ore-forming processes at Chuquicamata. Much of the Cu metal has been mined from the zone of supergene enrichment, which occupies an area of 3.5 km (N-S), with an average width and thickness of 500 m and 400 m respectively (Pirajno 1992). The 'blanket' enrichment zones of chalcocite and chalcocite + covellite have grades of up to 18% Cu and are commonly referred to as the 'chalcocite basin' (personal comm. 1996, M. Zentilli). These zones are underlain by an elongate and deeper zone of covellite enrichment, with grades of 10-15% Cu (Ambrus 1979).

1.4.2 Previous Work on Sulphide Mineral Assemblages at Chuquicamata

The deep hypogene sulphide mineral distribution at Chuquicamata has not been published, although several theses and internal reports summarize mine data. The most detailed description of the hypogene mineralisation at Chuquicamata (Lopez 1939) mentions that enargite is the main copper ore mineral, whereas bornite and chalcopyrite are present in minute amounts. More recently, in an internal report, Tobey (1971) described a central zone of hypogene low pyrite-to-copper sulphide ratio surrounded by successive zones of pyrite, chalcopyrite, and pyrite-chalcopyrite. Deeper mining showed that the zone of potassic alteration is overprinted by later sericitic alteration and associated hydrothermal mineralisation. In this study, sulphide mineral zoning has been looked at in terms of possibly being characteristic of the different alteration zones. Previous workers distinguished a "late-magmatic" potassic assemblage and a "hydrothermal" quartz-sericite assemblage. Modern use of the term "hydrothermal" includes any mineralisation/ alteration formed from hot waters, and for the purposes of this thesis both alteration assemblages at Chuquicamata are considered hydrothermal.

Soto (1979) wrote that the most common sulphide minerals in the potassic zone of

alteration (characterised by the association biotite-potassium feldspar-(anhydrite)-(sericite)) are bornite, chalcopyrite and pyrite, with variable amounts of hematite and magnetite. These descriptions are generally in good agreement with Tobey's (1971) internal report. Tobey and Soto both describe a central zone dominated by the association bornite-chalcopyrite, which locally contains 'inclusions' or a core of digenite. The digenite is associated with either, or both, of the other two sulphides. Bornite is the dominant copper sulphide in the core of the potassic zone. The central area with the bornite-chalcopyrite association gradually passes into a zone dominated by chalcopyrite-pyrite, in veins or disseminated in the host rocks, with hematite and magnetite. A zone of propylitic alteration, typically occurring at the margins of porphyry copper deposits, is restricted in Chuquicamata to the eastern margin, and is characterised by chlorite, calcite, epidote, quartz, and alkali feldspars. Copper mineralisation is limited in the propylitic zone, which is dominated by the alteration minerals pyrite, hematite, and chlorite.

The zone of quartz-sericite alteration is composed of several phases. Soto (1979) contends that the earliest (oldest formed) phase is one of large quartz veins with characteristic mineralisation, specifically molybdenite accompanied by copper and iron sulphides, most commonly pyrite and chalcopyrite. These make up the so-called 'blue veins', locally with halos of sericitic alteration.

The middle, and principal, phase of quartz-sericite alteration is characterised by both halos of sericitic alteration around sulphide (+/- quartz-alunite) veins, and large areas of sericitised wall-rock with significant kaolinite, where the original texture may be lost. Disseminated sulphides are abundant in the high-copper core zone (high bornite, chalcopyrite and chalcocite, with low pyrite) and rarer in the fringes of the quartz-sericite alteration, where the dominant sulphides are pyrite and chalcopyrite. In general, the mineralisation in the veins is the same as in the disseminations (Soto 1979).

Late-stage veining is considered the last phase of hydrothermal mineralisation, accompanied by low-temperature (hypogene) alteration characterised by the formation of clays. Common sulphide associations in the large cross-cutting veins are enargite-pyrite-(covellite), pyrite-chalcocite and pyrite-covellite, with minor sphalerite, galena, tennantite, and tetrahedrite (Soto 1979).

Figure 1.2. Index map locating Chuquicamata with respect to its Latitude and Longitude. Note the broad areal relationship between major Eocene-Oligocene porphyry copper systems in northern Chile and the regional Domeyko fault system (after Maksaev and Zentilli 1988).

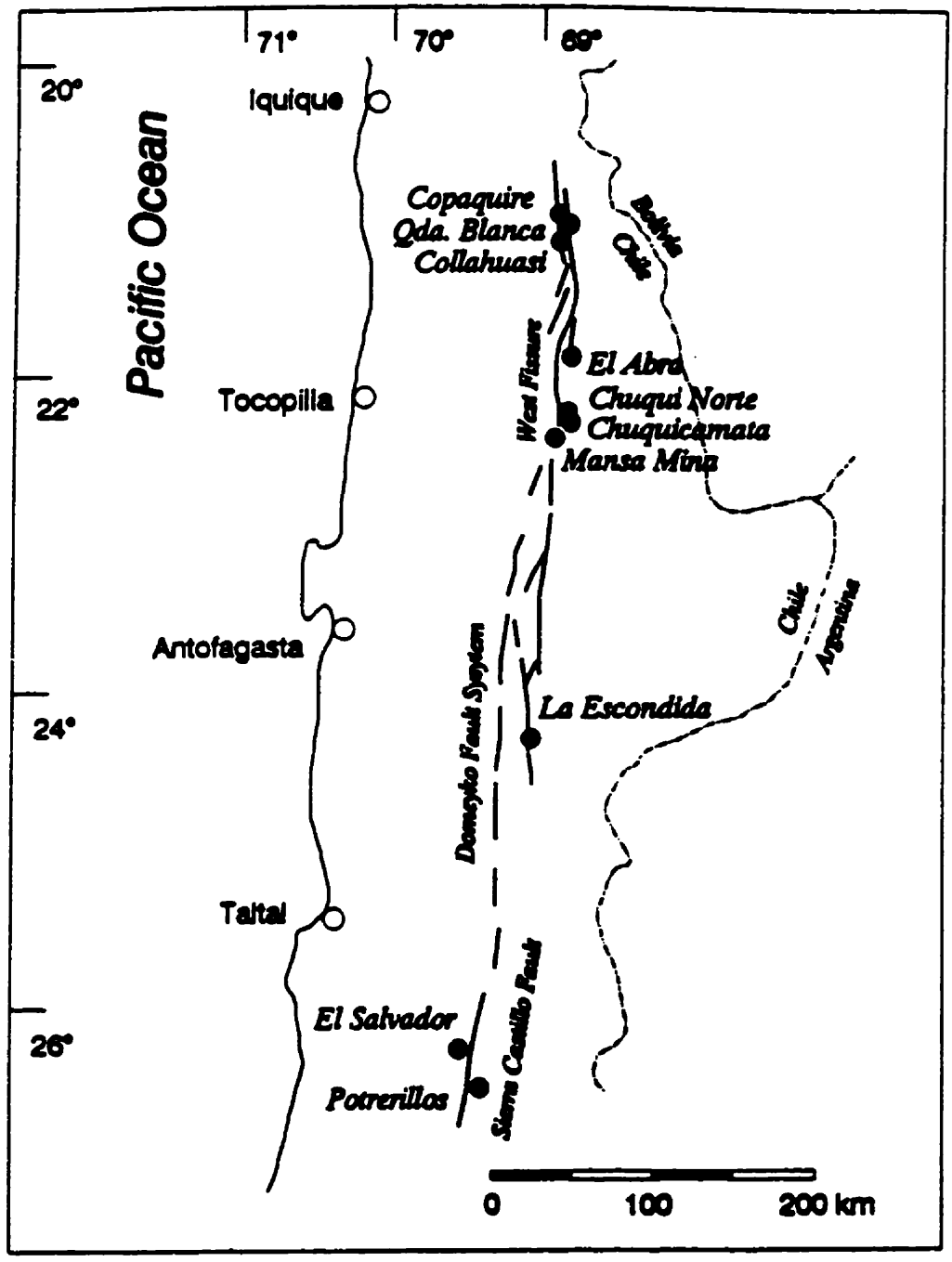

Figure 1.3. Simplified plan view of the Chuquicamata open pit as of 1979, with major alteration units outlined (modified after Martin et al. 1993).

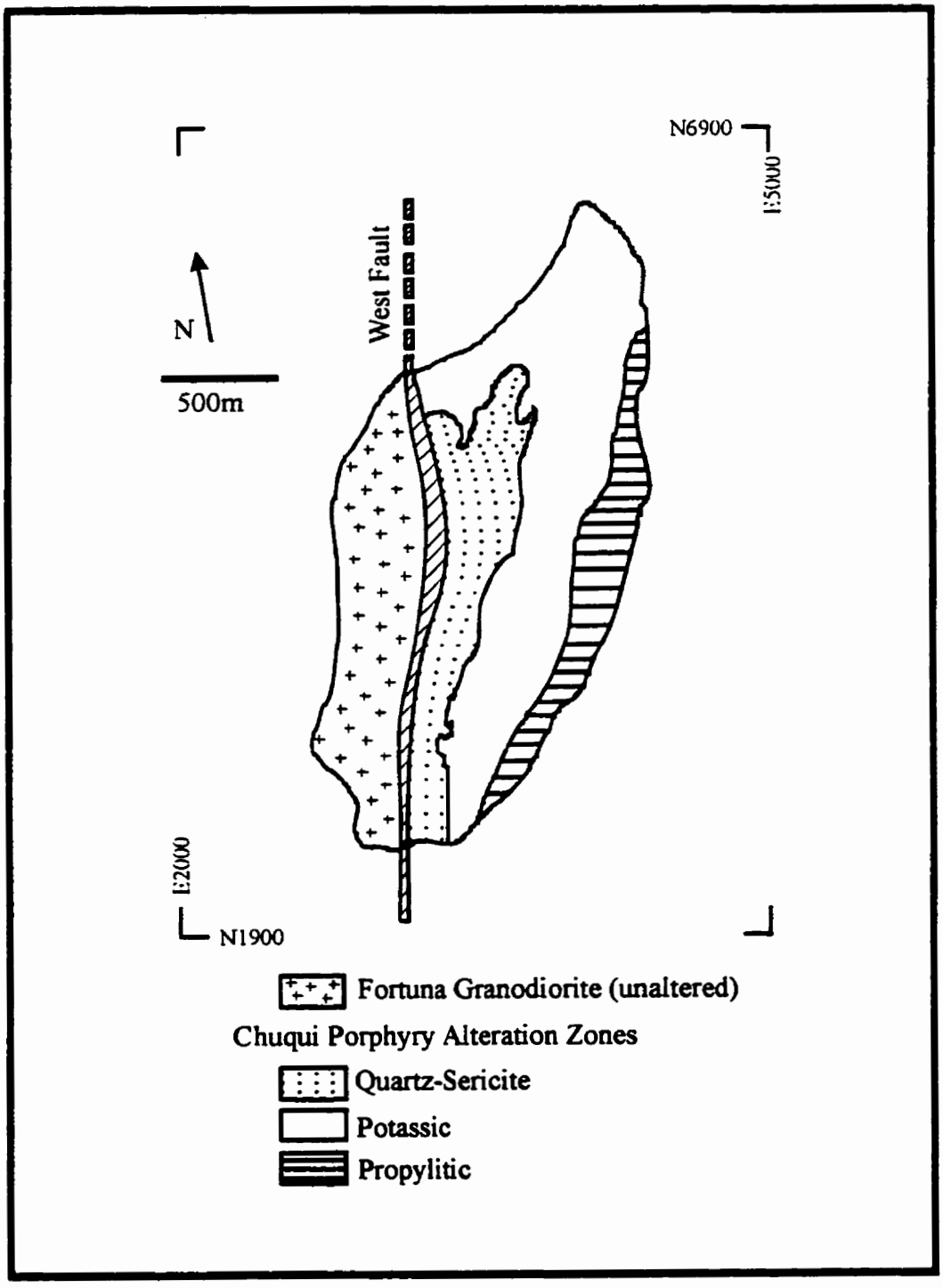

Tobey (1971) noted that insufficient data were available from the deeper levels of the ore deposit to permit accurate delineation of the zones of high primary chalcocite and covellite. Soto (1979) and Alvarez and Flores (1985) mention that covellite in the late-stage hydrothermal assemblages appears to be of hypogene origin, but later geologists continued to consider this mineral to be solely a result of the supergene enrichment process (for example, until recently covellite was used at Chuquicamata as the indicator mineral for supergene ore).

1.4.3 Present Geological Models

Chuquicamata is a deposit with a lower-temperature quartz-sericite core surrounded by a zone of higher-temperature potassic alteration, the reverse from the generalised Lowell and Guilbert (1970) model.

Published dates (mostly K/Ar dates with relatively large errors) from the Chuquicamata igneous host rocks show a range from 40 to 28 Ma; this was ascribed to a relatively continuous mineralisation/alteration history lasting about 10 m.y. (Sillitoe 1988). However, new $^{40}Ar/^{39}Ar$ dates indicate instead the results of two discrete periods of alteration with associated mineralisation: the first at ca. 34 +/- 1Ma, and the second at ca. 31 +/- 1Ma (Zentilli et al. 1994). The porphyritic texture of the quartz-monzonite intrusion and the ductile deformation of potassium feldspars shows the older event, characterised by potassic alteration, to have occurred fairly deep in the crust (>5 km?), while the younger event, dominated by quartz-sericite alteration and displaying evidence of brittle deformation such as wide quartz veins and open-space filling textures with distinct alteration halos, probably occurred relatively closer to surface (Zentilli et al. 1994; Lindsay et al. 1995). Further indication of two periods of alteration comes from the sericitic alteration-associated quartz veins that extend much farther than the range of the potassic alteration zone, and clearly cross-cut earlier veins associated with the potassic alteration (personal comm. 1995, D. Lindsay).

To explain the reversed zonation, Zentilli et al. (1994) hypothesized that the older alteration, at 34 Ma, could be associated with an intrusion that would have shown the 'typical' porphyry copper concentric zonation of alteration layers described extensively for the much smaller El Salvador deposit (Gustafson and Hunt 1975). This older Chuquicamata went through a period of rapid cooling accompanied by some exhumation before a second magmatic and

hydrothermal event at 31 Ma superimposed later quartz-sericite alteration over the earlier potassic alteration, now much nearer to surface. An apatite fission track age (Maksaev 1990, sample FT 19) indicates that the system cooled to about 100°C by 30 Ma. Dates from the zone of supergene mineralisation show that the deposit reached an extremely shallow stage by about 17 Ma and has remained there until the present (Sillitoe et al. 1996).

Figure 1.4 shows cross-section 4500N through the deposit, described by mine staff as being representative of the deposit. In addition, the 4500N section cuts all of the alteration zones and contains several deep drill holes with good core recovery that make it ideal for a petrologic study. The drill holes shown on the section are those for which sampling for this project concentrated. The alteration zones outlined were mapped by the mine staff during the last few years.

1.5 Objectives

The timing of the potassic and quartz-sericite alteration have been fairly well constrained through $^{40}Ar/^{39}Ar$ ages for potassium feldspars, biotite, and sericite (Ravenhurst et al. 1996). Much more work is required to constrain the temperature and pressure of mineralisation. With the advent of this new genetic model for the Chuquicamata porphyry copper deposit, many questions are being raised with regards to the mineralogy of the deposit (the possibility of two or more hypogene phases) and the temperature, pressure, and chemical character of the hydrothermal fluids responsible for the two periods of mineralisation/alteration.

The long-term objective of the ongoing study of Chuquicamata is to trace the evolution of the temperature, pressure, and composition of the fluids responsible for the formation of the deposit, leading to a comprehensive genetic model. The immediate problem is the question of the hypogene ore mineral assemblages, specifically those containing covellite, which, as mentioned above, have not been fully described or analyzed. Do different hypogene covellite assemblages correlate with the different periods of mineralisation? And how do these compare with the supergene covellite assemblages? In this context, this thesis focuses on the sulphide mineralogy and the information it can convey about the temperature and chemical character of the mineralising fluids. Specifically:

Figure 1.4. Cross-section 4500N through the deposit, showing drill hole and sample locations, and alteration zones as mapped by the mine staff. Ser = sericitic; SK = potassic overprinted by quartz-sericite; K = potassic; Clr = chloritic/propylitic.

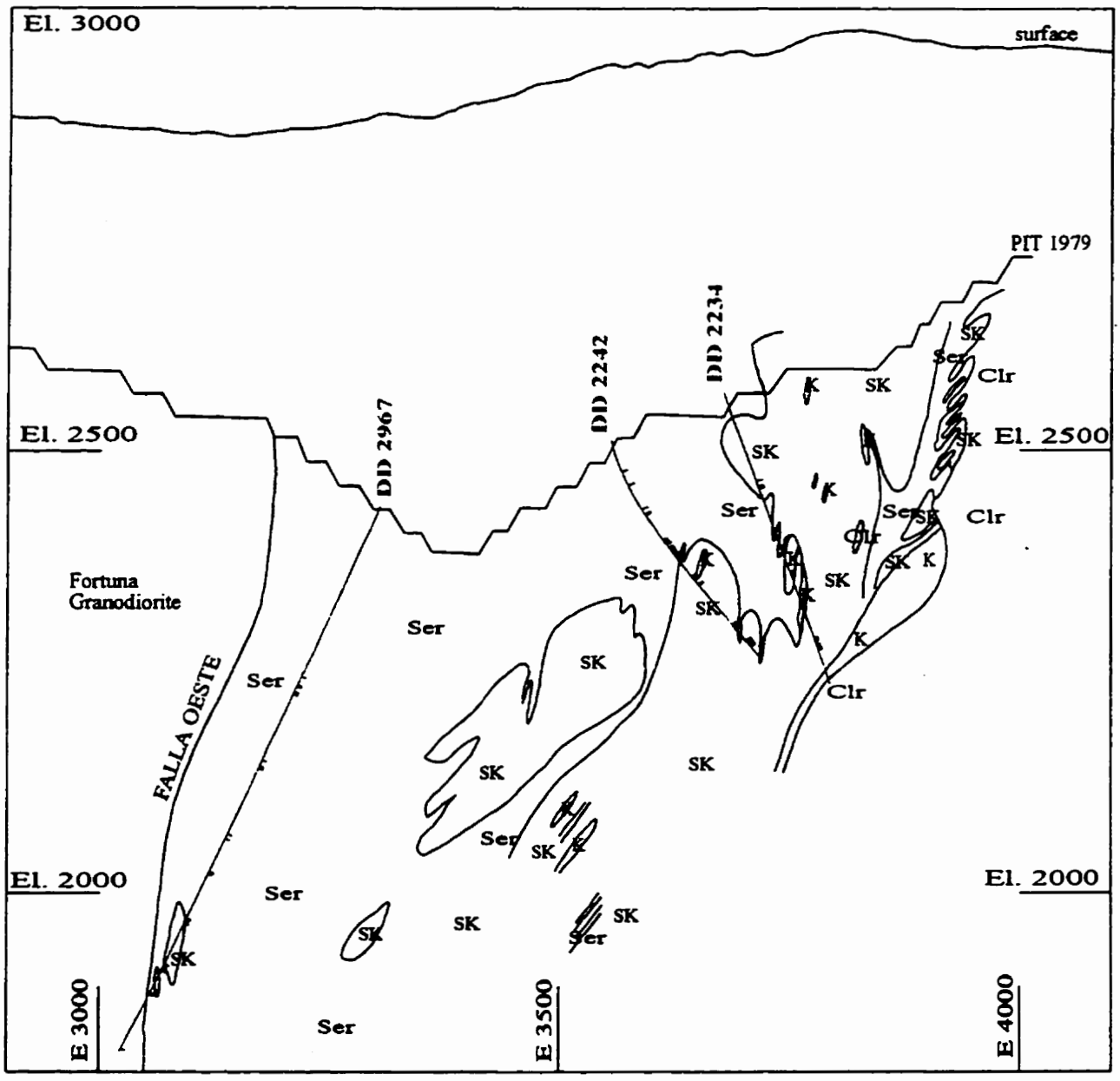

a) to determine the hypogene covellite assemblages associated with potassic and sericitic alteration in an E-W section representative of the hydrothermal system;

b) to establish the paragenetic sequence of the assemblages; and,

c) to use these assemblages to constrain the temperature and composition of the hydrothermal fluids as a contribution to the long-term objective described above.

In addition, a specific goal is to establish practical criteria for distinguishing hypogene from supergene covellite.

1.6 Methodology

The thesis uses two main approaches: sulphide petrology, which includes everything from textural descriptions to geochemical work, and sulphur isotope geothermometry. Initial samples were collected at Chuquicamata by M. Zentilli and M. Graves in 1993. Drill core was sampled on the basis of availability to represent ore mineral assemblages from all mapped ore and alteration zones. Further sampling was done by D. Lindsay in 1995 and 1996 as per the author's request, to fill gaps left by the original sampling technique and to answer specific questions.

1.6.1 Sulphide Petrology

A petrographic study was undertaken to recognize those primary assemblages that contain covellite. A paragenetic sequence was established, not only of the minerals within the assemblages, but also between the assemblages themselves. This work was carried out with a petrographic microscope under reflected light, on about 100 polished thin sections of drill core from mineralised porphyry and quartz veins from Chuquicamata.

Previously-determined experimental sulphide assemblages in the system Cu-Fe-S (-As-Sb) (e.g. Barton and Skinner 1979) are used to provide some constraints on the temperature, oxygen fugacity, and pH of the fluids responsible for ore deposition. For instance, I have used the metastable coexistence of covellite and chalcopyrite to infer a decomposition of idaite during cooling below ca. 200^{0}C (Chapter 3, Section 3.3.3).

Detailed mineral chemistry of the coexisting ore minerals can establish the presence of many of the ions/compounds in solution at the time of ore deposition. The two methods used for mineral composition analysis were the electron microprobe and the X-ray diffractometer. The

electron microprobe was essential for identification of Cu-Fe-S phases that are optically indistinguishable, of which there are several. For instance, the electron probe has allowed us to differentiate between blaubleibender, or 'blue-remaining', covellite and regular covellite, two copper sulphides with similar optical properties but very different temperature implications. The main use of the electron microprobe in this thesis was the determination of the chemical composition of sulphide minerals, and the study of the variation in chemical composition of the mienrals, regionally in the 4500N section. All analyses were performed using a JEOL 733 electron microprobe equipped with four wavelength spectrometers and an Oxford Link eXL energy dispersive detector operated by the Earth Science Department of Dalhousie University, with the assistance of R. MacKay.

1.6.2 Sulphur Isotope Thermometry

A study of the sulphur isotope fractionation between sulphide mineral pairs and between sulphide-sulphate pairs allows an estimate of the temperature of equilibration of the mineral pairs. The isotopic difference between two coexisting sulphur-bearing minerals may be produced by effects of temperature-dependent fractionation. The factor for isotope exchange between minerals, an inverse function of temperature, is determined from the measured isotopic difference between coexisting minerals. If the sulphur isotopic compositions can be determined for the two minerals, their temperature of equilibration can be calculated and compared to experimentally-determined fractionation factor vs temperature curves for many common sulphide pairs (e.g. Friedman and O'Neil 1977). As well, the sulphur isotopic composition of a mineral can give clues to the source of the sulphur.

Sulphur-bearing mineral grains were obtained by crushing, sieving, and hand picking the minerals. Twenty separated samples underwent X-ray diffraction to insure their purity, using the facility at Dalhousie University, and were sent to the NERC Isotope Geoscience Laboratory, where isotopic analyses were obtained under the supervision of Dr. Baruch Spiro, British Geological Survey, UK.

The sulphur isotope study is a complement to the sulphide petrology, used to confirm hypotheses formed from the petrologic study regarding temperature of mineralisation.

1.7 Organization of the Thesis

Several forms of presentation of the data were considered, ranging from organization of the data according to alteration zone, to organization according to environment of formation (supergene vs hypogene, for example). Since the focus of this study remains rooted in the sulphide petrology and the relationship between phases, arguably the best method of presentation is to concentrate on the ore minerals themselves. Chapter 2 presents general information on selected minerals at Chuquicamata and their occurrence and relationships in the geochemical systems that best define them (for example, experimental work and thermal studies are discussed here). Chapter 3 contains all information specific to Chuquicamata. Each phase is discussed with respect to its textural occurrence in the 4500N cross-section at Chuquicamata, its mineralogy, and its chemical composition and variations. The occurrence is expanded on in a section devoted to mineral groupings.

Chapter 3 details the assemblages and the paragenetic sequence of phases within each assemblage. The distribution of assemblages with respect to alteration zones is presented graphically, and leads to a discussion of the paragenetic sequence of assemblages.

Chapter 4 summarises the interpretations regarding temperature limits of assemblages using experimental work on the Cu(-Fe)-S system of several authors, summarised in Barton and Skinner (1979) and Vaughan and Craig (1978). The interpretations are based on the textural and chemical observations of phases within assemblages.

Chapter 5 presents sulphur isotope data, although this pilot study is intended to complement the petrologic study. Information about the physico-chemical conditions of the system that can be inferred from the isotopic data is linked back to mineralogy of the cross-section studied.

CHAPTER 2: THE CU-FE-S AND RELATED SYSTEMS

2.1 General Statement

The Cu-Fe-S system is complex--although it is the most-studied ternary sulphide system, many mineralogical relationships remain undetermined as a result of the presence of extensive solid solutions, metastability and unquenchable phases. Many phases in the system have closely-related crystal chemistry, resulting in similar physical appearance and X-ray powder diffraction patterns. Until the electron microprobe became widely-used as a tool for distinguishing optically-similar phases, the Cu-S system was thought to be relatively uncomplicated, consisting mostly of only 3 binary phases, covellite (CuS) digenite (Cu_9S_5), and chalcocite (Cu_2S). We now know that at least 8 distinct copper-sulphides exist (Barton and Skinner 1979), although the stability of some of these phases is still in question (Goble 1980). What follows is a summary of the state of understanding of the Cu(-Fe)-S system from the literature. This analysis is to a large extent based on a compilation and evaluation by MacInnis (1993).

2.2 Mineralogical Associations in the Binary Cu-S System

Experimental work on covellite and associated copper (-iron) sulphides dates back to Richardson and Jeffes (1952), and very little has been done since the late 1970s. Figure 2.1 is a schematic diagram of temperature vs composition for the phases in the Cu-rich portion of the Cu-S system. **Covellite**, CuS, possesses a hexagonal structure, with one type of Cu atom in tetrahedral coordination with S (the tetrahedra sharing corners to form layers), and a second type of Cu in trigonal coordination with S to build planar layers (Kalbskopf et al. 1975). Covellite has a fixed, nearly impurity-free chemical composition, and is stable up to 507°C (Kullerud 1965), above which it decomposes to digenite-chalcocite plus excess sulphur. Table 1 lists the minerals and phases, with notes on their thermal stabilities and cell structure, of the binary Cu-S system.

Between 507°C and 157°C, covellite forms with digenite and/or chalcocite. **Digenite**, Cu_9S_5, is the dominant high-temperature phase, and some workers conclude that digenite does not exist in the pure Cu-S system at low temperature (below about 70°C), suggesting that natural digenites contain a small amount of iron (~1%) as a necessary, stabilizing constituent (Morimoto and Koto 1970). As temperature rises above 25°C, digenite exists over an increasing

compositional range and becomes a stable phase in the Cu-S system at 70°C. At slightly higher temperatures, somewhere between 76 and 83°C, digenite inverts to a high-temperature cubic form, similar to high-temperature chalcocite (Roseboom 1966). At higher temperatures the solid solution expands to include compositions which are more sulphur- and iron-rich. For this reason digenite is included in both Table 1 and Table 2 (Minerals and phases of the Cu-Fe-S system). Solid solution between digenite and chalcocite is complete above 435°C.

Chalcocite, Cu_2S, is very common in both hypogene and supergene environments. It is stable up to 103°C; above this temperature, it inverts to a hexagonal form which is itself stable up to 435°C. Although the high-temperature cubic form exhibits a solid solution field (chalcocite-digenite) which extends from about 1.75 to 2:1 for Cu:S, chalcocite does not deviate measurably from Cu_2S.

Below 157°C covellite will coexist with a phase that is distinct, but similar to itself, the **blue-remaining covellite** (lacking the characteristic red-violet colour of optically-normal covellite in immersion oils, and possessing a different X-ray diffraction pattern). Frenzel (1959) recognized a phase he called "blaubleibender" or "blue-remaining" covellite, similar to regular covellite but lacking the pleochroism. He also found that it has a similar but distinct X-ray pattern. Moh (1964) synthesized blue-remaining covellite below 157°C, but its thermodynamic stability remains in doubt (refer to Section 2.3. Experimental studies with covellite). Blue-remaining covellite has a general formula of $Cu_{1+x}S$, where x=0.1 to 0.4, and is recognized as a separate phase (two, really: natural yarrowite has a composition approximating $Cu_{1.12}S$ and natural spionkopite has a composition around $Cu_{1.32\text{-}1.40}S$ (Goble 1980)). Blaubleibender covellites are indistinguishable from regular covellite in hand specimen.

Covellite has been shown in several studies not to depart measurably from the stoichiometric composition of Cu:S ratio in 1:1. Any mention in the literature of covellite or blue-remaining covellite containing iron is usually as an aside, where the authors report that analyses with iron are omitted due to microprobe calibration problems or some other technical difficulty. The one exception to this is the study on the products of supergene oxidation in the Copiapo mining district (Sillitoe and Clark 1969). They report that some of the iron content of the six samples of blue-remaining covellite may be due to minute inclusions of goethite, but 'some at

Figure 2.1. Phase relations of condensed phases in the central portion of the copper-sulphur system. Abbreviations are as follows: al, anilite $Cu_{1.75}S$; bcv, blue-remaining covellite $Cu_{1+x}S$; cc, chalcocite Cu_2S; cv, covellite CuS; dg, digenite $Cu_{1.8}S$; dj, djurleite $Cu_{1.96}S$ (after Barton, 1973).

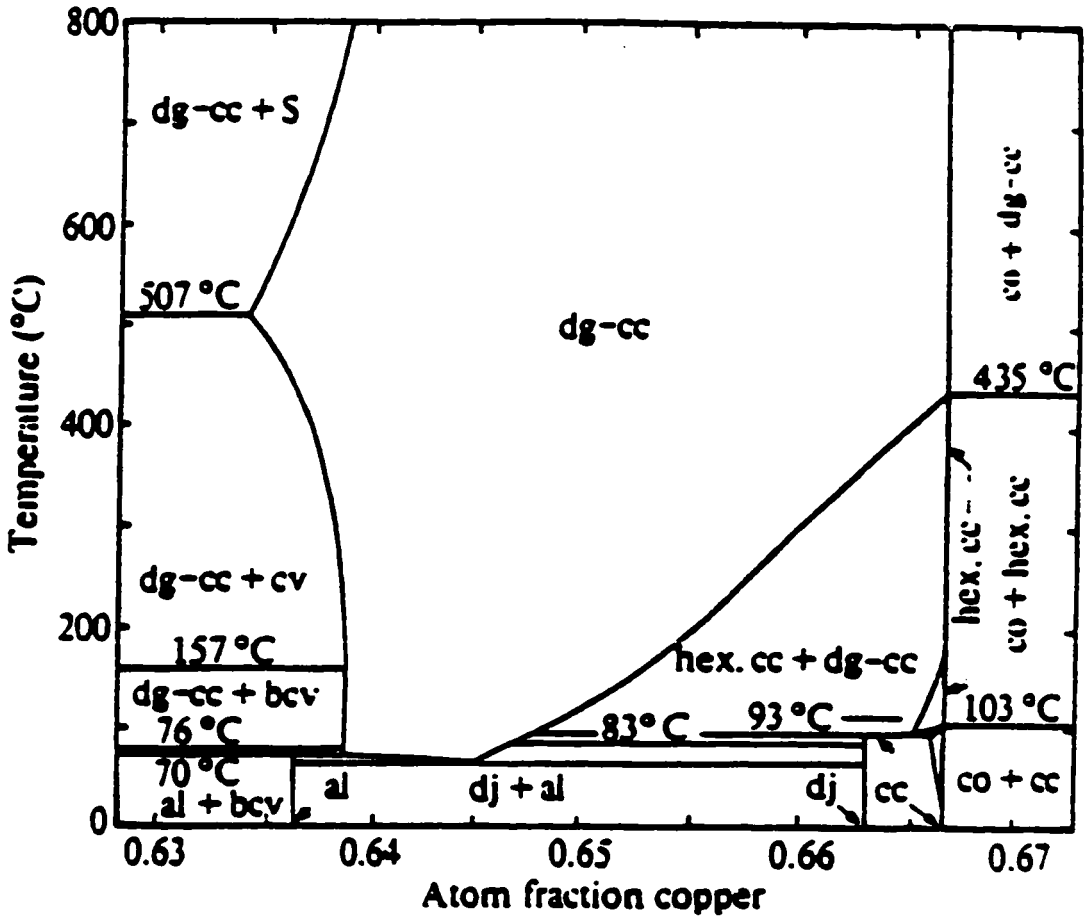

least of the blaubleibender covellite is ferroan'. Published references to hypogene covellite are rare.

Other stable copper sulphide phases at low temperature include **anilite** (Cu_7S_4) and **djurleite** ($Cu_{1.97}S$). Both anilite and djurleite closely resemble digenite, and may be easily overlooked without careful x-ray or microprobe examination. There seems to be some debate about the composition of anilite; some sources say Cu_7S_5, corresponding to $Cu_{1.4}S$ (the same composition as Cu-rich blue-remaining covellite), but others report $Cu_{1.75}S$. Above 70°C anilite decomposes to digenite and covellite (Morimoto and Koto 1970). Since it can also form from the breakdown of digenite + covellite below about 75°C, the presence of anilite, therefore, is not evidence of deposition below 75°.

Djurleite usually occurs as fine intergrowths with other copper suphides, and it decomposes above 93°C to hexagonal chalcocite and the cubic chalcocite-digenite phase (Roseboom 1966). Roseboom also found in the same study that the assemblage djurleite-covellite is not stable in the Cu-S system.

2.3 Mineralogical Associations in the Ternary Cu-Fe-S System

Figure 2.2 is a ternary diagram for the Cu-Fe-S system which plots the locations of the ternary sulphides according to their standard (accepted) chemical composition. **Chalcopyrite** is the most common of the ternary copper-iron sulphides, possessing an ordered tetragonal structure which is stable up to 557°C. Chemically, it deviates very little from ideal $CuFeS_2$, though it may be slightly metal-rich at high temperature (Barton 1973). Above the thermal maximum, chalcopyrite decomposes to pyrite plus the intermediate solid solution, which, although not a high-temperature polymorph of chalcopyrite, is nonetheless closely related in structure and composition.

Bornite exists in several polymorphic forms (Mormimoto and Kullerud 1961). The low-temperature form in most ores is tetragonal, inverting to cubic on heating to 228°C. Bornite, like digenite, exhibits extensive solid solution in the Cu-Fe-S system, especially with regard to the Cu/Fe ratio. Solid solution with digenite becomes complete above 335°C.

There are descriptions of 'anomalous' or 'x-' bornite from several locations (summarised in Brett and Yund 1964). These varieties of bornite contain a slight excess of sulphur relative to

Table 1. Minerals and phases of the Cu-S system. Numbers in brackets are references, compiled in Craig and Scott (1974).

Mineral Name	Composition	Thermal Max. (°C)	Thermal Min. (°C)	Structure Type
chalcocite	Cu_2S	103 (1)	----	monoclinic (15)
-----	Cu_2S	435 (1)	103	hexagonal (2,3)
----	Cu_2S	1129 (8)	435	cubic (4)
----	Cu_2S	500 (5)	----	tetragonal (7)
djurleite	$Cu_{1.97}S$	93 (1)	----	orthorhombic (10)
digenite	Cu_9S_5	83 (1)	----	cubic (4)
----	$Cu_{9+x}S_5$	1129 (8)	83	cubic (4)
anilite	Cu_7S_5	70 (12)	----	orthorhombic (11)
"blaubleibender" covellite	$Cu_{1+x}S$	157 (6)	----	hexagonal (18)
covellite	CuS	507 (13)	----	hexagonal (14)
----	CuS_2	550 (9)	?	cubic (16, 17)

References:

(1) Roseboom (1966)
(2) Buerger & Buerger (1944)
(3) Wuensch & Buerger (1963)
(4) Morimoto & Kullerud (1963)
(5) Skinner (1970)
(6) Moh (1964)
(7) Janosi (1964)
(8) Jensen (1947)
(9) Munson (1966)
(10) Morimoto (1962)
(11) Morimoto et al. (1969)
(12) Morimoto & Koto (1970)
(13) Kullerud (1965)
(14) Berry (1954)
(15) Evans (1968)
(16) Taylor & Kullerud (1971)
(17) Taylor & Kullerud (1972)
(18) Rickard (1972)

Table 2. Minerals and phases of the Cu-Fe-S system. Numbers in brackets are references, compiled in Craig and Scott (1974).

Mineral Name	Composition	Thermal Max. (°C)	Thermal Min. (°C)	Structure Type
digenite	$(Cu,Fe)_9S_5$	83	----	cubic
----	$(Cu,Fe)_9S_5$	1129	83	cubic (17)
bornite	Cu_5FeS_4	228 (13)	----	tetragonal (13)
----	Cu_5FeS_4	----	? Metastable	cubic (13)
----	Cu_5FeS_4	1100 (16)	228	cubic (13)
x-bornite	$Cu_5FeS_{4.05}$	125 (12)	----	tetragonal (19)
idaite	$Cu_{5.5}FeS_{6.5}$	501 (12)	----	hexagonal (14, 15)
fukuchilite	Cu_3FeS_8	200 (7)	----	cubic (8)
chalcopyrite	$CuFeS_2$	557	----	tetragonal (2, 11)
cubanite	$CuFe_2S_3$	200-210 (6)	----	orthorhombic (5)
intermediate ss	wide range	960 (16)	20-200	cubic (4)
talnakhite	$Cu_9Fe_8S_{16}$ (3)	186 (9)	----	cubic (1)
int. phase I	$Cu_9Fe_8S_{16}$ (?)	230 (9)	186	?
int. phase II	$Cu_9Fe_8S_{16}$ (?)	520 (9)	230	?
mooihoekite	$Cu_9Fe_9S_{16}$	167 (9)	?	tetragonal (2)
int. phase A	$Cu_9Fe_9S_{16}$	236	167	?
haycockite	$Cu_4Fe_5S_8$	?	----	orthorhombic
primitive cubic phase	wide range	20-200 (9)	20-200	cubic? (9)

References:

(1) Hall & Gabe (1972)
(2) Cabri & Hall (1972)
(3) Cabri & Harris (1971)
(4) Szymanski et al. (1973)
(5) Buerger (1947)
(6) Cabri et al. (1973)
(7) Kajiwara (1969)
(8) Shimazaki & Clark (1970)
(9) Cabri (1973)
(10) MacLean et al. (1972)
(11) Barton (1973)
(12) Yund & Kullerud (1966)
(13) Morimoto & Kullerud (1966)
(14) Yund (1963)
(15) Frenzel (1959)
(16) Kullerud et al. (1969)
(17) Morimoto & Kullerud (1963)
(18) Clark (1970)
(19) Morimoto (1970)

Figure 2.2. Minerals reported within the Cu-Fe-S system. Abbreviations are as follows: cc, chalcocite; dj, djurleite; di; digenite; al, anilite; bcv, blue-remaining covellite; cv, covellite; bn, bornite; a-bn, anomalous bornite; id, idaite; fk, fukuchilite; tal, talnakhite; cp, chalcopyrite; mh, mooihoekite; hc, haycockite; cb, cubanite; py, pyrite; mc, marcasite; gr, greigite; sm, smythite; m-po, monoclinic pyrrhotite; h-po, hexagonal pyrrhotite; tr, troilite; mk, mackinawite; ??, Cu-mackinawite? (data from several authors; refer to Tables 1 and 2).

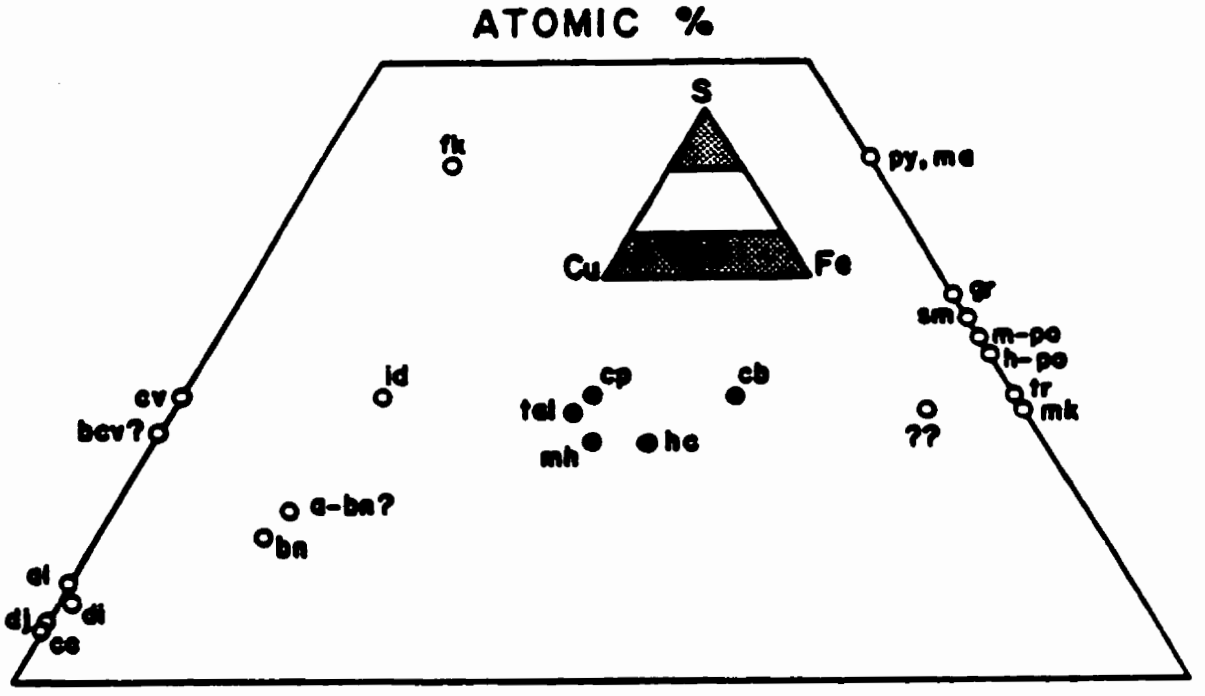

normal bornite, form below 125°C (from low-temperature solutions rather than through solid-state reactions on cooling), and are probably metastable (Yund and Kullerud 1966). Sillitoe and Clark (1969) describe a phase they refer to as **anomalous bornite**, forming as an intermediate stage in the alteration of bornite, on the way to the ultimate oxidation products of bornite, malachite and goethite.

Pyrite does not deviate measurably from the ideal composition FeS_2, except with respect to trace element distribution. The concentration of trace elements in a single phase (e.g., cobalt content of pyrite) has been used as a guide to temperature of mineralisation (Barton 1970). Pyrite is stable in the Cu-Fe-S system over a temperature range of 25-742°C, although equilibrium phase relations are not well established below 300°C (Toulmin and Barton 1964).

A synthetic phase of composition $Cu_{5-x}Fe_xS_{6+x}$ was first reported by Merwin and Lombard (1937), but a natural analog was not found until much later (Frenzel 1959). The similarity of this new phase, **idaite**, with bornite, except for an orange tint and a strong anisotropism, led some workers to refer to idaite as **'orange bornite'**. Yund and Kullerud (1966) found that idaite is stable below 501°C, although the phase relations remain in doubt. The high-temperature equilibrium assemblage of pyrite + bornite may be replaced by idaite + chalcopyrite at 300°C. At high temperatures idaite coexists with pyrite and digenite. Below 228°C, idaite may break down to give the metastable assemblage chalcopyrite + covellite in the absence of pyrite. Sillitoe and Clark (1969) describe a chalcopyrite-like phase, idaite, found as an intermediate stage in the oxidation of bornite. They describe the optical properties of this supergene sulphide as closely comparable to those described by Frenzel (1959), and the composition as close to Levy's idaite (1967), given the formula Cu_3FeS_4.

In the ternary Cu-Fe-S system, the tie-lines between covellite, on the Cu-S join, and other phases in the system, change with temperature. Figure 2.3a, a representation of the ternary phase diagram at 400°C, shows that when covellite appears at 507°C, it is tied to both idaite ($Cu_{5+X}FeS_{6+X}$), which forms at 501°C, and the extensive chalcocite-digenite-bornite solid solution. At high temperature (~400°C) this solid solution extends from the Cu-S join where it is continuous with the high chalcocite - high digenite solid solution, to a composition even more iron- and sulphur-rich than regular bornite (Cu_5FeS_4), up to 15 atomic % Fe. Below about 335°C,

this sulphur-rich bornite splits into a bornite solid solution and a digenite solid solution. Figure 2.3b shows that at this point covellite is tied to idaite and the digenite solid solution. These tie-lines remain in effect even at low temperature (25°C).

In some cases idaite will break down below 223°C (based on Schneeberg 1973), when it should decompose to pyrite + digenite + covellite:

$$2Cu_{5.5}FeS_{6.5}\ (id) \rightarrow 2FeS_2\ (py) + 2CuS\ (cv) + Cu_9S_5\ (dg)$$

This reaction appears to be prevented by the difficulty in nucleating pyrite: in the event that pyrite fails to grow, idaite may be represented by the chemically-equivalent, but non-equilibrium, decomposition products covellite + chalcopyrite:

$$2Cu_{5.5}FeS_{6.5}\ (id) \rightarrow 9CuS\ (cv) + 2CuFeS_2\ (cpy)$$ [Barton and Skinner 1976].

2.4 Covellite Crystal Chemistry

Covellite is not an abundant mineral but it occurs in most copper deposits, usually as a coating on other sulphides in the zone of supergene enrichment. It is associated with other copper minerals, especially chalcocite, chalcopyrite, bornite, and enargite, and is derived from them by alteration. It is often found as disseminations through these and other copper minerals. Mineralogical sources generally agree (e.g., Klein and Hurlbut, after Dana, 1977; Deer, Howie, and Zussman 1962) that hypogene covellite is known but uncommon. Although covellite is a hexagonal mineral, it rarely occurs in tabular hexagonal crystals. It possesses a {0001} cleavage, giving perfect flexible plates of metallic indigo-blue (or darker). Covellite has a fixed, nearly impurity-free composition by weight percent of Cu 66.4, S 33.6%. Although chemically very simple, it has a complex structure: one copper atom is in tetrahedral coordination with sulphur, with the tetrahedra sharing corners to form layers, and a second copper atom in trigonal coordination with sulphur to form planar layers. The excellent {0001} cleavage is parallel to this layer structure. The structure can be viewed as made of sheets of CuS_3 triangles between double layers of CuS_4 tetrahedra, where covalent sulphur-sulphur bonds link the layers (Figure 2.4).

2.5 Experimental Studies with Covellite

Blaubleibender, or blue-remaining, covellites (Section 2.2) have been observed in nature and described for several decades (Frenzel 1959). They had been attributed to a small excess of copper in the covellite structure (ranging from $Cu_{1.1\text{-}1.4}S$), until Moh (1971) synthesized two

distinct varieties of blaubleibender covellite, Type A ($Cu_{1.2}S$) and Type B($Cu_{1.4}S$), later named yarrowite and spionkopite respectively, after their type localities (Yarrow and Spionkop Creeks) in southwestern Alberta (Goble 1980). Potter (1977) used Moh's technique to synthesize phases with compositions $Cu_{1.1 +/- 0.1}S$ and $Cu_{1.4 +/- 0.1}S$, and showed that these phases are metastable in the Cu-S system; that is, they possess a more positive free energy at a given temperature, pressure, and bulk composition, as opposed to a stable phase which possesses the most negative free energy under the same conditions.

The observed presence of natural yarrowite and spionkopite, having compositions of approximately $Cu_{1.12}S$ and $Cu_{1.32-1.40}S$, respectively and produced by natural leaching of Cu-rich sulphides (Goble 1980), and metastable synthetic phases of approximately the same composition produced by synthetic leaching of Cu-rich sulphides suggest that yarrowite and spionkopite are naturally-occurring but metastable phases in the Cu-S system. However, it was later shown that synthetic varieties of blaubleibender covellite are not necessarily structurally-identical to natural varieties. Synthetic blaubleibender covellite may exist in a metastable pseudocubic structure that has a similar powder pattern to the hexagonal structure of natural blue-remaining covellites. Potter's conclusions, then, should be applied to natural yarrowite and spionkopite with caution. Although his synthetic samples were shown to be metastable, X-ray powder and optical data do not prove that these samples are in fact yarrowite and spionkopite. Single-crystal X-ray data is required to resolve the issue.

Other associations in the Cu-Fe-S system have been investigated. It was suggested that the assemblage covellite-djurleite, not stable in the system Cu-S, might be stable in the ternary system when djurleite contains significant iron, but Roseboom (1966) concluded that "because covellite does not take up any iron, this would require that the djurleite have a greater Fe:Cu ratio than any digenite that is also stable. Digenite is known to have considerable solid solution toward Cu_5FeS_4 and a djurleite solid solution having a comparable Fe:Cu ratio seems unlikely but no data are available". However, what about a situation where covellite does take up iron? As will be discussed in Chapter 3, covellites from Chuquicamata contain up to 5 weight percent iron, an amount not previously reported. Would this affect Roseboom's conclusions? In a case where covellite takes up as much iron as any 'pure' digenite that is also stable, would the combined

Figure 2.3 (a). Schematic phase relations in the central portion of the Cu-Fe-S system at 400°C and (b). at 300°C (after Craig and Scott, 1979).

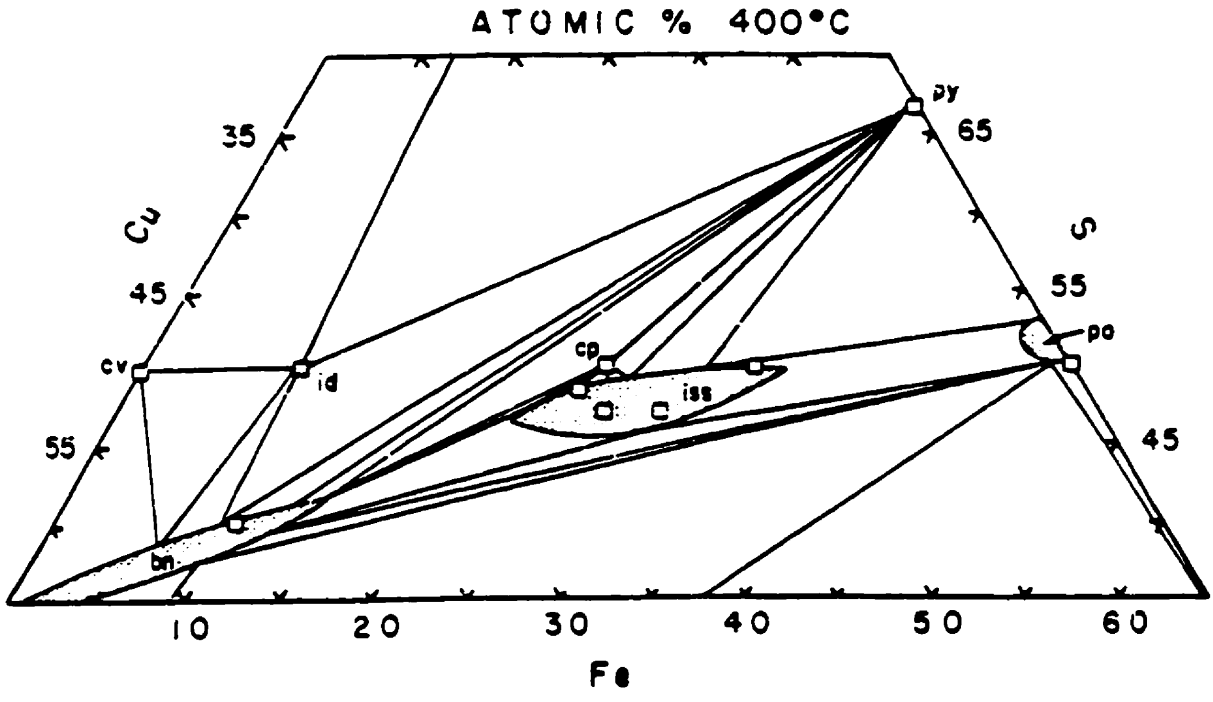

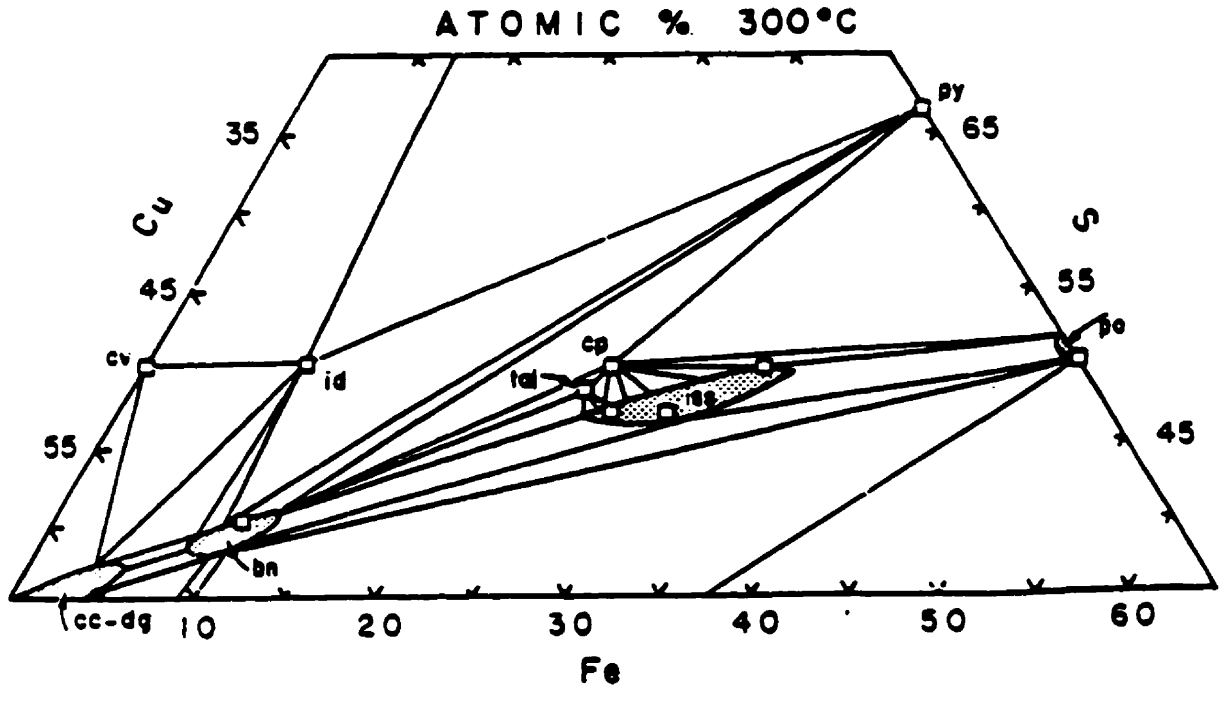

Figure 2.4. Structure of covellite, CuS. The dotted lines indicate covalent S-S bonds (after B.J. Wuensch, 1974, in *Sulfide Mineralogy*).

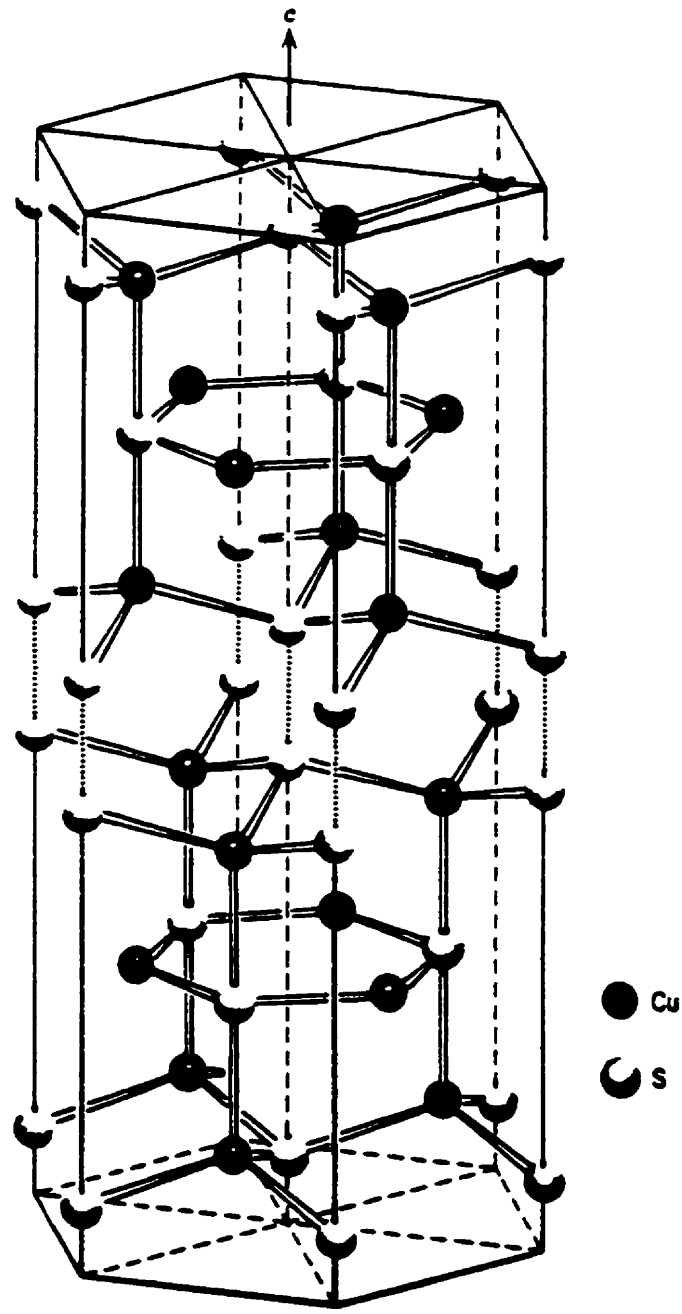

Fe:Cu ratio for covellite and djurleite have to be more than digenite? Or would the mere presence of iron in covellite affect the argument, and allow the assemblage covellite-djurleite to become stable in the system Cu-Fe-S? The assemblage djurleite-Fe-covellite is not observed in the 4500N section at Chuquicamata, so this study can provide no answers, but it is an intriguing question.

Other common ternary phases, such as cubanite, are not discussed here since they are not observed in the 4500N sample set chosen for this study.

2.6 Related Systems: Zn-Fe-S and Cu-As(-Sb)-S

Other common sulphides observed at Chuquicamata include sphalerite, and the sulphosalts enargite and colusite. The tungsten ore wolframite is a rare but interesting phase observed in a few samples from the 4500N section.

Sphalerite is the low-temperature (cubic) polymorph of ZnS, and wurtzite is the high-temperature hexagonal polymorph. For pure ZnS the inversion temperature is 1020°C (Allen and Crenshaw 1912); however, often in hydrothermal systems sphalerite is saturated with FeS, lowering the inversion temperature to approximately 875°C.

Buerger (1934) found that sphalerite could be considered the high-S form of ZnS, and wurtzite the low-S form. Other studies (e.g. Shalimova and Morozova 1965) confirmed, through optical absorption, that the hexagonal phase contained a deficiency of sulphur and that this deficiency was removed in the cubic phase. Nickel (1965) noted that most analyses of natural sphalerite show a sulphur:metal ratio >1. Since sphalerite and wurtzite vary slightly in composition, the phase change in general is not isocompositional or invariant, but likely a function of both temperature and f_{S2}.

Kullerud (1953) studied the dry binary system ZnS-FeS and concluded that: (a) the iron content of sphalerite is determined by the temperature of formation; and (b) the unit-cell parameter of sphalerite varies with Fe content. Later studies (e.g. Kudenko and Stetsenko 1964) found that minor elements can cause the same distortions of the crystal structure of sphalerite as iron. Several studies (e.g. Godovikov and Pitsyn 1965; Anfilogov et al. 1966) support the conclusion that the limit of substitution of Fe for Zn is raised substantially in aqueous solutions. Stroitelev and Babanskiy (1969) show that this is only sometimes true. The mechanism of entry of Fe into sphalerite is obviously complex, governed not only by temperature but also by

composition, concentration and pH of hydrothermal solutions.

Meagre data exists on the copper contents of zinc-sulphides, but Frenzel and Ottoman (1967) reported wurtzite containing 2.8 wt% Cu coexisting with sphalerite containing 0.2 wt% Cu. Clark and Sillitoe (1969) reported a supergene sphalerite from Copiapo containing 15+/-2 wt% Cu; this 'sphalerite' was interpreted as a metastable intermediate phase in the replacement of Cu-free sphalerite. The most recent study (Craig and Kullerud 1973) indicates the solubility of Cu in ZnS is very small between 200 and 800°C.

Enargite is orthorhombic and has an ideal composition of Cu_3AsS_4. In general, enargite varies little from the ideal (Maske and Skinner 1971), although natural enargite invariably contains some Sb substituting for the As (up to 6% by weight). Minor Fe and Zn may also be present (Klein and Hurlbut, after Dana, 1977).

The low-temperature polymorph of enargite, luzonite, has a tetragonal structure and does not show any marked deviation from the ideal composition of Cu_3AsS_4. The structure of enargite differs from that of luzonite in that luzonite has a structure derived from sphalerite, in which S atoms lie at the nodes of a face-centred cubic lattice. Enargite has a structure derived from wurtzite (the high-temperature polymorph of sphalerite), where S atoms lie at the nodes of a hexagonal close-packed lattice. The inversion temperature from luzonite to enargite has not been fixed and is tentatively placed in the range 275°C to 320°C (Maske and Skinner 1971). Famatinite, Cu_3SbS_4, the antimony "analogue" of enargite, is isostructural with, and shows an extensive solid solution toward, luzonite. Famatinite has a melting temperature of 627°C.

Colusite, $Cu_{26}V_2As_4Sn_2S_{32}$ or $Cu_3(As,Sn,V)S_4$, is a complex sulfosalt that can be thought of as a rather messy enargite. Most published analyses of colusite include 5-8 elements, although a broad range of isomorphous replacement is characteristic. An ideal crystal-chemical formula for colusite is $Cu_{26}V_2(As, Sn)_6S_{32}$ (Orlandi et al. 1981). The study by Orlandi indicates that iron may enter either the V site, as it does in samples from Butte (Levy 1967), or the (As, Sn) site, as shown in colusite from Gay (Pshenichnyi et al, 1974). Germanium may also substitute for (As, Sn) as in Gay.

With regards to common oxides, there have been several studies on the effect of temperature on the composition of wolframites. The chemistry of wolframites in the hubnerite

($MnWO_4$)-ferberite ($FeWO_4$) series varies to a great extent. The compositional changes depend on the conditions of formation: changes in temperature, composition of country rocks and of ore-forming solutions, and pH of solutions, to name a few.

Singh and Varma (1977) showed that the intermediate member of the series (wolframite with a composition between 75 and 25% MnO) has the highest crystallisation temperature (compared with hubnerites, 100 to 75% MnO, and ferberites, 25 to 0% MnO). Under lengthy conditions of high temperature and pressure, the most favourable conditions are created for mixing of hubnerite and ferberite components, and therefore the formation of wolframites, which are excluded at low temperature under near-surface conditions.

Others have shown a dependence on the influence of the country rocks. Barbanov (1975) concluded that during lengthy activity of high-temperature solutions on country rocks, a leaching of components and a change in the composition of solutions takes place, which translates into a change in ratios of Mn and Fe in wolframites. Denisenko (1971) identified "inverse dependence of composition of wolframites on the degree of iron content of the mineral paragenesis". In other words, with a low sulphur concentration in the solutions in a reducing environment, ferberite varieties should develop, whereas with an increase in the partial pressure of H_2S, most of the Fe present in the solutions will go into the composition of the sulphides, leaving hubnerite varieties to crystallize. Wolframite in an Fe-rich environment is related to the later stages of hydrothermal activity (Voyevodin, 1981).

2.7 Highlights Relevant to this Study

The main focus of this study is the characterization of hypogene, that is to say high temperature, covellite assemblages. As such, ternary phase diagrams for the Cu-Fe-S system in the 250° to 500° range and the experimental studies that refined them are referred to throughout this thesis.

Within the Cu-S system, specific points of interest include: the assemblage digenite-covellite and the various relationships it defines (e.g. equilibrium assemblage vs replacement assemblage); and the presence of blaubleibender covellites, which are documented and examined for the information they may provide about hypogene vs supergene assemblages.

Within the Cu-Fe-S system, particular attention is paid to the idaite-covellite tie, which is

linked to both the composition of covellites in the Chuquicamata system and to their mineralogical relationships.

3.1 Definitions of relevant terms

Just as each texture displayed by ore minerals can be formed by more than one process, so descriptive terminology can be interpreted in several ways. It is therefore necessary to define some terms that are commonly used throughout this thesis.

The initial goal of a petrologic investigation is to recognize (past or present) *equilibrium* mineral assemblages. A system (which can be any quantity we choose, in this case ore minerals) in equilibrium has no spontaneous tendency to change over a *reasonable* amount of time under fixed physical and chemical conditions (Barton et al. 1963). Minerals that *coexist* are not necessarily in equilibrium.

Any minerals occurring together, with unspecified spatial and equilibrium relationships, will be considered an *association*. A mineral *assemblage* will be defined as minerals occurring in direct contact with one another, and may or may not be in equilibrium.

For each assemblage, an attempt is made to infer the *paragenetic sequence* (i.e. the order of deposition) of the minerals through study of their textural relationships.

3.2 Main ore minerals

The face of the dominant mineralogical species found at Chuquicamata is an evolving one, with new phases at depth in the deposit competing with the common low temperature (and hence, nearer-surface) minerals. Early in the mining history, the most common minerals mined in Chuquicamata were copper oxides (Cook 1978); by the 1940's enargite and chalcopyrite were the dominant hypogene ore minerals (Lopez 1939). The following is an account of the main ore minerals found in the 4500N section of the deposit, as of the time of this study, including their occurrence, properties of identification and chemical character. For background information regarding the thermochemical properties of the minerals and an account of the experimental work associated with them, refer to Chapter 2. Table 3 details the locations of the samples chosen for study, including drill hole number, depth, and the alteration and mineralisation zone in which they occur (as mapped by mine staff at Chuquicamata). Figure 1.4 can be referred to for the spatial

distribution of the drill holes in cross-section 4500N. Appendix C offers brief descriptions of the drill core samples from which the polished sections for this petrographic study were made.

3.2.1 Analytical Methods

The electron mincoprobe was used to determine the chemical composition of sulphide minerals, and to study the variation in chemical composition of the mienrals through the 4500N cross-section. Analyses were carried out on a JEOL 733 electron microprobe equipped with four wavelength dispersive spectrometers and and Oxford Link eXL energy dispersive system. The energy dispersive system was used for all elements. Resolution of the energy dispersive detector was 137eV at 5.9Kev.

Each spectrum was acquired for 40 seconds with an accelerating voltage of 15Kv and a beam current of 15nA. Probe spot size was approximately 1 micron. The raw data was corrected using Link's ZAF matrix correction program. Instrument calibration was performed on cobalt metal. Instrument precision on cobalt metal (x=10) was +/- 0.5% at 1 standard deviation. Accuracy for major elements was +/- 1.5 to 2.0% relative.

Geological standards were used as controls. Sulphide standards used were natural chalcopyrite and synthetic $Cu_{1.8}S$, supplied by CANMET.

Appendix A contains the electron microprobe data from which representative samples were drawn for this section, and on which some conclusions are based.

X-ray diffractometry was performed by the author at the Fission Track Research Laboratory, Earth Sciences Department, Dalhousie University. The analyses were performed on small sub-samples by standard powder diffraction. An automated Philips 100kV generator and diffractometer unit was used for mineral identification by powder diffractometry. The very fine-grained granular material was powdered in acetone by hand in an agate mortar. The powdered sample was placed on a glass microscope slide and mounted in the diffractometer (in some cases, an amorphous, single crystal silica mount was used to reduce the background resonse from the mount itself). The sample and x-ray detector were rotated at a known rate with respect to a $CuK\alpha$ x-ray source. Energy detected was recorded and processed automatically. Output consists of a peak list, energy response curve, and peak match fit lists for various search routines (Cuesta Report, 1996). Peak lists are included for each sample (Appendix B).

Table 3. Chuquicamata, Section 4500N. Samples are documented with respect to drill hole, depth, alteration and mineralisation zones.

DDH	SAMPLE No.	DEPTH	ALTERATION	MINERALISATION	PTS	separates for sulphur isotopes	PTS described/ photo	comments
2967	CU-181	671.5m	Fortuna granod.		X		01/95	beyond Falla Oeste
2967	CU-182	224.76m	quartz-sericite	cv, en, py	X X	en + py	06/95	probed 09/95 for py, en, cv
2967	CU-183	225.10m	quartz-sericite	cv, en, py	X X	en + py	06/95	
2967	CU-184	233.04m	quartz-sericite	cv, en, py	X		05/95	
2967	CU-185	234.45m	quartz-sericite	cv, en, py	X	py + cv	05/95	
2967	CU-186	314.74m	quartz-sericite	cv, en, py				
2967	CU-187	316.26m	quartz-sericite	cv, en, py	X		01/95	
2967	CU-188	319.59m	quartz-sericite	cv, en, py				
2967	CU-189	324.69m	quartz-sericite	cv, en, py				
2967	CU-190	325.20m	quartz-sericite	cv, en, py	X			
2967	CU-191	325.49m	quartz-sericite	cv, en, py				
2967	CU-192	325.93m	quartz-sericite	cv, en, py	X		01/95	
2967	CU-193	408.00m	quartz-sericite	mass. py+/-cv, en	X		01/95	
2967	CU-194	411.38m	quartz-sericite	mass. py+/-cv, en				
2967	CU-195	413.77m	quartz-sericite	mass. py+/-cv, en			01/95	probed 01/95 for cv, dg; no hand sample
2967	CU-196	415.40m	quartz-sericite	mass. py+/-cv, en				
2967	CU-197	566.23m	quartz-sericite	mass. py+/-cv, en				
2967	CU-198	567.48m	quartz-sericite	mass. py+/-cv, en				
2967	CU-199	569.42m	quartz-sericite	mass. py+/-cv, en	X	gypsum + py		probed 11/95 for sph, en, cv
2967	CU-200	574.23m	quartz-sericite	mass. py+/-cv, en	X		06/95	
2967	CU-201	574.87m	quartz-sericite	mass. py+/-cv, en	X X X		01/95, 06/95	probed 01/95 for cv, dg
2967	CU-202	575.14m	quartz-sericite	mass. py+/-cv, en	X			
2967	CU-203	576.98m	quartz-sericite	mass. py+/-cv, en	X X		01/95	probed 01/95 for cv, dg, an, bcv, sph
2967	CU-204	513.05m	quartz-sericite	mass. py+/-cv, en	X	anh + py	01/95	probed 01/95 for cv, dg, wolf,
2967	CU-205	514.90m	quartz-sericite	mass. py+/-cv, en	X X		06/95	probed 09/95 for py, cv, dg, en; probed 11/95 for wolf
2967	CU-206	518.65m	quartz-sericite	mass. py+/-cv, en	X		01/95	probed 01/95 for sph, cv, dg
2967	CU-207	605.70m	quartz-sericite	py +/- cv	X		01/95	
2967	CU-208	607.96m	quartz-sericite	py +/- cv	X		01/95	
2967	CU-209	619.86m	quartz-sericite	py +/- cv				
2967	CU-210	455.90m	quartz-sericite	py +/- cv	X			probed 05/96 for cv, rutile
2967	CU-211	456.40m	quartz-sericite	py +/- cv	X X			probed 01/95 for cv, dg

Table 3. Chuquicamata, Section 4500N. Samples are documented with respect to drill hole, depth, alteration and mineralisation zones.

DDH	SAMPLE No.	DEPTH	ALTERATION	MINERALISATION	PTS	separates for sulphur isotopes	PTS described/ photo	comments
2967	CU-212	461.20m	quartz-sericite	py +/- cv				
2967	CU-213	209.10m	quartz-sericite	cv, en, py				
2967	CU-214	211.60m	quartz-sericite	cv, en, py	X X			probed 01/95 for cv, dg, mo, en, sulphosalt (?)
2242	CU-431	38.55m	quartz-sericite	cv, py, dg, mo	X		05/95	
2242	CU-432	40.91m	quartz-sericite	cv, py, dg, mo				
2242	CU-433	56.45m	quartz-sericite	cv, py, dg, mo	X	mo	05/95	
2242	CU-434	95.86m	quartz-sericite	dg, py, cpy, mo, sph, en	X	mo	05/95	
2242	CU-435	103.07m	quartz-sericite	dg, py, cpy, mo, sph, en	X			
2242	CU-436	103.83m	quartz-sericite	dg, py, cpy, mo, sph, en	X		05/95	QS overprinting K altn
2242	CU-437	138.24m	potassic	cv, cpy, dg, py				
2242	CU-438	139.15m	potassic	cv, cpy, dg, py	X	bn + cpy	05/95	
2242	CU-439	141.28m	potassic	cv, cpy, dg, py				
2242	CU-440	142.13m	potassic	cv, cpy, dg, py	X			
2242	CU-441	145.32m	potassic	cv, cpy, dg, py	X		06/95	fault gouge, massive sulphide, probed 09/95
2242	CU-442	149.60m	potassic	cv, cpy, dg, py	X			
2242	CU-443	151.38m	potassic	cv, cpy, dg, py	X		05/95	
2242	CU-444	154.42m	potassic	cv, cpy, dg, py				
2242	CU-445	153.63m	potassic	cv, cpy, dg, py	X		05/95	
2242	CU-446	156.77m	potassic	cpy, bn, dg, py, mo	X			
2242	CU-447	160.76m	potassic	cpy, bn, dg, py, mo	X		05/95	
2242	CU-448	161.04m	potassic	cpy, bn, dg, py, mo	X		05/95	
2242	CU-449	161.41m	potassic	cpy, bn, dg, py, mo	X			
2242	CU-450	161.98m	potassic	cpy, bn, dg, py, mo	X			probed 11/95 for cv, id, cpy
2242	CU-451	164.98m	potassic	cpy, bn, dg, py, mo	X			
2242	CU-452	189.86m	potassic	cpy, bn, dg, py, mo	X			
2242	CU-453	193.10m	potassic	cpy, bn, dg, py, mo	X	bn + cpy	05/95	
2242	CU-454	193.78m	potassic	cpy, bn, dg, py, mo	X X	gypsum + cpy	06/95	probed 09/95 for cv, cpy, dg, bn
2242	CU-455	193.86m	potassic	cpy, bn, dg, py, mo	X	cpy-cv mix	06/95	probed 09/95 for cv, cpy, Fe-oxide
2242	CU-456	194.20m	potassic	cpy, bn, dg, py, mo	X			
2242	CU-457	195.76m	potassic	cpy, bn, dg, py, mo	X X		05/95	

Table 3. Chuquicamata, Section 4500N. Samples are documented with respect to drill hole, depth, alteration and mineralisation zones.

DDH	SAMPLE No.	DEPTH	ALTERATION	MINERALISATION	PTS	separates for sulphur isotopes	PTS described/ photo	comments
2242	CU-458	196.55m	potassic	cpy, bn, dg, py, mo				cm-scale panels of kspar adjacent to QS altn
2242	CU-459	200.04m	potassic	cpy, bn, dg, py, mo				
2242	CU-460	200.75m	potassic	cpy, bn, dg, py, mo	X			probed 05/96 for cpy, Fe-oxide
2242	CU-461	202.52m	potassic	cpy, bn, dg, py, mo	X X		06/95	probed,09/95 for ga, dg, en, cv, py
2242	CU-462	252.55m	potassic	cpy, bn, dg, py, mo				
2242	CU-463	257.63m	potassic	cpy, bn, dg, py, mo				
2242	CU-464	258.45m	potassic	cpy, bn, dg, py, mo	X			
2242	CU-465	260.14m	potassic	cpy, bn, dg, py, mo	X			probed 05/96 for cv, id, cpy
2242	CU-466	261.02m	potassic	cpy, bn, dg, py, mo				
2242	CU-467	261.27m	potassic	cpy, bn, dg, py, mo	X X		06/95	probed 09/95 for bn, cpy, ga, dg, py; probed 05/11 for col
2242	CU-468	253.23m	potassic	cpy, bn, dg, py, mo	X X		05/95	
2242	CU-469	263.66m	potassic	cpy, bn, dg, py, mo				qtz vns w/ sericite, cutting K altn
2242	CU-470	264.53m	potassic	cpy, bn, dg, py, mo				
2242	CU-471	264.98m	potassic	cpy, bn, dg, py, mo				
2242	CU-472	265.60m	potassic	cpy, bn, dg, py, mo				
2242	CU-473	284.39m	potassic	cpy, bn, dg, py, mo	X		05/95	
2242	CU-474	286.75m	potassic	cpy, bn, dg, py, mo	X X		06/95	probed 05/96 for cv, dg, col, Fe-oxide
2242	CU-475	282.04m	potassic	cpy, bn, dg, py, mo	X X		05/95	
2242	CU-476	288.10m	potassic	cpy, bn, dg, py, mo	X X		06/95	probe 09/95 for bn, dg, cpy, py, cv; probed 11/95 for dg, bn, rt
2242	CU-477	288.65m	potassic	cpy, bn, dg, py, mo	X X		06/95	
2242	CU-478	288.95m	potassic	cpy, bn, dg, py, mo	X			probed 05/96 for Fe-oxide
2234	CU-479	294.20m	potassic	cpy, py, cv, dg	X	anh + py		
2234	CU-480	295.55m	potassic	py, cpy, bn, cv	X			probed 05/96 for tn, cv, en?
2234	CU-481	295.98m	potassic	py, cpy, bn, cv	X X		06/95	probed 05/96 for sph, dg, bn, en
2234	CU-482	297.53m	potassic	py, cpy, bn, cv	X		06/95	probed 09/95 for cv, cpy, Fe-oxide
2234	CU-483	297.89m	potassic	py, cpy, bn, cv				
2234	CU-484	298.65m	potassic	py, cpy, bn, cv				
2234	CU-485	299.82m	potassic	py, cpy, bn, cv				
2234	CU-486	301.37m	potassic	py, cpy, bn, cv				
2234	CU-487	301.95m	potassic	py, cpy, bn, cv	X		01/95	probed 01/95 for cv, bcv, dg, bn

Table 3. Chuquicamata, Section 4500N. Samples are documented with respect to drill hole, depth, alteration and mineralisation zones.

DDH	SAMPLE No.	DEPTH	ALTERATION	MINERALISATION	PTS	separates for sulphur isotopes	PTS described/ photo	comments
2234	CU-488	302.69m	potassic	py, cpy, bn, cv	X		01/95	
2234	CU-489	305.73m	potassic	py, cpy, bn, cv	X		06/95	probed 09/95 for sph, dg, col, py
2234	CU-490	307.95m	potassic	py, cpy, bn, cv	X			
2234	CU-491	306.79m	potassic	py, cpy, bn, dg	X			
2234	CU-492	308.20m	potassic	py, cpy, bn, dg				
2234	CU-493	216.30m	potassic	cpy, py, cv, dg, sph, ga	X	py + gyp		
2234	CU-494	219.84m	potassic	cpy, py, cv, dg, sph, ga	X		01/95	probed 01/95 for cv, dg, bcv, an
2234	CU-495	221.49m	potassic	cpy, py, cv, dg, sph, ga	X		01/95	probed 01/95 for cv, dg, id
2234	CU-496	244.40m	potassic	cpy, py, cv, dg, sph, ga	X		01/95	
2234	CU-497	245.49m	potassic	cpy, py, cv, dg, sph, ga				
2234	CU-498	245.68m	potassic	cpy, py, cv, dg, sph, ga				
2234	CU-499	249.15m	potassic	cpy, py, cv, dg, sph, ga	X	gyp/anh + py	01/95	
2234	CU-500	250.00m	potassic	cpy, py, cv, dg, sph, ga	X X		06/95	massive sulphide w/ massive sulphate, probed 09/95
2234	CU-501	250.70m	potassic	cpy, py, cv, dg, sph, ga	X			probed 11/95 for sph, dg, en
2234	CU-502	252.15m	potassic	cpy, py, cv, dg, sph, ga	X	gyp/anh + py		
2234	CU-503	253.27m	potassic	cpy, py, cv, dg, sph, ga	X		06/95	probed 09/95 for cv, mo, bn, sph, en, ga
2234	CU-504	107.86m	potassic	cc, cv, cpy, py, dg	X		01/95	
2234	CU-505	108.32m	potassic	cc, cv, cpy, py, dg				
2234	CU-506	111.09m	potassic	cc, cv, cpy, py, dg				
2234	CU-507	113.65m	potassic	cc, cv, cpy, py, dg	X X		06/95	probed 05/96 for cpy, dg, sph
2234	CU-508	114.71m	potassic	cc, cv, cpy, py, dg	X		01/95	
2234	CU-509	115.80m	potassic	cc, cv, cpy, py, dg	X			probed 05/96 for sph, dg, bn, cpy, rutile

3.2.1 Covellite (CuS)

Occurrence. In Chuquicamata, covellite has three main modes of occurrence:

a. an acicular form, on its own or in association with digenite, where covellite may be concentrated along the edges of digenite, or evenly distributed throughout (this assemblage is found in both of the major alteration zones studies, but considered by the author to be typical of quartz-sericite alteration);

b. thin lamellar crystals of covellite replacing other Cu-sulphides, mainly chalcopyrite; in some cases chalcopyrite has disappeared completely, and only the arrangement of covellite lamellae in loose lattices shows former chalcopyrite existence (size of lamellae varies widely) (this assemblage is typical of, but not necessarily restricted to, covellite in zones of potassic alteration); and,

c. massive covellite, interstitial to other minerals (pyrite or silicates, mainly), and small subrounded grains, some of which may not show pleochroism and may be blaubleibender (blue-remaining) covellite, or may be a basal section of regular covellite. Massive covellite may be of supergene or hypogene origin (textural differences will be discussed later, see Section 3.3).

Diagnostic properties. Covellite is easily recognizable in both hand sample and polished section by its deep blue colour. In hand sample, it is dark indigo-blue with a semi-metallic lustre and a black streak. In reflected light, covellite possesses extreme reflection pleochroism (from white to indigo-blue) and anisotropism (bright orange to copper-brown), both of which are even more striking in oil than they are in air. In the case of a basal section, which does not show pleochroism, the colour alone is enough to identify the mineral.

Chemistry. Of the approximately 100 samples of hypogene ore studied in polished section here, less than 15 have no covellite whatsoever. Analyses of over 150 samples of covellite from various hypogene mineral assemblages show that iron can substitute for copper up to 5 weight %. This phenomenon has not been described before. If only a few samples contained iron, we might be tempted to conclude that this aberration results from microprobe beam inaccuracies or micro-inclusions within the covellite. The large number of iron-bearing covellites, however, all interpreted as part of a hypogene environment, is enough to infer that covellite can indeed have a

significant iron content. A binary plot of Fe vs. Cu shows that the covellite analyses vary continuously from 0 weight % Fe (where many analyses are clustered around the standard stoichiometric covellite) to slightly less than 5% Fe. Figure 3.1 shows that a few (possibly spurious) samples contain between 5 and 7% Fe. If standard idaite is located on the same plot, the iron variation is seen to be systematic and may indicate crystallisation along the covellite-idaite tie line (Figure 2.4b). The few analyses of supergene covellite from the sample set have a fixed composition of CuS. Table 4 tabulates 3 representative electron microprobe analyses of covellite from Chuquicamata, along with the mean, maximum and minimum taken from the complete sample set (n) of covellites from Chuquicamata, where n for each element is the number of analyses of that element that fall above the limit of quantification (Appendix A). The calculated standard deviation and the detection limit and also provided. Representative samples were chosen on the basis of common mineral assemblages at Chuquicamata.

Table 4. Chemical composition (weight %) of hypogene covellite from Chuquicamata.

Sample	Cu	Fe	As	S	Total	assemblage
cu454B (77)	66.03	1.46		32.93	100.42	cv+cpy
cu195 (79)	67.13			32.80	99.93	cv+dg (no cpy)
cu495 (46)	65.63	1.99	0.28	32.95	100.85	py+cv
stoichiometric composition	66.47			33.53	100.00	
mean	66.18	1.56	0.28	33.06	100.07	
standard deviation	1.16	0.93	0.03	0.74		
maximum	69.39	4.36	0.35	34.52	101.99	
minimum	62.37	0.25	0.25	30.29	97.77	
# of analyses > LOQ	148	72	35	148	148	
detection limit (LOQ)	0.50	0.25	0.25	0.50		

Whatever its stability within the Cu-S system, blaubleibender covellite is recognised as a phase separate from regular covellite. It is reportedly enriched in copper over normal covellite by 1.5 to 2 percent (Frenzel 1959; Moh 1964), and can be enriched by as much as 6.7 percent

(Frenzel 1961, for synthetic samples; Sillitoe and Clark 1969, for samples of natural blaubleibender covellite). Although we have only 12 analyses of phases that fit unequivocally the composition of blaubleibender covellite, this dearth is due more likely to the failure of the author to recognize this phase than from its absence from the ore mineral assemblages. The samples of blaubleibender covellite range from about 68% Cu to 73.47%, enriched in copper by almost 7% over the regular covellites. As can be seen in Figure 3.2, a ternary Cu-Fe-S diagram, the blaubleibender covellites plot in a field distinct from that in which regular covellites from Chuquicamata plot. The blaubleibender covellites show a continuous range from 0 to about 3 weight % Fe, with at least one analysis at 4% Fe. This trend mimics the iron concentration of regular covellites from Chuquicamata. Table 5 gives the chemical composition of blue-remaining covellites from Chuquicamata. Two defined phases, yarrowite and spionkopite, are considered blaubleibender covellites, and their stoichiometric compositions are presented in Table 5 for comparison. The mean, standard deviation, maximum, and minimum are calculated from the number of analyses for each element that are above the limit of quantification.

Table 5. Chemical composition (weight %) of blaubleibender covellite from Chuquicamata.

Sample	Cu	Fe	As	S	Total	assemblage
cu203A (32)	72.65	1.59		25.13	99.37	cpy+dg+cv+sph+py
cu494 (26)	71.37	0.60		28.29	100.26	dg+cv
stoichiometric spionkopite	73.51			26.49	100.00	
stoichiometric yarrowite	72.35			27.65	100.00	
mean	70.30	1.78	0.25	27.76	99.42	
standard deviation	1.26	1.08		1.28		
maximum	72.65	3.92	0.25	29.51	101.21	
minimum	68.80	0.60	0.25	25.13	97.87	
# of analyses > LOQ	8	6	1	8	8	
detection limit (LOQ)	0.50	0.25	0.25	0.50		

Figure 3.1. Cu vs Fe plot of covellites from Chuquicamata. Standard idaite is represented by a solid triangle.

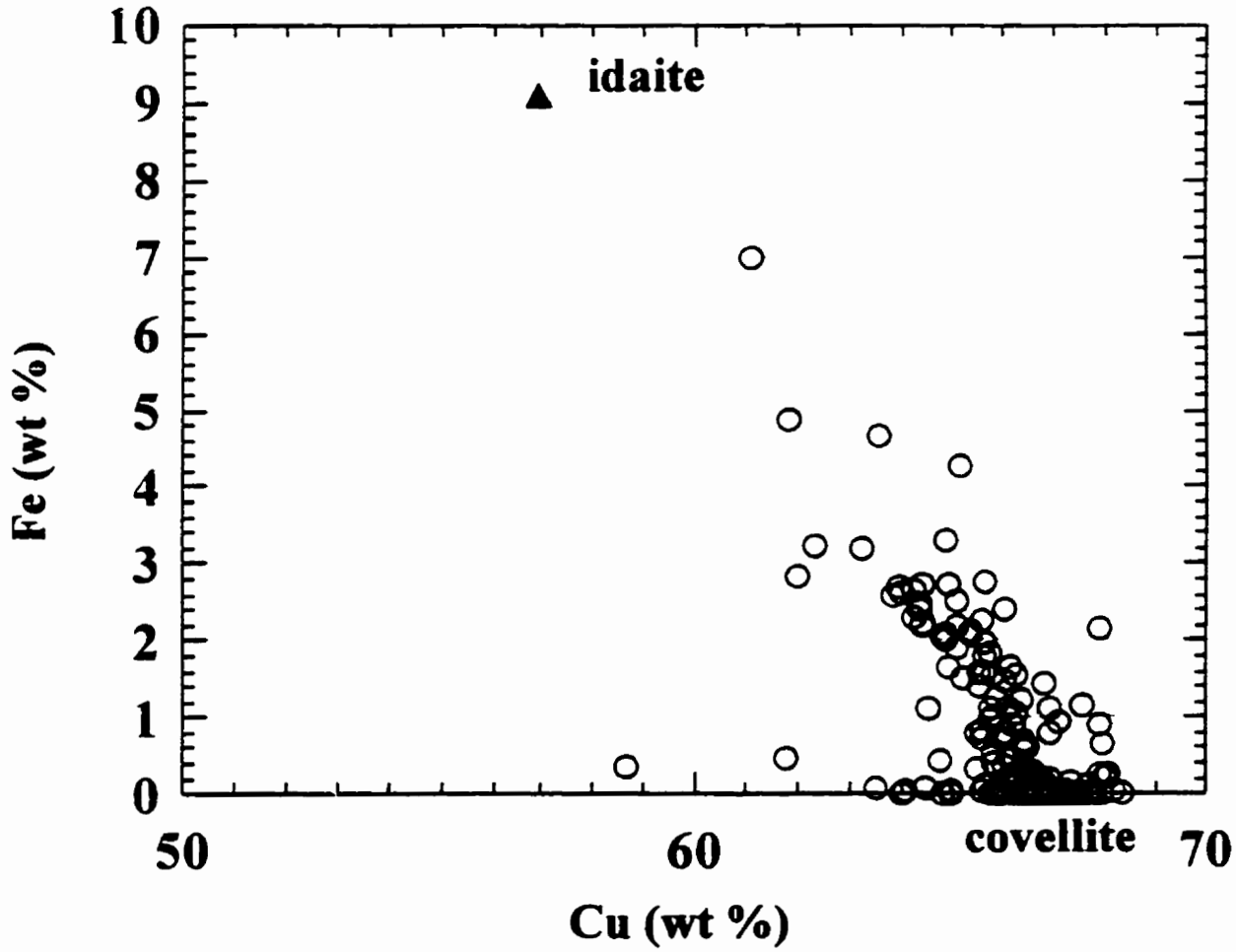

Figure 3.2. Cu-Fe-S diagram showing fields of covellite (open circles) and blue-remaining covellite (open squares) from Chuquicamata. Standard idaite is plotted as a solid triangle.

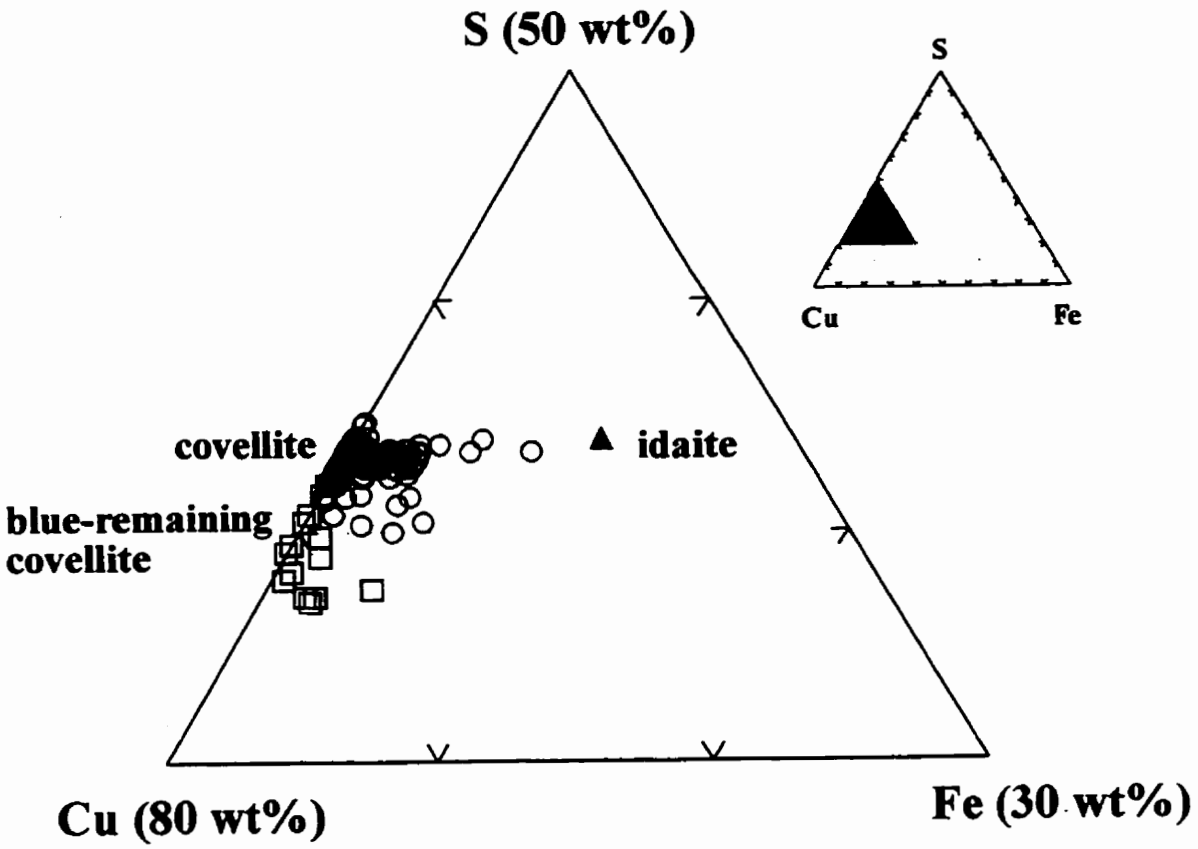

3.2.2 Anilite ($Cu_{1.75}S$)

Occurrence. Rarely identified from Chuquicamata, anilite occurs as individual grains or as small 'pods' in intimate intergrowths in massive digenite.

Diagnostic properties. Anilite from Chuquicamata has only been identified in polished section, where reflected light study shows it to be indistinguishable from digenite, varying from light blue to white-grey. All positive identifications of anilite from the samples studied here come from the electron microprobe. It is very likely that there is more of this mineral present than has been identified, and its rarity in Chuquicamata can probably be attributed to the difficulty in recognizing this phase.

Chemistry. As mentioned in Chapter 2, there is some confusion about the composition of anilite, with some sources quoting Cu_7S_5, which corresponds to $Cu_{1.4}S$ (the same composition as synthetic Cu-rich blaubleibender covellite), and other sources fixing the composition at $Cu_{1.75}S$. Anilites from Chuquicamata match the $Cu_{1.75}S$ composition, with copper content at 75.42 weight percent, but these may be copper-rich blaubleibender covellites and not anilites.

3.2.3 Digenite (Cu_9S_5)

Occurrence. Digenite is prevalent in Chuquicamata, where it occurs in three ways:

a. massive digenite, which may or may not be associated with acicular covellite and/or blocky to subrounded disseminated enargite, interstitial to other minerals, mainly silicates or pyrite aggregates;

b. disseminated grains of digenite with bornite in stable intergrowths, some from eutectic formation, some as exsolution products (this assemblage is found mainly in zones of potassic alteration; it is less common in quartz-sericite alteration, where the minerals may occur together in inclusions, interpreted as locked grains, in other sulphides); and

c. replacement digenite after other sulphides, particularly galena.

Diagnostic properties. In hand sample, digenite is metallic blue and lighter than covellite. In

reflected light, natural digenites show a dull blueish colour of moderate reflectivity. Some species may lose their blue colour more or less completely due to admixtures; the colour in this case turns greyish white. An octahedral cleavage is commonly visible, or the mineral may form an aggregate of blue to blue-white octahedral lamellae. Digenite may be, in some samples, optically indistinguishable from chalcocite (Cu_2S), unless the two occur together. In Chuquicamata, chalcocite plays a large role in the zone of supergene enrichment, where it is the most important copper mineral. The extent of chalcocite in the hypogene ore zones is unclear; judging from the 4500N section, it is rare in hypogene ore mineral assemblages. All of the copper-rich sulphide found in this study is considered too copper-deficient to be chalcocite (see Table 6, below). An X-ray diffractogram of a separate from sample cu192 shows that the phase in question can be structurally identified as digenite and not chalcocite (Appendix B).

Chemistry. Digenite can show extensive solid solution towards bornite at elevated temperatures, and even so-called 'pure' digenites commonly contain iron in excess of 1%. Figure 3.3 shows that samples of hypogene digenite from Chuquicamata plotted on a binary Fe vs.Cu diagram show, like the covellites, a continuous variation in iron content from 0 to 3 weight percent. A ternary Cu-Fe-S plot with standard bornite located on it shows that the same trend observed with covellite-idaite can be seen with digenite-bornite, as the digenites vary systematically with respect to iron content and appear to indicate crystallisation along the digenite-bornite tie line (Figure 3.4). High digenite is said to exhibit solid solution towards Cu_2S (Roseboom 1966), and although the cubic high digenite cell is not found below about 76^0, its compositional equivalent is preserved at lower temperatures. Digenites from Chuquicamata range from 74.53% Cu (about3.5% lower than standard digenites, both natural and synthetic), with significant iron, >2.5 weight %, to 79.60% copper (Table 6). Table 6 presents 3 representative samples of digenite from Chuquicamata, based mainly on mineral assemblages, with the maximum, minimum, calculated mean, and standard deviation based on the complete sample set, n, where n is the number of analyses for each element that are above the limit of quantification.

Figure 3.3. Cu vs Fe plot showing Fe content of digenites from Chuquicamata. Standard digenite contains 78.1 wt% Cu; standard chalcocite contains 79.9 wt% Cu.

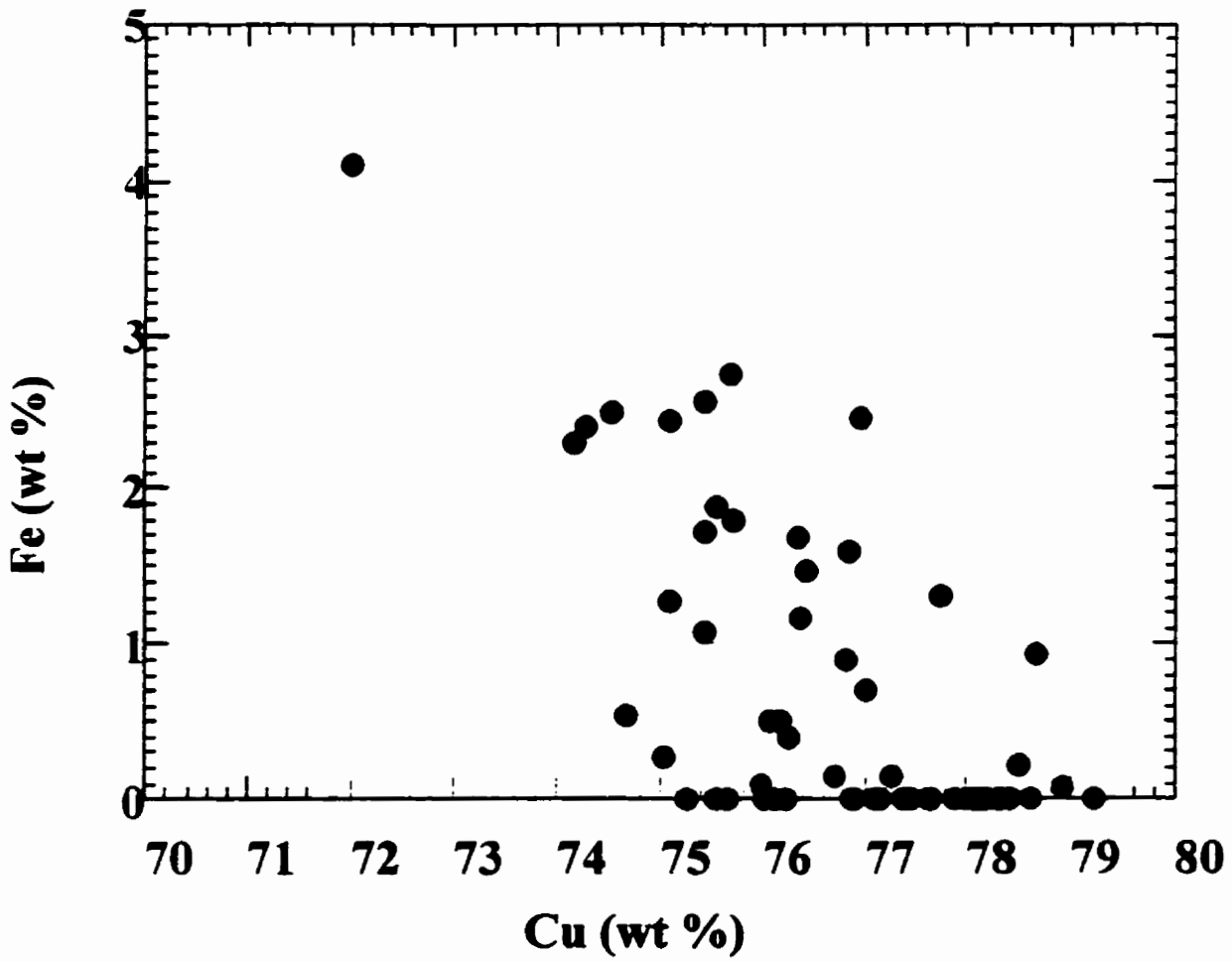

Figure 3.4. Cu-Fe-S plot showing digenties from Chuquicamata trending toward the standard bornite composition.

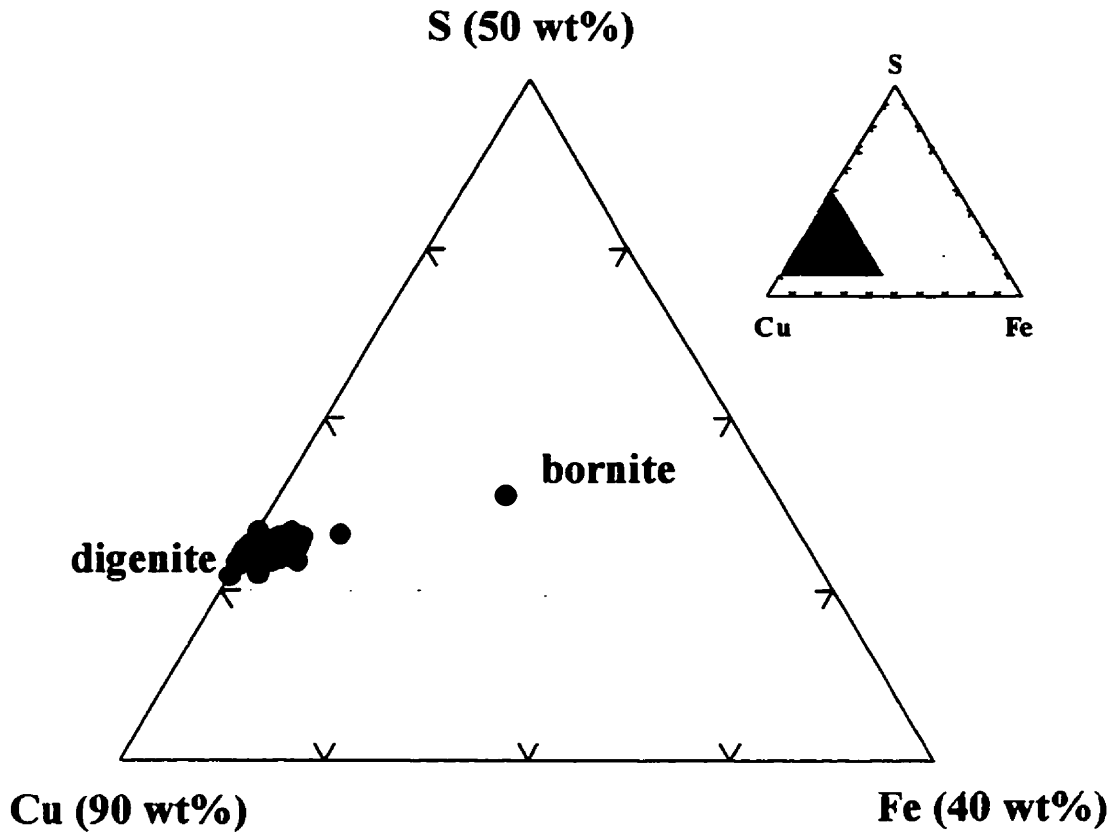

Table 6. Chemical composition (weight %) of digenite from Chuquicamata.

Sample	Cu	Fe	As	S	Total	assemblage
cu461b (30)	77.78			21.65	99.43	dg+cv+en+py
cu500B (82)	76.35	1.68		22.06	100.09	bn+dg
cu203B (20)	77.09		0.27	22.12	99.48	cov+dg
stoichiometric digenite	78.11			21.89	100.00	
stoichiometric chalcocite	79.86			20.14	100.00	
mean	76.98	1.38	0.37	22.02	99.66	
standard deviation	1.25	0.75	0.31	0.57	0.90	
maximum	79.60	2.74	1.40	23.51	102.08	
minimum	74.53	0.27	0.25	20.63	98.00	
# of analyses > LOQ	52	21	12	52	52	
detection limit (LOQ)	0.50	0.25	0.25	0.50		

3.2.4 Enargite ($Cu_3(As,Sb)S_4$)

Occurrence. In Chuquicamata, enargite occurs in two distinct assemblages:

a. in digenite + covellite, interstitial to pyrite aggregates or disseminated in gangue material, enargite is present locally in subhedral blocky to subrounded grains; and

b. veins of enargite + pyrite, where enargite occurs both in large blocky crystals and as massive anhedral intergrowths with pyrite, and fine-grained angular (wedge-shaped) crystals of enargite with angular pyrite, disseminated in sulphate veins. These veins are seen in the mid-to-shallow regions of the deposit and appear to be limited to zones of quartz-sericite alteration.

Diagnostic properties. Enargite has a submetallic lustre and is grey-black to black with a violet tint in hand sample. In reflected light enargite is pink-brown to light brown and shows moderate reflectivity. The reflected colour may be strongly influenced by accompanying minerals, and may be differently described according to adjacent phases. Reflection pleochroism is weak in air, but may be distinct along grain boundaries and is appreciably stronger in oil, grey cream to light rose-brown to violet-grey. Anisotropy is strong, with colours ranging from dark violet red to light

olive. Cleavage parallel to (110) is abundant and always visible in coarse-grained aggregates.

Chemistry. Enargites from Chuquicamata show a range from 0.40 to 4.32 weight % antimony substituting for arsenic. Several enargite-like minerals from one sample of quartz-sericite alteration range in antimony content from 8.50% to 11.66%, apparently at the expense of both arsenic and copper. (However, these samples have low totals, and are missing a component that makes up between 6 and 9 percent by weight of the composition; these samples are inferred tennantite-tetrahedrite series minerals). The arsenic content of the enargites ranges from about 16.05 to 18.99%, well within the range for standard enargites. Several samples from both quartz-sericite and potassic zones of alteration contain several percent zinc and/or iron. The samples that contain significant zinc show a range from 7.7 to 8.5% Zn, and a lower overall copper content (about 43%, whereas standard enargites have a copper content closer to 50%), suggesting that the zinc substitutes for copper in the unit cell; these samples are also probably sulfosalts from the tennantite-tetrahedrite series. Iron contents are low, 0 to <2. It is likely that the iron also substitutes for copper. Table 7 gives the chemical composition of enargite samples from Chuquicamata.

Table 7. Chemical composition (weight %) of enargite from Chuquicamata.

Sample	Cu	Fe	As	Sb	S	Total	assemblage
cu182B (57)	48.93		17.55	1.84	31.86	100.18	en+py
cu461B (32)	48.92		18.00	1.87	31.63	100.42	dg+cv+en+py
cu441 (94)	49.94		18.81		31.86	100.61	en+dg+cv+sph
stoichiometric enargite	48.41		19.02		32.57	100.00	
mean	49.37	1.22	18.09	1.40	32.14	100.62	
standard deviation	0.68	0.52	0.65	1.01	0.55	0.80	
maximum	50.54	1.64	18.99	4.32	33.02	101.95	
minimum	48.28	0.50	16.05	0.40	30.59	99.15	
# of analyses > LOQ	20	3	20	12	20	20	
detection limit (LOQ)	0.50	0.25	0.25	0.40	0.50		

3.2.5 Bornite (Cu_5FeS_4)

Occurrence. Bornite has several associations in Chuquicamata:

a. disseminated grains of bornite + digenite intergrowths, mainly from eutectic formation, although in some cases a cubic network is preserved, indicating exsolution on decomposition of high-temperature Cu_2S; the assemblage bornite + digenite is also found as subrounded to ovoid inclusions in pyrite, and is common interstitial to pyrite aggregates, where bornite >> digenite in zones of potassic alteration; and

b. stringers, veinlets and disseminated grains of bornite + chalcopyrite are common, mainly as equilibrium intergrowths, although there are cases where a film of chalcopyrite around bornite is clearly later---this relationship is also seen where bornite, interstitial to pyrite, contains narrow 'needles' of chalcopyrite, invading from a later chalcopyrite border around the bornite.

Diagnostic properties. Bornite is rose-brown in hand sample, similar to pyrrhotite when fresh, but tarnishes very quickly to copper-red, blue, and violet. In reflected light, bornite is light pinkish brown, of moderate reflectivity, one of the most readily recognised of the sulphides. The colour of a freshly-polished surface darkens quickly to red and then to violet-pink. Bornite may show a variable but weak anisotropy.

Chemistry. Bornites from Chuquicamata have iron contents ranging from 10.32 to 13.50%, the upper limit of which is approximately 2 percent higher than standard hypogene bornite. The excess iron in this case appears to substitute for copper. Table 8 gives the chemical composition of 3 representative samples of bornite from Chuquicamata. The calculated mean and standard deviation, as well as the maximum and minimum values, are taken from the sample set n, where n is the number of analyses for each element that are above the limit of quantification.

Table 8. Chemical composition (weight %) of bornite from Chuquicamata.

Sample	Cu	Fe	S	Total	assemblage
cu467B (61)	62.68	11.27	25.13	99.08	bn+cpy+dg-cv
cu476B (65)	62.71	11.49	25.72	99.92	bn+dg
cu467B (49)	62.46	11.69	25.30	99.45	sph+bn+cpy
stoichiometric bornite	63.32	11.13	25.55	100.00	
mean	62.41	11.61	25.48	99.50	
standard deviation	1.06	0.70	0.38	0.88	
maximum	64.94	13.50	26.37	101.46	
minimum	60.47	10.32	24.55	97.81	
# of analyses > LOQ	36	36	36	36	
detection limit (LOQ)	0.50	0.25	0.50		

Although the composition of anomalous bornites are generally defined by a slight excess of sulphur combined with a decreased copper content over regular bornites, several samples from Chuquicamata which may fit the description of anomalous bornite contain about the same amount of sulphur as regular hypogene bornites (i.e. 25-26.5 weight percent). However, as seen in Table 9, these samples are characterised by an increased iron content, in the range of 12-13.5%, and a lower copper content (60-61.6%) than regular bornite.

Table 9. Electron microprobe analyses of possible anomalous bornites, Chuquicamata, 4500N

Sample	Wt.% Cu	Wt.% Fe	Wt.% S	Total	Location
Cu5FeS4 (standard hypogene bornite)	63.33	11.12	25.55	100.00	
Anomalous bornite (von Gehlen, 1964)	61.5	11.5	26.5	99.5	Sommerkahl (Spessart)
Cu503 possible anomalous bornite?	60.69	13.50	25.30	99.49	DD2234, 253.27m
Cu503 possible anomalous bornite?	61.93	12.17	25.36	99.46	DD2234, 253.27m
Cu482 possible anomalous bornite?	61.66	12.36	25.53	99.54	DD2234, 297.53m
Cu482 possible anomalous bornite?	60.79	13.06	25.32	99.17	DD2234, 297.53m

3.2.6 Chalcopyrite ($CuFeS_2$)

Occurrence. Chalcopyrite is found throughout the system and occurs in several ways:

a. narrow veins and stringers of massive chalcopyrite, usually at least partially replaced by massive covellite, where covellite lamellae are arranged in loose lattices after the chalcopyrite, and massive chalcopyrite interstitial to silicate minerals (this is mainly restricted to zones of potassic alteration); and

b. disseminated anhedral to subhedral grains of chalcopyrite + bornite intergrowths, and veinlets of the same assemblage, which occurs in both zones but dominantly in the potassic.

Diagnostic properties. Chalcopyrite is metallic yellow in hand sample, and may show a somewhat greenish-yellow hue in contact with pyrite. In reflected light, chalcopyrite is light yellow and has a high lustre. In time, chalcopyrite in polished sections will turn a dark yellow golden colour in a uniform or spotty manner. Reflection pleochroism is rare, but in some instances lamellar structure of chalcopyrite grains can be recognised due to pleochroic effects. Anisotropy is weak but usually recognizable under oil.

Chemistry. Chalcopyrite from Chuquicamata does not deviate significantly from the ideal composition (Table 10).

Table 10. Chemical composition (weight %) of chalcopyrite from Chuquicamata.

Sample	Cu	Fe	S	Total	assemblage
cu454B (75)	35.00	30.53	34.72	100.25	cv+cpy
cu467B (50)	36.17	29.58	34.34	100.09	sph+bn+cpy
cu494 (24)	35.30	29.87	34.56	99.73	cpy+bn+dg+cv
stoichiometric chalcopyrite	34.63	30.43	34.94	100.00	
mean	34.90	30.45	34.85	100.20	
standard deviation	0.79	0.48	0.42	1.10	
maximum	36.17	31.26	35.51	101.75	
minimum	33.41	29.58	34.29	98.25	
# of analyses > LOQ	14	14	14	14	
detection limit (LOQ)	0.50	0.25	0.50		

3.2.7 Sphalerite (ZnS)

Occurrence. Although sphalerite may be difficult to spot in hand specimen as a result of the (generally) small grain size in samples from Chuquicamata, it occurs in many assemblages. In general, the addition of sphalerite to any of the assemblages described below is as a later phase (possibly the latest, as in the case of possible supergene sphalerite described in section 3.3.4), though some notable exceptions do exist:

a. massive sphalerite, composed of a 'welded' aggregate of fine-grained euhedral to subhedral sphalerite crystals, where remnant grain boundaries are still visible; in some samples the massive sphalerite is interstitial to aggregates of subrounded pyrite grains +/- other sulphide minerals; and

b. skeletal sphalerite within digenite + covellite, interstitial to pyrite aggregates; sphalerite looks like a strange intergrowth---possibly the digenite + covellite is a result of the unmixing of mineral A, where the high-temperature assemblage was mineral A + sphalerite, but more likely the sphalerite is earlier.

Diagnostic properties. Sphalerite can be resinous, white to completely black, green or reddish, but most often brown, or metallic in hand sample. In reflected light, sphalerite is light grey with a very delicate blue or brownish tint, depending on mineral associations and intensity of illumination. It has a very low reflectivity, and usually has numerous internal reflections, ranging from white in the iron-poor sphalerites, to yellow, light brown and dark brown.

Chemistry. The bulk of the sphalerite samples analyzed from Chuquicamata fall within the standard ZnS range, with zinc contents around 67 weight percent. A few samples show decreased zinc contents (around 65%), but these same samples contain copper up to 4.5%, which apparently substitutes for zinc in the sphalerite structure. Analyses from samples of possible supergene sphalerite (Section 3.3.4) contain between 4.68 and 10.02 percent copper by weight, whereas the zinc content of these samples is as low as 60 percent. These very high copper content of these samples may be due to microbeam inaccuracies, or the samples may represent an intermediate phase in the replacement of copper-sulphides by sphalerite. Figure 3.5, a binary plot of Cu vs. Zn shows a more or less linear relationship, suggesting that copper substitutes for zinc in the low-

temperature environment. The iron content of Chuquicamata sphalerites varies from 0 to almost 1 percent by weight. There is no clear relationship to the zinc and copper contents, but in general the samples containing more iron are the possible supergene sphalerites, at the lower limit of the zinc range. Table 11 presents 3 representative sphalerite samples from the sample set n, where n is the number of analyses for each element that are above the limit of quantification.

Table 11. Chemical composition (weight %) of sphalerite from Chuquicamata.

Sample	Zn	Cu	Fe	S	Total	assemblage
cu467B (55)	68.33			32.54	100.87	sph(massive)+bn+dg+ga
cu203A (30)	65.40	1.35		32.58	99.33	cv+sph+dg
cu501 (25)	67.36			33.42	100.78	bn+cpy+dg+sph
stoichiometric sphalerite	66.41			33.59	100.00	
mean	67.66	0.96	0.63	32.76	100.99	
standard deviation	1.39	0.38	0.27	0.43	0.87	
maximum	69.33	1.58	0.90	33.64	101.82	
minimum	62.98	0.58	0.36	32.22	99.33	
# of analyses > LOQ	15	8	2	15	15	
detection limit (LOQ)	0.80	0.50	0.25	0.50		

3.2.8 Pyrite (FeS_2)

Occurrence. Pyrite is ubiquitous in Chuquicamata samples, and was likely formed throughout the mineralising history. Successive stages of pyrite precipitation are even found within the same 'grain'. Pyrite mainly occurs as aggregates of coarse- to fine-grained sub- to euhedral crystals, either welded together (where grain boundaries may still be visible) or cemented with: massive chalcopyrite, digenite + covellite, bornite +/- digenite, massive covellite, or massive sphalerite. The occurrence of veins of pyrite + enargite intergrowths are also noted, as well as fine-grained cubic pyrite crystals disseminated throughout many samples.

Figure 3.5. Zn vs Cu plot showing variation in sphalerite compositions from Chuquicamata. Standard sphalerite is plotted as a solid circle.

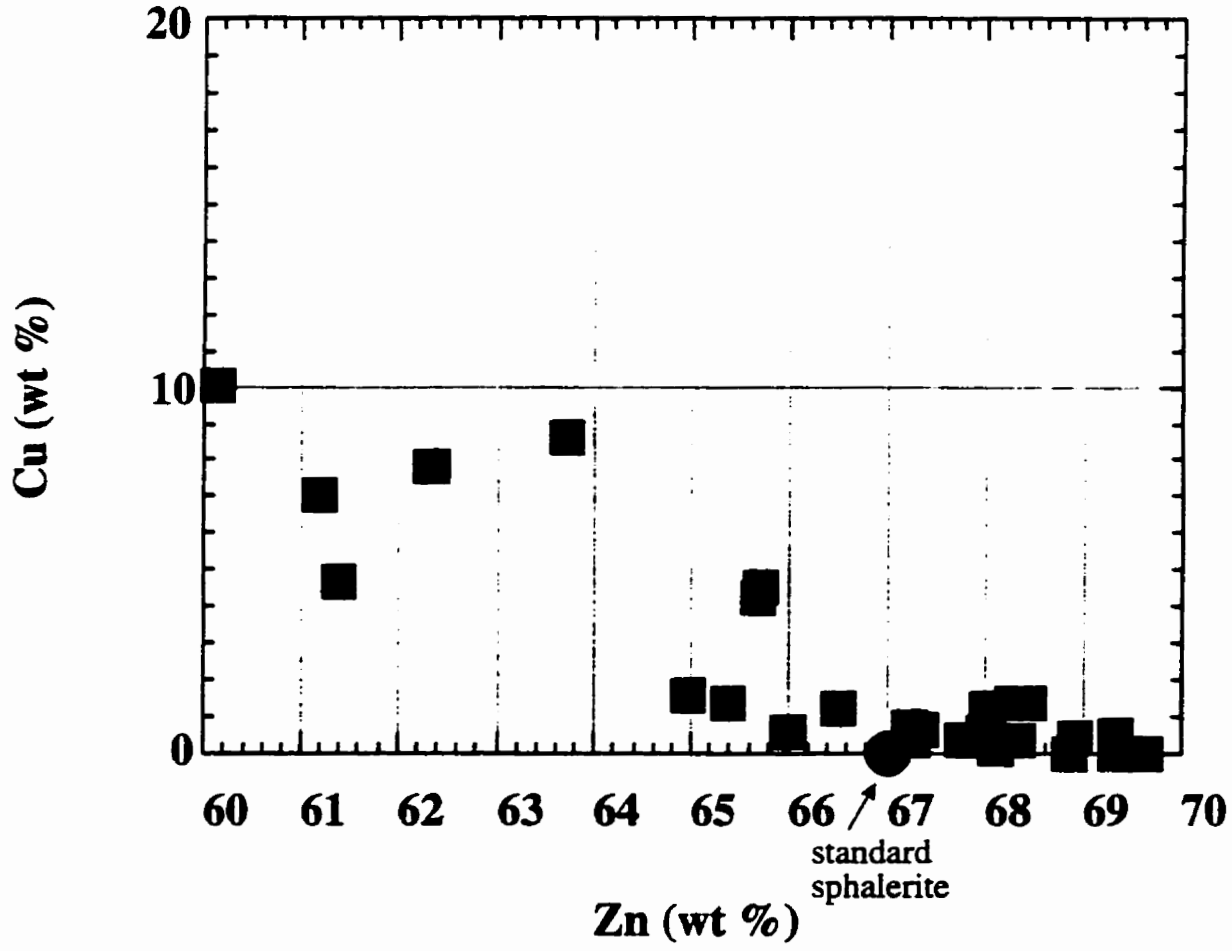

Diagnostic properties. Pyrite is light brass-yellow with a highly metallic lustre in hand sample. Reflectivity of pyrite is very high, exceeded only by some of the native metals and a few rare ore minerals. In reflected light pyrite is very light yellow, and in the majority of cases anisotropic effects are not observed.

Chemistry. Pyrites from Chuquicamata deviate little from the ideal composition. Two groups of pyrite can be defined on the basis of their trace elements, specifically arsenic. Whereas some pyrite samples are arsenic-free, those that do contain trace amounts have arsenic contents that fall within a very small range, between 0.20 and 0.34 weight percent. In general, samples that contain arsenic also carry trace gold, up to 0.50 weight percent. Table 12 gives the chemical composition of pyrite from Chuquicamata.

Table 12. Chemical composition (weight %) of pyrite from Chuquicamata.

Sample	Cu	As	Fe	S	Total	assemblage
cu182B (59)		0.34	46.45	53.56	100.35	en+py
cu489 (96)			47.15	53.79	100.94	py+dg
cu482 (36)			47.59	53.78	101.37	cpy+py+cv
stoichiometric pyrite			46.55	53.45	100.00	
mean	0.61	0.33	46.88	53.75	100.85	
standard deviation	0.08	0.02	0.37	0.29	0.46	
maximum	0.69	0.34	47.59	54.17	101.79	
minimum	0.54	0.29	46.14	53.12	99.92	
# of analyses > LOQ	2	7	16	16	16	
detection limit (LOQ)	0.50	0.25	0.25	0.50		

3.2.9 Molybdenite (MoS_2)

Occurrence. Veins of molybdenite in quartz and sulphate (the 'blue veins', found in the 4500N section only in zones of quartz-sericite alteration) are easily recognizable in hand specimen. Minor molybdenite is associated with several other assemblages:

a. aggregates of very fine-grained curved tabular strands of molybdenite, either replacing or overprinting other sulphides, such as covellite or bornite (+/- chalcopyrite) (this association is found in both major zones of alteration); and

b. fine-grained molybdenite in curved tabular form and spindles growing with digenite + covellite, interstitial to pyrite aggregates; the lack of molybdenite-digenite and molybdenite-covellite intergrowths may suggest that an assemblage of molybdenite + mineral B broke down to form molybdenite + digenite + covellite.

Diagnostic properties. Molybdenite is light silver-grey and flaky in hand sample, with a highly metallic lustre. In reflected light molybdenite is generally pure white and possesses a high reflectivity. The reflection pleochroism, from grey-white to white to slate-blue, is very high, exceeded only by a few minerals. Effects of anisotropism are also very high, with colours ranging from white with a pink tint to deep ink-blue, very visible with the characteristic undulatory extinction of bent leaves of molybdenite.

Chemistry. Molybdenite analyzed from Chuquicamata, both from the 'blue veins' and disseminated molybdenite in other hypogene assemblages, is more or less stoichiometric MoS_2. Copper is a minor component of most of the samples (< 1 weight percent).

3.2.10 Wolframite ($(Fe,Mn)WO_4$)

Occurrence. Its grain size in Chuquicamata samples make it unidentifiable in hand specimen, and although it is not common, wolframite occurs in one of two forms in the same basic assemblage :

a. rounded masses of wolframite, full of holes and inclusions of pyrite and covellite, in contact with pyrite + digenite + covellite, in quartz-sericite-associated assemblages; and

b. fine-grained (locally curved) tabular to wedge-shaped grains of wolframite in digenite + covellite, interstitial to pyrite aggregates or disseminated in silicates.

Diagnostic properties. Wolframite is black to blackish brown in hand sample, with a greasy,

submetallic lustre. The reflectivity of wolframite is quite low, approximately that of sphalerite, and the colour effect varies in reflected light according to the accompanying minerals, grey to greyish-white to brown. Anisotropic effects are weak but distinct, possibly varying with chemical composition. Brownish-red to blood-red internal reflections are almost always visible in oil, but rarely in air.

Chemistry. All of the wolframites in Chuquicamata tend towards the hubnerite variety, with manganese contents varying from 11.94 to 15.22 weight percent. A few samples are pure hubnerites, but most contain minor iron, ranging from 0.65 to 3.88 percent. Copper contents in the wolframites range continuously from 0 to 1.84 weight percent.

3.2.11 Colusite $Cu_{26}V_2As_4Sn_2S_{32}$ or (approximately) $Cu_3(As,Sn,V)S_4$

Occurrence. Although there is not very much of it in Chuquicamata, colusite does occur, either as part of the digenite-covellite-enargite assemblage where it is found as individual grains separated by digenite-covellite intergrowths, or as very fine round inclusions in massive digenite (+ covellite).

Diagnostic properties. Colusite occurs in tetrahedral bronze-brown crystals in hand sample. In reflected light colusite appears coppery-cream coloured to creamy-tan, of moderate reflectivity. It is completely isotropic, and cleavage is not observed, although zonal textures are common, visible by differences in colour shade and polishing hardness.

Chemistry. As can be seen from Table 13, colusites from Chuquicamata comprise at least three distinct groups, differentiated on the basis of major elements tin and arsenic, and minor elements zinc, vanadium, and iron. There is a clear distinction between those samples that contain zinc and those that do not. Tin is a trace to major element; samples that contain zinc also contain tin as a major element, making up 12.51 to 20.36 percent. A distinction is also made between samples that contain zero to trace amounts of iron and those with significant iron content, up to 12.00 percent. These samples contain little or no arsenic. Samples with high arsenic (up to 16.71%) are

Table 13. Chemical composition (weight %) of colusite from Chuquicamata.

Sample	Zn	Cu	Fe	As	S	Sn	Sb	V	Total	assem.
cu481A (101)		45.04	12.00		29.44	14.80			101.28	cv+dg+col
cu467A (22)		52.30		10.64	31.89		0.74	3.30	98.87	dg+col
cu489 (98)	4.15	44.89		2.06	28.85	16.51	1.93		98.39	dg+cv+col
mean	3.56	47.70	4.01	6.74	30.23	14.57	1.64	2.91	99.05	
standard deviation	1.56	4.81	4.21	4.82	1.44	4.55	0.77	0.40	1.04	
maximum	6.29	59.31	12.00	16.71	32.98	20.36	2.85	3.30	101.44	
minimum	1.24	39.82	0.61	0.26	28.52	4.42	0.46	2.16	97.73	
# of analyses> LOQ	9	18	9	17	18	11	9	7	18	
detection limit (LOQ)	0.50	0.25	0.25	0.40	0.50	0.50	0.40	0.20		

also those that contain measurable vanadium. All samples fall into either a high-arsenic or a high-tin category; the high-arsenic samples contain no zinc and trace iron. The high tin content samples can be further subdivided between those that contain zinc and/or significant iron, those that contain zinc and trace iron, and those without zinc. While it is clear that arsenic and tin substitute for each other, it is also apparent that samples containing zinc and significant iron do so at the expense of copper.

3.2.12 Idaite $Cu_{5.5}FeS_{6.5}$

Occurrence. Idaite occurs as 'streaks' or curved tabular 'grains' interfingered with similar-looking grains of covellite disseminated in silicate gangue in zones of potassic alteration. It also occurs as rounded but irregular-shaped grains which may or may not be associated with covellite, rimmed by irregular and angular chalcopyrite.

Diagnostic properties. Both macro- and microscopically, idaite resembles bornite with a copper-reddish colour and metallic lustre. Idaite is of moderate reflectivity, and reflection pleochroism is high, from red-orange to almost brown. Anisotropic effects are enormous, with sharp extinction and a yellowish-green colour at the 45° position.

Chemistry. All of the idaites found at Chuquicamata have a composition very close to $Cu_{5.5}FeS_{6.5}$. Copper contents fall within a limited range, from 57.20 to 58.97 weight percent. The iron content ranges from 8.11 to 11.35 percent. Most of the samples contain trace tungsten, up to 0.47%, and at least one sample of idaite contains trace arsenic. Table 14 gives the chemical composition of idaite from Chuquicamata. Three representative samples of idaite are presented from 2 samples; the mean and standard deviation are calculated from the complete sample set (number of analyses for each element that are above the limit of quantification.

Table 14. Chemical composition (weight %) of idaite from Chuquicamata.

Sample	Cu	Fe	S	Total	assemblage
cu450 (3)	57.20	9.71	34.71	101.62	cv+id+dg+bn
cu465 (57)	57.41	11.35	29.42	98.18	cpy+bn+dg+id
cu465 (65)	58.05	9.38	34.21	101.64	cpy+cv+id
stoichiometric idaite	56.14	9.87	33.99	100.00	
mean	57.91	9.73	33.55	101.20	
standard deviation	0.63	0.85	1.86	1.35	
maximum	58.97	11.35	34.71	101.95	
minimum	57.20	8.69	29.42	98.19	
# of analyses > LOQ	6	6	6	6	
detection limit (LOQ)	0.50	0.25	0.50		

3.3 Mineral Groupings/ Assemblages

For ease of reference, each assemblage described below has been given a number code, where the first number classes the assemblage by its dominant phases (for example, all of the 100 number assemblages are dominated by covellite(-digenite), all of the 400 number assemblages are dominated by chalcopyrite, etc). The assemblages have been described from a purely textural point of view, and paragenetic interpretations have been made based on the textures.

In most assemblages, pyrite is the first phase formed, evidenced by the euhedral to subrounded grains (where most other phases are in a massive/anhedral form) common to almost every sample studied, with other sulphides filling spaces between pyrite grains, surrounding the pyrite, and/or filling cracks or fractures in pyrite grains. In the common assemblage pyrite + digenite + covellite, pyrite is clearly the earliest phase, often in fine euhedral grains surrounded by massive digenite-covellite intergrowths (cu195). Covellite, occurring here as fine needles distributed throughout the digenite, is probably an equilibrium assemblage with the digenite (possible exsolution?).

There has obviously been, however, more than one pulse of pyrite precipitation. In some

Table 15. DISTRIBUTION OF ORE MINERAL ASSEMBLAGES AT CHUQUICAMATA, SECTION 4500N
mineral names as column headings denote mineral(s) dominating a given group of assemblages

DRILL HOLE	SAMPLE	DEPTH (m)	ALTERATION	covellite(-digenite)	digenite(-bornite)	chalcopyrite	sphalerite	molybdenite	other pyrite	iron oxide
DDH 2967	cu214	211.60	quartz-sericite	100, 102, 101						
DDH 2967	cu182	224.76	quartz-sericite	102					200	
DDH 2967	cu183	225.10	quartz-sericite							
DDH 2967	cu184	233.04	quartz-sericite	101, 102					200, 201	
DDH 2967	cu185	234.45	quartz-sericite	100, 102				800		
DDH 2967	cu187	316.26	quartz-sericite			400			202	
DDH 2967	cu189	324.69	quartz-sericite		300, 304	400				
DDH 2967	cu190	325.20	quartz-sericite		300, 304, 303, 305					
DDH 2967	cu192	325.93	quartz-sericite		300, 303		600, 601			
DDH 2967	cu193	408.00	quartz-sericite	103	300					
DDH 2967	cu195	413.77	quartz-sericite	103	304					
DDH 2967	cu210	455.90	quartz-sericite	103	304					
DDH 2967	cu211	456.40	quartz-sericite	101, 103	305		600			
DDH 2967	cu204	513.05	quartz-sericite	103, 105	304					
DDH 2967	cu205	514.90	quartz-sericite	103, 105, 104	304					
DDH 2967	cu206	518.65	quartz-sericite	106	304	400			202	
DDH 2967	cu199	569.42	quartz-sericite	101, 103, 106					202	
DDH 2967	cu200	574.23	quartz-sericite	101, 103	305	400, 401				
DDH 2967	cu201	574.87	quartz-sericite	103, 105			600	800		
DDH 2967	cu202	575.14	quartz-sericite	103, 106?	304, 300					
DDH 2967	cu203	576.98	quartz-sericite	106		400?				
DDH 2967	cu207	605.70	quartz-sericite		304				202	
DDH 2967	cu208	607.97	quartz-sericite	101		401			202	
DDH 2967	cu181	671.50	quartz-sericite							

Table 15. DISTRIBUTION OF ORE MINERAL ASSEMBLAGES AT CHUQUICAMATA, SECTION 4500N
mineral names as column headings denote mineral(s) dominating a given group of assemblages

DRILL HOLE	SAMPLE	DEPTH (m)	ALTERATION	covellite(-digenite)	digenite(-bornite)	chalcopyrite	sphalerite	molybdenite	other pyrite	iron oxide
DDH 2234	cu504	107.86	QS over K?			406			202	
DDH 2234	cu507	113.65	potassic				700			
DDH 2234	cu508	114.71	potassic			407, 400			200	
DDH 2234	cu509	115.80	potassic				701, 700			
DDH 2234	cu493	216.30	potassic		304	400, 409, 410				
DDH 2234	cu494	219.84	QS over K??			401, 407, 409, 410				
DDH 2234	cu495	221.49	potassic			405			202	
DDH 2234	cu496	244.40	potassic			409, 401				
DDH 2234	cu499	249.15	QS over K?	103	304	409		800		
DDH 2234	cu500	250.00	potassic		304, 301	407		800		
DDH 2234	cu501	250.70	potassic	100, 103		411, 401				
DDH 2234	cu503	253.27	potassic	100		411, 405		800		
DDH 2234	cu479	294.20	potassic	100	300	409			202	
DDH 2234	cu480	295.55	QS over K?	103, 104	304	401				
DDH 2234	cu481	295.98	QS over K?	103, 106	304					
DDH 2234	cu482	297.53	potassic	103		405, 407				
DDH 2234	cu487	301.95	potassic		305	401				
DDH 2234	cu488	302.69	potassic			400			202, 201	
DDH 2234	cu489	305.73	QS over K?	108	304	407				
DDH 2234	cu491	306.79	potassic		304	402				
DDH 2234	cu490	307.95	potassic			402		800		

Table 15. DISTRIBUTION OF ORE MINERAL ASSEMBLAGES AT CHUQUICAMATA, SECTION 4500N
mineral names as column headings denote mineral(s) dominating a given group of assemblages

DRILL HOLE	SAMPLE	DEPTH (m)	ALTERATION	covellite(-digenite)	digenite(-bornite)	chalcopyrite	sphalerite	molybdenite	other pyrite	iron oxide
DDH 2242	cu431	38.55	quartz-sericite			405, 404				
DDH 2242	cu433	56.45	quartz-sericite	101, 103				800		
DDH 2242	cu434	95.86	quartz-sericite	103, 106				800		
DDH 2242	cu435	103.07	quartz-sericite	100, 103	304, 300			800		
DDH 2242	cu436	103.83	quartz-sericite	101, 106	300					
DDH 2242	cu438	139.15	potassic			401, 407				
DDH 2242	cu440	142.13	potassic			408, 406, 401				
DDH 2242	cu441	145.32	fault gouge	103, 106				800		
DDH 2242	cu442	149.60	potassic			400, 401, 406				
DDH 2242	cu443	151.38	potassic		301	409, 401, 406	602	800		
DDH 2242	cu445	153.63	QS over k?	103, 106						
DDH 2242	cu446	156.77	potassic			408				
DDH 2242	cu447	160.80	QS over K?	103		404, 407				
DDH 2242	cu448	161.00	QS over K?	103				800		
DDH 2242	cu449	161.41	potassic	103	304	404	600			
DDH 2242	cu450	161.98	potassic			402, 407				
DDH 2242	cu451	164.98	potassic			402		800		
DDH 2242	cu452	189.86	potassic		303	400, 407, 406				
DDH 2242	cu453	193.10	potassic		303	401, 407		800		
DDH 2242	cu454	193.78	potassic		302	401, 404, 402, 407		800		
DDH 2242	cu455	193.86	potassic			408				
DDH 2242	cu456	194.20	potassic		303	401, 402				
DDH 2242	cu460	200.75	potassic			409, 401				900
DDH 2242	cu461	202.52	QS over K?	104, 106	300, 302			800		
DDH 2242	cu464	258.45	potassic	103		402	600			
DDH 2242	cu465	260.14	potassic			406, 404				
DDH 2242	cu467	261.27	QS over K?			407, 403	700			
DDH 2242	cu468	263.23	QS over K?	108			602, 603			
DDH 2242	cu475	282.04	potassic			400, 409				900
DDH 2242	cu473	284.39	potassic	103	300	401	600			
DDH 2242	cu474	286.75	QS over K?			404, 401				
DDH 2242	cu476	288.10	QS over K??	1.01E+02		401, 406				
DDH 2242	cu477	288.65	potassic			400, 409, 401	700			
DDH 2242	cu478	288.95	potassic			401, 404	600			900

cases (cu489), coarse-grained subrounded pyrites are marked with 'inclusion trails' of teardrop-shaped digenite, outlining a grain shape in the pyrite. This assemblage is interpreted as the formation of pyrite grains followed by a lapse in pyrite precipitation. During this lapse, digenite was precipitated and surrounded the earlier pyrite grains. A subsequent period of pyrite formation then surrounded the digenite and conformed to the earlier pyrite grain shape, squeezing the digenite into separate inclusions, leaving a pyrite core, an inner rim of digenite inclusions, and an outer rim of later pyrite. Other evidence of more than one period of pyrite formation comes from looking at samples from the two main alteration zones. In the zone of potassic alteration, pyrite aggregates are commonly surrounded by digenite-bornite intergrowths (cu490), where the digenite and bornite may show smooth intergrowths or the cubic network pattern suggesting exsolution (either way, it is interpreted as an equilibrium assemblage). In quartz-sericite alteration, pyrite is always surrounded by the digenite-covellite assemblage, and is the earlier phase. However, it is not necessarily the earliest one, as some euhedral pyrite grains in the zone of quartz-sericite alteration contain fine round to ovoid inclusions of the assemblage digenite + bornite (cu205), interpreted as locked grains and, therefore, representing an assemblage of phases earlier than the pyrite. Figure 3.6 is an excellent example.

Table 15 details the distribution of the coded assemblages according to sample number. The codes were chosen arbitrarily and do not have genetic (temporal) implications, except where the assemblage paragenesis is described (Section 3.5), when one sulphide mineral 'assemblage' is referred to as having formed later than another 'assemblage'. Conclusions of parageneis are based only on direct observation in this chapter, and Chapter 4 discusses temperature limits imposed by some of the sulphide assemblages. For instance, in sample cu205 described above, the *assemblage* covellite + digenite +/- pyrite (where pyrite, when it is present, is the first phase formed of the three, described as code 103) is interpreted to have formed later than the *assemblage* digenite + bornite (described as code 303). In general, the 100 and 200 code numbers are the sulphide assemblages that are characteristic of quartz-sericite alteration, whereas the higher-coded assemblages are characteristic of potassic alteration. Many of the assemblages described can be considered subsets of a few main assemblages (e.g., digenite + covellite + wolframite and digenite + covellite + enargite are variations of the same basic assemblage, probably changing through time

as a function of temeprature and composition of the ore fluids), but they are separated here for easier comprehension.

3.3.1 Covellite (-Digenite) Assemblages

100 covellite

Disseminated grains of covellite, in fine-grained columnar form (sample cu454) and semi-massive anhedral masses interstitial to euhedral silicate minerals (sample cu205) are commonly associated with disseminated to veinlet sulphate, mainly anhydrite (Figure 3.7a). Narrow stringers of covellite undulate and pinch and swell in silicate gangue (sample cu480).

101 covellite + pyrite

One example of this is in sample cu184, where a fused aggregate consisting of fine- to medium-grained subrounded to rounded pyrite grains contains interstitial massive covellite; a very fine film of covellite runs along the edges of individual pyrite grains in the aggregate, and covellite fills tension fractures in pyrite grains.

The same assemblage with a slightly different appearance is seen in sample cu476, where a narrow veinlet of pyrite in irregular globular texture encloses covellite--in this way, covellite may appear to be earlier than pyrite, but upon close inspection, minor grain boundaries are still apparent between fine rounded pyrite grains. It seems most likely then that the pyrite vein is enclosing remnant interstitial covellite.

102 covellite + pyrite + enargite

Sample cu185 contains mini-aggregates of 3+ grains of medium-grained pyrite adjacent to subrounded fine-grained covellite, with blocky tabular grains of enargite.

Figure 3.6. Sample cu205. DDH 2967, 514.90m. Reflected light photograph of a euhedral pyrite grain surrounded by massive digenite-covellite, where covellite (dark blue) occurs in an acicular form in the digenite (light blue). The pyrite (yellow) contains very fine round to ovoid inclusions of bornite and bornite-digenite intergrowths. Scale bar 0.09mm.

In sample cu214 a completely different texture is in the form of a vein of minor subrounded pyrite remnants and fine-grained subrounded to blocky enargite grains surrounded by a thick blanket of covellite, where the edges of enargite grains are partially dissolved; there are several occurrences here of blue-remaining covellite (Figure 3.7b). This texture, of massive to wide, almost banded, veins of covellite completely enveloping earlier minerals, partially dissolving and replacing some, such as enargite, and simply flooding others that are more resistant, such as pyrite, is interpreted as supergene enrichment of pre-existing sulphides by low-temperature covellite.

103 pyrite + digenite + covellite

Sample cu199 is a typical example of this common assemblage, where disseminated grains of pyrite and welded aggregates of fine-grained subrounded pyrite are disseminated throughout silicate gangue and in narrow veinlets and stringers. Some areas show disseminated 'groupings' of pyrite aggregates with a globular texture, while others have minor interstitial covellite +/- digenite. Many pyrite grains contain very fine-grained rounded to ovoid inclusions of covellite and/or digenite, probably not locked grains.

In sample cu210, sulphides in veins consist mainly of pyrite + digenite + covellite, with digenite and covellite filling spaces between massive elongate irregular pyrite masses (1-2 mm). The digenite-covellite assemblage fills spaces to varying degrees; in some veins, there are almost equal amounts of pyrite and digenite-covellite, with spaces between pyrite masses filled by massive-textured digenite with abundant 'strokes' and radiating spindles of covellite, very concentrated along edges of digenite. Abundant tabular strokes of covellite are distributed throughout the massive digenite. Sulphides are bordered by (and spaces in digenite-covellite filling are filled by) sulphates; where the sulphides thin out, sulphates continue in a narrow vein, 0.5 mm in width. In other veins, semi-massive to massive rounded elongate pyrite masses are in contact with very minor amounts of covellite + digenite in small patches. No sulphate is associated with these veins. Other than the veins, there are abundant grains of disseminated pyrite, subrounded elongate to irregular, average size 0.2 mm, +/- surrounded by or in contact with angular digenite (+covellite).

In general, as described above, this assemblage consists of early-formed euhedral to sub-rounded pyrite grains surrounded by later equilibrium digenite-covellite, where covellite occurs as fine needles disseminated in digenite. Covellite and digenite also occur together when variably-sized interlocking lamellar crystals of covellite replace grains of massive digenite (sample cu476).

104 pyrite + digenite + covellite + enargite

The most common form of this assemblage is coarse-grained subrounded to subangular pyrite with interstitial digenite + covellite + enargite, where the enargite is massive-textured and smooth, no visible grain boundaries are apparent, just angular and irregular-shaped enargite in contact with digenite + covellite, where covellite occurs as narrow needles in digenite (e.g., sample cu205).

The other type of this assemblage (e.g., sample cu461) shows aggregates of small subrounded pyrite grains with massive interstitial covellite and digenite (very minor digenite compared to covellite, where covellite may even have replaced digenite, covellite occurs in an interlocking mass of very fine needles) and enargite, where the enargite occurs as discrete small blocky to subrounded grains in the covellite (-digenite).

Where enargite occurs with digenite and covellite, it appears to be the earlier phase (after pyrite?). It occurs as coarse to fine blocky grains partly surrounded by (where the enargite is in contact with pyrite) or disseminated in the assemblage digenite-covellite (cu501, cu205). Although no obvious textures show mineral paragenesis for these assemblages, (unlike the wolframite described below), the enargite likely formed after pyrite. Pyrite in this association occurs in fine to medium-grained spaced aggregates, with blocky to irregular-subrounded grains of enargite disseminated in the spaces between pyrite grains. The enargite is not always in contact with pyrite, but where it is, the contact is usually smooth, with the edges of the enargite grain conforming to the shape of the rounded pyrite. Spaces between pyrite and enargite, and surrounding enargite, are filled by digenite-covellite, assumed to be an equilibrium assemblage. Since no direct intergrowths between enargite and covellite and enargite and digenite are observed, the enargite is interpreted to have formed before the digenite-covellite.

105 pyrite + wolframite + digenite + covellite

This assemblage is seen in sample cu204, where abundant curved tabular crystals of wolframite, fine to coarse-grained, are disseminated in gangue with massive-textured angular grains of digenite-covellite and are interstitial to aggregates of subrounded medium-grained pyrite with massive digenite + covellite; in some places, pyrite has closed around the interstitial assemblage, leaving apparent inclusions, in massive pyrite, of small subrounded wolframite grains surrounded by digenite + covellite. In these samples, wolframite > digenite/covellite (Figure 3.8).

In sample cu205, coarse elongate to blocky subrounded pyrite grains are surrounded by digenite + covellite + wolframite, where covellite occurs in narrow needles and strokes concentrated along edges of massive digenite (to give massive covellite), and wolframite occurs in fine-grained subrounded to ovoid disseminated grains in the digenite-covellite.

A few samples show wolframite occurring in a blobby pocked mass with pyrite aggregates, where paragenesis becomes difficult to ascertain, but where it occurs in long tabular to stubby grains, disseminated in silicate gangue and in contact with pyrite, the long blades of wolframite (cu204) contain very fine-grained round inclusions of pyrite, suggesting that the wolframite formed after the pyrite. However, very fine cracks running across the wolframite grains are filled or partially filled by digenite, +/- covellite, and where all three minerals are interstitial to pyrite aggregates, the assemblage digenite-covellite clearly surrounds the wolframite blades and stubby grains.

106 pyrite + digenite + covellite (+ enargite) + sphalerite

Stringers and veinlets of medium-grained subrounded to rounded separate pyrite grains with spaces filled with digenite + covellite + sphalerite + enargite are not uncommon; sphalerite occurs in fine subrounded to slightly irregular grains in massive covellite-digenite; enargite occurs in contact with both covellite-digenite and sphalerite, in small blocky to irregular grains (sample cu199).

In a sample of fault gouge (sample cu441), not typical of other ore samples, an aggregate of spaced medium-grained pyrite grains is filled with interstitial digenite + covellite, where digenite is massive and covellite occurs as narrow needles distributed throughout digenite. In

Figure 3.7 (a). Sample cu192. DDH 2967, 325.93m. Reflected light photograph of fine-grained sub-rounded thin-lamellar grains of covellite (cornflower blue to blue-white) disseminated in vein sulphate (anhydrite, dark brown, cleavage visible), around subhedral silicate grains (light brown-grey). Space bar 0.18mm.

Figure 3.7 (b). Sample cu214. DDH 2967, 211.60m. Reflected light photograph of vein of massive covellite (blue) surrounding small subrounded disseminated grains of pyrite and enargite. This is a typical sample of supergene ore, where covellite envelops all earlier sulphides. Space bar 0.36mm.

Figure 3.8. Sample cu204. DDH 2967, 513.05m. Reflected light photograph of an aggregate of fine subrounded to subangular pyrite grains with spaces infilled by curved tabular wolframite grains (brown) and massive digenite-covellite, where covellite occurs as needles in the digenite. Digenite- covellite network is clearly later than the wolframite, as it has infiltrated along fine fractures in the wolframite grain. Field of view 0.72mm.

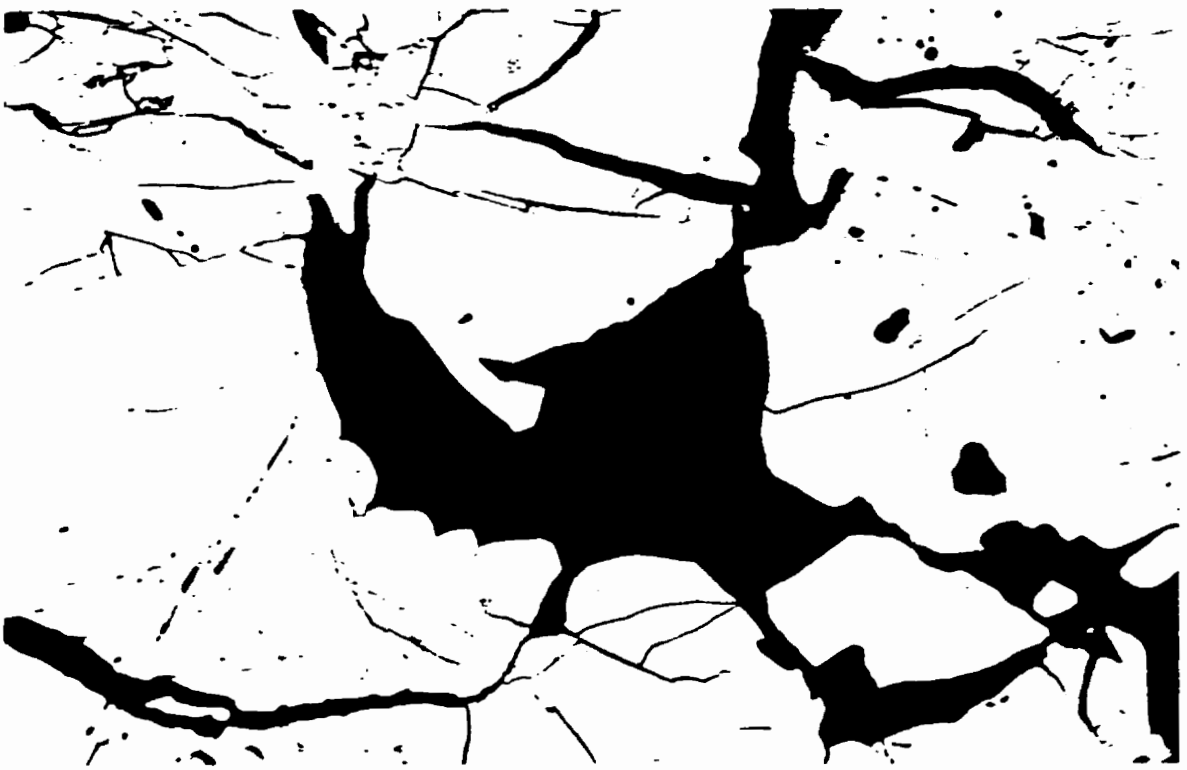

massive interstitial digenite + covellite, sphalerite occurs as skeletal blocky grains; no direct intergrowths are observed between sphalerite and digenite, or sphalerite and covellite, and the sphalerite is rarely in contact with the pyrite (being dominantly disseminated in the once-open spaces between the grains). Enargite in this assemblage occurs as very fine rounded globular grains disseminated in the interstitial digenite + covellite + sphalerite.

Since no direct intergrowths occur between sphalerite and covellite, and sphalerite and digenite, and the minor spaces open in the grains of skeletal sphalerite are filled with digenite-covellite intergrowths, sphalerite is interpreted to have formed after pyrite, but before the assemblage digenite-covellite (Figure 3.9). The exact relationship of enargite to the rest of the assemblage is yet to be determined.

107 pyrite + digenite + covellite + molybdenite

The sample of fault gouge (cu441)contains an unusual assemblage consisting of abundant fine-grained molybdenite in curved tabular grains and fine spindles with digenite +/- covellite, interstitial to rounded medium-grained pyrite grain aggregates; the assemblage molybdenite + digenite + covellite also occurs as narrow fracture fillings in the pyrite; no direct intergrowths of digenite-molybdenite, or covellite-molybdenite are observed, but the fine grain size and optical similarity of the phases makes interpretation of paragenesis difficult.

Molybdenite may be the earliest phase (after pyrite?), with later digenite-covellite, or molybdenite may have formed in equilibrium with another phase, which subsequently broke down to give digenite + covellite, as suggested by the occurrence of fine needles of molybdenite in the digenite (a texture similar to that of covellite needles in massive or lamellar digenite).

108 pyrite + digenite + covellite + colusite

In sample cu489 creamy brown-beige colusite in fine-grained aggregates of rounded to irregular grains or in disseminated subrounded grains with digenite and covellite is found between and surrounding coarse subrounded to subangular grains of pyrite in a spaced aggregate; the colusite grains and fine aggregates occur disseminated in digenite-covellite intergrowths where covellite occurs as fine needles and streaks in massive digenite; no direct intergrowths between

covellite-colusite or digenite-colusite are observed; colusite is sometimes is found as subrounded to rectangular inclusions in pyrite, alone or in smooth contact with digenite in digenite(-covellite) + colusite inclusions.

Where the colusite is in contact with pyrite, it conforms to the rounded to irregular edges of the pyrite grains. Where several 'grains' or masses of colusite occur together in the digenite-covellite, narrow spaces between the grains are filled with digenite-covellite intergrowths (digenite > covellite, where covellite occurs as fine needles in random orientation distributed through massive digenite). Like enargite, colusite is interpreted to have formed before the equilibrium assemblage digenite-covellite.

Colusite is also found as very fine round inclusions in veins of massive covellite + digenite, where covellite occurs as coarse feather and brush-strokes, and covellite > digenite (cu481). In another texture, colusite is observed in disseminated grains of digenite and veins of massive digenite + covellite, where digenite > covellite and the covellite mainly occurs as fine needles in small groups in the digenite (cu467, cu474). A very narrow film of colusite rims fine-grained irregular grains of digenite (+/- 0.1 mm) disseminated in silicate gangue, and leaves very fine-grained 'inclusion trails' in veins of massive digenite + covellite, sometimes appearing to outline subrounded grains or delineate grain boundaries within the massive digenite (Figure 3.9b).

3.3.2 Digenite (-Bornite) Assemblages

300 (pyrite +) digenite

Veins consist of coarse-grained (1-3 mm) subrounded elongate and slightly irregular pyrite grains, with spaces between grains filled by (and aggregates surrounded by) massive digenite + sulphate (e.g., cu189).

Digenite is one of the most common sulphide phases found at Chuquicamata. It is commonly seen in an open framework of massive digenite surrounding euhedral silicate 'cut-outs', and in large angular flakes of irregular-shaped digenite filling space between euhedral silicate minerals (cu435). As mentioned above, it occurs in two ways with covellite, one interpreted as an equilibrium assemblage and the other as a replacement, with digenite as the

Figure 3.9 (a). Sample cu441. DDH 2242, 145.32m. Reflected light photograph of a sample of fault gouge, showing skeletal sphalerite (brown) in open spaces between subrounded pyrite grains (yellow). The open spaces were later filled with a digenite-covellite network, where covellite occurs as dark blue needles in massive digenite. Space bar 0.09mm.

Figure 3.9 (b). Sample cu467, DDH 2242, 261.27m. Reflected light photograph of a vein of massive digenite (light blue), surrounding fine-grained euhedral to subhedral silicates (brown). Needles of covellite (dark blue) form networks in the digenite; inclusion 'trails' of colusite (beige) appear to delineate grain boundaries in massive digenite. Scale bar 0.09mm.

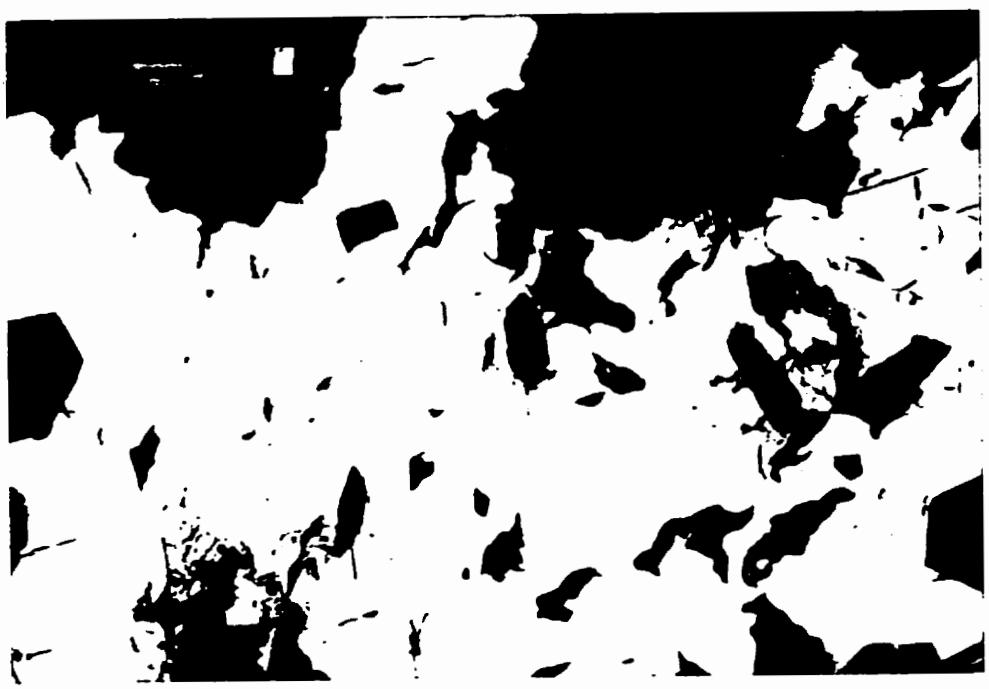

earlier phase.

301 digenite + galena

Digenite + galena is a rare assemblage that is seen as minor occurrences of angular irregular cores of galena, +/- 0.2mm across, in an open framework of semi-massive digenite + sulphate, surrounding euhedral to subhedral silicate minerals (e.g., sample cu461). At least some of the digenite appears to be controlled by the shape of sulphate minerals (anhydrite).

The irregularity of the shape of the galena cores are evidence of the replacement of galena by digenite.

302 bornite + galena

Also rare, seen only in sample cu500, is this assemblage, consisting of very fine-grained cores of subrounded galena in massive bornite (interstitial to spaced coarse-grained pyrite aggregate).

No obvious replacement textures can be seen, but galena is clearly earlier than the surrounding bornite +/- digenite.

303 digenite + bornite

This assemblage is seen as a film of digenite + bornite around euhedral to subrounded silicate minerals, and irregular masses of digenite + bornite interstitial to silicates; bornite-digenite assemblage shows smooth intergrowths in some areas; in others, digenite forms a cubic network in bornite (e.g., sample cu476).

Other than covellite, the most common intergrowth with digenite is bornite. This assemblage occurs in several ways. The one most often observed is the smooth intergrowth, where disseminated grains are made up of digenite and bornite in approximately equal volumes, and the contacts between the two phases are smooth (cu454). This appears to be an equilibrium assemblage, shown by the eutectic intergrowth. Also interpreted as an equilibrium assemblage is the exsolution texture, rarely preserved in these samples, but locally seen in small grains (+/-0.2 mm) where digenite forms a cubic network with bornite (cu476). This texture is typical of the

exsolution of bornite from digenite upon the decomposition of β-Cu_2S (Ramdohr 1980) (Figure 3.10a). Similar to this texture is a replacement texture that mimics exsolution. In some samples, bornite grains disseminated in silicate gangue and/or associated with sulphate veinlets have been rimmed or partially replaced by digenite. Where the digenite is rimming bornite grains (cu509), the rim is composed of very fine bands of digenite interlocking at 90° around the bornite grain (Figure 3.10b). Where digenite has partially to almost completely replaced bornite (cu491), the 'massive' digenite is actually a cubic network advancing across the bornite.

304 pyrite + digenite + bornite

Sample cu500 consists of massive pyrite, in aggregates of fine-grained to coarse-grained (0.05 mm to +1 mm) subrounded, inclusion-filled, variably smooth to shattered grains of pyrite with interstitial massive bornite + digenite (bornite >> digenite), where digenite in the bornite occurs as small speckled areas or irregular smooth intergrowths.

Similarly, sample cu490 consists of veins and stringers of pyrite + digenite + bornite + sulphate in a silicate matrix, where the sulphide stringers consist of single grains and welded aggregates of several grains of pyrite, all sizes, separated by interstitial massive digenite-bornite intergrowths.

In contrast, sample cu205 consists of euhedral pyrite crystals, 0.3 to 0.5 mm, which contain fine-grained round to ovoid inclusions of bornite-digenite smooth intergrowths.

In general, this assemblage consists of early pyrite grains or aggregates surrounded by later digenite-bornite intergrowths, except in the case (described elsewhere in this thesis), where second-generation pyrite contains inclusions of digenite-bornite grains.

3.3.3 Chalcopyrite Assemblages

400 chalcopyrite

Chalcopyrite occurs in massive form in narrow veins and stringers in silicate gangue, and in open frameworks around fine euhedral silicate crystals (sample cu474). Many samples in both the quartz-sericite and potassic zones of alteration contain very fine-grained disseminated grains

Figure 3.10 a. Sample cu476. DDH 2242, 288.10m. Reflected light photograph of bornite and digenite in an exsolution relationship. Digenite (light blue) forms a cubic network in bornite (tarnished purplish-blue) as it exsolves from a high-temperature Cu_2S phase (Ramdohr, 1980). Bornite-digenite grains are disseminated in silicate matrix (light brown). Space bar 0.18mm.

Figure 3.10 b. Sample cu491. DDH 2234, 306.79m. Reflected light photograph of bornite and digenite in a replacement relationship. digenite (light blue) advances across the bornite grain (pink), with digenite lamellae forming a cubic network very similar to that seen in exsolution. Bornite-digenite grains are disseminated in a silicate- sulphate matrix (sulphate veinlet is dark brown). Space bar 0.09mm.

of chalcopyrite, +/- associated with other sulphide minerals.

401 chalcopyrite + bornite

A very common assemblage, where chalcopyrite is usually the most abundant phase, in subrounded to irregular grains, very fine-grained up to 1.0 mm, as well as minor tabular grains with subrounded ends, +0.05 mm, with minor to moderate component of bornite in irregular intergrowths (e.g., sample cu442).

Chalcopyrite-bornite intergrowths are very common in small amounts in quartz-sericite alteration, and as one of the main ore assemblages in zones of potassic alteration. Although earlier workers originally assumed that most of the chalcopyrite-bornite assemblage seen in Chuquicamata represented a eutectic intergrowth, a detailed examination shows that only a minor amount is likely an equilibrium assemblage. Many clear examples of small 'grains' (+/-0.2 mm) composed of welded aggregates of very fine-grained euhedral to subhedral chalcopyrite grains occur with massive bornite filling spaces between chalcopyrite and in some instances almost outlining fine euhedral chalcopyrite grains (cu442). Remnant interstitial bornite is preserved as inclusions in the chalcopyrite.

402 chalcopyrite + digenite + bornite

One common example of this assemblage is in sample cu450, which contains irregular subrounded to angular disseminated grains of chalcopyrite + bornite + digenite, where the intergrowths between chalcopyrite and bornite, and digenite and bornite, are smooth fronts; no direct intergrowths between chalcopyrite and digenite are observed.

Sample cu491 is an example of euhedral to subrounded fine-grained chalcopyrite surrounded by massive-textured bornite with minor granular digenite along edges of bornite; some grains show a chalcopyrite core surrounded by bornite and digenite, where digenite is a cubic network in bornite.

The assemblage chalcopyrite + digenite + bornite is really an extension of digenite + bornite, since the chalcopyrite is generally the first phase formed of the three, and the mineral paragenesis is determined by the bornite and digenite. In one process, subrounded grains of

chalcopyrite in a welded aggregate, to massive chalcopyrite, are partially surrounded by (spaces filled by) minor to moderate bornite, with digenite replacing the bornite in the cubic network described above (cu509). Where there is no bornite in contact with chalcopyrite, digenite forms a rim around the chalcopyrite and fills cracks/ fractures in the cubic-network replacement pattern. For other grains disseminated in silicate-sulphate gangue paragenesis is difficult to determine, with contacts between all three minerals very smooth, almost like a eutectic intergrowth. However, close inspection of the assemblage in fine-grained disseminations shows that euhedral chalcopyrite grains are partly surrounded by the equilibrium assemblage bornite + digenite (cu454). This association probably carries over to other grains where irregular chalcopyrite + bornite + digenite offers no clues. Another texture documented for this assemblage is in disseminated grains to massive bornite with minor digenite, containing fine needles or rims of chalcopyrite, or fine speckled 'grains' of chalcopyrite in the bornite (cu500). While the partial narrow rims around bornite would seem to show that chalcopyrite is later, the needles and speckled grains of chalcopyrite in bornite are probably remnants of earlier chalcopyrite that has been replaced. As well, the minor digenite in bornite is interpreted as an equilibrium intergrowth, and the lack of digenite-chalcopyrite intergrowths suggest that bornite-digenite is the later assemblage.

403 chalcopyrite + covellite + idaite

This assemblage is usually in the form of very irregular grains and small masses of chalcopyrite disseminated in silicate gangue, with covellite and idaite. Idaite occurs in curved tabular streaks within or adjacent to the same kind of streaks of covellite, and weird little irregular 'grains', not necessarily in contact with covellite (although it may exhibit the same texture spatially close by), as almost the core of a grain, where the rim is made up of a film of chalcopyrite (of varying thickness, depending on the 'grain' shape of the idaite +/- covellite) (e.g., sample cu465). Covellite occurs in streaks and irregular grains in the chalcopyrite as well, +/- associated with the idaite, but it also occurs in a fine granular form clustered at the edges of the chalcopyrite (cu465) (Figure 3.11).

Mineral paragenesis is exceedingly difficult to determine: idaite and covellite sometimes appear to be streaks of one 'grain', suggesting the possibility that a high-temperature phase

exsolved both on cooling. Chalcopyrite definitely looks to be later in this assemblage, but this is complicated by later covellite replacing parts of the chalcopyrite + covellite + idaite assemblage in the network of lamellae discussed above.

404 covellite + chalcopyrite

The best example of this assemblage is seen where massive covellite is in contact with massive chalcopyrite, or in chalcopyrite with intersecting lines of covellite in it at about 90°; covellite has an almost graphic texture next to the chalcopyrite, formed from a network of covellite lamellae (e.g., sample cu455).

Texturally, covellite of this type differs from the other covellites we see at Chuquicamata, in that covellite replacing another phase forms an interlocking network of lamellae of widely varying sizes. This texture is often seen as a thick rim around digenite (cu476), but the most remarkable examples of replacement are seen in the assemblage covellite + chalcopyrite. In many cases, covellite can be seen starting to replace veins and grains of chalcopyrite around the edges and from cleavage planes in the chalcopyrite (cu455) (figure 3.12a). In some cases the chalcopyrite has disappeared completely, and only the arrangement of covellite lamellae in loose lattices shows the former chalcopyrite existence (cu455).

In sample cu494, covellite and chalcopyrite occur together in an assemblage that bears little resemblance to the replacement texture described above (Figure 3.12b). The (probably metastable) coexistence of these two minerals can be explained by the breakdown of high-temperature idaite (see Chapter 2 for details).

405 pyrite + covellite + chalcopyrite

This assemblage is seen in veins, where a vein of massive chalcopyrite surrounds fine-grained separated subrounded to rounded grains of pyrite, with narrow stringers of covellite cutting through both the chalcopyrite and the pyrite; covellite also rims the massive chalcopyrite at the edges of veins; also, in some samples we see covellite + minor chalcopyrite as a small rounded inclusion in pyrite (e.g., sample cu495).

This assemblage is especially interesting in terms of mineral paragenesis, since the textures

are very clear indicators of the order of mineral deposition: fine to coarse-grained disseminated pyrite grains surrounded by a vein of massive chalcopyrite, where massive covellite has begun to take over in a network of lamellae, working in from the edges of the chalcopyrite (cu495). Covellite 'stringers' or fracture fillings cut across the chalcopyrite and through the rounded grains of pyrite, but the 'massive' covellite preferentially attacks the chalcopyrite and leaves the pyrite grains undisturbed.

406 chalcopyrite + bornite + covellite

A relatively common assemblage, typified in sample cu487, consists of fine-grained rounded to subangular chalcopyrite disseminated in silicate gangue, with bornite + covellite filling cracks and fractures in chalcopyrite; bornite also occurs in smooth intergrowths with chalcopyrite in fine-grained rounded grains, with covellite partially rimming the grains or invading the grains in fine needles.

407 (pyrite +) chalcopyrite + bornite + digenite + covellite

Sample cu454 contains irregular to subrounded fine to medium-grained chalcopyrite grains disseminated in silicate gangue or in 2-3 mm masses, surrounded by bornite-digenite in smooth intergrowths, and rimmed or partially rimmed by very fine needles and/or granular covellite; some speckled or partly 'dissolved' fine grains of chalcopyrite are disseminated in bornite-digenite intergrowths in contact with massive chalcopyrite.

Sample cu500 contains massive bornite (interstitial to variably spaced to welded aggregate of fine to coarse-grained pyrite) with narrow needles of chalcopyrite in the bornite, starting from the outer edges, as well as minor occurrences of finely speckled chalcopyrite grains as 'inclusions' in the bornite; digenite occurs as small irregular smooth intergrowths with massive bornite, and covellite occurs as fine needles in small patches at the edges of the bornite + digenite + chalcopyrite.

Figure 3.11. Sample cu450. DDH 2242, 161.98m. Reflected light photograph of semi-massive covellite (light to dark blue) + idaite (light blue to dark red), where the two minerals occur as interfingered needles or 'strokes' and curved tabular 'grains'. Matrix is silicate with some sulphate in upper right corner. Field of view 0.75mm.

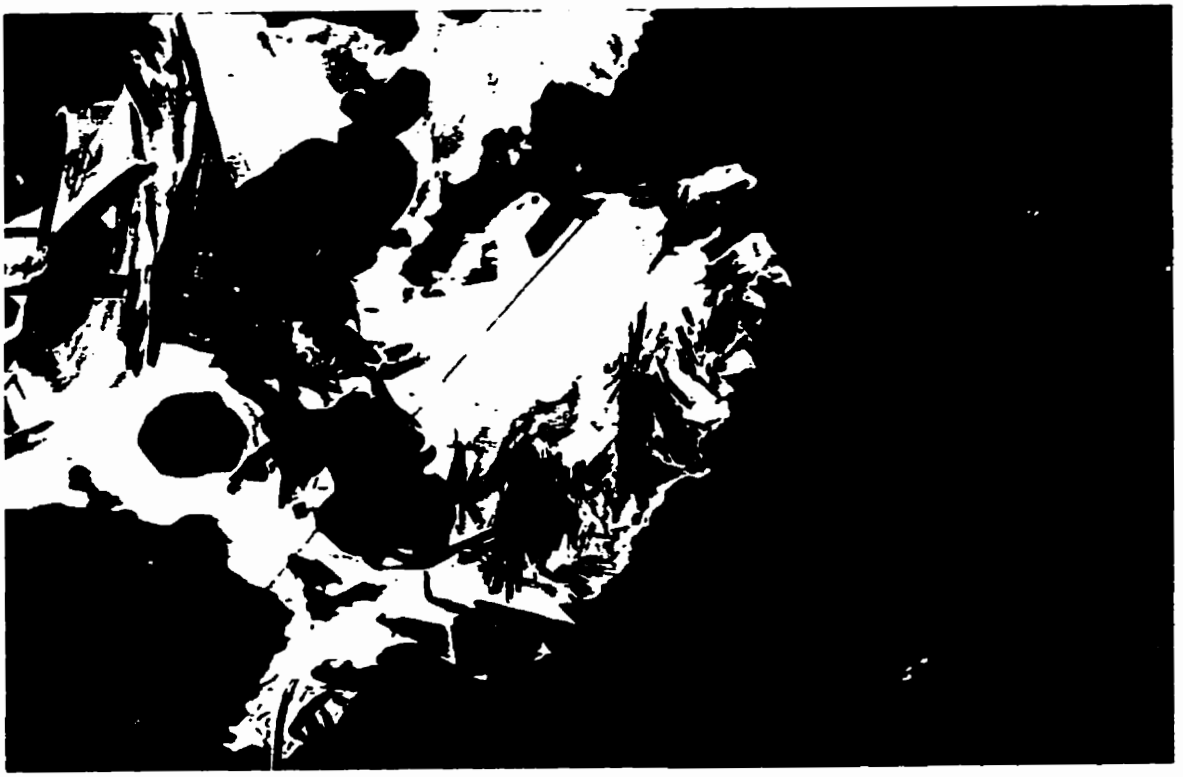

Figure 3.12 a. Sample cu455. DDH 2242, 193.86m. Reflected light photograph of covellite (dark blue) replacing chalcopyrite (bright yellow) in a lattice of loosely-spaced lamellae. Covellite-chalcopyrite is in a matriix of silicate (brown). Scale bar 0.18mm.

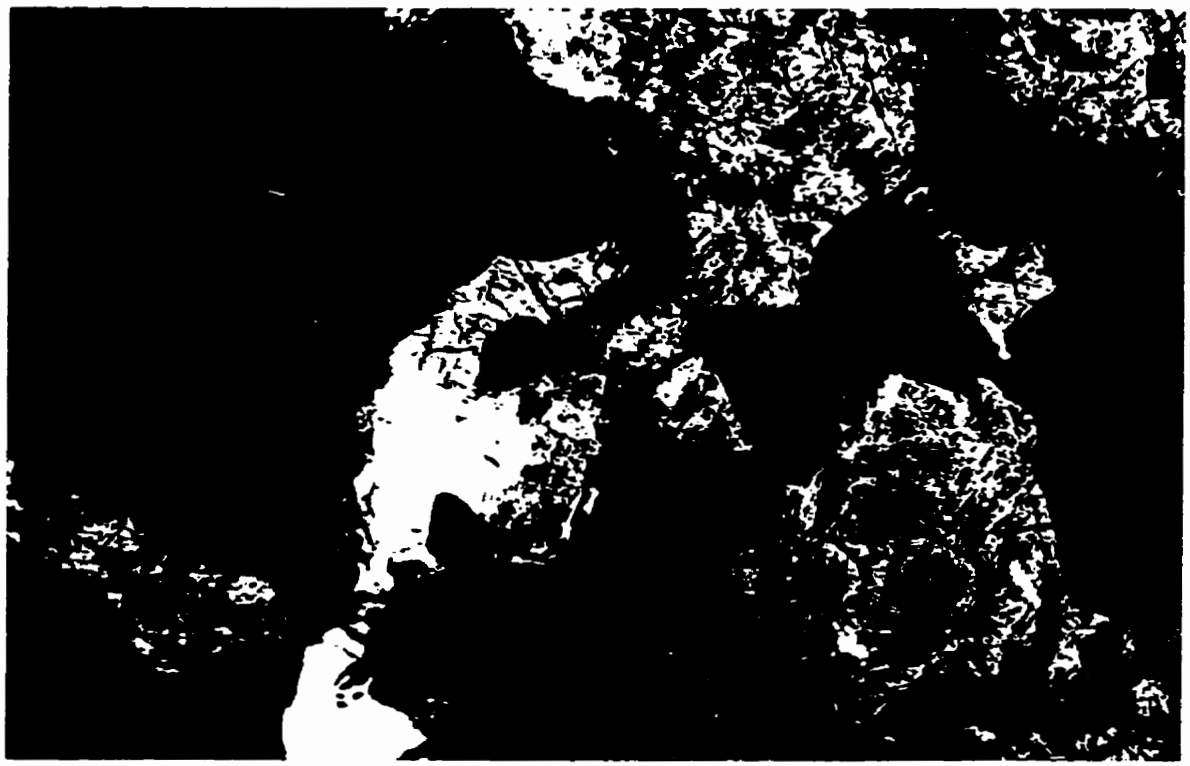

Figure 3.12 b. Sample cu494. DDH 2234, 219.84m. Reflected light photograph of metastable assemblage covellite (dark blue) + chalcopyrite (bright yellow) as an inclusion (locked grain) in pyrite (light yellow). Ratio of covellite to chalcopyrite is approximately 9:2. Scale bar 0.09mm.

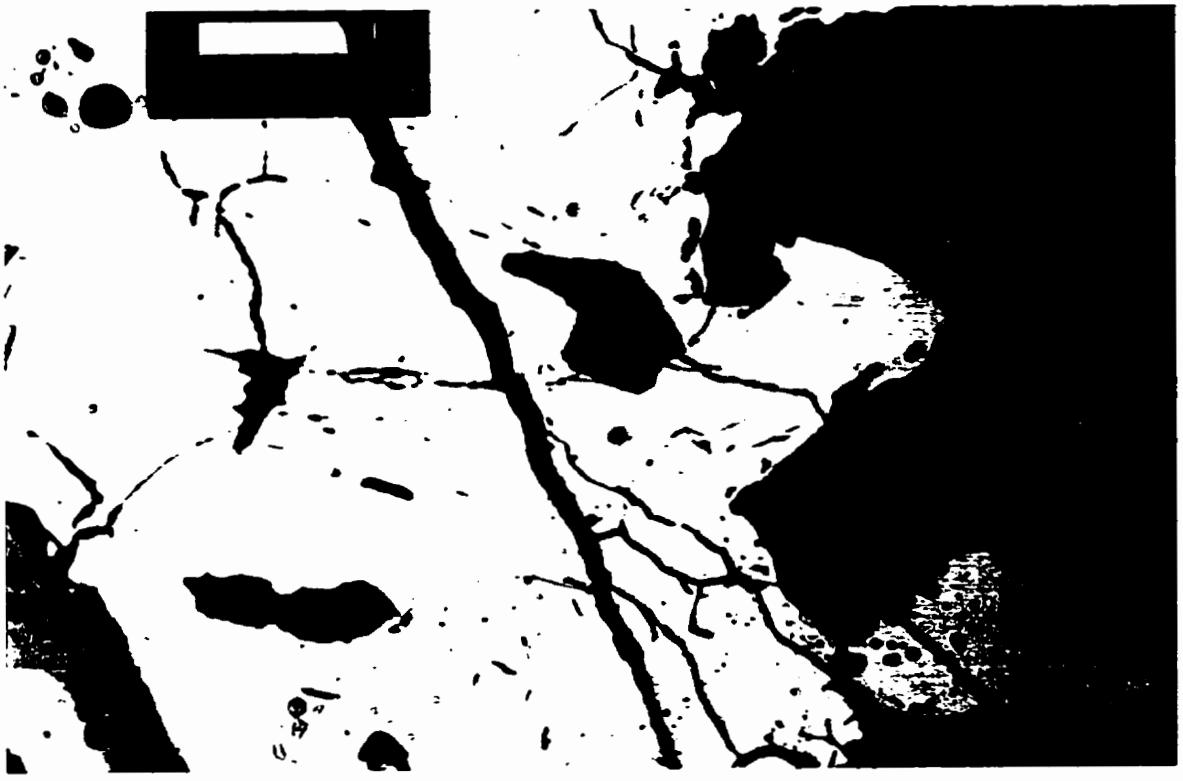

There appear to be two major subgroups of this assemblage defined by their respective mineral paragenesis. Some cases are very difficult to judge, such as ones where there appears to be remnant chalcopyrite and bornite (impossible to determine earlier relationship, possible equilibrium, but now very minor bornite left and only trace chalcopyrite) attacked first by digenite, then by covellite in a very regular lattice network, surrounding euhedral medium- to very fine-grained pyrite grains, where the pyrite remains virtually unaffected (cu482). In other cases, indeed most of them, chalcopyrite is obviously surrounded by equilibrium digenite-bornite, with later covellite intruding in fine needles and splatshots (cu442). A third possibility exists, in that bornite + pyrite react to produce digenite + chalcopyrite below 228°C (Yund and Kullerud, 1966). If this reaction were in fact proceeding here, we would see the products at the interface between bornite and pyrite, instead of within or at the edges of the massive bornite.

408 covellite + chalcopyrite + Fe-oxide

Again in sample cu455, where massive covellite is in contact with massive chalcopyrite, and covellite has a graphic texture and is rimmed by a narrow film of iron oxide; the iron-oxide also forms as streaks in the massive covellite, and rims holes/gouges in the covellite and chalcopyrite.

3.3.4 Sphalerite Assemblages

600 sphalerite

Sphalerite mainly occurs as a minor phase in various assemblages which can be found throughout the deposit. It commonly occurs as skeletal grains disseminated in silicate gangue and as small subrounded grains and irregular masses adjacent to, and possibly overprinting, other sulphides, such as pyrite with surrounding digenite + covellite (cu481).

601 sphalerite + pyrite + galena

Sample cu467 contains this assemblage in minor amounts, where welded to spaced aggregates of fine-grained subrounded to subangular pyrite grains, are surrounded by (and have

spaces filled by) galena + sphalerite; galena is a very minor phase, in very fine rounded grains and subrounded slightly irregular-shaped grains, surrounded by massive sphalerite.

The galena apparently formed after the pyrite grains, as it fills angular open spaces left by the pyrite (see below for further discussion).

602 sphalerite + bornite + chalcopyrite

In sample cu467, massive sphalerite, pocked and with irregular edges, is cut by narrow veins, pinching and swelling, of bornite + chalcopyrite; the bornite and chalcopyrite occur in irregular intergrowths in veins full of holes and gouges, and very fine-grained euhedral to subhedral silicate minerals.

The veins and stringers of chalcopyrite + bornite are interpreted as an equilibrium assemblage. The massive sphalerite is scratched and gouged, and contains fine-grained subrounded to subangular inclusions of pyrite. In some instances, remnant grain boundaries of subhedral fine-grained sphalerite grains are apparent in the massive sphalerite. Elsewhere in the section, semi-massive pyrite is made up of spaced to welded aggregates of subrounded variably-sized pyrite grains (<0.05 to 0.2 mm), with very minor fine grains of galena disseminated between the pyrite grains, and massive sphalerite surrounding the pyrite and galena. In the same section, we observe a small amount of semi-massive galena adjacent to massive sphalerite, with spaces around/between the galena and sphalerite filled by massive smooth digenite-bornite intergrowths. Mineral paragenesis for these associations is interpreted as: pyrite, followed by minor galena, followed by massive sphalerite. Since the veinlets of bornite-chalcopyrite, interpreted as an equilibrium assemblage, are not in contact with the presumably eutectic intergrowth of digenite-bornite, it is difficult to ascertain the order. However, based on the placement of chalcopyrite in other samples, the chalcopyrite-bornite veinlets likely formed before the massive-textured digenite-bornite.

603 sphalerite + bornite + digenite + galena

Sample cu467 consists of massive sphalerite, possibly a welded grain aggregate (outlines of apparent grain boundaries are sometimes visible) in contact with semi-massive irregular galena,

with spaces in and between sphalerite and galena filled by approximately equal amounts of bornite and digenite in smooth intergrowths. The mineral paragenesis of this assemblage is discussed above, in conjunction with the other sphalerite-dominated assemblages.

700 chalcopyrite + covellite + sphalerite

This unique assemblage is typified in sample cu507, where a vein of massive chalcopyrite with abundant cracks and fractures is filled with very fine granular digenite +/- covellite; the digenite + covellite also borders the chalcopyrite vein. The digenite is then rimmed and in some areas taken over by fine granular sphalerite, which forms a film around the edges of the chalcopyrite vein and invades along cracks and fractures. Where the digenite-covellite pinches out, granular sphalerite rims the massive chalcopyrite vein; massive chalcopyrite is also found in an open framework surrounding euhedral to subhedral silicate minerals, most of which also have a thin coating of digenite and/or sphalerite (Figure 3.13).

This assemblage occurs at relatively shallow depths in the porphyry system, and may be indicative of low-temperature sphalerite replacing earlier high-temperature phases.

701 sphalerite + (chalcopyrite +) digenite + bornite (+covellite)

Sample cu509 is an example of this unique assemblage, where disseminated grains and interrupted stringers of elongated chalcopyrite grains, +/- 0.25 mm, and grains of bornite-digenite intergrowths, are all rimmed by a narrow film of sphalerite. Bornite occurs in isolated or small groupings of grains disseminated in silicate gangue, and as a minor component in the chalcopyrite stringers, surrounding euhedral to subhedral chalcopyrite and concentrating along edges of the veinlets; digenite occurs as a granular coating, very fine-grained, around the edges of the chalcopyrite stringers, and as granular rims around and partial cubic networks in bornite grains, with interlocking 'needles' of digenite starting at edges of bornite grains and projecting part or all the way across the grains. Each grain is rimmed by a fine film of granular to massive-textured sphalerite, which also rims the outer edges of, and the fractures/cracks in, the chalcopyrite veinlets. Where covellite is part of this assemblage, it occurs as a minor component, as very fine needles in the granular digenite rimming bornite and/or chalcopyrite. This texture is tentatively

interpreted as supergene sphalerite.

3.3.5 Molybdenite Assemblages

800 molybdenite

Molybdenite occurs as isolated curved tabular grains, <0.5 mm long, to veins of massive molybdenite in massive quartz; minor flakes of molybdenite occur with disseminated grains of covellite (e.g., sample cu434).

Massive molybdenite occurs in late-stage veins (+/- 5 mm wide) in massive quartz, the so-called 'blue veins' in the upper regions of quartz-sericite zones of alteration (cu433)(Figure 3.14).

801 molybdenite + other sulphide phases

Sample cu500 contains +/- 0.1 mm aggregates of curved molybdenite strands associated with semi-massive and disseminated grains of bornite + chalcopyrite; individual strands are disseminated in massive interstitial bornite and molybdenite masses are disseminated in gangue and in contact with edges of interstitial bornite.

In sample cu201, minor molybdenite in splayed flakes is in contact with subangular to subrounded very fine-grained pyrite grains disseminated in silicate gangue.

Molybdenite, though rarely the dominant sulphide, nevertheless occurs in many mineral associations covering a range of sulphide assemblages and alteration zones. Other than the possible equilibrium assemblage with digenite and covellite described above, molybdenite occurs in most associations as fine curved tabular grains and spindles disseminated in silicate gangue, spatially associated with other sulphides, or in contact with them. Fine-grained curved tabular 'balls' of molybdenite overprint areas of disseminated to semi-massive covellite, where covellite has completely replaced earlier chalcopyrite (cu503). Aggregates of very fine-grained molybdenite strands are disseminated in gangue and overprint parts of massive interstitial bornite and disseminated grains of bornite + chalcopyrite (cu500). In most cases, molybdenite occurs as a later phase, overprinting earlier sulphides where it is in contact with them, and disseminated in the spaces left where it is not.

Figure 3.13. Sample cu507. DDH 2234, 113.65m. Reflected light photograph of chalcopyrite (yellow) - covellite (blue) - sphalerite (grey) - sulphate (dark brown) vein in silicate matrix. Covellite occurs as fine lamellae replacing chalcopyrite, with very fine-grained granular sphalerite rimming. This texture represents possible supergene sphalerite. Space bar 0.18mm.

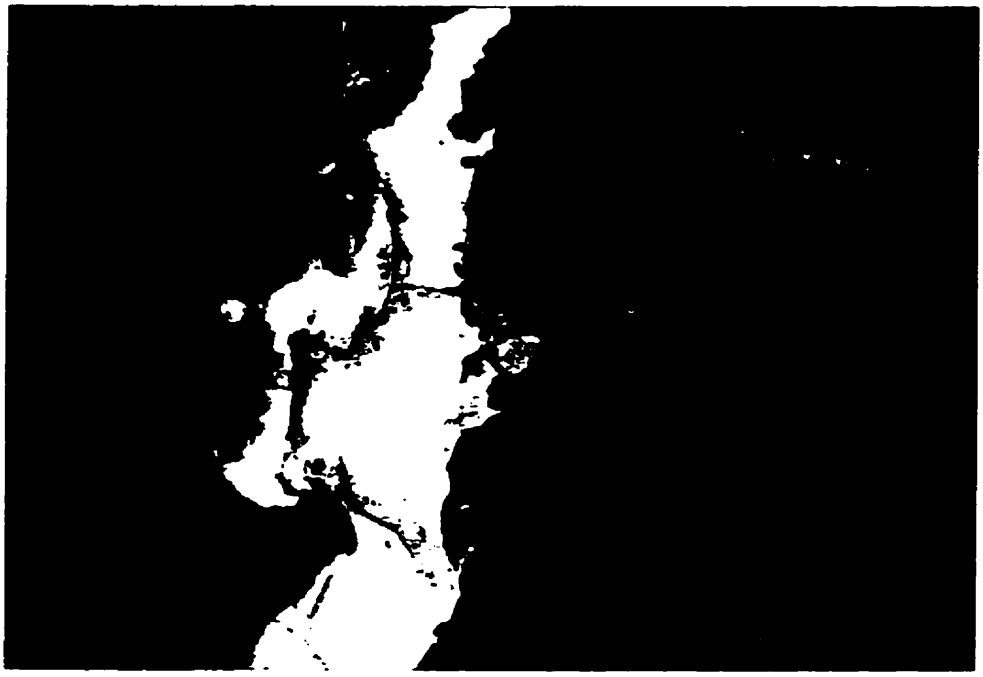

Figure 3.14. Sample cu433. DDH 2242, 56.45m. Plane light photograph of a cut section of drill core through a 'blue vein', made up of massive molybdenite (metallic grey) + quartz + anhydrite.

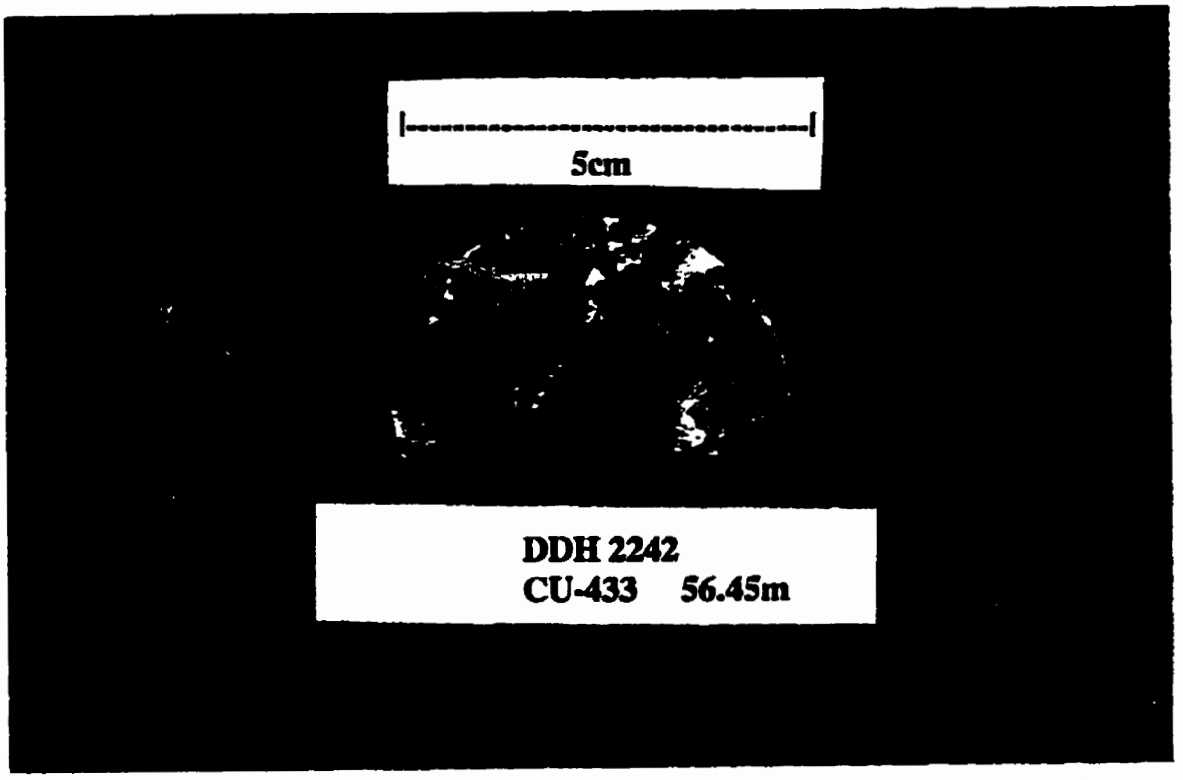

3.3.6 Other Pyrite Assemblages

200 pyrite

201 (pyrite +) enargite + sphalerite

Spatially associated with the coarse enargite-pyrite veins is minor sphalerite in skeletal grains (possibly due to rapid crystallization) adjacent to large blocky grains of enargite, with edges slightly dissolved-- indicative of a possible enargite-sphalerite assemblage, with enargite not as susceptible to later dissolution by percolating fluids (e.g., sample cu183)?

202 pyrite + sphalerite

203 pyrite + enargite

This coarse-grained assemblage consists of veins of massive enargite + pyrite + sulphate in silicate matrix; massive enargite-pyrite consists of angular to irregular subrounded intergrowths of the two minerals, each commonly containing inclusions of the other; there are minor areas of very fine-grained disseminated grains of enargite and pyrite in sulphate, with an almost 'shattered' appearance, which may be right alongside massive enargite-pyrite veins; enargite also occurs as large blocky grains (1.0+ mm) with distinct cleavage almost at 90°; both enargite and pyrite occur as small blocky to wedge-shaped and tabular randomly-oriented grains grouped together in massive sulphate adjacent to larger grains--possibly pieces broken off of larger grains during quartz-sericite veining (e.g., sample cu182)?

Veins of coarse-grained pyrite + enargite + sulphate represent another generation of both pyrite and enargite. The enargite in these veins is up to several millimetres in size, large blocky grains with semi-massive pyrite (cu182). Both the pyrite and enargite also occur in these veins as abundant fine wedges and randomly-oriented angular grains disseminated in massive sulphate. This assemblage is interpreted as an equilibrium assemblage.

204 pyrite + wolframite

Wolframite occurs in two forms: in one, massive blobby pocked wolframite is in contact with massive pyrite, where the pyrite is made up of welded aggregates of fine-grained subrounded to subangular pyrite grains, where grain boundaries are still apparent in some places (e.g., sample cu201); in the other, narrow tabular grains of wolframite are disseminated in silicate gangue and in contact with (abutting) subrounded coarse-grained pyrite (e.g., sample cu204). As discussed earlier, paragenesis is difficult to determine where massive wolframite is intergrown with pyrite, but the small tabular grains of wolframite can be observed to have been deposited after the pyrite, and this interpretation can be extended to encompass other textures of the same assemblage.

3.4 Distribution of Assemblages

The distribution of minerals is one clue to the relative timing of emplacement of one mineral assemblage over another. Since recent Ar/Ar dates from Dalhousie University, Nova Scotia, put the event that produced the quartz-sericite zone of alteration at approximately 31 Ma, 2 to 3 Ma later than the episode of potassic alteration, mineral assemblages from each event will be treated as separate entities for now. The remaining question is whether each episode of alteration has a characteristic ore mineral assemblage.

3.4.1 Assemblages Characteristic of Quartz-sericite Alteration

Figure 3.15, a cross-sectional view of the Chuquicamata deposit with the alteration zones clearly outlined, shows that quartz-sericite alteration dominates the western half of the deposit, and abuts the West Fissure. In the central portion of the deposit this alteration zone dominates at shallow depths, and continues this way even further east. At greater depths, however, the quartz-sericite alteration grades into elongated pods, oriented up and to the east, of quartz-sericite overprinting earlier potassic alteration. These zones are discussed further in Section 3.4.3.

As has been described above, covellite occurs in many mineral associations, the most common being with digenite in stringers and veins, disseminated in silicate-sulphate gangue, or surrounding euhedral to subhedral spaced to semi-massive pyrite grains. The covellite and

digenite are assumed to be in equilibrium, either as eutectic intergrowths or as exsolution products (see Chapter 4 for discussion on temperature implications). This equilibrium assemblage is typical of quartz-sericite alteration and occurs throughout the zone. As can be seen in Table 15 and Figure 3.16, where the distribution of covellite-digenite-dominated assemblages are plotted on the 4500N section, these assemblages dominate in the quartz-sericite zone. They are also found in zones of potassic alteration, albeit in much lesser amounts (see discussion in section 3.4.3). Some of the covellite, occurring as disseminated grains or with digenite, is actually blaubleibender covellite, which is found in minor amounts throughout the zone, regardless of depth or mineral associations.

Within the basic scheme of covellite + digenite +/- pyrite comes enargite. Enargite in this association occurs as blocky to subrounded grains disseminated adjacent to pyrite and surrounded by covellite + digenite. The addition of wolframite makes a fourth assemblage characteristic of quartz-sericite alteration. Wolframite only occurs in this zone.

Another assemblage containing enargite is the coarse-grained enargite + pyrite, which forms veins above the typical hypogene assemblages described above. These veins occur only in the zone of quartz-sericite alteration, and are interpreted as late-stage hydrothermal veins.

The so-called 'blue veins', made up of massive molybdenite + quartz, may have formed before the quartz-sericite alteration, as they possess a degree of shearing and deformation that is not necessarily matched elsewhere in this zone. Since the absolute age of the veins has yet to be determined, and the relative age is difficult to interpret based on textures and mineralogical associations (since the blue veins in section 4500N are not in contact with the more common assemblages), the interpretation must be made based on the distribution of the veins. The blue veins in section 4500N occur exclusively in the zone of quartz-sericite alteration, at relatively shallow depths. What this means in terms of deformational history, uplift, etc. is unclear. Molybdenite is also found at much greater depths in this zone, as curved tabular grains disseminated in gangue and sometimes associated with other sulphides, namely covellite, digenite and pyrite.

Sphalerite in quartz-sericite alteration is found mainly as skeletal grains disseminated in gangue and as small subrounded grains associated with other sulphides (pyrite, digenite,

covellite). Most samples that do contain sphalerite have only a minor amount. Figure 3.17 details the distribution of sphalerite assemblages in the 4500N section.

Bornite and chalcopyrite, although not rare in this zone, occur in minor amounts as fine-grained disseminations in silicate-sulphate gangue. They may be spatially associated with the more common sulphides here, such as covellite and digenite, but they are rarely in contact with them. There are minor occurrences of digenite-bornite intergrowths in disseminated grains or in contact with pyrite, but most of the bornite and digenite-bornite 'grains' occur as fine round to ovoid inclusions in pyrite. These inclusions are interpreted as locked grains.

3.4.2 Assemblages Characteristic of Potassic Alteration

Potassic alteration dominates the eastern side of the deposit, and a portion of the central area, where it occurs underneath a 'blanket' of quartz-sericite alteration. Further east, potassic alteration grades into the (poorly mineralised) propylitic alteration.

Most of the chalcopyrite and bornite that occurs in the system is concentrated in the zone of potassic alteration. They often occur together, but bornite occurs even more commonly with massive digenite, in equilibrium intergrowths and sometimes as replacement intergrowths, on their own or surrounding pyrite or chalcopyrite. The assemblage bornite + digenite + chalcopyrite is extremely common in this zone. Massive chalcopyrite is found in several samples, and is commonly partially or completely replaced by massive covellite. This texture is not seen in the zone of quartz-sericite alteration. Covellite in the potassic zone also occurs as fine needles and acicular bundles at the edges of other sulphides, particularly bornite and chalcopyrite. Covellite in the potassic zone is in contrast to covellite in the quartz-sericite zone, where it dominantly occurs in equilibrium with digenite. Figure 3.18 shows the distribution of chalcopyrite-dominated assemblages in the 4500N section.

Where pyrite in the quartz-sericite zone is mainly surrounded by digenite-covellite, here it is usually surrounded by digenite-bornite intergrowths or by massive chalcopyrite (which may or may not be invaded by later stringers of covellite).

Sphalerite is common in potassic alteration. The massive sphalerite described earlier in section 3.3, possibly made up of welded grain aggregates and part of an assemblage that may

contain galena, pyrite, bornite, digenite, and/or chalcopyrite, occurs exclusively in this zone. Another sphalerite assemblage exclusive to potassic alteration is the possible supergene sphalerite, where it occurs as narrow rims around disseminated grains and/or veins composed of chalcopyrite, digenite, and bornite (or any combination thereof) (Figure 3.17). Other sphalerite occurrences in this zone consist of minor isolated grains disseminated in gangue or associated with other suphides.

Molybdenite in potassic alteration occurs much the same way as in quartz-sericite alteration, as isolated curved tabular grains or fine bundles of grains disseminated in gangue near other sulphides, or overprinting other sulphides. Veins of massive molybdenite are not seen, although there is at least one occurrence of semi-massive to disseminated grains and curved flaky bundles of molybdenite in silicate gangue in a sample that contains little else in the way of sulphides.

Galena, which occurs only in minor amounts in a few samples, has been described texturally as one of the earliest phases. Whatever mineral associations it occurs with, it is only found in zones of potassic alteration.

Other sulphides that occur in minor amounts are idaite and colusite. The idaite assemblage, with covellite and chalcopyrite, is observed only in potassic alteration. Assemblages containing colusite are discussed below.

3.4.3 Assemblages Characteristic of Quartz-sericite Overprinting Potassic Alteration

Several samples of ore, ostensibly in the zone of potassic alteration, show a marked departure from both the potassic and the quartz-sericite alteration, although they contain elements of both. These samples are interpreted as lower-temperature quartz-sericite alteration overprinting the earlier, high-temperature potassic alteration.

In terms of distribution, relatively vast areas in the deep central and eastern portions of the deposit that were once dominated by potassic alteration have been affected by the later hydrothermal fluids. The zones of quartz-sericite overprinting potassic alteration occur as large 'stretched' pods surrounded by regular quartz-sericite alteration, or with quartz-sericite alteration

to the west and pure potassic alteration as a rim to the east (refer to Figure 3.15). Smaller elongated pods of pure potassic alteration also occur within the larger areas of this combined alteration.

The mark of this type of alteration in terms of ore minerals is generally the presence of the equilibrium assemblage digenite + covellite in contact with assemblages charactersitic of potassic alteration.

Above and below these samples is pure potassic alteration, and while the samples themselves may contain typical potassic minerals such as chalcopyrite and bornite-digenite intergrowths, they also appear to have been 'flooded' by digenite + covellite, which fills any available space between the earlier sulphides. For instance, colusite is only found in the zone of quartz-sericite overprinting potassic. As described above, the colusites occur in one assemblage as fine rounded to subrounded individual grains disseminated in spaces between large pyrite grains. Elsewhere in the same sample, pyrite is partially surrounded by massive digenite + bornite, taken as a eutectic intergrowth. The spaces between colusite grains are flooded with massive digenite + covellite, which also surrounds the pyrite and other sulphides.

The same type of texture is repeated in other samples of potassic alteration, where spaced pyrite grains with skeletal sphalerite between (but not in contact with) the grains are filled/surrounded by covellite + digenite in a texture typical of quartz-sericite alteration.

In some samples, covellite and digenite may not be the only later minerals to make their way into earlier assemblages. Several samples of potassic alteration contain veins and disseminated stocks of pyrite grains with interstitial digenite + covellite + enargite, where the enargite occurs in small subrounded blocky grains or more angular intergrowths with the other two phases; this texture, as has been mentioned above, is relatively common in quartz-sericite alteration.

Other examples of quartz-sericite overprinting potassic alteration are seen in samples where stringers and veins of massive covellite + digenite (+/- surrounding rounded pyrite grains) cut through silicate-sulphate gangue and are spatially associated with, but not in contact with, typical potassic assemblages, such as digenite + bornite + chalcopyrite. A few such samples have veins of massive digenite-covellite, interpreted as an equilibrium intergrowth, that contain very

fine round inclusions or subrounded irregular inclusion trails of colusite. The question is whether, in these instances, the colusite is high-temperature, charactersitic of potassic alteration, or whether it may have come in with the typical quartz-sericite-associated sulphides. What is clear is that to date, colusite has only been found in zones of potassic alteration that appear to have been overprinted by quartz-sericite alteration.

3.5 Paragenetic Sequence of Assemblages

A much more difficult task than the mineral paragenesis within each assemblage comes when we try to reconstruct the paragenetic sequence of the assemblages themselves. Many assemblages appear from the scale of sampling done for this study to be virtually 'isolated' from each other, making interpretation of relative timing somewhat ambiguous. However structural and textural clues are very valuable, and though this study does not answer all the questions of paragenesis it does provide the basis for a more detailed sampling scheme for further in-depth analysis.

Figure 3.19 is a graphical representation of the mineral paragenesis as constructed from a detailed petrologic study of the ore assemblages in the 4500N cross-section at Chuquicamata. While the paragenetic sequence is organised by *mineral*, the author would like to stress that it is the order of the *mineral assemblages* that is really being defined. The assemblages, by mineral, are broken into those characteristic of potassic alteration vs sericitic alteration.

Pyrite is the first sulphide formed, and occurs surrounded by and as inclusions in other very high-temperature minerals, such as galena and massive chalcopyrite. Galena and chalcopyrite are also among the earliest phases, along with the rare samples of massive sphalerite.

The (probably equilibrium) assemblage of chalcopyrite + bornite is seen cutting massive sphalerite and is obviously later. Bornite shows continuous mineralisation from the early varieties in eutectic growth with chalcopyrite, to massive bornite replacing chalcopyrite after chalcopyrite precipitation had ceased, to eutectic formation with high-temperature digenite. Also early, forming before or contemporaneously with bornite, is idaite. How long precipitation of idaite lasted is anyone's guess; it is not very common in these samples, but this may be due in part to its decomposition on cooling.

The covellite found in the potassic zone is undoubtedly a higher-temperature variety than that found in the later hydrothermal ores, but it come at the tail end of the other high-temperature minerals. It is found almost exclusively as a replacement mineral, resulting from hydrothermal leaching, where the covellite appears to have formed during dissolution of the primary phase (commonly chalcopyrite or digenite; 'primary' in this case refers only to the relative timing of the minerals involved, since they are all obviously in the hypogene environment). Although leaching without immediate replacement is common in other deposits, no evidence is seen for it here.

Recent argon dates from Dalhousie University for the two main periods of alteration confirm what can be observed from a textural study of the ores: that quartz-sericite alteration is considerably later than potassic alteration. As mentioned before, the best example of this, seen time and again, is that of euhedral pyrite grains containing inclusions of bornite or bornite-digenite intergrowths, and surrounded by covellite-digenite intergrowths. Therefore at least one generation of pyrite was formed after the bornite-digenite assemblage and the other high-temperature minerals. Other mid-temperature assemblages are pyrite + enargite and pyrite + wolframite, both of which precede the dominant quartz-sericite-associated ore assemblage covellite + digenite.

Molybdenite assemblages are difficult to place. Those containing only a small amount of molybdenite in isolated or small groups of grains are probably early in the mid-temperature range characteristic of quartz-sericite alteration. However the so-called 'blue veins' pose a problem. On the one hand the molybdenite veins occur mainly (or in the case of our samples, only) in quartz-sericite alteration, but there is evidence to suggest that the sericite cuts the veins. As well, molybdenite in this zone is very sheared, suggesting that the blue veins formed before the quartz-sericite alteration event.

Coarse-grained pyrite-enargite veins are limited to the quartz-sericite alteration zone and form an upper boundary between earlier hypogene ore and the supergene ore above. These veins are evidence of late-stage hydrothermal veining.

Supergene assemblages, dominated by rims of chalcocite/ djurleite or sphalerite around grains and veins of other copper sulphides, and blankets of covellite overlying and enveloping other phases, are the most recent sulphide assemblages to have formed.

Figure 3.15. Chuquicamata cross-section 4500N, detailing alteration zones.

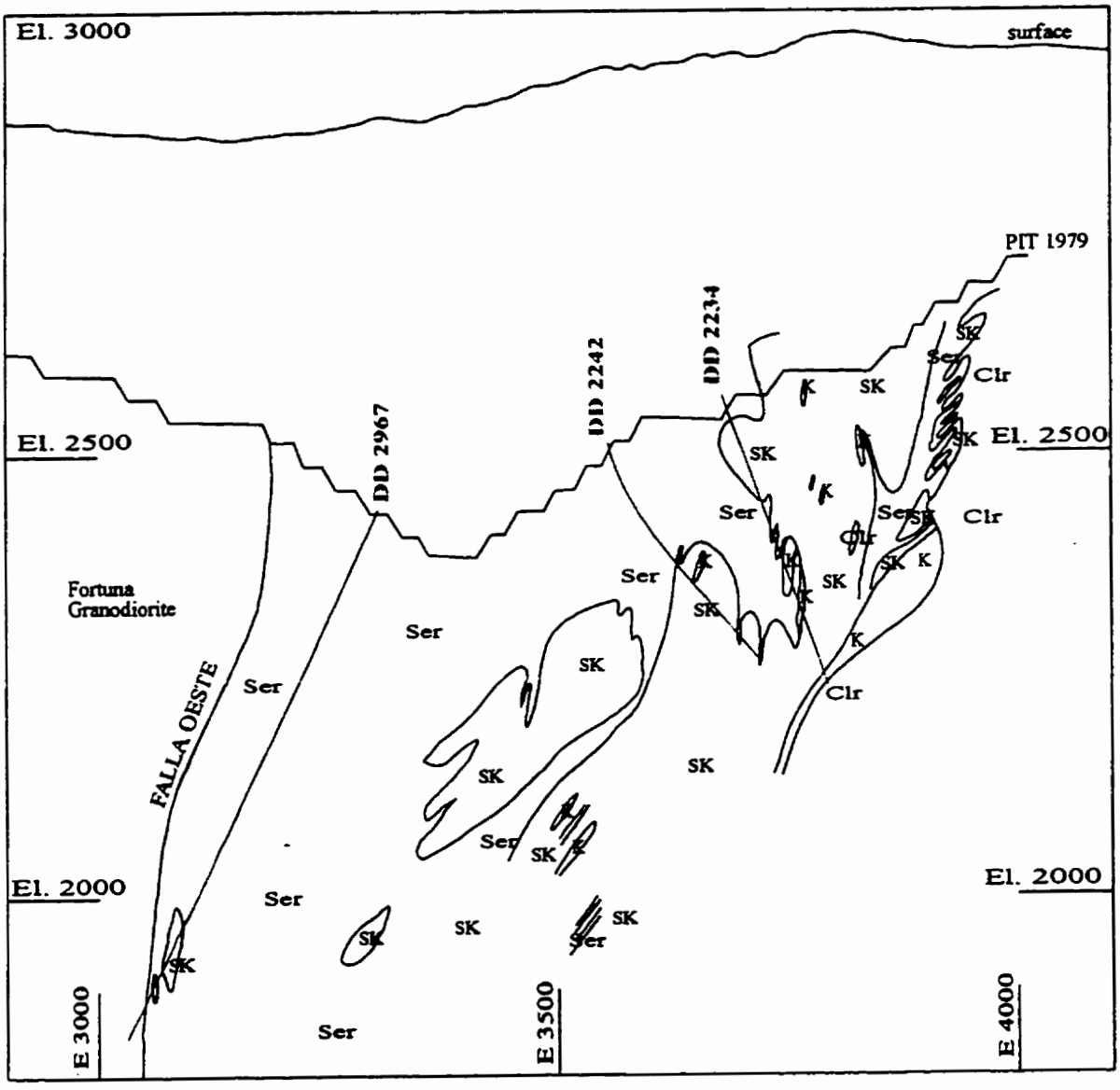

Figure 3.16. Distribution of covellite-digenite assemblages in cross-section 4500N.

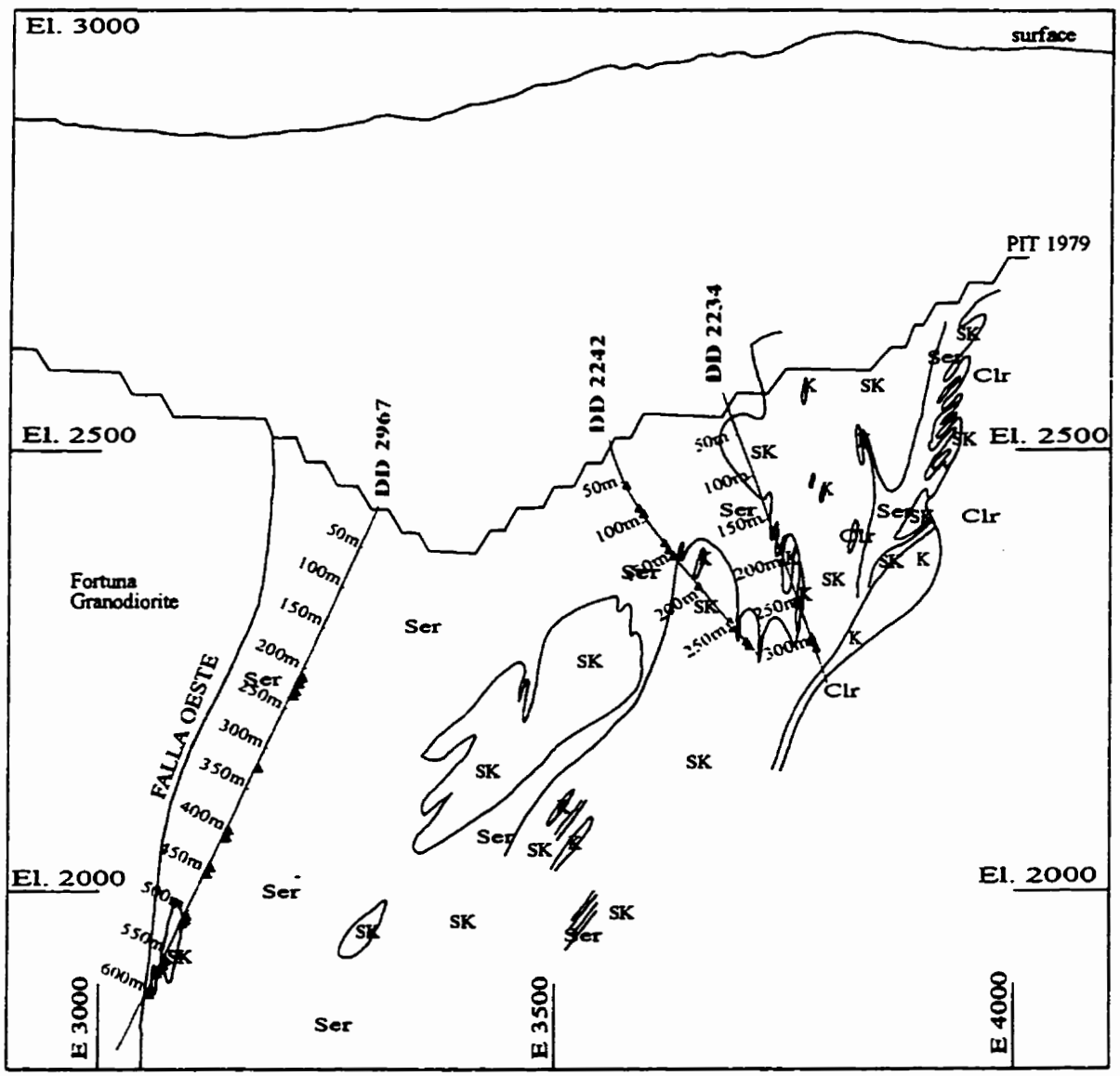

Figure 3.17. Distribution of sphalerite assemblages in cross-section 4500N.

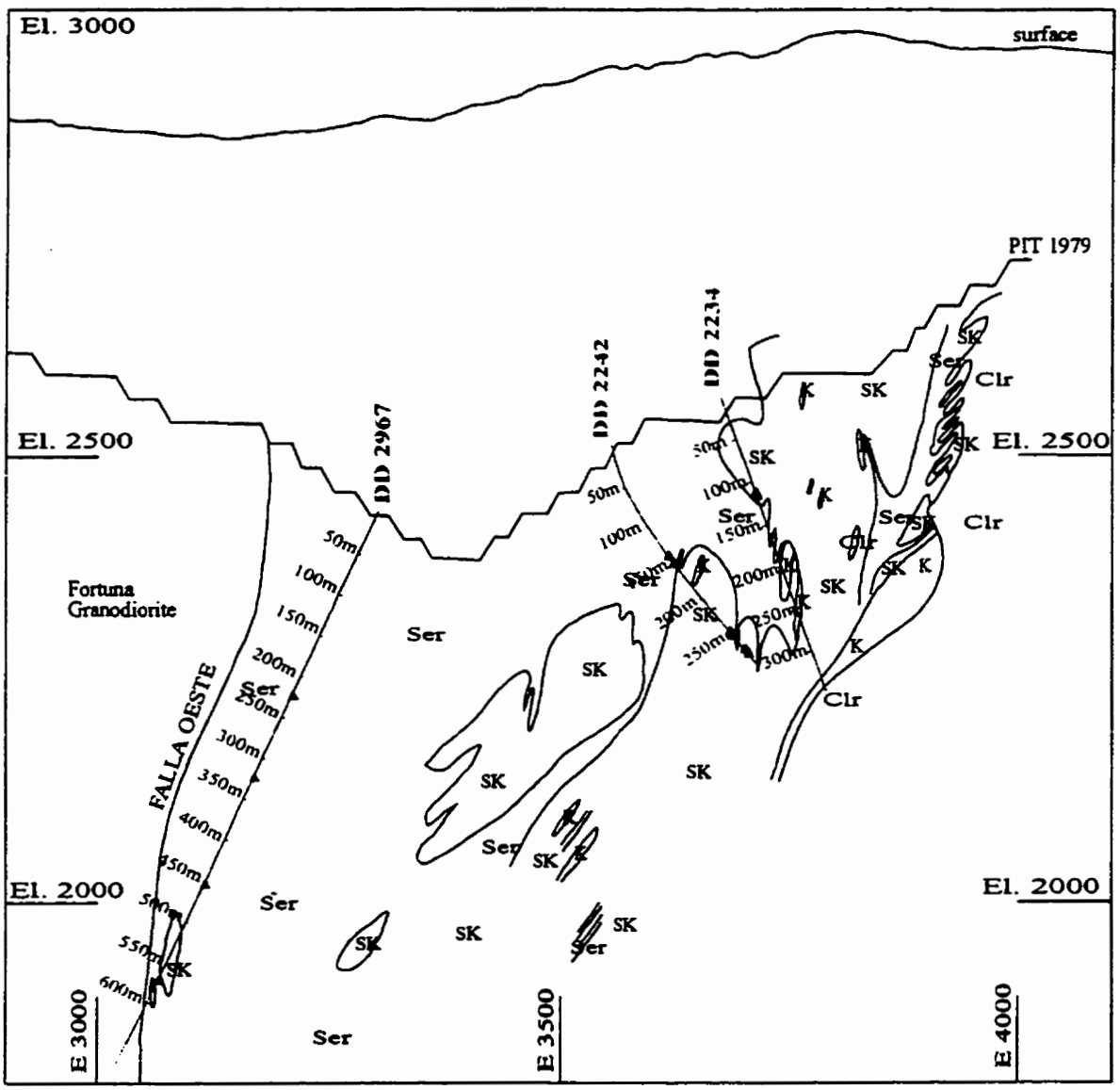

Figure 3.18. Distribution of chalcopyrite-dominated assemblages in cross-section 4500N.

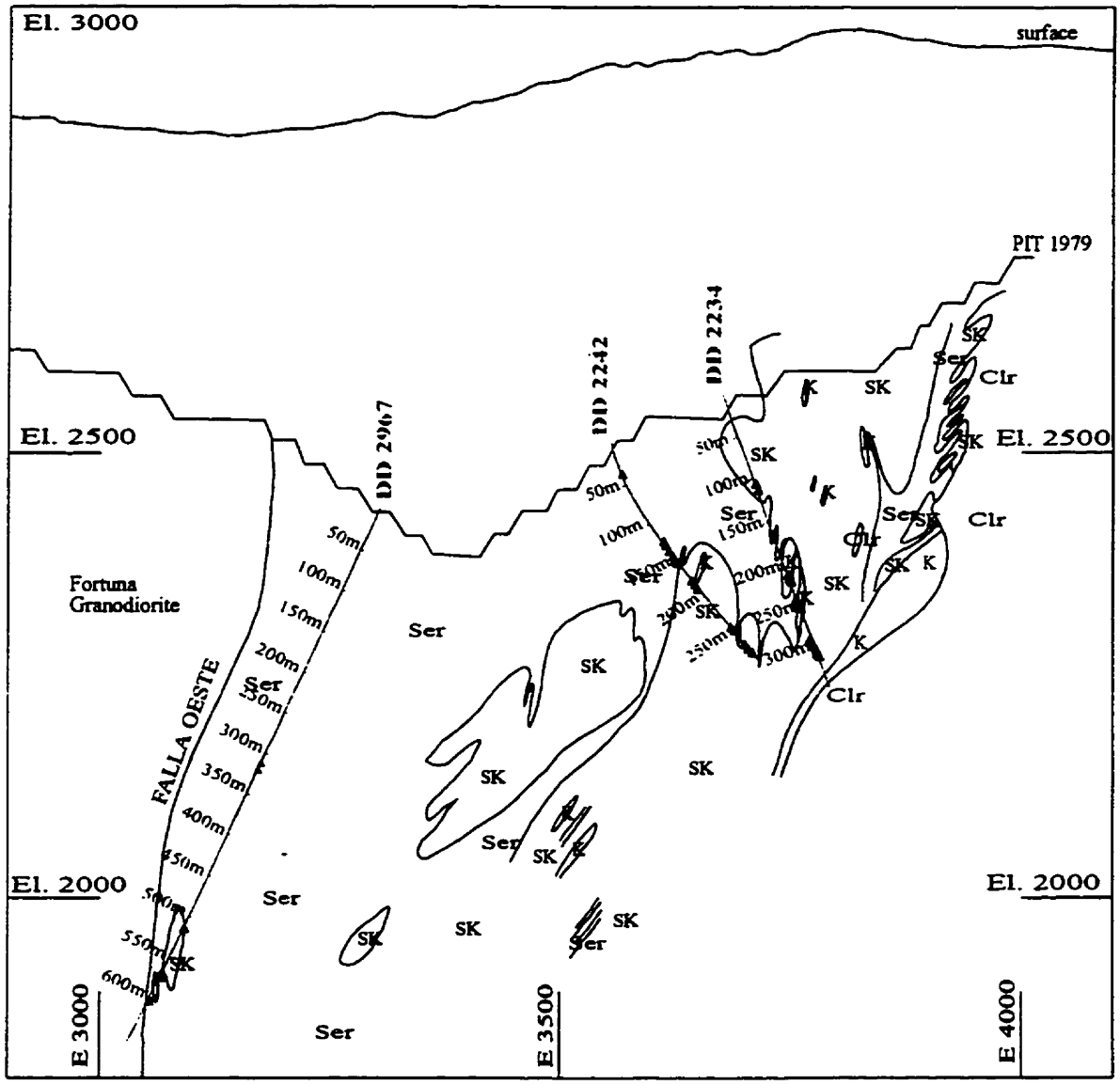

Figure 3.19. Inferred paragenetic sequence of minerals at Chuquicamata, section 4500N.

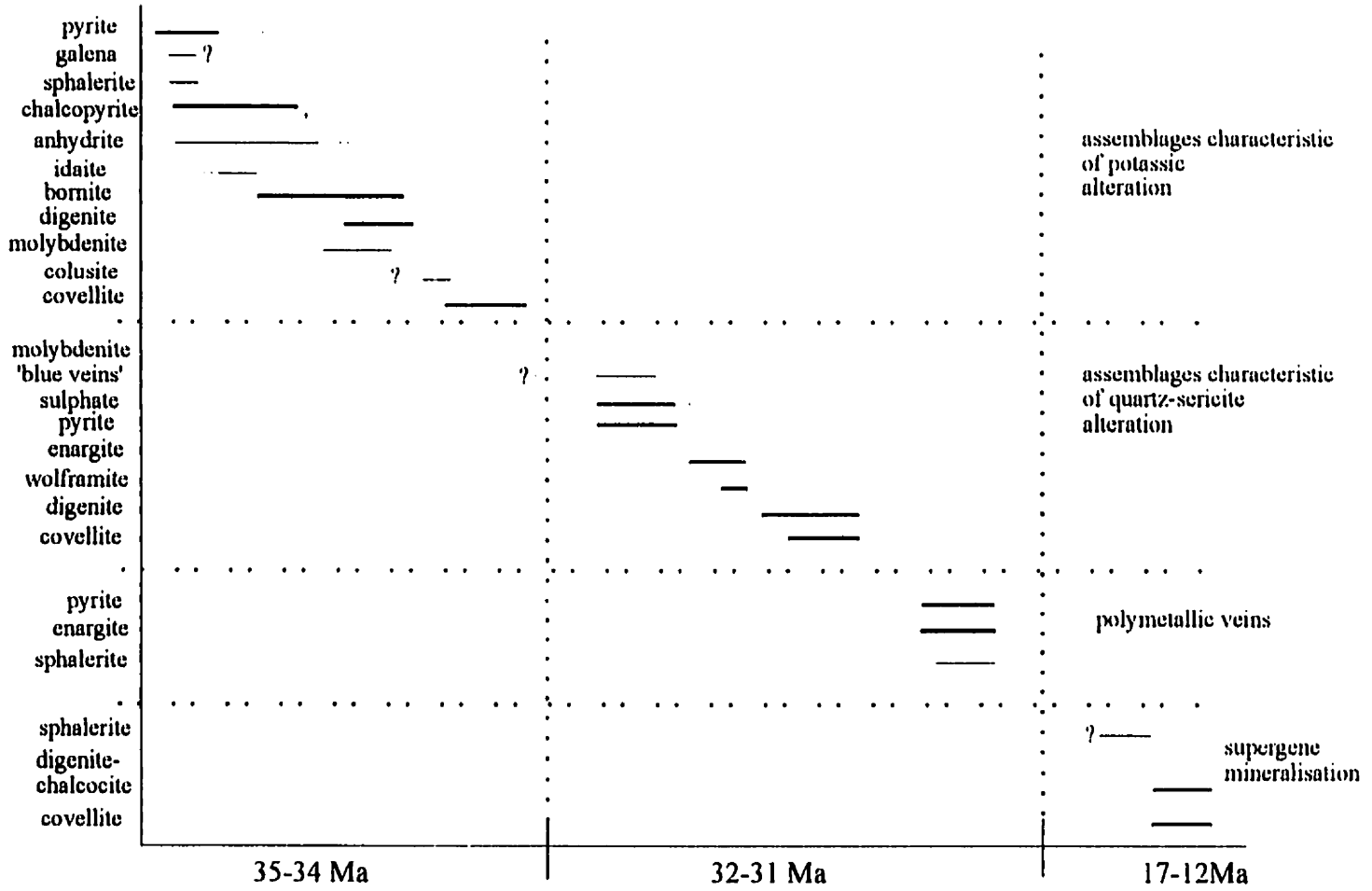

3.6 Hypogene vs Supergene Covellite

Are hypogene and supergene covellite different, and can we come up with a set of criteria to distinguish them? This was one of the major questions we started out with. After detailed study of the sulphide assemblages in Chuquicamata's 4500N section, we can summarise the observations and data gathered regarding covellite in the porphyry system in the following way: with respect to mineralogy (grain morphology and mineral assemblages) and to chemistry (minor elements, specifically iron).

How does covellite occur in Chuquicamata? In the high-temperature potassic zone, covellite is most often found as a replacement mineral. It is most common as a decomposition product of chalcopyrite (e.g., cu455), although it can also be found originating from more copper-rich sulphides, such as digenite (e.g., cu482). Although obviously a secondary phase in these samples, covellite is still of hypogene origin, a fact which is left in no doubt due to the common association of hypogene anhydrite with these assemblages. In the quartz-sericite zone, covellite occurs in a very fine-grained acicular form associated with digenite (e.g., cu192), or as disseminated fine subhedral grains in massive-to-vein sulphate (usually anhydrite, although it has been associated with barite). By contrast, most of the typical supergene covellite found at Chuquicamata is massive (e.g., cu214).

With respect to mineral asssemblages, we have seen that covellite occurs in many assemblages. In the hypogene environment, covellite occurs as a replacement phase in the potassic zone, where it is also associated with high-temperature idaite. In the quartz-sericite zone, covellite is mainly associated with digenite in what is taken to be an equilibrium assemblage, whether by eutectic growth or by exsolution. While we do observe samples of supergene covellite attacking aggregates of small rounded pyrite grains and chalcopyrite veinlets, the most typical samples at Chuquicamata are associated with the later-stage hydrothermal veins, specifically the coarse enargite-pyrite veins (e.g., cu213).

The most striking difference between hypogene and supergene covellites at Chuquicamata is seen in their chemical composition. As we have seen, hypogene covellite contains significant iron, up to about 5 weight percent. This has not been described before, as any reference to iron-bearing hypogene covellite in the literature has been dismissed as due to calibration or

identification problems. In direct contrast, samples of supergene covellite from Chuquicamata show almost no variaton from stoichiometric CuS. Where it does deviate, the small iron content can be attributed to an inherited impurity.

The first two points brought up here may be useful in mapping the deposit, in aiding to distinguish hypogene from supergene ore. While the chemical character of covellite is not useful for field mapping, it may help to differentiate assemblages in other sections of the deposist, where the mineralogical relationships outlined above may not hold true.

CHAPTER 4: Temperature limits on assemblages from experimental work on Cu-Fe-S phases

4.1 Introduction

The Cu-Fe-S system is the most-studied ternary sulphide system. Still, it remains one of the most confusing, due to the extensive solid solutions and the presence of metastable and unquenchable phases. Much work has gone into defining the minerals and phases and coming up with an accurate phase diagram, but it still has many problems, especially at low temperature (Barton and Skinner 1979). It was suggested long ago that the ranges in composition of the solid solutions might offer precise geothermometers, but most phases fail to preserve these compositions upon cooling. However, enough experimental work has gone into the most common phase relations to make them useful in the study of natural systems, although caution must be used in the application of equilibrium diagrams to natural assemblages.

4.2 Assemblages in the Cu-Fe-S System

Interpretation of ore mineral textures in this system are notoriously difficult, since equilibration between minerals such as bornite, chalcocite, digenite, and copper is so rapid, even at low temperatures, that the compositions and textures of the minerals record only their most recent histories (Barton et al. 1963). It has been frequently observed that reactions involving chalcopyrite are slower than the rest, and those involving pyrite are much slower; the tendency for ores representing the copper-rich porion of the Cu-Fe-S system to violate the phase rule is attributed to the inertness of pyrite (Barton et al. 1963).

One excellent example of this behaviour is seen in the coexistence of chalcopyrite and covellite in an apparently eutectic intergrowth (documented in sample cu494, Section 3.3.3). While equilibrium phase diagrams clearly show that these two minerals do not occur together, their observation in natural systems seems to defy the phase rule. The assemblage covellite + chalcopyrite is the chemical equivalent of, and appears to represent, idaite. The absence of idaite from the assemblage is explained by Schneeberg (1973): idaite decomposes to digenite + covellite + pyrite at temperatures below 223°C. Covellite and chalcopyrite do not react at 200°C but do at

higher temperature. The reluctance of pyrite to grow permits idaite to decompose to the metastable assemblage covellite + chalcopyrite at lower temperature.

Not all of the original idaite in Chuquicamata is represented by chemically-equivalent breakdown assemblages. The compositions of the idaite specimens found at Chuquicamata (described in Section 3.2.11) correspond to $Cu_{5.5}FeS_{6.5}$, the composition of the phase described by Frenzel (1959) and found to be stable below 501°C (Yund and Kullerud 1966), as opposed to the supergene phase, also (confusingly) called idaite; this supergene phase seems to have the same optical properties as the high-temperature idaite, but its composition has been fixed at Cu_3FeS_4. We are obviously dealing with the high-temperature phase at Chuquicamata, but questions still abound. Should the preserved idaite in the potassic zone of alteration be interpreted as having been quenched at a temperature above about 225°C? This is one possibility, that would give some mineralogical credence to the suggestion that the system underwent (possibly quite rapid) uplift and some exhumation after the event that resulted in potassic alteration (Zentilli et al. 1995).

Many individual temperature points for specific reactions can be specified for the Cu-Fe-S system; in the direct determination of phase relations, the most useful data direct attention to the circumstance where one assemblage of phases replaces another. Table 18 lists the invariant points of the reactions which are of particular interest to this study.

Normal hypogene ores in a hydrothermal environment already serve to place assemblages between 200 and 500°C; the question is, can specific assemblages help to place further constraints on temperature? It is obvious from Table 16 and from data presented in Chapter 2 that assemblages in the Cu-Fe-S can be at least somewhat useful in this regard. Several samples from the zone of potassic alteration at Chuquicamata preserve the assemblage covellite + idaite (documented in Chapter 3); since above 482°C the same bulk composition would precipitate digenite + sulphur melt, we can conclude that this assemblage formed below 482°C. In one of those samples (cu465), idaite is found with chalcopyrite, and minor bornite. Since idaite does not normally form ties with chalcopyrite (Figure 4.1), this assemblage is most likely due to the breakdown of high-temperature pyrite + bornite to idaite + chalcopyrite at 300°C (Yund and Kullerud 1966). In this way the temperature of formation for sample cu465 can be constrained to between 300 and 482°C.

Figure 4.1. 300°C isothermal section. Assemblages consisting of two condensed phases are indicated by numeral 2; tie-lines are not shown in these fields. Compositional limits of solid solutions and compositions of coexisting phases are only approximate (from Yund and Kullerud 1966).

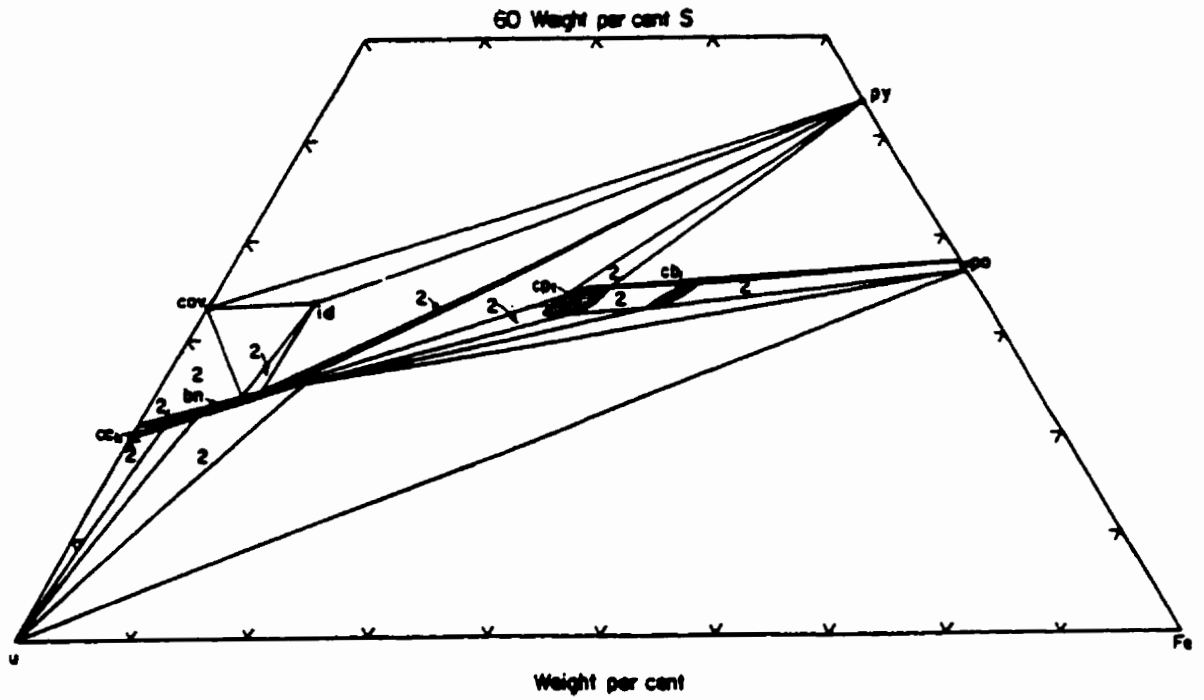

Table 16. Summary of invariant points from the condensed Cu-Fe-S system of possible interest to the geothermometry of ore deposits (after Barton and Skinner 1967).

Low-T Assemblage	High-T Assemblage	Temperature (C)	Remarks
sulphur-rich bornite	bornite + digenite + chalcopyrite	~75	
digenite	high digenite	120	in presence of bornite
bornite	high bornite	<200	in presence of high digenite
cubanite	tetragonal (?) cubanite	~200	not reversible
bornite	high bornite	228	not quenchable
digenite + chalcopyrite	bornite + pyrite	230 +/- 5	
tetragonal (?) cubanite	isometric cubanite	260	
high bornite + high digenite	complete fcc solid solution	335	
copper + isometric cubanite	bornite + pyrrhotite	~325	
pyrrhotite + chalcopyrite	isometric cubanite + pyrite	330 +/- 5	
pyrite + covellite	idaite + sulphur melt	434	
pyrrhotite + copper	bornite + iron	475	
covellite + idaite	high digenite (ss) + sulphur melt	482	
idaite	high digenite (ss) + pyrite + sulphur melt	501	
chalcopyrite	isometric chalcopyrite	547 +/- 5	sulphur saturated compounds; in presence of cubanite, inversion lowers to ~480 C
isometric cubanite + isometric chalcopyrite	isometric chalcopyrite (ss)	~550	
pyrite + bornite	isometric chalcopyrite + sulphur melt	568	
pyrite + isometric chalcopyrite	pyrrhotite + sulphur melt	739	
pyrrhotite + digenite + iron	melt (eutectic, 15% Cu, 41% Fe)	912	

References: Brett (1963), Brett and Yund (1964), Greigg et al. (1955), Kullerud (1960), Morimoto and Kullerud (1961), Roseboom and Kullerud (1958), Yund and Kullerud (1961, 1963), Merwin and Lombard (1937).

This is useful, but to be able to translate approximate temperatures across more than just one sample, we need to look at the more common sulphide assemblages. In the potassic zone, the digenite-bornite assemblage, for instance, is prevalent and may have some temperature implications of its own. Can we say anything about temperature based on textural observations? Digenite-bornite is found here in exsolution relationships, where reconstruction of the original state of the grain is possible (that is, it is unlikely that part of the exsolved material has migrated out of the host grain). Even so, can we say that the preserved digenite-bornite exsolution relationships formed at higher temperature than the abundant digenite-bornite eutectic intergrowths found in both potassic and quartz-sericite zones of alteration? Exsolution occurs on cooling below solid solution, where one phase becomes saturated with the other as the temperature decreases. Although a precise temperature connot be determined, for digenite and bornite exsolution occurs somewhere in the neighbourhood of 335°C. Preserved exsolution assemblages probably formed from grains that were precipitated above 335°C, whereas eutectic intergrowths should have formed below that, because there is not much solid solution in the samples studied here (i.e., both digenite and bornite are relatively pure when they occur together). It is possible that what we have interpreted as eutectic intergrowths are actually high-temperature grains where the pattern of exsolution is characterised by the two phases separating completely.

In the quartz-sericite zone, the most common assemblages are those with digenite + covellite. Experimental studies show that covellite is CuS without, so far as has been shown, the capacity to form solid solutions (except possibly with blue-remaining covellite) (Ramdohr 1980). However, with increasing temperature above 300°C digenite has an increasing capacity to dissolve CuS or Cu_2S; high-temperature digenite in natural occurrences can dissolve up to 32% of CuS in excess of Cu_2S (Buerger 1941). At Chuquicamata we see numerous exsolution patterns of digenite with covellite, where covellite occurs as lamellae parallel to (111) (e.g., sample cu441), or in thin tabular tufted to feather-like masses in digenite (e.g., sample cu205). These digenite assemblages must have formed with excess CuS well above 300°C, whereupon covellite was exsolved on cooling. However, compositional variations in digenites from Chuquicamata (detailed in Chapter 3, Section 3.2.3) show that they had not dissolved much Cu_2S. Solid solution between digenite and Cu_2S becomes complete above 435°C, and since digenites from Chuquicamata are

compositionally closest to the 'digenite' end-member of the solid solution, an upper limit of 435°C can be placed on these assemblages.

4.3 Other Assemblages

Wolframite assemblages, which were described in some detail in Section 3.2.10, are found only in the zone of quartz-sericite alteration at Chuquicamata. We would therefore suspect them to have formed at a lower temperature than some other assemblages. The composition of the wolframites is decidedly toward the hubnerite variety, with minor iron contents. As described previously, studies show that the intermediate member of the hubnerite-ferberite series (i.e., wolframites with the highest degree of mixing of Mn and Fe components) has the highest crystallisation temperature, while formation of the end-members depends more on factors such as the Eh and pH of the solutions and the partial pressure of H_2S than it does on temperature (Singh and Varma 1977; Voyevodin 1981). It would then make sense to interpret the observed wolframite assemblages at Chuquicamata as lower temperature (in the 250°C range), since high-sulphidation systems take most of the iron into the early sulphides, leaving Mn-rich wolframites to crystallize in later-stage hydrothermal activity.

Also interpreted as a result of later-stage hydrothermal activity are the coarse enargite-pyrite-(sphalerite) veins found in quartz-sericite alteration zones. The temperature of these veins is difficult to fix, but the composition of the enargites is a clue. Enargite in these veins contains significant antimony, which the low-temperature polymorph of enargite, luzonite, usually does not. Also, X-ray diffraction studies on three samples of enargite from these veins confirm that we are dealing with enargite and not luzonite. Since the inversion temperature from enargite to luzonite has not been fixed but is somewhere in the range of 275°C to 320°C (Maske and Skinner 1971), we can conclude that the veins formed above the inversion temperature, and that the late-stage hydrothermal activity was still at relatively elevated temperatures. Other enargite assemblages are interpreted as having formed at even higher temperature.

Other sulfosalts in Chuquicamata are potentially useful as well. Hall (1967; compiled with other data in Barton 1970) demonstrated that a given sulfosalt is not appreciably more stable than any of several alternative configurations that represent the same bulk composition. Therefore,

relatively small changes in temperature and composition have the ability to strongly modify the configuration of sulfosalt phase fields, and for this reason natural sulfosalt assemblages may contain precise thermochemical information (Barton 1970). Unfortunately, data for complex sulfosalts such as colusite are few.

4.4 Summary

Figure 4.2 provides a graphical summary of the inferred temperatures of mineralisation for sulphide assemblages in the 4500N section. In the potassic zone, pyrite was the first mineral to crystallize, probably at temperatures of 500°C or higher and continuing down to lower temperature. Chalcopyrite could have formed anywhere below 557°C, but probably precipitated above 400°C or so, since the common digenite-bornite assemblage is interpreted to have formed later than chalcopyrite. Digenite-bornite assemblages formed at +/- 335°C, where the +/- (although it was more likely at a higher temperature than a lower one) could be 50° or greater. Idaite assemblages, although not very common, are in good agreement with other assemblages in this zone, having formed between 300 and 482°C. Temperatures for the duration of the potassic event could have been between about 600 and 275°C, but it is extremely unlikely that temperatures reached below 300° at this stage, and they may have stayed well above that, in the 400 to 450° range.

Less interpretation can be made using various sulphide assemblages in the quartz-sericite zone, but the most common assemblages have been well-documented. The digenite-covellite assemblages formed between 300 and 435°C. Wolframite and enargite, crystallizing with or soon after pyrite, must have formed in this range as well, or at slightly higher temperatures, since covellite-digenite follows these phases in the paragenetic sequence. Later assemblages such as the 'late-stage' hydrothermal veins of enargite-pyrite must have formed above 275 to 320°C. Since the absolute ages of the alteration events and their associated mineralisation have been determined at 34+/-1 Ma for the potassic zone and 31+/-1 Ma for the sericitic zone, we can make some interpretations about the cooling of the system. If the potassic event cooled from 600°C or higher to 350-450°C in <<1 m.y., it is improbable that the system stayed at that temperature for the next 2-3 m.y., especially when the spatial associations are considered (i.e. the fluids would have to

Figure 4.3. Summary of temperatures of mineralisation estimated from sulphide assemblages at Chuquicamata, section 4500N. See text for specific samples. Temperatures for pyrite and chalcopyrite are inferred only from paragenesis.

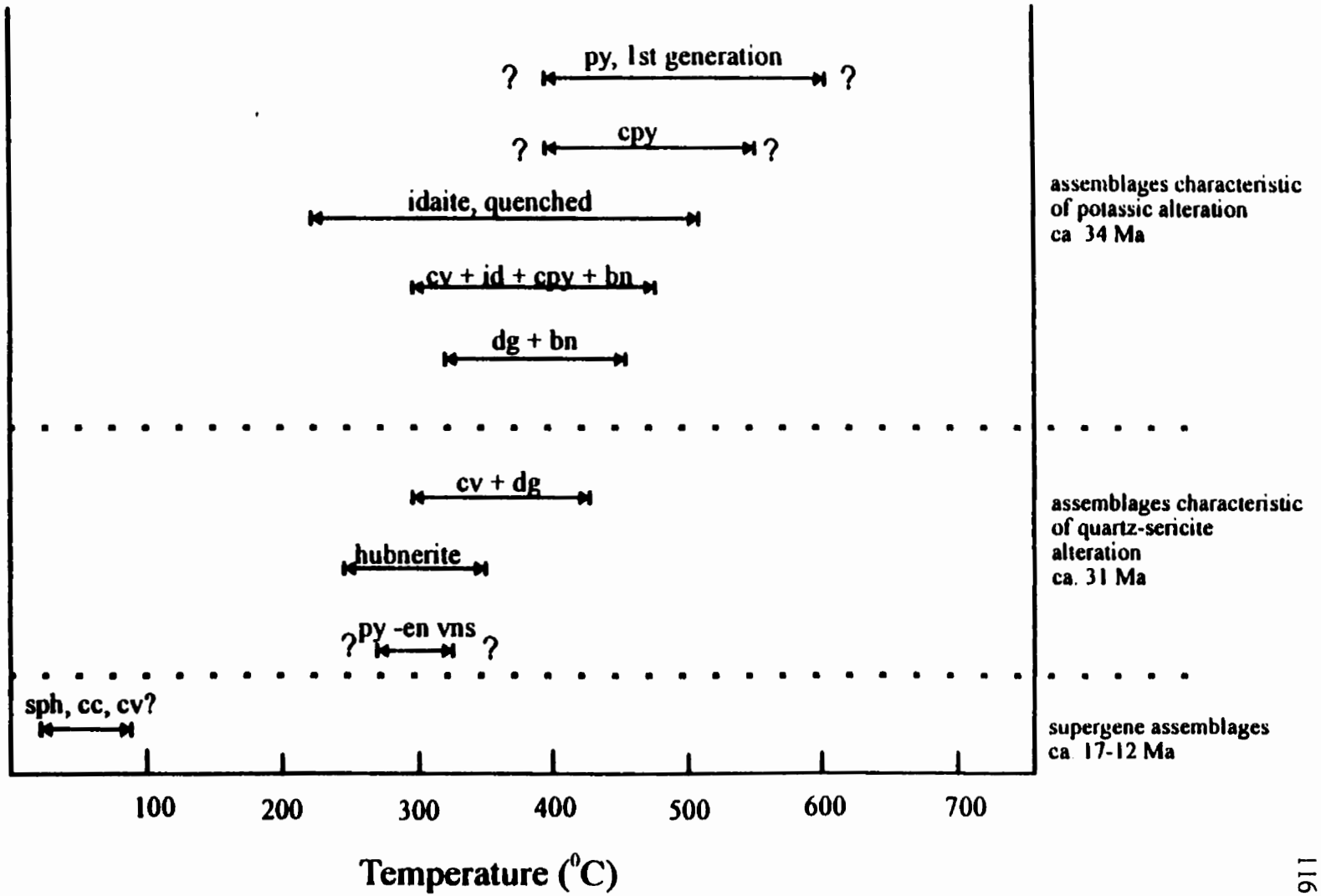

have travelled up to several kilometres without losing their heat to the country rocks). A more likely interpretation is that a second heating event at 31 Ma produced the hydrothermal fluids responsible for ore deposition in the quartz-sericite zone, in agreement with the theory postulated by Zentilli et al. (1994).

Other assemblages that can provide information about the formation of the system include those containing low-temperature phases like anomalous bornite, and the supergene assemblages. The so-called 'anomalous bornite' or sulphur-rich bornite, has been found to form from low-temperature solutions below 125^{0}C (Yund and Kullerud 1966). It is unclear whether this implies only supergene processes, or whether it can form from very late hydrothermal fluids. Recognition of this phase is difficult, and the Chuquicamata samples that may correspond to it should be studied further for positive identification and for possible evidence of supergene enrichment.

In the supergene environment, dated at 17-12 Ma (Sillitoe et al. 1996), the possible 'supergene' sphalerite is a new phenomenon and to date there is not much information on which to rely. It may have formed up to 100^{0}C, well above what would usually be considered reasonable for supergene processes. Supergene covellite and chalcocite probably formed between 25 and 75^{0}C.

CHAPTER 5: STABLE ISOTOPE STUDY

A stable isotope study can yield valuable information when used in conjunction with other mineralogical and geochemical studies of a mineral deposit. With an integrated study, some insight can be gained into the physical/chemical conditions of ore formation (e.g., temperature, pH, redox state, pressure, depth), the source of the ore constituents (especially sulphur, carbon and metals), the mechanisms of transport, and composition of the fluids, specifically sulphide/sulphate ratios. The scope of the isotopic study done here was limited to a few well-chosen samples from the 4500N section at Chuquicamata to gain some insight into temepratures of equilibration and the possible source of the sulphur.

Thirty-four samples of sulphides and sulphates were analyzed for their sulphur isotope compositions at the NERC Isotope Geoscience Laboratory (British Geological Survey) in Nottingham, UK (three samples were duplicates to assess precision of the results), under the supervision of Dr. Baruch Spiro.

All of the samples were separated manually by crushing and sieving the rock to between 80 and 60 mesh (corresponding to 180-250 microns), and hand-picking the individual grains. Sample sizes sent for analysis varied between 8.0 and 30.0 mg.

5.1 Sulphur Isotope Theory and Mechanisms of Fractionation

Sulphur has four stable isotopes. Their atomic numbers and natural abundances are as follows:

S^{32}	S^{33}	S^{34}	S^{36}
95.1%	0.74%	4.2%	0.02%

The isotopic ratio in any given reservoir is expressed as the heavy isotope over the light isotope, in this case for the two most abundant isotopes, i.e. the ratio of S^{34}/S^{32}. Different reservoirs (e.g., minerals) may have different isotopic ratios. These differences are measurable and imply that there must be fractionation of the sulphur isotopes. There are two mechanisms of fractionation in the sulphur system. The first is fractionation during kinetic reactions, i.e,. a unidirectional reaction that directly affects the sulphur bond (Nielson 1979), of which an excellent

example is the bacterial reduction of sulphate to H_2S; this bacterial reduction accounts for most of the fractionation in the sulphur cycle. The second mechanism is isotopic exchange under equilibrium fractionation. Typical equilibrium systems include sulphate and sulphide in a magmatic environment, and dissolved sulphide and precipitating sulphide minerals in hydrothermal fluids. For sulphur-bearing minerals, the fractionation effect at constant temperature is largest between sulphate-sulphide pairs (where S^{34} is preferentially taken into the sulphate), and smallest but still measurable between many sulphide-sulphide pairs, where there is a preferential order of concentrating S^{34}.

If evidence can be obtained that indicates the source of the sulphur in the sulphides, it helps in determining the processes by which some base-metal deposits have formed (Jensen 1967). The isotopic composition of any compound A can be expressed as a "del" value:

$$\delta_A = ((R_A - R_{st}) / R_{st}) * 10^3$$

where R_A is the isotopic ratio in compound A

and R_{st} is the isotopic ratio defined for a standard sample

and del values are measured in per mil, parts per thousand.

For sulphur:

$$\delta S^{34}\,‰ = ((S^{34}/S^{32}_{\text{sample}} - S^{34}/S^{32}_{\text{CDT}}) / S^{34}/S^{32}_{\text{CDT}}) * 10^3$$

where CDT is troilite from the Canon Diablo iron meteorite, the standard for sulphur, where $S^{34}/S^{32} = 0.0450045$.

Positive per mil deviations indicate enrichment of S^{34} relative to the standard, while negative per mil deviations indicate depletion.

Ohmoto (1972) pointed out that the δS^{34} of an ore-bearing fluid indicates (loosely) the origin of the sulphur in the fluid. Sulphur of mantle magmatic origin is assumed to have a del value around zero, comparable to the standard (approximating the primordial earth and the mantle) (Ohmoto and Rye 1974). A δS^{34} of about +20‰, approximately that of seawater, implies marine evaporites or seawater as a source of the sulphur. Intermediate values suggest that the sulphur may have been remobilized from the surrounding rock.

In magmatic hydrothermal ore deposits the ore solutions are derived at high temperatures and there is not much isotope fractionation resulting from exchange reactions (Jensen 1967).

Magmatic hydrothermal solutions become well-mixed during crystallization of the parent magma; the result is homogenization of the isotopic composition. Therefore, when mineralizing solutions escape from the magma, very little sulphur isotope fractionation occurs. The majority of δS^{34} values of sulphides from porphyry copper deposits are between -3‰ and +1‰, which has led to the proposal of a deep crustal or mantle origin of the sulphur (Hoefs 1987).

The isotopic difference between two coexisting (equilibrated) sulphur-bearing minerals or mineral phases may originate from temperature-dependent fractionation effects. The fractionation factor, α, is defined as the ratio of the isotopic ratios of any two compounds A and B, i.e. $\alpha_{A\text{-}B} = R_A/R_B$. This fractionation factor for isotope exchange between minerals is a linear function of $1/T^2$, where T is temperature in degrees Kelvin. The relationship between fractionation and temperature is given by the equation:

$$10^3 \ln\alpha = A/T^2 + B$$

where A and B are experimentally- or theoretically-determined equilibrium constants for a given system, i.e., A and B are specific for any mineral pair. Experimentally-determined curves for common sulphate- sulphide mineral pairs are based on the work of Sakai (1968), and are used in this thesis. If the fractionation factor is known, these curves can be used to find the temperature of equilibration.

5.2 Method of Analysis

Sulphur-bearing mineral phases must be separated and analyzed individually. Samples from Chuquicamata were chosen based mainly on ease of separation; many of the copper-sulphides are very finely intergrown, and separation of sulphur-bearing phases is difficult. Samples of coexisting sulphates (usually anhydrite) and sulphides (pyrite or chalcopyrite) were picked from fine to medium-grained sulphate veins in the quartz-sericite and sericite-overprinting-potassic zones of alteration. Electron microprobe analyses of the samples to be separated ensure the homogeneity of the phases. The samples were hand-picked and X-ray diffraction was performed on most of the separated samples to assess their purity. The minerals or mineral phases are converted to SO_2, in one of several ways. The two most common are direct oxidation and oxidation of the sulphide to a sulphate. In the latter method, the sulphate is then precipitated as

barium-sulphate and reduced to barium-sulphide at a temperature of about 1000°C when mixed with excess carbon. The barium-sulphide is treated with acid to evolve H_2S, and precipitated as silver- or cadmium-sulphide, which is rapidly and easily oxidized to SO_2. The gas is then analyzed in a mass spectrometer, a device that separates charged atoms and molecules on the basis of their masses, based on their behaviour in a magnetic field. Figure 5.1 is a simplified diagram of a basic mass spectrometer. The spectrometer is made up of: the inlet system; the ion source, where ions are formed, accelerated and focused into a beam, usually by bombardment of electrons; the mass analyzer, where ion beams are separated according to their mass:charge ratio by passing them through a magnetic field (the ions are deflected into circular paths, with radii proportional to the square root of M/e (mass/charge)); and the ion detector, which collects the separated ions, converts them into electrical impulses and feeds them into an amplifier. The ion beams of the two isotopes desired must be collected simultaneously so that the isotopic ratios of two samples can be compared under nearly identical conditions.

Values of $\delta S^{34}/S^{32}$ can be determined in a mass spectrometer to +/- 0.2 $‰_0$.

5.3 Purpose

If measurable equilibrium fractionation can be shown to occur in the formation of coexisting minerals, then sulphur isotopes can be used to estimate the temperature of equilibration. How valid are these isotopic temperature estimates? One must assume not only equilibrium between coexisting mineral phases at the time of deposition, but also preservation of isotopic equilibrium and accuracy of calibration curves where α is related to temperature.

If equilibrium cannot be shown, sulphur isotopes are useful for indicating the source of the sulphur, a major factor in controlling the sulphur isotopic composition of hydrothermal ore deposits.

Del (δS^{34}) values of sulphides and sulphates reflect not only temperature and source, but the pH (relative acidity) and f_{O2} (oxygen fugacity) of the ore-bearing solutions as well (Ohmoto 1972). Any knowledge gained about these factors brings us closer to understanding the complex conditions of ore deposition.

Figure 5.1. Schematic diagram of a basic mass spectrometer.

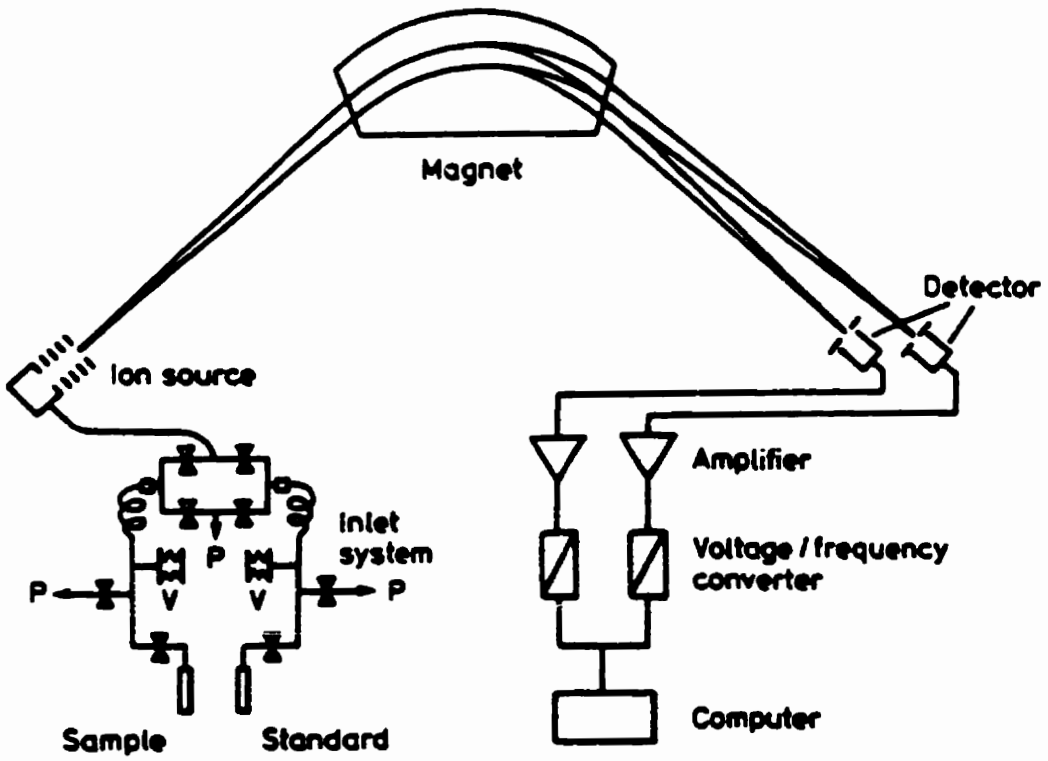

5.4 Results for the Present Study

Table 17 lists isotopic data for the 34 sulphur-bearing mineral separates from Chuquicamata.

Isotope fractionation theory predicts that hypogene sulphate should be enriched in δS^{34} relative to any coexisting (equilibrated) sulphide (Sakai 1968). For vein samples of sulphate-sulphide, then, such as sample cu199, which has gypsum veinlets with disseminated to semi-massive pyrite and lesser digenite, a significantly higher δS^{34} value is expected for the gypsum than for the pyrite. As shown in Table 19, actual $\delta^{34}S$ values agree with the theory of fractionation. In a 'typical' porphyry copper deposit (Field and Gustafson 1976), hypogene sulphates range in δS^{34} values from about +7.3 to +17.0 permil, with a mean of +10.7. Some of the Chuquicamata samples (e.g., cu499, cu502) contain both gypsum and anhydrite, as massive gypsum with anhydrite cores; the gypsum in these samples is interpreted to have formed by simple (supergene?) hydration of hypogene anhydrite. As such, it is expected to inherit the sulphur isotopic composition of the anhydrite, and should be enriched in S^{34}. The data clearly indicates this enrichment; samples cu499 and cu502 have gypsum values above +17 permil, in good agreement with hypogene anhydrite isotopic compositions, and considerably heavier than the sample of primary gypsum (cu199). In contrast, any supergene sulphate derived from the oxidation of sulphide-sulphur is expected to be enriched in S^{32} (Field 1966). The mean $\delta^{34}S$ value of sulphates from Chuquicamata is 15.9 permil, considerably higher (i.e., the sulphates are considerably heavier) than at El Salvador.

Hypogene sulphides from most deposits generally range about 0 permil or are slightly negative; the well-studied El Salvador deposit shows a mean of hypogene sulphides of -3.0 permil (Field and Gustafson 1976). A general S^{34} enrichment in the order molybdenite >= pyrite > chalcopyrite >bornite has been predicted theoretically from bond strengths (Bachinski 1969), and observed in several deposits (Ayres et al. 1981; Field and Gustafson 1976).

Hypogene sulphides from Chuquicamata have a mean of -2.3 permil, about what would be expected for primary sulphides from a magmatic hydrothermal environment. Molybdenite shows the greatest enrichment in S^{34} over the other sulphides; pyrite is next, varying from +0.6 to -4.5 permil. A general trend can be observed, where most pyrite is compositionally heavier than

chalcopyrite and bornite, although there is significant overlap. In the two samples where coexisting chalcopyrite + bornite were analyzed (cu438 and cu453), individual values are different but chalcopyrite is consistently isotopically heavier than bornite, as has been predicted by Bachinski (1969).

Two samples of supergene sulphide, cu109 and cu214, from two cross-sections 1300m apart, have been analyzed to determine whether or not supergene covellite is isotopically distinctive relative to the hypogene sulphides. Any isotopic effect is unlikely to have formed by sulphide-sulphide equilibria in the low-temperature supergene environment (i.e., there is no fractionation (Sakai 1968)); instead, the isotopic ratio of supergene sulphides is most likely an inherited characteristic from the dominant hypogene sulphides serving as host for supergene replacement. With the sulphur isotope analyses of supergene minerals, it is sometimes possible to identify isotopically the primary host mineral (Field and Gustafson 1976). Samples of supergene covellite from Chuquicamata are between -5.0 and -5.8 permil, very consistent and significantly depleted in S^{34} compared to all of the hypogene sulphides. This depletion may be due to the effect of extremely acidic conditions in the supergene environment, since changes in pH affect the isotopic compositions of sulphides (Hoefs 1987). Another possibility (discussed in Chapter 4) is that the supergene environment at Chuquicamata was not at 25°C, as in 'typical' supergene zones, but actually at temperatures up to 100°C, where some isotopic fractionation is still expected.

5.5 Sulphate- sulphide Equilibria

Specific samples of sulphate- sulphide pairs were chosen for this study in an effort to confirm and further constrain hypotheses made about the temperature of mineralisation from sulphide phase equilibria. Sulphate- sulphide pairs work best for this kind of interpretation due to the large degree of fractionation between the two mineral species; some coexisting sulphide pairs have also been used, although they generally give lower temperatures of mineralisation, possibly due to their continued equilibration down to lower temperatures. The common equilibrium sulphide pairs at Chuquicamata, such as chalcopyrite + bornite or covellite + digenite, have not been well-calibrated and are not very useful for inferring temperatures.

Table 17. Analytical data given as δS^{34} per mil values for mineral concentrates of the Chuquicamata samples.

Sample	Description	Sulphide δS^{34}	Sulphate δS^{34}	ΔS^{34}
3200N, DD3472				
cu105enargite cu105pyrite	143.77m; sulphide-rich cc-en-py veins in shattered quartz	En -4.8 Py -3.8		
cu109covellite cu109Asulphide cu109sulphide	453.35m; veins of massive covellite in quartz, looks supergene, blanketing disseminated fg pyrite	Cv -5.0 Cv -5.8 Py -3.1		
4500N, DD2967				
cu214covellite	211.60m; typical supergene covellite in quartz-sericite rock	Cv -5.7		
cu183enargite cu183pyrite	225.10m; quartz + altered feldspars, and semi-mass. to massive vns of pyrite + enargite (large striated crystals)	En -3.6 Py -4.0		
cu185covellite cu185pyrite	234.45m; dissem. fg-mg pyrite and covellite in sericitized matrix	Cv -3.6 Py -1.6		
cu204anhydrite cu204sulphide	513.05m; abundant semi-mass. to dissem. pyrite with minor interstitial digenite, in vein of pink anhydrite in sericitized porphyry	Py -2.4	Anh +19.2 Anh +17.3	+21.6 +19.7
cu199gypsum cu199sulphide	569.42m; fg dissem. pyrite + digenite (+/- bn) and gypsum vnlets in qtz-rich rock	Py +0.6	Gyp +7.0	+6.4
4500N, DD2242				
cu433molybdenite	56.45m; abundant mo in veins and minor dissem. mo in dominantly qtz host	Mo +1.1		
cu434molybdenite	95.86m; narrow vnlets of mo, pinching and swelling, and dissem. cv +py in qtz vein host	Mo +1.3		
cu438bornite cu438chalcopyrite	139.15m; smeared-out altered porphyry with dissem. to stringer chalcopyrite + bornite	Bo -2.0 Cp -1.1		
cu453bornite cu453chalcopyrite	193.10m; abundant dissem. fg bornite + chalcopyrite, in mainly qtz host	Bo -3.6 Cp -2.4		
cu454gypsym cu454Asulphate cu454sulphide	193.78m; vnlet of mo, semi-massive and dissem. bn-cpy in potassically-altered porphyry with abundant narrow sulphate veins	Py -2.4	Gyp +16.0 Gyp +16.9	+18.4 +19.3
cu455sulphide	193.86m; abundant semi-mass. to massive cpy being replaced by massive cv	Cv-Cp -0.5		
4500N, DD2234				
cu493gypsum cu493pyrite	216.30m; semi-massive and dissem. chalcopyrite + pyrite in pink gypsum veins in sericitized porphyry	Py -4.5	Gyp +16.2	+20.7
cu499gyp/anhydrite cu499sulphide	249.15m; semi-massive pyrite aggregate +/- cpy with interstitial dg in gyp rock with anhydrite cores	Cp -3.6	Gyp/Anh +17.2	+20.8
cu502gyp/anhydrite cu502pyrite	252.15m; semi-massive patches and dissem. py+dg+cv in sericitized porphyry with abundant sulphate (blueish--anhydrite?)	Py -3.3	Gyp/Anh +17.3	+20.6
cu479anhydrite cu479sulphate cu479pyrite	294.20m; patches of massive pyrite with minor digenite in potassically-altered porphyry with minor sulphate.	Py -1.5	Anh +15.9 Anh +16.1	+17.4 +17.6

Figure 5.2 plots individual $\delta^{34}S$ values of sulphides and sulphates from coexisting pairs against the isotopic difference, or delta value, which is a function of temperature as discussed above. The delta value is a direct measurement, but the superimposed temperature scale is an interpretation only, based on an assumption of equilibrium. For sample cu199, for instance, the isotopic data suggest that the gypsum-sulphide veins formed at temperatures in excess of 700°C. This temperature is obviously not realistic for veins in the quartz-sericite zone, and we must conclude that the assemblage is not in equilibrium.

Assuming the fractionation between coexisting sulphates and sulphides in Chuquicamata is due entirely to temperature effects, the assemblages point to a restricted range for temperature of mineralisation between 300 and 375°C. All but one of the pairs that plot in this field are from the zone of potassic alteration (although sample cu204, from the quartz-sericite zone, suggests the same range of temperature or a little lower); while this is not an unreasonable temperature of mineralisation for a system as large as Chuquicamata, it is significantly lower than what would be expected for a typical high-temperature potassic zone (for instance, the El Salvador deposit, which is similar in many ways to Chuquicamata and has been well-studied). Sulphur isotope data from El Salvador, plotted in Figure 5.2, are taken from Field and Gustafson (1976) and are shown for comparison only. They will not be discussed further here. Isotopic temperatures are also low in comparison with the temperatures of mineralisation determined for Chuquicamata from sulphide equilibria (Chapter 4), although there is of course leeway in the temperature ranges determined from the sulphide petrology. So what could serve to lower the temperature of mineralisation in the potassic zone?Because much of the potassic alteration is overprinted by later quartz-sericite alteration, with which the veins of massive anhydrite + disseminated pyrite are associated, the low temperatures of equilibration from sulphur isotopic compositions point to samples, ostensibly from potassic alteration, that are in actuality the result of quartz-sericite alteration. A system the size of Chuquicamata almost certainly benefitted from the mixing of meteoric waters and magmatic waters, which, had it happened during the quartz-sericite event, would have affected the fluid temperatures. Oxygen and strontium isotopes are required to test this possibility. Mixing of magmatic water with oxidising meteoric waters could also have affected the $\delta^{34}S$ values of sulphates from Chuquicamata, which are clearly isotopically heavier than those

at El Salvador (Figure 5.2). the higher oxidation potential of the resulting fluids would result in the precipitation of 'heavier' sulphates coexisting with sulphides. However, while temperature determines the fractionations between sulphur-bearing minerals, other factors can affect the $\delta^{34}S$ values in hydrothermal deposits (Ohmoto 1972), and the isotopic data should be studied for other information it can provide about the system.

Disregarding sample cu199 then, a linear regression analysis was performed on the remaining sulphates and sulphides using Yorkfit, a weighted fit based on uncertainties in the data points (Figure 5.3). The large amount of scatter in the individual isotopic analyses (compared to the small number of analyses) gives a significant margin of error, and when the regressions are extended back to the Y-axis, the intercept estimates do not overlap. Table 18 gives the statistical analysis for the points, as performed by Yorkfit (York 1969).

Table 18. Regression analysis performed by Yorkfit for individual $\delta^{34}S$ values of sulphates and sulphides plotted against Δsulphate-sulphide for Chuquicamata, section 4500N. Absolute error for individual $\delta^{34}S$ values is 0.2 permil; error for Δ values are 0.4 permil.

	Sulphates	Sulphides
Iterations	5	5
Slope	0.7747673	-0.7094318
Intercept	1.742888	11.22243
XBar	19.57778	19.57778
YBar	16.91111	-2.666667
Sum S	34.96793	40.57881
Intercept error without Sum S	1.685688	1.585744
Intercept error with Sum S	3.767585	3.817981
Slope error without Sum S	8.58729E-02	8.078158E-02
Slope error with Sum S	0.1919298	0.194497

The important point to consider is that, although the intercepts of the lines from the sulphide data and the sulphate data do not converge, the Sum S value, a measure of whether or

Figure 5.2. Plot of sulphate and sulphide $\delta^{34}S$ permil values vs delta (Δ) values of coexisting sulphate-sulphide mineral pairs for Chuquicamata and El Salvador. El Salvador data taken from Field and Gustafson (1976). Temperature scale based on experimental work by Sakai (1968). Sulphates are samples of anhydrite from Chuquicamata, whereas sulphides are samples of pyrite or chalcopyrite from Chuquicamata. Readers are referred to Field and Gustafson (1976) for details of sulphate and sulphide samples from El Salvador.

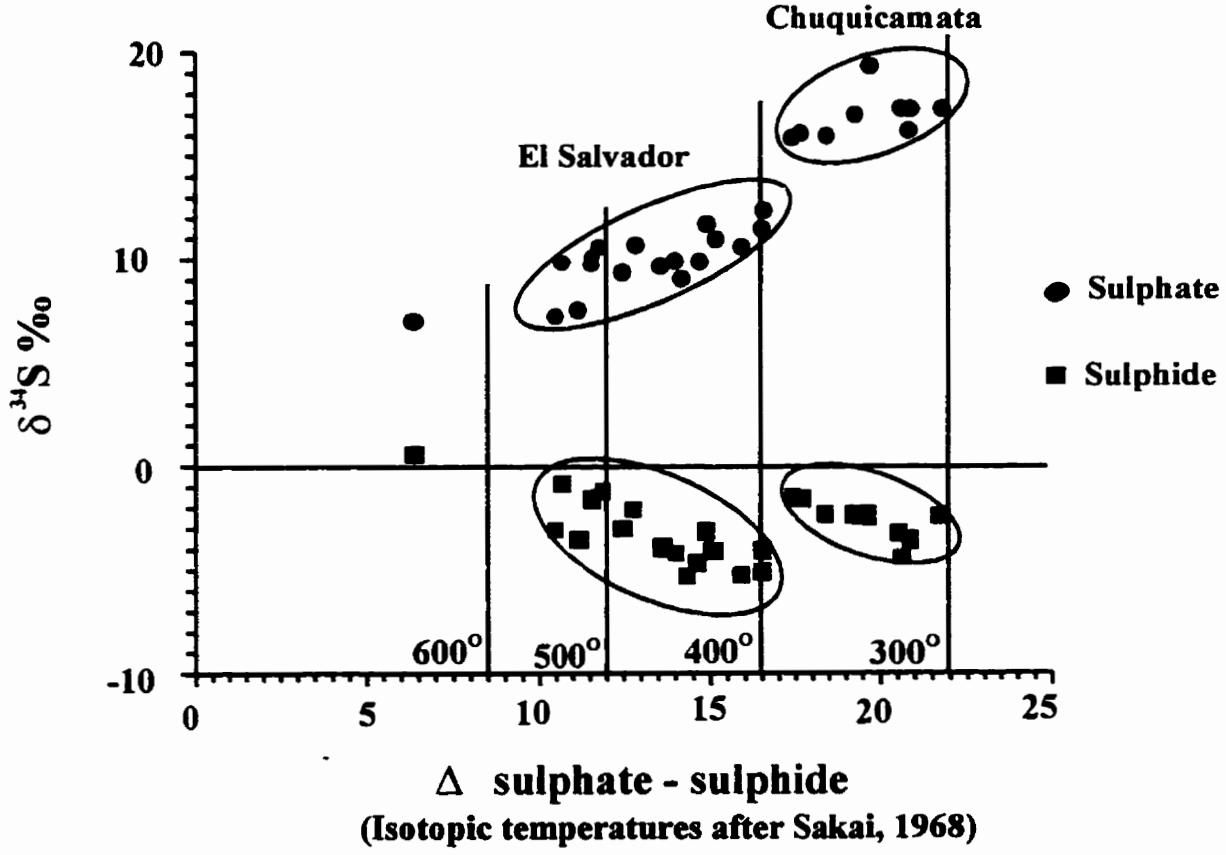

not the points fit the line *within error*, is very high. The high Sum S value implies real scatter of the data points, i.e., the points do not really fit the line. This suggests that the linear approximation is not a good model. We note, however, that a linear relationship should not be expected, since temperature, a function of the Δ value, varies. Figure 5.4 does show that the lines do diverge from a point, i.e., one line has a positive slope and one has a negative slope, therefore, the linear model can be used as a first-order approximation. If the lines, +/- errors, were to intersect along the Y-axis, this point would give a $\delta^{34}S_{\Sigma S}$ of the system that is consistent with the data (i.e., at very high temperature there is no fractionation, so at the limit we are left with the total sulphur content). In the case where the lines do not converge on the Y-axis, we are left with the question of what to use as the $\delta^{34}S_{\Sigma S}$ value. It can be seen in Figure 5.4 that the gap between the errors for the intercepts is quite small, from about +5.5 to +7.5 permil. Given that there is so much scatter in the data points, it is reasonable to assign a total sulphur content (i.e., convergence of the lines) around +6.5 permil.

If the total sulphur content ($\delta^{34}S$ value) at Chuquicamata is around +6.5 permil, and we use the isotopic composition of sulphides to represent H_2S and the sulphates to represent SO_4, we end up with a dissolved sulphate to sulphide ratio for the 31 Ma sericitic alteration/mineralisation event of 0.8:1. This ratio implies that the system would produce about 55% sulphide to 45% sulphate, a conclusion that is in reasonable agreement with direct observations. Most vein sulphides in the potassic zone at Chuquicamata are associated with sulphates, while the disseminated sulphides tend to be associated with silicate gangue. Further study is needed to assess the true extent of sulphate mineralisation in the quartz-sericite alteration zone, but from this optical study we can at least conclude that there is significantly more sulphate than has been described previously at Chuquicamata. Isotopic data place Chuquicamata in a sulphide-rich system, but shifted toward an equal sulphate-sulphide system; this placement is borne out by the assemblages described above. The dissolved sulphate:sulphide ratio implies that at the time of mineralisation concurrent with the event that resulted in quartz-sericite alteration, Chuquicamata was a slightly reducing system.

Figure 5.3. Estimate of $\delta^{34}S$ value for total sulphur content for the Chuquicamata hydrothermal system as determined from convergent lines of regression for plots of sulphate and sulphide $\delta^{34}S$ permil values vs delta (Δ) values of coexisting sulphate-sulphide mineral pairs.

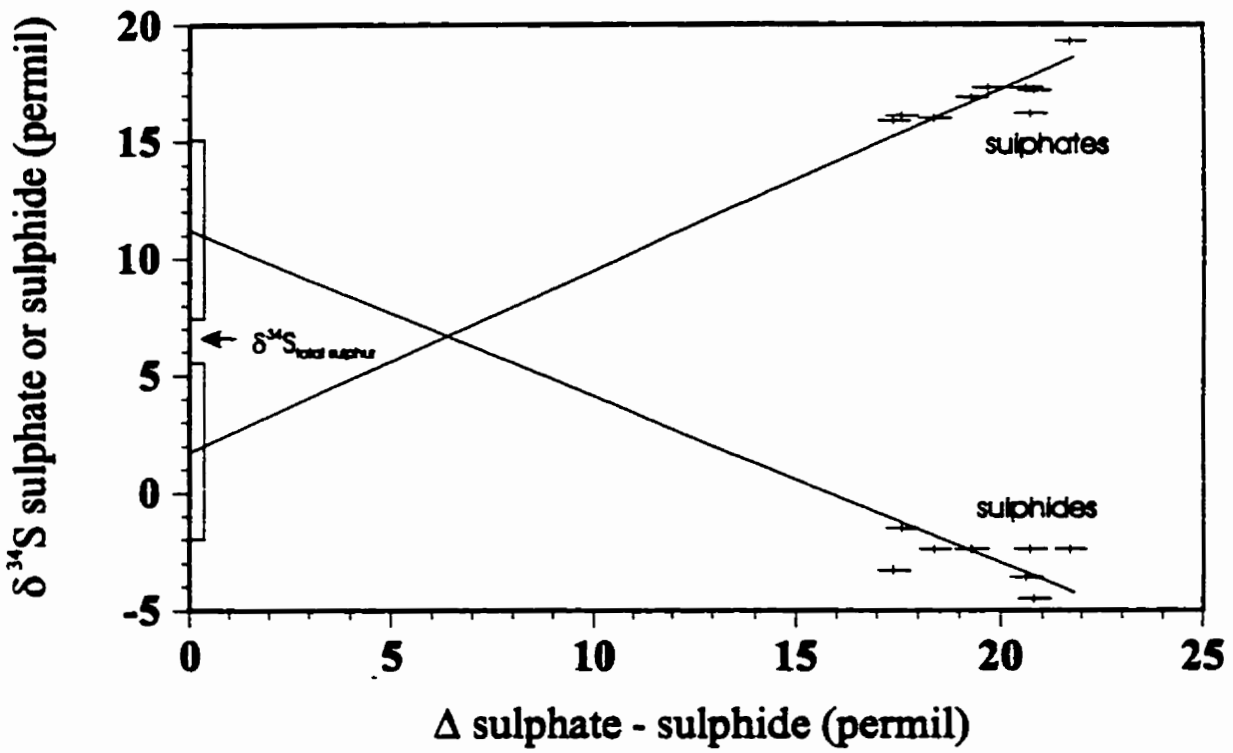

The proportions of oxidized and reduced sulphur species in solution can be evaluated in terms of temperature, pH and f_{O_2} of hydrothermal fluids (Rye and Ohmoto, 1974). Figure 5.4a shows the stability fields of sulphur phases in a pH-log f_{O_2} diagram. Figure 5.4b plots the $\delta^{34}S$ values at points A, B, C, and D, detailing the extreme effects that changes in f_{O_2} have on the sulphur isotopic composition. An increase in oxygen fugacities has a much stronger effect on the $\delta^{34}S$ values than a change in pH due to the large isotopic fractionation between sulphates and sulphides (Hoefs, 1987). Figure 5.5 is the same type of diagram, but it shows the mole fractions of aqueous sulphur species relative to the total sulphur content. Figure 5.5 can be compared to Figure 5.4a to see how changes in the physico-chemical conditions of a system can affect the mineralogy. For instance, in very reducing conditions the sulphide fraction would be dominated by phases like pyrrhotite, and there would be no sulphate mineralisation. In very basic conditions, the dominant sulphur species is S^{2-}; by assuming that the bulk of the sulphides present in Chuquicamata (pyrite, chalcopyrite, bornite, idaite, and the other copper sulphides) can be represented by H_2S, an upper limit of about 7 for the pH of the system can be inferred. Also by assuming that all of the sulphides can be represented as H_2S, and knowing that the ratio of sulphate to sulphide is close to 1, Chuquicamata must plot in the upper left quadrant of Figure 5.5, corresponding approximately to area B in Figure 5.4a. In other words, the potassic zone was produced in a relatively acidic, moderate-to-high oxygen fugacity environment (i.e., there was a significant amount of oxygen available).

Figure 5.4 a. Stability fields of sulphur phases in a pH-log f_{O2} diagram at 250°C for total sulphur content 0.1 and $Ba^{2+} = 10^{-3}$ mol kg^{-1} ; b. $\delta^{34}S$ values of sulphides and sulphate at 250°C (from Nielson 1985).

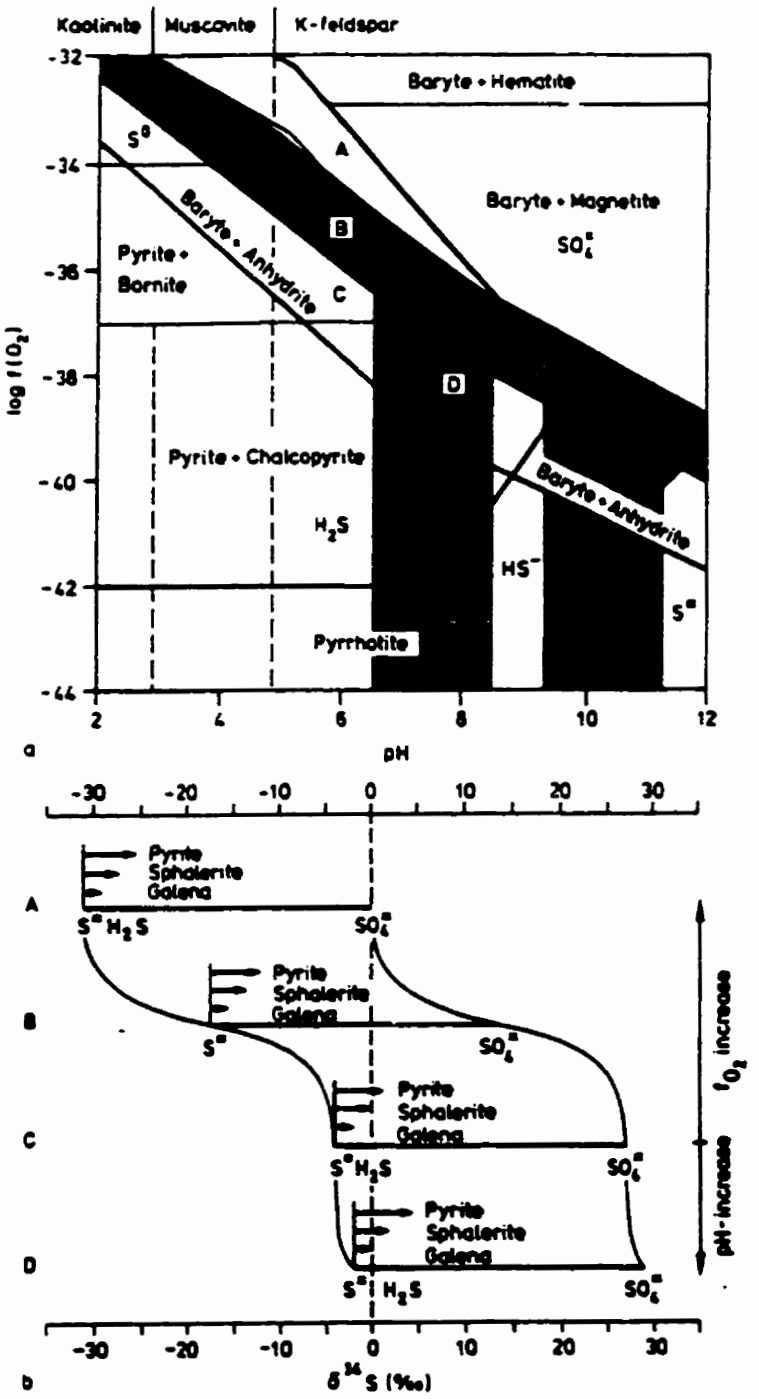

Figure 5.5. Mole fractions of aqueous sulphur species relative to total sulphur content plotted on a pH- log f_{O2} diagram. T = 250°C and I = 1.0. $\sum SO_4 = SO_4^{2-} + HSO_4^- + KSO_4^- + NaSO_4^-$ (from Ohmoto 1972).

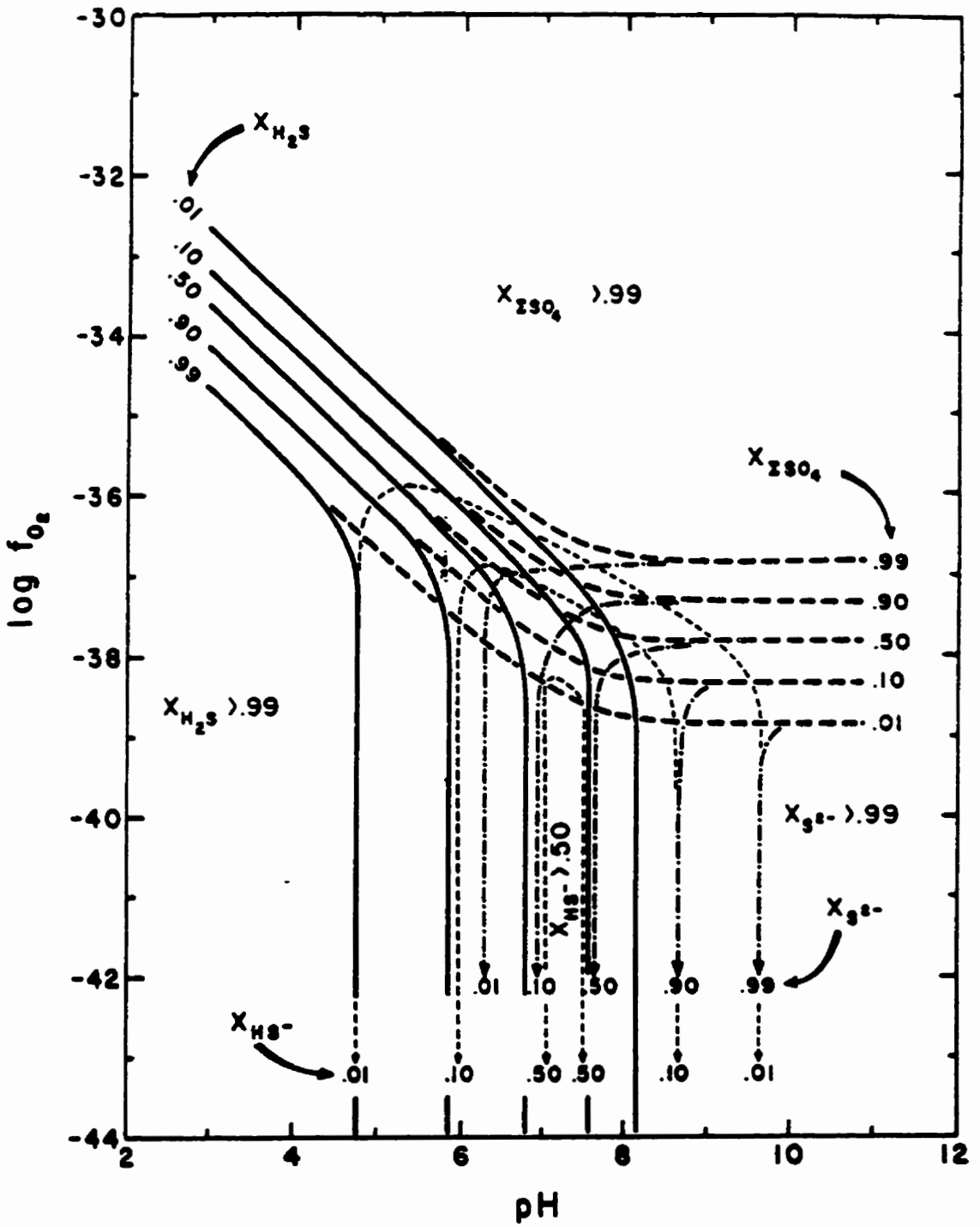

5.6 Summary

The sulphur isotopic compositions of the sulphides from Chuquicamata are very similar to hydrothermal sulphides from other deposits, such as El Salvador, and show the expected relative S^{34} enrichment predicted by Bachinski (1969). Isotopic temperatures derived from coexisting sulphates and sulphides in the quartz-sericite (overprinting potassic) zone of alteration are between 300 and 375^{0}C. These temperatures are lower than what would be expected from the hypogene environment at Chuquicamata, and are possibly explained by hydrothermal fluids mixing with meteoric waters.

The total sulphur at Chuquicamata during the 31 Ma sericitic alteration event, determined from the limited number of isotopic analyses performed, has a $\delta^{34}S$ value of approximately +6.5 permil. Such S^{34}-enriched total sulphur implies a sulphur source derived from either local country rocks (not likely in the case of Chuquicamata) or (more likely) from a mixture of magmatic and sulphate-rich water (Hoefs, 1987). However, the isotopic study undertaken here was a preliminary one, and further work on sulphur, oxygen and hydrogen isotopes will provide more concrete evidence of sources.

The dissolved sulphate-to-sulphide ratio represented in Chuquicamata shows that the environment that produced the sericitic alteration was acidic and had available a significant amount of oxygen.

CHAPTER 6 CONCLUSIONS AND RECOMMENDATIONS

6.1 Conclusions

1) Different hypogene covellite assemblages correlate with the different periods of mineralisation/ alteration at Chuquicamata. In the potassic zone of alteration, covellite occurs almost exclusively as a hypogene replacement phase; most commonly it originates from chalcopyrite, bornite and/or digenite. Although covellite in this zone is secondary in nature, it is still clearly of hypogene origin, evidenced by its common association with hypogene anhydrite. In the quartz-sericite zone, covellite occurs as subhedral crystals disseminated in massive sulphate (-silicate) gangue, as tufted and feathery masses exsolved from digenite, and as acicular crystals in eutectic intergrowths with digenite, all hypogene in character.

2) Supergene and hypogene covellite can be distinguished on the basis of mineralogy (grain morphology and ore mineral assemblages) and chemical composition (minor elements). The textural occurrence of hypogene covellite has been described above; supergene covellite in Chuquicamata is generally massive or has a fine granular texture. Hypogene covellite is associated with high-temperature idaite, digenite and sulphates (anhydrite and barite), while covellite in the supergene environment is associated with late-stage hydrothermal veins (specifically the coarse enargite-pyrite veins) or with disseminated to semi-massive pyrite, chalcopyrite and/or bornite. Chemically, hypogene covellites have been shown to contain significant Fe, up to 5 weight %. It must be stressed that this is a real phenomenon; the results are reproducible and not likely to be due to calibration or identification problems, as has been suggested in the literature. Supergene covellite rarely deviates from stoichiometric CuS, unless it contains Fe or other minor elements inherited from the replaced phase(s).

3) Based on sulphide phase equilibria, temperatures of mineralisation at Chuquicamata are between approximately 400 and 600^{0}C for the potassic alteration phase (although they may have been as low as 300^{0}C), and between 300 and 435^{0}C for the quartz-sericite alteration phase. Late stage hydrothermal veins crystallized at temperatures above 275-320^{0}C. Given that the two periods of alteration/ mineralisation are separated by 2-3 m.y., these temperature implications support the hypothesis that the quartz-sericite zone resulted from a second heating event. Some

types of supergene enrichment, such as the possible supergene sphalerite, may have formed up to 100°C.

4) Temperatures of equilibration based on sulphur isotopic compositions of coexisting sulphides and sulphates are between 300 and 375°C for samples from the potassic zone at Chuquicamata, and are interpreted as representing the sericitic, and not potassic, alteration phase, because anhydrite in veins in the potassic zone probably formed during later quartz-sericite alteration. However, the temperature is still low, and may have resulted from mixing of magmatic and meteoric waters. The limited number of analyses point to a total sulphur content ($\delta^{34}S$ value) of the system of +6.5 permil for the quartz-sericite (overprinting potassic) zone, which could suggest that the sulphur was derived from a mixture of magmatic water and water with heavier sulphur (i.e., magmatic water alone is not enough to explain the relatively S^{34}-enriched total sulphur). The sulphate to sulphide ratio for the system at about 31 Ma is approximately 0.8:1, showing that the environment at the time of quartz-sericite alteration was acidic with a moderate to high oxygen fugacity.

6.2 Recommendations

The covellite-bearing hypogene assemblages have been characterised with respect to their sulphide mineralogy and chemical composition. To further round out the work started here and to apply it to the Chuquicamata system as a whole, several projects will be instrumental.

1) Minerals with high bond strength, such as sphalerite and pyrite, are much more likely to preserve a record of their history than minerals in which rates of solid-state diffusion are high (chalcocite, digenite, bornite, and chalcopyrite). Most of the minerals studied in detail in the 4500N section tend to equilibrate very quickly. An optical study of sphalerites from this cross-section would determine crystal zoning, and electron probe work on compositionally-banded sphalerites would confirm if, and to what extent, re-equilibration had occurred in these samples (this could change the conclusions drawn on the basis of sulphide equilibria).

2) Sulphur isotopic data should be gathered for samples in the potassic zone for comparison with (a) temperatures determined from sulphide phase equilibria, and (b) temperatures determined from sulphur isotopic fractionation between coexisting sulphur phases in the quartz-

sericite zone.

3) Samples from both the potassic and sericitic zones should be analyzed for oxygen and strontium isotopes to determine if perhaps mixing occurred with (more oxidising) meteoric waters during mineralisation.

4) A detailed study of non-ore minerals in the 4500N and other cross-sections will determine the true extent of sulphate mineralisation. This is necessary for comparison with the implications, from the limited sulphur isotope study conducted here. that the dissolved sulphate:sulphide ratio was close to 1:1, which could mean that the environment was much more oxidising than what has been interpreted so far.

5) A fluid/melt inclusion study of silicates, sulphates, and some sulphides (sphalerite and enargite can be studied under infrared light) would aid in constraining temperatures of mineralisation and would give, indirectly, the composition of the hydrothermal fluids, including their equivalent salinity. As well, since an independent estimate of temperature is available from isotopic data, fluid inclusions can be used as geobarometers when the compositional data is used with experimental P-V-T-X properties for a fluid composition similar to that at Chuquicamata.

The implementation of these recommendations would make significant advances in further constraining the temperature, pressure and chemical character of the fluids responsible for mineralisation at Chuquicamata, which will in turn lead to greater understanding of the processes responsible for concentrating such large volumes of copper and sulphur in one spot in the earth's crust.

APPENDIX A

ELECTRON MICROPROBE ANALYSES

The electron mincoprobe was used to determine the chemical composition of sulphide minerals, and to study the variation in chemical composition of the mienrals through the 4500N cross-section. Analyses were carried out on a JEOL 733 electron microprobe equipped with four wavelength dispersive spectrometers and and Oxford Link eXL energy dispersive system. The energy dispersive system was used for all elements. Resolution of the energy dispersive detector was 137eV at 5.9Kev.

Each spectrum was acquired for 40 seconds with an accelerating voltage of 15Kv and a beam current of 15nA. Probe spot size was approximately 1 micron. The raw data was corrected using Link's ZAF matrix correction program. Instrument calibration was performed on cobalt metal. Instrument precision on cobalt metal (x=10) was +/- 0.5% at 1 standard deviation. Accuracy for major elements was +/- 1.5 to 2.0% relative.

Geological standards were used as controls. Sulphide standards used were natural chalcopyrite and synthetic $Cu_{1.8}S$, supplied by CANMET.

Tables of chemical analyses are organised by mineral. Each table includes the mean, maximun, minimum, and calculated standard deviation for the number of analyses for each element that are above the detection limit (limit of quantification).

Digenite - Weight Percent

52 acceptable analyses from 24 samples

Sample	Point	Analyzed	Assemblage	CuK	FeK	AsL	S K	Total	
cu195	73	dg	cv+dg	78.50		0.25	21.86	100.61	
cu195	75	dg	dg+cv+ba	78.91		0.36	21.74	101.01	
cu195	76	dg	dg+cv+ba	78.07			21.77	99.84	
cu195	77	dg	dg+cv	77.99			22.40	100.40	
cu199	10	dg	py+dg+cv	78.42			22.73	101.15	
cu201	10	dg	dg+cv	76.42	1.47		22.41	100.29	
cu201	22	dg-incl	py+cv+dg	75.71	1.80		23.20	100.71	
cu203B	20	dg	cv+dg	77.09		0.27	22.12	99.47	
cu203B	28	dg	cv+dg	76.06	0.50		22.40	98.96	
cu203B	31	dg	cv+sph+dg	74.66	0.54	0.32	22.48	98.00	sph
cu204	40	dg	cv+dg+wolf	76.12		0.26	21.81	98.20	
cu204	44	dg	py+dg+cv+wolf	76.17	0.51		22.15	99.32	
cu204	48	dg-incl	wolf+cv+dg	75.97		0.27	22.26	98.50	
cu204	52	dg	cv+dg+wolf	76.69		0.28	22.13	99.10	
cu204	57	dg	dg+cv+py	77.26			21.80	99.06	
cu205B	3	dg	py+dg+cv	77.46			22.02	99.48	
cu205B	8	dg	cv+dg+sulfate	78.30			21.81	100.11	
cu205B	13	dg	en+cv+dg+py	75.53	1.89		21.63	99.06	en
cu205B	18	dg	dg+py	75.68	2.74		21.77	100.19	
cu205B	20	dg	cv+dg+en+py	77.37			21.89	99.26	en
cu206	12	dg	sph+dg+cv	76.25	0.40		22.84	99.49	sph
cu211	7	dg	dg+cv	75.04	0.27	0.29	22.40	98.01	
cu211	8	dg-incl	py+dg	76.82	0.90	0.25	22.37	100.34	
cu441	90	dg	cv+dg+py	77.16			21.79	98.95	
cu441	93	dg	dg+cv+py+mo	76.00			22.04	98.04	
cu441	98	dg	en+dg+cv+sph	77.42			21.70	99.12	en
cu441	99	dg	en+dg+cv+sph	76.89			21.80	98.69	en
cu454B	79	dg	dg+bn+sulf	77.02	0.70	0.27	22.03	100.02	
cu461B	24	dg	dg+ga+sulfate	76.22			21.99	98.21	

Digenite - Weight Percent

52 acceptable analyses from 24 samples

Sample	Point	Analyzed	Assemblage	CuK	FeK	AsL	S K	Total	
cu461B	27	dg	dg+cv	78.18			20.63	98.81	
cu461B	28	dg	dg+cv	79.23			20.76	99.99	
cu461B	30	dg	dg+cv+en+py	77.78			21.65	99.43	en
cu461B	31	dg	dg+cv+en+py	78.44			20.72	99.16	en
cu461B	37	dg	dg+py	76.85	1.59		21.79	100.23	
cu467A	25	dg	dg+col	78.14			21.76	99.90	
cu467A	32	dg	dg+bn+col+py	76.36	1.17		22.12	99.66	
cu467B	59	dg	sph+bn+dg+ga	77.65			21.82	99.47	
cu474A	3	dg	dg+cv	79.60			22.04	101.65	
cu474A	4	dg	dg+cv+bcv?	77.63			21.96	99.59	
cu474A	9	dg	dg+cv+col?	75.54		1.40	23.15	100.08	
cu476B	66	dg	bn+dg-exsol	77.43			21.20	98.64	
cu481A	94	dg	py+dg+bn+sph+en	78.66	0.93		22.49	102.08	en
cu489	91	dg	dg+X+sph+py	75.08	1.27		22.92	99.27	sph
cu489	97	dg	py+dg	75.41	2.57		21.74	99.72	
cu489	102	dg-incl	py+dg+X	77.87			21.90	99.77	
cu489	107	dg	dg+X+en?(Y)	78.33			21.63	99.97	en
cu494	35	dg	cpy+bn+dg+cv	75.41	1.73	0.27	23.51	100.92	
cu494	40	dg	bn+cpy+dg+cv	75.08	2.44		22.74	100.26	
cu500B	79	dg	bn+dg+py	74.53	2.49		22.18	99.19	
cu500B	82	dg	bn+dg	76.35	1.68		22.06	100.09	
cu501	26	dg	bn+cpy+dg+sph	77.73	1.31		20.95	100.00	sph
cu509	86	dg	dg+sph	78.60			22.15	100.75	sph
covellite				66.47			33.53	100.00	
bornite				63.32			25.56	88.88	
yarrowite				72.35			27.65	100.00	
splonkopite				73.51			26.49	100.00	
digenite				78.11			21.89	121.89	

Digenite - Weight Percent

52 acceptable analyses from 24 samples

Sample	Point	Analyzed	Assemblage	CuK	FeK	AsL	S K	Total	
djurleite				79.53			20.47	120.47	
chalcocite				79.86			20.14	120.14	
								0.00	
cu509	88	dg	cpy+dg+bn	76.95	2.46		23.21	104.40	high total
cu467B	56	dg	sph+bn+dg+ga	75.65			21.81	99.34	high zinc; probable sph inclusion mixed analyses
cu204	53	dg	cv+dg+woll	75.26		0.33	21.60	97.19	low total
cu489	100	dg	dg+cv+X	74.29			24.33	98.62	intermediate composition; dg/bcov
cu214A	73	dg-incl	py+cv+dg	74.28	2.40	0.31	23.00	100.60	closer to bcov or mixed analyses
cu204	56	dg-incl	py+bn+dg	74.15	2.29	0.37	22.90	99.71	bcov
cu500B	76	dg	dg+cv+bn+cpy	72.60	2.18		25.83	100.61	bcov
cu476A	20	dg	py+cp+dg+bn	72.47	2.00		27.35	101.83	bcov
cu494	25	dg?	dg+cv	72.45	0.48		28.14	101.08	bcov or mixed analyses dg/cv
cu507A	69	dg	cpy+dg+sph	71.15	1.31		29.38	101.84	closer to bcov
cu211	10	dg?-incl	py+cv+dg	56.74	13.04		31.76	101.54	likely a bornite inclusion
cu487	86	dg?	cpy+bn+cv	46.01	16.65		32.02	95.12	likely a bornite inclusion
cu205B	4	dg-incl	dg-bn	26.29	5.82		10.35	42.46	low total
cu467A	28	dg	dg+bn+ga+py	72.02	4.11		23.08	99.20	intermediate digenite/bornite composition; suspect mixed analyses
cu489	93	dg	dg+X+sph+py	72.24			23.72	98.60	suspect mixed analyses with inclusions
cu509	85	dg	dg+bn	76.87			21.78	99.57	probable sphalerite inclusion; sph in this sample
Stoichiometric Compositions									
digenite				78.11			21.89		
djurleite				79.53			20.47		
chalcocite				79.86			20.14		
mean				76.98	1.38	0.37	22.02	99.66	
std				1.25	0.75	0.31	0.57	0.90	
max				79.60	2.74	1.40	23.51	102.08	
min				74.53	0.27	0.25	20.63	98.00	

Digenite - Weight Percent

52 acceptable analyses from 24 samples

Sample	Point	Analyzed	Assemblage	CuK	FeK	AsL	S K	Total
n				52	21	12	52	52
samples with enargite and/or sphalerite								
mean				76.93	0.96	0.29	22.26	99.73
std				1.27	0.56	0.04	0.40	1.03
max				78.91	1.80	0.36	23.20	101.15
min				74.66	0.50	0.25	21.74	98.00
n				13	5	6	13	13
detection limit (3sigma LOQ)				0.50	0.25	0.25		
Section	Point	analyzed	assemblage	CuK	FeK	AsL	S K	Total
cu203A	34	an?	cpy+dg+cv+sph+py	75.42	1.08		22.78	99.27
cu203A	26	an?	cv+dg	74.17	0.44	0.29	24.42	99.31

Covellite - Weight Percent
148 acceptable analyses from 29 samples

Sample	Point	analyzed	assemblage	CuK	FeK	AsL	S K	Total
cu182B	61	cv	en+cv+py	64.37	2.42		32.87	99.66
cu182B	63	cv	en+cv+py	65.88			33.08	98.96
cu195	72	cv	cv+dg	67.30			32.86	100.16
cu195	78	cv-needle	dg+cv	68.14			32.61	100.74
cu195	79	cv-massive	dg+cv	67.13			32.80	99.93
cu199	11	cv	py+dg+cv	67.53	1.15		32.98	101.65
cu199	16	cv	py+cv+en+sph	66.80			33.68	100.48
cu201	2	cv	cv+wolf	66.60			33.45	100.04
cu201	4	cv		66.48		0.27	33.36	100.10
cu201	5	cv		66.81			33.23	100.04
cu201	6	cv		66.45	0.58	0.26	33.59	100.87
cu201	7	cv		66.27		0.31	33.30	99.87
cu201	8	cv		66.70		0.28	33.27	100.25
cu201	9	cv	dg+cv	65.79	1.55	0.35	33.40	101.08
cu201	11	cv	dg+cv	66.47			33.48	99.95
cu201	12	cv		66.28	1.05		33.28	100.62
cu201	13	cv		66.18			33.39	99.57
cu201	14	cv		65.59		0.29	33.80	99.68
cu201	15	cv	cv+py	67.68			33.37	101.05
cu201	16	cv		69.16		0.25	32.58	101.99
cu201	17	cv		67.23		0.30	33.27	100.80
cu201	18	cv		67.05			33.26	100.31
cu201	19	cv	py+cv	66.15	0.48		33.33	99.96
cu201	20	cv		66.51	0.25		33.31	100.06
cu201	21	cv-incl	py+cv+dg	65.55	1.58		33.41	100.54
cu203A	23	cv	py+cv+sph	64.73	0.43	0.33	33.37	98.87
cu203A	25	cv	cv+dg	66.39			33.17	99.55
cu203A	27	cv	cv+dg	66.95		0.29	32.89	100.13
cu203A	29	cv	cv+sph+dg	66.59	0.28		31.53	98.40
cu203A	33	cv	cpy+dg+cv+sph+py	65.47	0.32		33.23	99.01
cu203A	36	cv	cpy+dg+cv+sph+py	66.11	1.11	0.35	32.19	99.76
cu203B	18	cv	cv+dg	67.44			33.47	100.91
cu203B	19	cv	cv	64.47		0.26	33.23	97.96

Covellite - Weight Percent

148 acceptable analyses from 29 samples

Sample	Point	analyzed	assemblage	CuK	FeK	AsL	S K	Total
cu203B	21	cv	cv+dg	67.39			32.21	99.59
cu203B	22	cv	cv+dg	67.75		0.25	33.22	101.23
cu204	39	cv	cv+dg+wolf	66.48			32.09	98.57
cu204	43	cv	wolf+cv+py	64.54	1.13		32.09	97.77
cu204	45	cv	py+dg+cv+wolf	65.61	0.73		33.49	99.83
cu204	47	cv-incl	wolf+cv+dg	64.07			33.11	97.17
cu204	51	cv	cv+dg+wolf	66.20			33.13	99.33
cu204	58	cv	cv+dg	65.79	0.54	0.34	33.19	99.86
cu205B	2	cv	py+dg+cv	67.03			32.83	99.86
cu205B	7	cv	cv+dg+sulfate	68.95			30.54	99.49
cu205B	9	cv	cv+dg+sulfate	67.31			31.81	99.12
cu205B	12	cv	en+cv+dg+py	67.19			32.44	99.63
cu205B	16	cv	en+cv+dg	69.39			30.29	99.69
cu206	11	cv	sph+dg+cv	65.99		0.27	33.40	99.66
cu210	74	cv	py+cv+rt	65.89			33.16	99.05
cu211	3	cv	cv+sulphate	65.91			33.12	99.02
cu211	4	cv	cv+dg	65.87		0.25	33.71	99.82
cu211	5	cv	cv+dg	64.83			32.94	97.77
cu211	9	cv-incl	py+cv+dg	67.90	2.14	0.29	30.44	100.76
cu214A	65	cv	cv+sulf	66.59			33.79	100.38
cu214A	66	cv	cv+sulf	66.59			34.52	101.11
cu214A	67	cv	py+cv	65.08	1.89		33.35	100.31
cu214A	68	cv	py+cv	66.20			33.61	99.80
cu214A	69	cv	py+cv	64.39	2.21		33.61	100.21
cu214A	70	cv-incl	py+cv	63.87	2.57	0.32	33.87	100.62
cu214A	71	cv-incl	py+cv+dg	64.24	2.30		33.53	100.07
cu214A	72	cv-incl	py+cv+dg	65.36	2.09		32.21	99.66
cu214A	74	cv-incl	py+cv	64.84	2.07		33.73	100.64
cu214A	75	cv		66.60			33.72	100.32
cu214A	77	cv	cv+mo	65.00			34.48	99.48
cu214A	78	cv	cv+mo	65.62			33.50	99.12
cu214A	79	cv	mo+cv	65.00			33.37	98.37
cu214A	80	cv		67.22			33.70	100.92

Covellite - Weight Percent
148 acceptable analyses from 29 samples

Sample	Point	analyzed	assemblage	CuK	FeK	AsL	S K	Total
cu214A	81	cv		66.97			33.44	100.41
cu214A	82	cv		65.76			33.67	99.43
cu214B	83	cv	cv+py	67.33		0.26	33.45	101.04
cu214B	84	cv	cv+py	65.97		0.33	33.89	100.19
cu214B	85	cv	py+cv	65.63	1.81	0.25	33.68	101.37
cu214B	86	cv-incl	py+cv	64.39	2.73	0.25	33.78	101.14
cu214B	87	cv	py+cv	65.97	0.74	0.35	33.52	100.58
cu214B	88	cv		66.91			33.80	100.71
cu214B	89	cv		66.69			33.73	100.42
cu214B	90	cv	py+cv	65.80	0.41		33.06	99.26
cu214B	91	cv-incl	py+cv	64.34	2.47		33.15	99.97
cu214B	93	cv	cv+en+py	66.62		0.26	33.81	100.68
cu441	89	cv	cv+dg+py	66.19			32.94	99.12
cu450	2	cv-mix?	cv+id+dg+bn	63.14	4.36		34.32	101.82
cu450	6	cv	cv+id+dg+bn	67.15			34.03	101.19
cu454B	69	cv	cv+sulfate	66.43			32.96	99.39
cu454B	71	cv	cv+sulfate	65.97			32.84	98.81
cu454B	77	cv	cv+cpy	66.03	1.46		32.93	100.42
cu455	42	cv	cv+cpy+oxide	66.75			33.32	100.06
cu455	44	cv	cv+cpy	66.24			32.89	99.14
cu455	46	cv-needle	cv+cpy+oxide	65.10	2.52		32.93	100.55
cu455	48	cv	cv>>cpy	66.45			33.33	99.79
cu455	50	cv	cv>>cpy	66.23			33.30	99.53
cu461B	26	cv	dg+cv	66.61			31.87	98.48
cu461B	35	cv	cv+en	67.51			32.02	99.53
cu465	56	cv	cv+id?	66.94	1.11		33.69	101.75
cu465	60	cv	cpy+cv+id	66.25	1.56		33.68	101.49
cu474A	5	cv	dg+cv+bcv?	67.95			33.40	101.35
cu476B	70	cv	cv+py	65.78	0.99		32.56	99.32
cu480	42	cv	cv+dg+bcv?	67.18			32.55	99.73
cu482	28	cv-incl?	py+cv	64.91	2.72		33.03	100.65
cu482	30	cv-incl	py+cv	65.58	2.25		32.98	100.81
cu482	31	cv-incl	py+cv	64.43	2.18		33.05	99.66

Covellite - Weight Percent
148 acceptable analyses from 29 samples

Sample	Point	analyzed	assemblage	CuK	FeK	AsL	S K	Total
cu482	33	cv-incl?	py+cv	64.86	3.30		31.24	99.40
cu482	37	cv	cpy+py+cv	65.86	1.27		32.75	99.89
cu482	44	cv	cv+cpy+oxide	67.90	0.91		31.68	100.49
cu482	46	cv	cv+oxide	67.94		0.28	32.12	100.34
cu482	47	cv	cv+oxide	67.63			32.95	100.58
cu487	84	cv	bn+cv	66.84	1.45	0.29	31.46	100.04
cu489	101	cv	dg+cv+X	66.91			32.82	99.73
cu494	27	cv	cpy+py+cv	68.00		0.26	31.18	99.44
cu494	28	cv	py+cv	65.48	0.78		33.09	99.34
cu494	31	cv?	cpy+bn+dg+cv	62.37	3.22		33.41	99.00
cu494	33	cv	cpy+bn+dg+cv	66.44	0.65		33.08	100.17
cu494	34	cv	cpy+bn+dg+cv	66.21	0.90		32.77	99.89
cu494	36	cv	cv+dg+cpy	65.21	1.52		33.68	100.42
cu494	37	cv	cv+cpy	66.92			33.28	100.20
cu494	39	cv	bn+cpy+dg+cv	67.88	0.25		32.73	100.85
cu494	41	cv	bn+cpy+dg+cv	68.07	0.25		32.38	100.70
cu494	42	cv	bn+cpy+dg+cv	66.15			33.02	99.17
cu495	45	cv	cv+cpy+py	64.91	1.64		32.42	98.97
cu495	46	cv-incl	py+cv	65.63	1.99	0.28	32.95	100.84
cu495	50	cv	py+cv	66.50			33.11	99.60
cu495	52	cv-incl	py+cv	64.78	2.06		33.30	100.14
cu495	53	cv-incl	py+cv+cpy	64.86	2.01		33.18	100.05
cu495	54	cv	py+cv	65.78	1.12	0.27	33.44	100.62
cu495	55	cv	py+cv	63.99	2.69		33.06	99.73
cu495	56	cv	py+cv	66.95	0.79		33.17	100.91
cu495	57	cv	py+cpy+cv	66.07	0.74	0.28	33.83	100.92
cu495	59	cv	cv+cpy	66.73		0.26	33.87	100.87
cu495	60	cv	cv+cpy	65.84	1.02		33.11	99.97
cu495	61	cv	cv+cpy	64.05	2.63	0.27	33.50	100.45
cu495	62	cv	py+cpy+cv	66.01	0.36		33.83	100.20
cu495	63	cv	cv+cpy	66.51	0.63		33.39	100.54
cu495	64	cv	cv+cpy	66.42	0.67		33.56	100.65
cu495	65	cv	cpy+cv	65.77	1.82		33.73	101.32

Covellite - Weight Percent

148 acceptable analyses from 29 samples

Sample	Point	analyzed	assemblage	CuK	FeK	AsL	S K	Total	
cu495	66	cv-incl	py+cv+cpy	65.65	1.58		33.69	100.93	
cu495	67	cv	py+cpy+cv	65.37	2.13		33.69	101.19	
cu495	68	cv	cpy+cv	65.51	1.39	0.26	33.09	100.24	
cu495	69	cv-incl	py+cv+cpy	67.11	0.93	0.26	33.52	101.82	
cu495	71	cv	cv+cpy	66.36	1.21		33.63	101.20	
cu500B	77	cv	dg+cv+bn+cpy	65.15	4.26		30.32	99.73	
cu503	2	cv-incl	cv+py	66.13	1.64		33.54	101.31	
cu503	4	cv-incl	cv+py	65.10	2.19		33.12	100.40	
cu503	5	cv-incl	cv+py	65.62	2.77		32.78	101.17	
cu503	6	cv-incl	cv+py	64.26	2.65		32.86	99.77	
cu503	10	cv	cv+cpy	68.97		0.27	31.90	101.14	
cu503	12	cv	massive cv	66.27			33.33	99.59	
cu503	13	cv	massive cv	67.44			32.92	100.36	
cu503	14	cv	massive cv	65.76			32.80	98.56	
cu503	19	cv	cv+cpy	67.02			32.97	99.99	
cu503	23	cv	cv+bn+cpy	65.61	0.84		32.48	98.94	
rejected analyses (reason in last comment column)									
cu204	49	cv-incl	wolf+cv+dg	64.02		0.29	30.81	98.47	wolf in same sample, suspect mixed analyses
cu214B	94	cv-incl	cv+en+py	63.51		3.39	33.89	100.79	suspect enargite in part
cu465	61	cv	cpy+cv+id	63.55	4.65		34.32	102.52	high total
cu465	63	cv?	cpy+cv+id	61.09	6.98		34.21	102.28	high total
cu465	66	cv	cpy+cv+id	68.34			33.86	102.19	high total; not covellite (too much Cu)
cu455	40	cv	cv+cpy+oxide	38.57	23.71		18.08	80.37	mix with oxide;
cu482	42	cv	cv+cpy+oxide	50.51	13.55		25.36	89.42	low total
cu503	3	cv-incl	cv+py	66.06	2.42		33.62	102.09	high total
cu206	17	cv	sph+cv	66.07			30.61	98.88	probable mixed analyses
cu482	45	cv	cv+cpy+oxide	38.04	23.20		19.31	80.55	low total; Fe - not covellite
cu487	82	cv	cpy+bn+cv	63.24	3.20	0.32	28.46	95.23	low total
cu487	83	cv	cpy+bn+cv	62.03	2.84		29.38	94.79	low total
cu494	36	cv	cpy+cv	58.64	0.35		28.23	93.45	low total
cu495	47	cv	py+cv	61.76	0.48		32.20	95.51	low total
cu495	58	cv	py+cpy+cv	67.92	0.64		33.71	102.27	high total

Covellite - Weight Percent

148 acceptable analyses from 29 samples

Sample	Point	analyzed	assemblage	CuK	FeK	AsL	S K	Total	
cu476B	71	cv	cv+py	48.61	1.75		8.40	58.76	low total - oxide
cu500B	75	cv	dg+cv+bn+cpy	30.10	1.17		22.50	53.76	low total - mix with oxide
overall									
min				62.37	0.25	0.25	30.29	97.174	
max				69.39	4.36	0.35	34.52	101.99	
mean				66.18	1.56	0.28	33.06	100.07	
std dev				1.16	0.93	0.03	0.74	0.8652	
n				148	72	35	148	148	
with chalcopyrite				identical to overall stats					
min				63.87	0.54	0.25	30.29	97.17	
max				69.39	2.57	0.34	34.52	101.37	
mean				66.07	1.77	0.28	33.07	99.71	
std dev				1.27	0.64	0.03	0.97	0.98	
n				39	11	10	39	39	
with digenite but without cpy					marginally higher Cu and lower Fe - could be because of dg filaments				
min				63.14	0.41	0.25	31.24	98.48	
max				67.95	4.36	0.35	34.32	101.82	
mean				66.01	2.00	0.29	33.12	100.16	
std dev				1.04	1.03	0.05	0.64	0.88	
n				30	15	3	30	30	
with enargite (or py only)					higher Fe and As				
min				62.37	0.25	0.26	30.32	98.97	
max				68.07	4.26	0.28	33.87	101.82	
mean				65.83	1.45	0.27	33.19	100.34	
std dev				1.12	0.94	0.01	0.65	0.69	
n				31	27	7	31	31	
detection limit				0.50	0.25	0.25			

Bornite - Weight Percent
36 acceptable samples in 14 samples

Sample	Point	Analyzed	Assemblage	CuK	FeK	S K	Total
cu204	55	bn-incl	py+bn+dg	61.23	11.43	25.58	98.24
cu205B	5	bn-incl	dg-bn	60.47	12.52	25.33	98.33
cu205B	6	bn-incl	dg-bn	61.36	12.31	25.13	98.80
cu450	1	bn?	cpy+dg+bn	62.69	11.66	25.97	100.32
cu450	4	bn	cv+id+dg+bn	62.84	10.85	26.18	99.87
cu450	5	bn?	cv+id+dg+bn	62.85	11.24	26.31	100.40
cu454B	80	bn	dg+bn+sulf	62.88	11.32	24.96	99.17
cu454B	84	bn	mo+bn+cpy	62.69	11.41	25.34	99.43
cu467A	27	bn	dg+bn+ga+py	62.92	11.05	25.31	99.28
cu467A	33	bn	dg+bn+col+py	63.30	10.32	25.09	98.71
cu467B	49	bn	sph+bn+cpy	62.46	11.69	25.30	99.45
cu467B	57	bn	sph+bn+dg+ga	61.28	11.33	25.20	97.81
cu467B	58	bn	sph+bn+dg+ga	63.26	10.41	25.09	98.76
cu467B	61	bn	bn+cpy+dg-cv	62.68	11.27	25.13	99.07
cu476A	21	bn	py+cpy+dg+bn	62.35	12.24	25.77	100.36
cu476A	22	bn	dg+bn+en	62.66	11.59	26.18	100.44
cu476B	65	bn	bn+dg-exsol	62.71	11.49	25.72	99.92
cu476B	68	bn	cpy+bn+dg+py	61.49	12.51	25.28	99.28
cu481A	95	bn	py+dg+bn+sph+en	64.35	11.52	25.59	101.46
cu482	26	bn	bn+py	62.51	11.82	25.31	99.65
cu482	27	bn	bn+py	61.66	12.36	25.53	99.54
cu482	29	bn	py+bn+cv	62.53	11.25	24.55	98.33
cu482	32	bn-incl	py+bn	60.79	13.06	25.32	99.17
cu494	23	bn	cpy+bn+dg+cv	62.94	11.27	25.50	99.72
cu494	80	bn	bn+rutile	62.96	11.45	25.69	100.10
cu500B	73	bn	dg+cv+bn+cpy	60.53	12.67	26.37	99.57
cu500B	74	bn	dg+cv+bn+cpy	61.68	11.88	25.34	98.91
cu500B	80	bn	bn+dg+py	61.43	11.30	25.39	98.12
cu500B	81	bn	bn+dg	64.14	11.04	25.37	100.55
cu500B	83	bn	bn+dg	61.73	11.35	25.34	98.41
cu503	7	bn-incl	py+bn	60.69	13.50	25.30	99.49
cu503	17	bn-incl	bn+cpy	61.93	12.17	25.36	99.46
cu503	24	bn	bn+ga	62.55	11.55	25.33	99.43

Bornite - Weight Percent
36 acceptable samples in 14 samples

Sample	Point	Analyzed	Assemblage	CuK	FeK	S K	Total	
cu509	80	bn	dg+bn	63.58	10.78	25.80	100.15	
cu509	87	bn	dg+bn	64.94	10.53	25.73	101.20	
cu509	89	bn	cpy+dg+bn	63.80	11.71	25.67	101.19	
Rejected Analyses								
cu476A	24	bn	bn+dg+cv	58.80	13.32	30.06	102.18	low Cu; high total
cu205B	19	bn-incl	bn+dg	34.65	27.54	40.19	102.38	high total
cu454B	85	bn-incompl	mo+bn+dg+py	48.02	9.45	23.29	80.75	low total
cu454B	86	bn-incompl	mo+bn+dg+py	50.42	9.37	23.46	83.25	lo2 total
cu500A	36	bn?	bn+ga+py	35.72	25.27	40.41	101.40	closer to cpy
stoichiometric bornite				25.55	11.13	63.32	100.00	
mean				62.41	11.61	25.48	99.50	
std				1.06	0.70	0.38	0.88	
max				64.94	13.50	26.37	101.46	
min				60.47	10.32	24.55	97.81	
n				36	36	36	36	
detection limit (3sigma LOQ)				0.50	0.25			

Idaite - Weight Percent

6 acceptable analyses from 2 samples

Sample	Point	Analyzed	Assemblage	CuK	FeK	S K	Total	
cu450	3	id?	cv+id+dg+bn	57.20	9.71	34.71	101.62	
cu465	53	id?	cpy+cv+id	58.97	8.69	34.26	101.92	
cu465	55	id?	cpy+cv+id	58.39	9.15	34.41	101.95	
cu465	57	id?	cpy+bn+dg+col	57.41	11.35	29.42	98.19	
cu465	59	id	cpy+id	57.42	10.13	34.32	101.87	
cu465	65	id	cpy+cv+id	58.05	9.38	34.21	101.63	
Rejected analyses								
cu210	76	id?	py+cv+rt	46.23	12.29	29.18	102.18	not colusite
cu454B	72	id?	cv+sulfate	51.45	15.73	24.51	91.69	low total
cu465	58	id?	cpy+bn+dg+col	53.91	8.63	32.37	94.92	low total
cu455	47	cv-massive	cv+cpy+oxide	58.37	7.57	33.54	99.49	probably an idaite
cu182B	64	cv-incl	en+cv+py	61.87	4.86	34.32	101.05	probably an idaite
cu450	8	id?	cp+id+cv+bn	57.35	10.13	34.87	102.35	high total
cu465	62	id	cpy+cv+id	57.79	10.17	34.29	102.25	high total
cu495	51	id?	py+id?	57.92	8.11	36.48	102.51	high total
bornite				63.32	11.13	25.55		
stoichiometric idaite				56.14	9.87	33.99		
mean				57.91	9.73	33.55	101.20	
std				0.63	0.85	1.86	1.35	
max				58.97	11.35	34.71	101.95	
min				57.20	8.69	29.42	98.19	
n				6	6	6	6	
detection limits (3sigma LOQ)				0.50	0.25			

Blaubleibend Covellite - Weight Percent
8 acceptable analyses from 5 samples

Sample	Point	analyzed	assemblage	CuK	FeK	AsL	S K	Total	
cu203A	32	bcv	cpy+dg+cv+sph+py	72.65	1.59		25.13	99.37	
cu467B	52	bcv	bn+dg+cpy	69.62			28.52	98.14	
cu474A	13	bcv	dg+cv+col	69.05			28.82	97.87	
cu487	65	bcv	cpy+bn+cv	69.28	3.92	0.25	27.76	101.21	
cu487	87	bcv	bn+cv	71.12	1.66		27.09	99.87	
cu494	26	bcv	dg+cv	71.37	0.60		28.29	100.26	
cu494	30	bcv	cpy+bn+dg+cv	70.48	2.04		26.95	99.47	
cu494	32	bcv	cpy+bn+dg+cv	68.80	0.85		29.51	99.16	
Stoichiometric Compositions									
covellite				66.47			33.53		
yarrowite				72.35			27.65		
spionkopite				73.51			26.49		
mean				70.30	1.78	0.25	27.76	99.42	
std				1.26	1.08	0.00	1.28	1.01	
max				72.65	3.92	0.25	29.51	101.21	
min				68.80	0.60	0.25	25.13	97.87	
n				8	6	1	8	8	
Rejected Analyses									
cu487	88	bcv?	cpy+cv	66.20	0.78	0.26	29.67	96.91	low total; covellite Cu
detection limits (3sigma LOQ)				0.50	0.25	0.25			

Chalcopyrite - Weight Percent

14 acceptable analyses from 12 samples

Sample	Point	Analyzed	Assemblage	CuK	FeK	S K	Total	
cu203A	37	cpy	cpy+dg+cv+sph+py	33.72	29.82	34.71	98.25	
cu204	60	cpy	py+cpy+?	33.41	30.82	34.93	99.16	
cu454B	75	cpy	cv+cpy	35.00	30.53	34.72	100.25	
cu455	51	cpy	cpy+cv	33.76	30.29	34.47	98.52	
cu465	64	cpy	cpy+cv+id	35.47	30.77	35.51	101.75	
cu467B	50	cpy	sph+bn+cpy	36.17	29.58	34.34	100.09	
cu467B	67	cpy	cpy+bn+dg+py	34.52	30.44	34.29	99.25	
cu478	50	cpy	cpy+cv+oxide	35.62	30.51	35.09	101.23	
cu482	35	cpy	cpy+py+cv	34.49	31.24	34.47	100.20	
cu482	43	cpy	cv+cpy+oxide	35.24	30.35	34.62	100.22	
cu494	24	cpy	cpy+bn+dg+cv	35.30	29.87	34.56	99.73	
cu503	25	cpy	bn+cpy+ga	35.29	30.07	35.51	100.87	
cu507A	68	cpy	cpy+dg+sph	34.92	31.26	35.43	101.61	
cu509	91	cpy	cpy+bn+dg+sph	35.74	30.73	35.20	101.67	
Rejected Analyses								
cu455	43	cpy	cv+cpy	47.74	17.36	33.95	99.06	not cpy
cu455	52	cpy	cpy+cv	48.84	16.78	33.51	99.13	not cpy
cu495	70	cv-cpy	cv+cpy	53.78	13.44	33.94	101.16	not cpy
cu450	7	cpy	cp+id+cv+bn	35.62	30.86	35.65	102.12	high total
stoichiometric chalcopyrite				34.63	30.43	34.94		
mean				34.90	30.45	34.85	100.20	
std				0.79	0.48	0.42	1.10	
max				36.17	31.26	35.51	101.75	
min				33.41	29.58	34.29	98.25	
n				14	14	14	14	

Colusite - Weight Percent
18 analyses from 5 samples

Sample	Point	Analyzed	Assemblage	ZnK	CuK	FeK	AsL	S K	SnL	SbL	V	Total	
cu467A	22	col	dg+col		52.30		10.64	31.89		0.74	3.30	98.88	x
cu467A	24	col	dg+col		59.31		8.45	29.20		1.07	2.16	100.19	o
cu467A	30	col	dg+bn+col+py		49.46	1.37	16.71	31.71				99.26	x
cu467A	31	col	dg+bn+col+py		50.33	2.76	11.09	31.83			2.96	98.98	x
cu467A	34	col	dg+bn+col		50.89		12.28	32.29			3.19	98.65	x
cu474A	17	col	dg+cv+col		52.43		11.00	32.98			3.25	99.67	x
cu474A	20	col	dg+col		51.31	0.61	11.35	31.88			3.04	98.19	x
cu480	44	col	dg+cv+en		50.13		8.67	30.85	4.42	0.46	2.47	97.84	x
cu481A	101	col	cv+dg+col		45.04	12.00		29.44	14.80			101.28	o
cu489	90	col	dg+col+sph+py	1.24	48.22		5.57	29.60	10.43	2.85		98.13	o
cu489	92	col	dg+col+sph+py	2.84	46.36	0.76	4.29	29.14	12.51	2.65		98.79	o
cu489	98	col	dg+cv+col	4.15	44.89		2.06	28.85	16.51	1.93		98.39	o
cu489	99	col	dg+cv+col	3.42	45.39	0.71	2.99	29.71	15.02	1.98		99.43	o
cu489	103	col-incl	py+dg+col	1.44	47.79		6.13	30.05	10.45	1.76		97.83	o
cu489	105	col	dg+cv+col(2?)	6.29	42.30	0.63	0.60	28.68	20.36			99.05	o
cu489	106	col	dg+cv+col(2?)	2.93	40.30	8.52	1.17	28.52	17.78			99.22	o
cu489	108	col	dg+cv+col(2?)	5.01	42.25		1.28	28.65	18.93	1.35		97.73	o
cu489	109	col	dg+cv+col(2?)	4.67	39.82	8.75	0.26	28.91	19.03			101.44	o
min				1.24	39.82	0.61	0.26	28.52	4.42	0.46	2.16	97.73	
max				6.29	59.31	12.00	16.71	32.98	20.36	2.85	3.30	101.44	
mean				3.56	47.70	4.01	6.74	30.23	14.57	1.64	2.91	99.05	
std				1.56	4.81	4.21	4.82	1.44	4.55	0.77	0.40	1.04	
n				9	18	9	17	18	11	9	7	18	
Rejected analyses													
cu489	104	col-incl	py+dg+col		49.63	0.80	10.51	31.50	3.15	1.73		97.33	low total
cu474A	10	col	dg+cv+col?		49.94		9.39	28.14			2.76	90.23	low total
cu474A	12	col	dg+cv+col		52.18		9.59	31.22		0.56	3.28	96.84	low total
cu474A	14	col?	single grain		51.83		9.19	31.58		0.47	2.80	95.86	low total
cu467A	23	col	dg+col		50.97		7.83	27.90		0.46	2.59	89.75	low total
cu481A	100	col?	cv+dg+col?		46.41	12.13		29.50	15.02			103.07	high total
cu441	91	en-col?	dg+cv+en		49.74		7.63	30.64	5.04	3.05		96.10	low total
Detection Limit (3sigma LOQ)				0.80	0.50	0.25	0.25		0.50	0.40	0.20		

Enargite Analyses - Weight Percent
20 acceptable analyses in 8 samples

Sample	Point	Analyzed	Assemblage	ZnK	CuK	FeK	AsL	S K	SbL	Total		
cu182B	53	en	en+sulfate+py		48.38		16.05	30.59	4.32	99.34		
cu182B	56	en	en+sulfate+py		49.24		18.83	31.97		100.03		
cu182B	57	en-grain	en+py		48.93		17.55	31.86	1.84	100.19		
cu182B	58	en-massive	en+py		48.62		18.22	31.83	0.92	99.59		
cu182B	60	en	en+cv+py		48.33	1.54	17.91	31.75	0.92	100.44		
cu182B	84	en	en+py		48.28		17.92	31.72	1.86	99.79		
cu199	17	en	py+cv+en+sph		50.29		17.95	33.02		101.26		
cu199	18	en	py+cv+en+sph		49.89	0.50	17.88	32.95		101.22		
cu214B	92	en?	cv+en+py		49.64		18.99	32.37		101.00		
cu441	94	en	en+dg+cv+sph		49.94		18.81	31.86		100.61		
cu441	95	en	en+dg+cv+sph		49.43		18.82	32.17		100.42		
cu461B	29	en	dg+cv+en+py		48.52		17.55	32.47	1.44	99.98		
cu461B	32	en	dg+cv+en+py		48.92		18.00	31.63	1.87	100.42		
cu461B	33	en	cv+dg+en+py		50.04		18.61	32.00	0.75	101.39		
cu461B	34	en	en+cv		49.84		18.53	32.16	1.09	101.61		
cu465	52	en?	cpy+cv+en		49.38		18.62	33.00		101.01		
cu480	39	en	dg+cv+en+py		49.55		17.62	31.98		99.15		
cu481A	96	en	py+dg+bn+sph+en		50.13		17.63	32.49	1.01	101.26		
cu481A	97	en	py+dg+bn+sph+en		50.54		18.25	32.60	0.40	101.79		
cu481A	99	en	cv+dg+en		49.44	1.64	18.00	32.43	0.44	101.95		
Tennantite												
cu501	27	en	dg+cv+en	8.11	43.55		19.58	28.05		99.28	tennantite	
cu501	28	en	dg+cv+en	7.77	44.15		19.56	28.29		99.76	tennantite	
cu503	15	en	cv+en+cpy	8.45	43.42		20.03	27.30		99.20	tennantite	
cu503	18	en	cv+en+cpy	7.83	44.17	0.75	20.29	27.30		100.34	tennantite	
cu199	14	en	py+cv+en+sph	8.41	44.51		19.47	28.51		100.89	tennantite	
Tennantite/Tetrahedrite + missing component												
cu205B	11	en	en+cv+dg+py	5.92	42.89		8.67	25.79	8.50	91.77	low total	tetrahedrite missing a component
cu205B	14	en	en+cv+dg+py	6.49	41.90		8.59	25.77	10.74	93.49	low total	tetrahedrite missing a component
cu205B	15	en	en+cv+dg	6.92	42.25		8.81	25.89	11.66	95.53	low total	tetrahedrite missing a component
cu205B	17	en	en+cv+dg	6.49	40.96		8.55	25.82	10.92	92.73	low total	tetrahedrite missing a component
cu205B	21	en	cv+dg+en+py	6.43	42.14		10.56	25.93	8.71	93.77	low total	tetrahedrite missing a component

Enargite Analyses - Weight Percent
20 acceptable analyses in 8 samples

Sample	Point	Analyzed	Assemblage	ZnK	CuK	FeK	AsL	S K	SbL	Total	
enargite				48.41			19.02	32.57			
mean				ERR	49.37	1.22	18.09	32.14	1.40	100.62	
std				ERR	0.68	0.52	0.65	0.55	1.01	0.80	
max				ERR	50.54	1.64	18.99	33.02	4.32	101.95	
min				ERR	48.28	0.50	16.05	30.59	0.40	99.15	
n				0	20	3	20	20	12	20	
Other rejected analyses											
cu476A	23	en	dg+bn+en		50.61		19.10	34.69		104.40	high total
Detection limit (3sigma LOQ)				0.80	0.50	0.25	0.25		0.40		

Sphalerite - Weight Percent

15 acceptable samples in 7 samples

Sample	Point	analyzed	assemblage	ZnK	CuK	FeK	S K	Total	
cu199	9	sph	py+sph	68.09			33.64	101.73	
cu203A	24	sph	py+cv+sph	64.98	1.58	0.36	32.50	99.42	
cu203A	30	sph	cv+sph+dg	65.40	1.35		32.58	99.33	
cu203A	35	sph	cpy+dg+cv+sph+py	66.52	1.22	0.90	32.49	101.43	
cu206	13	sph	sph+dg+cv	67.23	0.76		32.83	100.81	
cu206	14	sph	sph+dg+cv	68.00	0.61		32.71	101.32	
cu206	15	sph	sph+dg+cv	66.00	0.58		32.82	99.40	
cu206	16	sph	sph+dg+cv	67.36	0.63		33.59	101.82	
cu441	96	sph	en+dg+cv+sph	69.33			32.22	101.55	
cu441	97	sph	en+dg+cv+sph	68.92			32.41	101.32	
cu467B	51	sph-mass.	sph+bn+cpy	69.33			32.48	101.81	
cu467B	55	sph-mass.	sph+bn+dg+ga	68.33			32.54	100.88	
cu467B	66	sph	sph+py+ga	68.85			32.73	101.58	
cu489	89	sph	dg+X+sph+py	69.33			32.39	101.72	
cu501	25	sph	bn+cpy+dg+sph	67.26			33.42	100.68	
cu509	82	sph	sph+dg+cv	63.71	8.62		32.16	104.49	high Cu - possible multigrain beam point
cu509	83	sph	sph+dg+cv	60.13	10.02		31.80	102.25	high Cu - possible multigrain beam point
cu509	90	sph	cpy+bn+dg+sph	62.35	7.84	1.04	32.22	103.46	high Cu - possible multigrain beam point
cu199	13	sph	py+cv+sph	61.19	7.05	1.21	32.38	101.82	high Cu - possible multigrain beam point
cu441	86	sph	dg+cv+sph	65.69	4.22		31.51	102.25	high Cu - possible mix
cu503	16	sph	sph+cv	68.28	1.41		32.43	102.11	high total
cu507A	70	sph	cpy+dg+sph	65.72	4.49	0.93	32.82	103.97	high total
cu199	12	sph	py+cv+sph	67.76		0.79	33.71	102.26	high total
cu199	15	sph	py+cv+en+sph	68.03	1.20		33.59	102.82	high total
cu481A	93	sph	py+dg+bn+sph+en	69.65			33.34	102.99	high total
cu481A	98	sph	py+dg+bn+sph+en	68.45	1.41		32.76	102.61	high total
cu507A	72	sph	cpy+dg+sph	61.39	4.68	2.85	32.55	101.48	
stoichiometric sphalerite				66.41			33.59	100.00	
mean				67.66	0.96	0.63	32.76	100.99	
std				1.39	0.38	0.27	0.43	0.87	

Sphalerite - Weight Percent
15 acceptable samples in 7 samples

Sample	Point	analyzed	assemblage	ZnK	CuK	FeK	S K	Total
max				69.33	1.58	0.90	33.64	101.82
min				64.98	0.58	0.36	32.22	99.33
n				15	7	2	15	15
detection limit (3sigma LOQ)				0.80	0.50	0.25		

Pyrite - Weight Percent
16 acceptable analyses from 9 samples

Sample	Point	Analyzed	Assemblage	ZnK	CuK	FeK	AsL	S K	Total	
cu182B	54	py	en+sulfate+py			46.61	0.33	53.67	100.61	
cu182B	59	py	en+py			46.45	0.34	53.56	100.35	
cu182B	62	py	en+cv+py			46.66		53.26	99.92	
cu203A	38	py	cpy+dg+cv+sph+py		0.54	46.92		53.76	101.21	
cu204	54	py-incl	woll+py			46.14		54.17	100.31	
cu205B	1	py	py+dg+cv			46.65		53.83	100.48	
cu461B	36	py	dg+py			46.93	0.34	53.77	101.03	
cu461B	38	py	dg+py		0.69	46.61		53.12	100.42	
cu467A	29	py	dg+bn+ga+py			47.34		53.65	100.99	
cu467B	68	py	sph+py+ga			47.35	0.29	54.15	101.79	
cu476B	69	py	cpy+bn+dg+py			46.77	0.34	53.77	100.87	
cu476B	72	py	cv+py			46.97		54.13	101.11	
cu482	34	py	py+cv+dg			46.67	0.33	54.06	101.06	
cu482	36	py	cpy+py+cv			47.59		53.78	101.38	
cu489	95	py	py+dg			47.22	0.32	53.56	101.10	
cu489	96	py	py+dg			47.15		53.79	100.94	
stoichiometric pyrite						46.55		53.45	100.00	
mean				ERR	0.61	46.88	0.33	53.75	100.85	
std				ERR	0.08	0.37	0.02	0.29	0.46	
max				ERR	0.69	47.59	0.34	54.17	101.79	
min				ERR	0.54	46.14	0.29	53.12	99.92	
n				0	2	16	7	16	16	
Rejected Analyses										
cu467B	60	py	sph+py	2.18		46.29	0.26	53.89	102.62	high total; possible mixed analyses with sph
detection limit (3sigma LOQ)				0.80	0.50	0.25	0.25			

Wolframite - Weight Percent

13 analyses from 2 samples - All incomplete analyses

Sample	Point	Analyzed	Assemblage	CuK	FeK	AsL	MnK	W M	Total	
cu204	41	wolf	cv+dg+wolf		0.65			51.86	52.51	
cu204	42	wolf	wolf+cv+py		1.04	0.29		52.10	53.43	
cu204	46	wolf	wolf+py+dg+cv		1.11	0.27		51.24	52.62	
cu204	50	wolf	wolf+cv+dg	0.52	1.73			52.51	54.77	
cu204	61	wolf	wolf+cv+dg+py	1.21	1.13			52.55	54.88	
cu204	62	wolf-incl	py+wolf		2.21			52.73	54.93	
cu204	63	wolf-incl	py+wwolf		3.24	0.25		53.36	56.85	
cu205A	29	wolf	dg+cv+wolf	1.13	0.97		14.23	58.89	75.22	
cu205A	30	wolf	dg+cv+wolf	0.54	3.88		11.94	58.92	75.29	
cu205A	31	wolf	dg+cv+wolf				15.22	58.37	73.59	
cu205A	32	wolf	dg+cv+wolf		2.86		12.24	58.95	74.05	
cu205A	33	wolf	dg+cv+wolf	0.73	1.65		13.58	58.17	74.13	
cu205A	34	wolf	dg+cv+wolf	1.84			14.67	59.25	75.76	
stoichiometric hubnerite MnWO4							18.14	60.72	78.86	21.14
mean				0.99	1.86	0.27	13.65	55.30	63.69	
std				0.46	1.01	0.02	1.21	3.24	10.23	
max				1.84	3.88	0.29	15.22	59.25	75.76	
min				0.52	0.65	0.25	11.94	51.24	52.51	
n				6	11	3	6	13	13	
detection limit (3sigma LOQ)				0.50	0.25	0.25	0.40	0.50		

Galena - Weight Percent
13 analyses from 6 samples

Sample	Point	Analyzed	Assemblage	ZnK	CuK	FeK	S K	PbM	Total
cu461B	22	ga	ga+dg				12.09	85.83	97.92
cu461B	23	ga	ga+dg		2.23		12.24	86.73	101.20
cu467A	26	ga	dg+bn+ga+py				12.78	88.85	101.64
cu467B	53	ga	sph+bn+dg+ga				12.02	86.05	98.08
cu467B	54	ga	sph+bn+dg+ga				12.39	85.86	98.26
cu467B	65	ga	sph+py+ga			0.55	12.40	85.86	98.82
cu467B	67	ga	sph+py+ga			0.84	12.46	85.41	98.71
cu474A	18	ga	ga+py			1.51	13.10	89.53	104.14
cu474A	19	ga	ga+py		0.54	1.92	12.80	89.25	104.51
cu500A	35	ga	bn+ga+py		1.17		12.66	88.86	102.69
cu500A	37	ga	ga+bn+dg		0.61	1.03	12.92	89.08	103.63
cu503	20	ga	ga+bn+cpy		3.13		12.58	85.31	101.02
cu503	21	ga	ga+bn+cpy		1.59		12.41	86.61	100.61
detection limit (3sigma LOQ)				0.80	0.50	0.25	0.25	1.20	

Fe-oxides - weight percent

Sample	Point	Analyzed	Assemblage	ZnK	CuK	FeK	AsL	S K	MnK	CaK	V K	SiK	AlK	TiK	Total
cu441	87	Fe-oxide	py+oxide			54.55									54.55
cu441	88	Fe-oxide	py+oxide	5.99		24.97			1.88	1.11					33.96
cu455	39	Fe-oxide	cv+cpy+oxide			55.41	0.32								55.73
cu455	41	Fe-oxide	cv+cpy+oxide		0.53	55.48	0.27								56.27
cu455	45	Fe-oxide	cv+cpy+oxide		0.50	55.02	0.37								55.89
cu460	2	Fe-oxide	oxide			62.80				0.29	0.20		0.15		63.45
cu460	21	Fe-oxide	oxide			62.62					0.22				62.84
cu474A	15	Fe-oxide	dg+oxide		1.38	50.38	0.50			0.19		2.22	1.23		55.89
cu474A	16	Fe-oxide	dg+oxide		1.24	50.08	0.75			0.66		4.89	2.24		59.85
cu478	47	Fe-oxide	cpy+cv+oxide			63.92	0.26				0.35	0.25	0.19		64.98
cu478	48	Fe-oxide	cpy+cv+oxide			61.89	0.38					0.94	0.81	0.19	64.21
cu478	51	Fe-oxide	cpy+cv+oxide			64.15						0.13			64.28
cu482	38	Fe-oxide	cv+cpy+oxide		1.98	52.89	0.36	1.81							57.04
cu482	39	Fe-oxide	cv+cpy+oxide		1.61	53.87	0.25	0.55							56.29
cu482	40	Fe-oxide	cv+cpy+oxide		1.53	53.64	0.40								55.57
cu482	41	Fe-oxide	cv+cpy+oxide		1.45	54.94	0.34								56.73
cu482	48	Fe-oxide	cv+oxide			52.91	0.37								53.28

Sample	Point	Analyzed	Assemblage	CuK	FeK	AuM	W M	CaK	V K	SiK	AlK	TiK	Total
cu503	11	rutile			1.44	1.09						50.00	52.54
cu503	22	rutile	rutile+cpy			0.59		0.10				50.81	51.50
cu183B	85	rutile										53.11	53.11
cu476A	19	rutile	cpy+rt				0.25					52.94	53.20
cu478	49	rutile	cpy+cv+oxide		1.01		0.63					53.24	54.88
cu210	73	rutile	py+cv+rt				1.23					52.87	54.10
cu210	75	rutile	py+cv+rt				0.98					53.05	54.03
cu210	79	rutile	py+cv+rt		0.61		1.89	0.08				52.31	54.89
cu509	81	rutile	rutile					0.18				53.96	54.13
cu509	92	rutile	cpy+bn+dg+sph		0.70		0.39	0.10		0.22		53.33	54.73

Sulphate Minerals - weight percent

Sample	Point	Analyzed	Assemblage	CuK	S K	CaK	Total	
cu182B	55	sulfate	en+sulfate+py		20.47	27.49	47.96	anhydrite
cu205B	10	sulfate	cv+dg+sulfate		21.07	27.69	48.76	anhydrite
cu454B	73	sulfate	cv+sulfate	1.40	21.84	27.64	50.89	anhydrite
cu454B	74	sulfate	cv+sulfate		20.92	27.67	48.59	anhydrite
cu454B	78	sulfate	cv+cpy+sulf		21.44	27.93	49.37	anhydrite
cu454B	81	sulfate	dg+bn+sulf		18.99	25.87	44.86	anhydrite
cu461B	25	sulfate	dg+ga+sulfate	0.54	20.75	27.55	48.84	anhydrite
cu489	94	sulfate	py+sph+sulf		21.78	27.89	49.67	anhydrite

APPENDIX B

X-RAY DIFFRACTION ANALYSES

X-ray diffraction analyses were done at the Fission Track Research Laboratory, Earth Sciences Department, Dalhousie University. The analyses were performed on small sub-samples by standard powder diffraction. An automated Philips 100kV generator and diffractometer unit was used for mineral identification by powder diffractometry. The very fine-grained granular material was powdered in acetone by hand in an agate mortar. The powdered sample was placed on a glass microscope slide and mounted in the diffractometer (in some cases, an amorphous, single crystal silica mount was used to reduce the background response from the mount itself). The sample and x-ray detector were rotated at a known rate with respect to a CuKα x-ray source. Energy detected was recorded and processed automatically. Output consists of a peak list, energy response curve, and peak match fit lists for various search routines (Cuesta Report, 1996). Peak lists are included for each sample. Sample numbers are descriptive terms, e.g., cu199gyp is a sample of gypsum from cu199.

File: CU199GYP.DI 18-Dec-1996 15:52

Phillips Analytical X-Ray B. V. PC-APD, Diffraction software

Sample identification: cu199gyp
Data measured at: 20-Apr-1996 11:14:00

Diffractometer type: PW3710 BASED
Tube anode: Cu
Generator tension [kV]: 40
Generator current [mA]: 45
Wavelength Alpha1 []: 1.54060
Wavelength Alpha2 []: 1.54439
Intensity ratio (alpha2/alpha1): 0.500
Divergence slit: 1x
Receiving slit: 0.1
Monochromator used: YES

Start angle [x2i]: 10.000
End angle [x2i]: 90.000
Step size [x2i]: 0.020
Maximum intensity: 2959.360
Time per step [s]: 0.800
Type of scan: CONTINUOUS

Minimum peak tip width: 0.00
Maximum peak tip width: 1.00
Peak base width: 2.00
Minimum significance: 0.75
Number of peaks: 62

Angle [x2i]	d-value '1 []	d-value '2 []	Peak width [x2i]	Peak int [counts]	Back. int [counts]	Rel. int [%]	Signif.
11.560	7.6488	7.6676	0.200	2959	42	100.0	43.91
17.565	5.0451	5.0575	0.320	11	21	0.4	1.06
20.590	4.3102	4.3208	0.080	1832	18	61.9	2.26
20.665	4.2947	4.3053	0.080	1467	18	49.6	1.71
23.300	3.8146	3.8240	0.100	2510	17	84.8	11.30
25.405	3.5031	3.5118	0.160	16	16	0.5	1.06
26.585	3.3503	3.3585	0.280	72	16	2.4	5.87
28.000	3.1841	3.1919	0.160	38	16	1.3	1.13
29.040	3.0724	3.0799	0.220	2663	15	90.0	44.27
31.005	2.8820	2.8891	0.140	296	15	10.0	5.26
31.985	2.7959	2.8028	0.200	67	14	2.3	2.73
33.165	2.6991	2.7057	0.040	266	14	9.0	1.90
33.270	2.6908	2.6974	0.100	303	14	10.2	2.26
34.415	2.6038	2.6102	0.100	180	14	6.1	2.13
35.300	2.5406	2.5468	0.100	52	14	1.8	1.44
35.880	2.5008	2.5070	0.160	45	14	1.5	1.06
36.475	2.4614	2.4674	0.060	114	14	3.9	1.32
37.270	2.4107	2.4166	0.120	34	13	1.1	1.17
39.270	2.2924	2.2980	0.240	10	13	0.3	1.07
40.565	2.2221	2.2276	0.100	372	13	12.6	2.56
42.090	2.1451	2.1504	0.160	37	13	1.3	0.82
43.205	2.0923	2.0974	0.100	169	13	5.7	0.97

File: CU199GY9.DI 18-Dec-1996 15:52

Phillips Analytical X-Ray B. V. PC-APD, Diffraction software

Angle [x2i]	d-value '1 []	d-value '2 []	Peak width [x2i]	Peak Int [counts]	Back. Int [counts]	Rel. Int [%]	Signif.
43.495	2.0790	2.0841	0.060	210	13	7.1	0.89
44.090	2.0523	2.0574	0.160	50	13	1.7	0.99
44.490	2.0348	2.0398	0.120	36	13	1.2	0.84
45.370	1.9973	2.0022	0.080	137	13	4.6	1.11
46.250	1.9614	1.9662	0.240	15	13	0.5	1.43
47.810	1.9009	1.9056	0.220	303	12	10.2	9.86
48.265	1.8841	1.8887	0.200	125	12	4.2	2.81
50.160	1.8172	1.8217	0.060	1722	12	58.2	4.98
50.295	1.8127	1.8171	0.060	992	12	33.5	2.89
51.035	1.7881	1.7925	0.160	146	12	4.9	1.05
51.220	1.7821	1.7865	0.080	169	12	5.7	0.78
53.510	1.7111	1.7153	0.240	19	12	0.7	0.80
54.265	1.6891	1.6932	0.240	29	12	1.0	2.33
55.010	1.6679	1.6720	0.060	85	12	2.9	1.45
55.720	1.6484	1.6524	0.120	72	12	2.4	1.09
56.680	1.6227	1.6267	0.100	237	12	8.0	1.67
57.440	1.6030	1.6070	0.160	25	12	0.8	2.13
58.085	1.5867	1.5907	0.080	56	12	1.9	0.85
60.240	1.5350	1.5388	0.160	74	12	2.5	2.53
61.240	1.5123	1.5161	0.240	28	12	0.9	0.99
62.320	1.4887	1.4924	0.240	21	12	0.7	1.70
63.645	1.4609	1.4645	0.160	69	12	2.3	2.92
64.615	1.4413	1.4448	0.320	25	13	0.8	1.19
65.180	1.4301	1.4336	0.120	36	14	1.2	0.96
68.575	1.3674	1.3707	0.060	161	14	5.5	2.27
69.860	1.3453	1.3486	0.120	25	14	0.8	1.28
70.530	1.3342	1.3375	0.120	49	13	1.7	1.49
71.085	1.3251	1.3284	0.280	38	13	1.3	1.69
72.805	1.2980	1.3012	0.200	6	12	0.2	0.78
74.030	1.2795	1.2827	0.080	46	12	1.6	0.97
74.745	1.2690	1.2722	0.240	35	12	1.2	2.13
76.475	1.2446	1.2476	0.320	46	12	1.6	1.30
77.415	1.2318	1.2348	0.080	37	12	1.3	1.39
79.520	1.2044	1.2074	0.120	48	12	1.6	1.67
81.940	1.1748	1.1777	0.320	15	12	0.5	0.92
83.220	1.1600	1.1628	0.120	52	12	1.8	1.19
83.690	1.1547	1.1575	0.120	34	12	1.1	0.88
84.800	1.1424	1.1452	0.160	98	13	3.3	1.29
85.085	1.1393	1.1421	0.120	106	13	3.6	0.77
85.820	1.1314	1.1342	0.160	22	13	0.7	1.02

File: CU502SUL.DI 8-Dec-1996 17:46

Phillips Analytical X-Ray B. V. PC-APD, Diffraction software

Sample identification: cu502sulf
Data measured at: 19-Apr-1996 13:15:00

Diffractometer type: PW3710 BASED
Tube anode: Cu
Generator tension [kV]: 40
Generator current [mA]: 45
Wavelength Alpha1 []: 1.54060
Wavelength Alpha2 []: 1.54439
Intensity ratio (alpha2/alpha1): 0.500
Divergence slit: 1x
Receiving slit: 0.1
Monochromator used: YES

Start angle [x2i]: 10.010
End angle [x2i]: 119.990
Step size [x2i]: 0.020
Maximum intensity: 691.6900
Time per step [s]: 0.500
Type of scan: CONTINUOUS

Minimum peak tip width: 0.00
Maximum peak tip width: 1.00
Peak base width: 2.00
Minimum significance: 0.75
Number of peaks: 38

Angle [x2i]	d-value '1 []	d-value '2 []	Peak width [x2i]	Peak int [counts]	Back. int [counts]	Rel. int [%]	Signif.
10.290	8.5898	8.6109	0.480	0	30	0.0	0.77
11.635	7.5996	7.6183	0.080	416	31	60.2	4.25
18.900	4.9241	4.9362	0.960	8	41	1.1	0.89
20.705	4.2865	4.2970	0.160	28	48	4.1	0.95
23.385	3.8010	3.8103	0.080	142	55	20.5	1.67
28.490	3.1304	3.1381	0.080	169	52	24.4	1.32
29.130	3.0631	3.0706	0.120	59	50	8.6	0.81
31.455	2.8418	2.8488	0.160	55	42	7.9	0.80
33.035	2.7094	2.7160	0.120	692	41	100.0	10.98
37.105	2.4210	2.4270	0.060	488	32	70.6	1.88
40.765	2.2117	2.2171	0.060	174	28	25.2	1.25
40.885	2.2055	2.2109	0.040	85	28	12.2	0.78
47.420	1.9157	1.9204	0.060	216	29	31.2	1.26
56.265	1.6337	1.6377	0.060	339	27	48.9	1.84
56.425	1.6294	1.6334	0.060	193	27	27.9	1.37
59.030	1.5636	1.5674	0.060	62	27	9.0	3.35
59.185	1.5599	1.5637	0.060	28	27	4.1	0.80
61.690	1.5024	1.5061	0.040	310	27	44.8	29.98
61.865	1.4986	1.5022	0.060	144	27	20.8	1.00
64.275	1.4481	1.4516	0.100	66	27	9.5	2.45
64.465	1.4443	1.4478	0.060	40	27	5.7	1.49
76.595	1.2429	1.2460	0.060	35	29	5.0	2.05

File: CU502SUL.DI 8-Dec-1996 17:46

Phillips Analytical X-Ray B. V. PC-APD, Diffraction software

Angle [x2i]	d-value '1 []	d-value '2 []	Peak width [x2i]	Peak Int [counts]	Back. Int [counts]	Rel. Int [%]	Signif.
78.955	1.2116	1.2146	0.120	23	19	3.3	1.82
81.310	1.1823	1.1853	0.120	28	18	4.1	2.31
82.970	1.1629	1.1657	0.280	3	18	0.4	0.84
83.665	1.1550	1.1578	0.060	46	18	6.7	2.03
83.925	1.1520	1.1549	0.080	18	18	2.7	1.12
88.285	1.1060	1.1088	0.080	69	15	10.0	1.76
88.575	1.1032	1.1059	0.060	24	15	3.5	1.33
95.250	1.0427	1.0453	0.080	161	14	23.3	3.04
95.585	1.0399	1.0425	0.100	48	13	6.9	1.68
99.940	1.0060	1.0085	0.080	50	14	7.3	1.23
100.290	1.0034	1.0059	0.120	22	14	3.2	1.80
102.290	0.9892	0.9916	0.100	35	14	5.0	1.46
102.645	0.9867	0.9891	0.060	22	14	3.2	1.09
107.070	0.9578	0.9602	0.060	36	12	5.2	1.49
113.160	0.9229	0.9252	0.120	8	13	1.2	0.82
117.095	0.9030	0.9052	0.120	18	13	2.6	1.46

File: CU493GYP.DI 8-Dec-1996 17:44

Phillips Analytical X-Ray B. V. PC-APD, Diffraction software

Sample identification: cu493gyp
Data measured at: 20-Apr-1996 9:07:00

Diffractometer type: PW3710 BASED
Tube anode: Cu
Generator tension [kV]: 40
Generator current [mA]: 45
Wavelength Alpha1 []: 1.54060
Wavelength Alpha2 []: 1.54439
Intensity ratio (alpha2/alpha1): 0.500
Divergence slit: 1x
Receiving slit: 0.1
Monochromator used: YES

Start angle [x2i]: 10.010
End angle [x2i]: 89.990
Step size [x2i]: 0.020
Maximum intensity: 5640.010
Time per step [s]: 0.800
Type of scan: CONTINUOUS

Minimum peak tip width: 0.00
Maximum peak tip width: 1.00
Peak base width: 2.00
Minimum significance: 0.75
Number of peaks: 67

Angle [x2i]	d-value '1 []	d-value '2 []	Peak width [x2i]	Peak int [counts]	Back. int [counts]	Rel. int [%]	Signif.
11.580	7.6356	7.6544	0.140	5640	38	100.0	36.60
17.660	5.0181	5.0305	0.080	142	29	2.5	0.94
17.740	4.9957	5.0080	0.060	119	29	2.1	0.83
19.850	4.4692	4.4802	0.080	98	28	1.7	0.80
20.695	4.2885	4.2991	0.140	2134	28	37.8	20.33
22.875	3.8845	3.8941	0.120	53	27	0.9	1.11
23.320	3.8114	3.8208	0.120	1376	27	24.4	12.83
23.790	3.7372	3.7464	0.120	50	27	0.9	1.06
25.445	3.4977	3.5063	0.080	90	27	1.6	0.76
26.670	3.3398	3.3480	0.100	353	26	6.3	1.34
26.735	3.3318	3.3400	0.080	324	26	5.7	0.96
27.835	3.2026	3.2105	0.100	94	26	1.7	1.27
29.075	3.0688	3.0763	0.160	3102	26	55.0	35.81
29.825	2.9933	3.0006	0.100	110	25	2.0	0.82
31.030	2.8797	2.8868	0.180	286	25	5.1	9.17
32.015	2.7933	2.8002	0.080	121	25	2.1	1.11
33.290	2.6892	2.6958	0.100	266	25	4.7	2.46
33.390	2.6814	2.6880	0.080	234	25	4.2	1.75
34.450	2.6013	2.6077	0.060	151	24	2.7	2.95
35.005	2.5613	2.5676	0.160	100	24	1.8	1.90
35.330	2.5385	2.5447	0.080	74	24	1.3	0.76
35.920	2.4981	2.5043	0.080	79	24	1.4	0.76

File: CU493GYP.DI 8-Dec-1996 17:44

Phillips Analytical X-Ray B. V. PC-APD, Diffraction software

Angle [x2i]	d-value '1 []	d-value '2 []	Peak Width [x2i]	Peak Int [counts]	Back. Int [counts]	Rel. Int [%]	Signif.
36.560	2.4558	2.4619	0.060	110	24	2.0	1.87
37.330	2.4069	2.4129	0.160	40	23	0.7	0.98
37.775	2.3796	2.3854	0.100	34	23	0.6	0.98
40.575	2.2216	2.2271	0.120	303	24	5.4	4.32
42.100	2.1446	2.1499	0.240	38	24	0.7	2.30
42.445	2.1280	2.1332	0.200	31	24	0.6	0.84
43.310	2.0874	2.0926	0.080	149	25	2.6	0.93
43.560	2.0760	2.0811	0.060	174	25	3.1	1.20
44.185	2.0481	2.0531	0.160	55	25	1.0	2.01
44.535	2.0328	2.0378	0.120	46	25	0.8	0.77
45.305	2.0000	2.0050	0.060	185	25	3.3	0.76
45.430	1.9948	1.9997	0.060	193	25	3.4	1.53
47.785	1.9019	1.9066	0.080	296	26	5.2	1.19
48.310	1.8824	1.8871	0.120	102	26	1.8	1.09
50.260	1.8139	1.8183	0.100	243	26	4.3	2.93
51.080	1.7867	1.7910	0.100	130	26	2.3	1.70
51.315	1.7790	1.7834	0.120	139	27	2.5	1.74
52.805	1.7323	1.7365	0.240	15	27	0.3	0.88
53.475	1.7121	1.7164	0.240	18	27	0.3	1.49
54.405	1.6851	1.6892	0.240	14	27	0.2	0.92
55.090	1.6657	1.6698	0.200	66	27	1.2	2.58
55.760	1.6473	1.6513	0.160	72	28	1.3	1.23
56.645	1.6236	1.6276	0.140	142	28	2.5	3.50
57.500	1.6015	1.6054	0.120	26	28	0.5	1.11
58.090	1.5866	1.5905	0.120	40	28	0.7	1.21
60.280	1.5341	1.5379	0.100	48	29	0.8	1.14
61.315	1.5107	1.5144	0.160	24	29	0.4	0.94
61.850	1.4989	1.5026	0.240	32	29	0.6	3.69
63.715	1.4594	1.4630	0.120	41	30	0.7	0.95
64.800	1.4376	1.4411	0.400	16	31	0.3	1.03
65.295	1.4279	1.4314	0.160	22	31	0.4	0.86
68.635	1.3663	1.3697	0.120	112	27	2.0	1.72
69.385	1.3534	1.3567	0.240	28	27	0.5	1.17
70.050	1.3421	1.3454	0.240	28	27	0.5	0.82
70.610	1.3329	1.3361	0.120	48	27	0.8	1.16
71.265	1.3222	1.3255	0.320	19	27	0.3	0.88
73.005	1.2949	1.2981	0.480	10	26	0.2	1.14
74.030	1.2795	1.2827	0.120	28	26	0.5	1.39
74.810	1.2681	1.2712	0.120	40	26	0.7	2.17
76.315	1.2468	1.2499	0.560	25	26	0.4	1.91
77.485	1.2309	1.2339	0.320	25	26	0.4	0.90
79.595	1.2035	1.2064	0.320	21	26	0.4	0.92
83.245	1.1597	1.1626	0.120	44	24	0.8	2.34
84.850	1.1418	1.1446	0.060	62	23	1.1	1.12
85.125	1.1388	1.1416	0.100	61	23	1.1	0.96

File: CU479SUL.DI 8-Dec-1996 17:42

Phillips Analytical X-Ray B. V. PC-APD, Diffraction software

Sample identification: cu479sulf
Data measured at: 19-Apr-1996 14:22:00

Diffractometer type: PW3710 BASED
Tube anode: Cu
Generator tension [kV]: 40
Generator current [mA]: 45
Wavelength Alpha1 []: 1.54060
Wavelength Alpha2 []: 1.54439
Intensity ratio (alpha2/alpha1): 0.500
Divergence slit: 1x
Receiving slit: 0.1
Monochromator used: YES

Start angle [x2i]: 10.010
End angle [x2i]: 119.990
Step size [x2i]: 0.020
Maximum intensity: 1169.640
Time per step [s]: 0.800
Type of scan: CONTINUOUS

Minimum peak tip width: 0.00
Maximum peak tip width: 1.00
Peak base width: 2.00
Minimum significance: 0.75
Number of peaks: 43

Angle [x2i]	d-value 1 []	d-value 2 []	Peak width [x2i]	Peak int [counts]	Back. int [counts]	Rel. int [%]	Signif.
11.545	7.6587	7.6775	0.100	762	44	65.1	8.24
20.780	4.2712	4.2817	0.100	320	41	27.4	6.72
23.310	3.8130	3.8224	0.100	146	40	12.5	3.02
26.635	3.3441	3.3523	0.080	90	40	7.7	0.97
28.440	3.1358	3.1435	0.100	303	37	25.9	4.14
29.090	3.0672	3.0748	0.140	77	36	6.6	3.39
32.965	2.7150	2.7217	0.060	740	32	63.3	1.69
33.065	2.7070	2.7137	0.040	543	32	46.4	8.60
37.015	2.4267	2.4327	0.060	353	27	30.2	1.48
37.115	2.4204	2.4263	0.040	369	27	31.5	3.74
40.700	2.2151	2.2205	0.120	253	24	21.6	4.37
41.170	2.1909	2.1963	0.040	44	24	3.7	1.77
46.265	1.9608	1.9656	0.480	10	24	0.9	0.76
47.380	1.9172	1.9219	0.060	462	23	39.5	1.99
47.510	1.9122	1.9169	0.060	193	23	16.5	0.84
50.395	1.8195	1.8239	0.100	36	23	3.1	1.03
51.245	1.7813	1.7857	0.240	13	23	1.1	1.00
56.220	1.6349	1.6389	0.060	1170	26	100.0	3.99
56.375	1.6308	1.6348	0.060	543	25	46.4	1.96
58.970	1.5650	1.5689	0.060	76	24	6.5	2.60
61.575	1.5049	1.5086	0.060	132	24	11.3	1.05
64.215	1.4493	1.4528	0.080	142	24	12.1	1.91

File: CU479SUL.DI 8-Dec-1996 17:43

Phillips Analytical X-Ray B. V. PC-APD, Diffraction software

Angle [x2i]	d-value '1 []	d-value '2 []	Peak width [x2i]	Peak int [counts]	Back. int [counts]	Rel. int [%]	Signif.
64.390	1.4458	1.4493	0.080	62	24	5.3	0.86
69.285	1.3551	1.3584	0.100	52	24	4.4	1.76
76.550	1.2435	1.2466	0.120	37	23	3.2	0.80
78.910	1.2122	1.2152	0.120	92	22	7.9	3.24
79.130	1.2094	1.2123	0.060	46	22	4.0	1.78
81.275	1.1828	1.1857	0.080	117	21	10.0	2.34
81.515	1.1799	1.1828	0.080	38	21	3.3	1.08
83.590	1.1558	1.1586	0.080	21	21	1.8	0.97
88.255	1.1063	1.1091	0.080	62	18	5.3	1.24
95.205	1.0431	1.0456	0.080	488	18	41.8	5.27
95.520	1.0405	1.0430	0.060	237	18	20.3	1.47
99.895	1.0063	1.0088	0.080	123	17	10.5	2.02
100.230	1.0039	1.0063	0.120	35	17	3.0	0.87
102.260	0.9894	0.9918	0.060	52	17	4.4	1.59
102.615	0.9869	0.9893	0.120	19	17	1.7	1.31
107.040	0.9580	0.9604	0.080	231	17	19.8	3.12
107.425	0.9556	0.9580	0.080	114	16	9.8	2.20
114.465	0.9161	0.9183	0.160	18	16	1.5	1.09
117.065	0.9031	0.9053	0.100	48	16	4.1	1.24
117.535	0.9009	0.9031	0.120	19	16	1.7	1.41
119.670	0.8910	0.8931	0.060	35	15	3.0	1.42

File: CU479ANH.DI 8-Dec-1996 17:41

Phillips Analytical X-Ray B. V. PC-APD, Diffraction software

Sample identification: cu479anh
Data measured at: 20-Apr-1996 10:08:00

Diffractometer type: PW3710 BASED
Tube anode: Cu
Generator tension [kV]: 40
Generator current [mA]: 45
Wavelength Alpha1 []: 1.54060
Wavelength Alpha2 []: 1.54439
Intensity ratio (alpha2/alpha1): 0.500
Divergence slit: 1x
Receiving slit: 0.1
Monochromator used: YES

Start angle [x2i]: 10.010
End angle [x2i]: 89.990
Step size [x2i]: 0.020
Maximum intensity: 4984.360
Time per step [s]: 0.800
Type of scan: CONTINUOUS

Minimum peak tip width: 0.00
Maximum peak tip width: 1.00
Peak base width: 2.00
Minimum significance: 0.75
Number of peaks: 57

Angle [x2i]	d-value '1 []	d-value '2 []	Peak width [x2i]	Peak int [counts]	Back. int [counts]	Rel. int [%]	Signif.
11.715	7.5479	7.5665	0.240	692	36	13.9	33.73
20.755	4.2763	4.2868	0.140	279	21	5.6	4.83
22.930	3.8753	3.8849	0.120	86	18	1.7	1.71
23.440	3.7922	3.8015	0.160	279	18	5.6	9.21
25.500	3.4903	3.4989	0.240	4984	18	100.0	84.63
26.600	3.3484	3.3566	0.100	372	18	7.5	2.24
26.720	3.3336	3.3418	0.080	428	18	8.6	1.42
28.580	3.1208	3.1285	0.200	66	16	1.3	3.77
29.160	3.0600	3.0675	0.200	357	16	7.2	14.70
30.035	2.9728	2.9801	0.120	11	16	0.2	0.77
31.375	2.8488	2.8559	0.180	835	15	16.8	18.07
31.940	2.7997	2.8066	0.240	71	14	1.4	4.72
33.390	2.6814	2.6880	0.140	67	14	1.3	1.95
34.560	2.5932	2.5996	0.200	22	14	0.4	1.49
35.430	2.5315	2.5378	0.160	12	14	0.2	0.88
36.290	2.4735	2.4796	0.100	266	14	5.3	2.11
37.425	2.4010	2.4069	0.240	7	14	0.1	1.14
38.585	2.3315	2.3372	0.080	420	14	8.4	1.60
38.690	2.3254	2.3311	0.080	524	14	10.5	1.58
39.485	2.2804	2.2860	0.160	32	14	0.7	1.48
40.765	2.2117	2.2171	0.120	462	14	9.3	3.81
41.260	2.1863	2.1917	0.060	306	14	6.1	1.14

File: CU479ANH.DI 8-Dec-1996 17:41

Phillips Analytical X-Ray B. V. PC-APD, Diffraction software

Angle [x2i]	d-value '1 []	d-value '2 []	Peak width [x2i]	Peak int [counts]	Back. int [counts]	Rel. int [%]	Signif.
41.370	2.1807	2.1861	0.040	310	14	6.2	3.23
42.490	2.1258	2.1310	0.060	86	14	1.7	2.84
43.285	2.0886	2.0937	0.100	207	14	4.2	1.77
45.410	1.9957	2.0006	0.140	137	14	2.7	3.45
46.815	1.9390	1.9438	0.200	64	14	1.3	2.66
47.860	1.8991	1.9037	0.240	79	14	1.6	4.61
48.690	1.8686	1.8732	0.100	339	14	6.8	2.21
49.155	1.8520	1.8566	0.160	106	14	2.1	2.63
50.145	1.8178	1.8222	0.160	66	14	1.3	1.25
51.245	1.7813	1.7857	0.320	30	14	0.6	1.83
52.215	1.7505	1.7548	0.080	441	14	8.8	1.96
52.345	1.7464	1.7507	0.060	408	14	8.2	3.28
55.680	1.6495	1.6535	0.100	250	14	5.0	1.96
56.815	1.6192	1.6231	0.240	38	14	0.8	2.54
57.760	1.5949	1.5988	0.200	46	14	0.9	1.38
58.960	1.5653	1.5691	0.100	121	14	2.4	1.41
59.960	1.5415	1.5453	0.200	46	14	0.9	1.85
60.650	1.5256	1.5294	0.240	88	14	1.8	3.80
62.210	1.4911	1.4947	0.100	135	14	2.7	1.30
63.890	1.4559	1.4594	0.320	8	14	0.2	2.61
65.045	1.4328	1.4363	0.080	12	14	0.2	0.76
65.385	1.4261	1.4296	0.120	52	14	1.0	0.76
66.850	1.3984	1.4018	0.240	61	14	1.2	2.82
67.710	1.3827	1.3861	0.060	21	14	0.4	0.95
68.650	1.3661	1.3694	0.160	40	14	0.8	0.78
71.365	1.3206	1.3239	0.240	62	15	1.3	3.24
72.795	1.2981	1.3013	0.120	22	15	0.4	0.90
74.160	1.2776	1.2807	0.240	130	15	2.6	4.78
75.605	1.2567	1.2598	0.240	11	16	0.2	1.06
77.005	1.2373	1.2404	0.320	22	16	0.4	1.12
78.555	1.2168	1.2197	0.160	49	16	1.0	1.18
79.820	1.2006	1.2036	0.200	46	16	0.9	1.73
81.430	1.1809	1.1838	0.160	22	18	0.4	1.37
82.735	1.1656	1.1684	0.120	94	22	1.9	2.25
88.325	1.1056	1.1084	0.120	156	15	3.1	1.50

File: CU214CV.DI 8-Dec-1996 17:38

Phillips Analytical X-Ray B. V. PC-APD, Diffraction software

Sample identification: cu214cv
Data measured at: 19-Apr-1996 11:28:00

Diffractometer type: PW3710 BASED
Tube anode: Cu
Generator tension [kV]: 40
Generator current [mA]: 45
Wavelength Alpha1 []: 1.54060
Wavelength Alpha2 []: 1.54439
Intensity ratio (alpha2/alpha1): 0.500
Divergence slit: 1x
Receiving slit: 0.1
Monochromator used: YES

Start angle [x2i]: 10.010
End angle [x2i]: 119.990
Step size [x2i]: 0.020
Maximum intensity: 10795.21
Time per step [s]: 1.000
Type of scan: CONTINUOUS

Minimum peak tip width: 0.00
Maximum peak tip width: 1.00
Peak base width: 2.00
Minimum significance: 0.75
Number of peaks: 35

Angle [x2i]	d-value '1 []	d-value '2 []	Peak width [x2i]	Peak int [counts]	Back. int [counts]	Rel. int [%]	Signif.
10.805	8.1815	8.2016	0.100	605	144	5.6	6.41
21.690	4.0940	4.1041	0.160	204	253	1.9	5.03
23.715	3.7488	3.7580	0.960	37	250	0.3	0.86
25.440	3.4984	3.5070	0.120	92	250	0.9	1.16
27.165	3.2800	3.2881	0.240	81	250	0.8	1.49
27.665	3.2219	3.2298	0.060	231	250	2.1	0.91
29.205	3.0554	3.0629	0.080	484	246	4.5	0.84
29.310	3.0447	3.0522	0.080	571	246	5.3	0.98
31.775	2.8139	2.8208	0.180	1082	243	10.0	11.07
32.820	2.7266	2.7333	0.100	10795	243	100.0	21.86
32.925	2.7182	2.7249	0.040	5506	243	51.0	8.00
38.820	2.3179	2.3236	0.200	139	219	1.3	2.45
43.090	2.0976	2.1027	0.120	66	222	0.6	1.09
44.265	2.0446	2.0496	0.060	773	222	7.2	1.62
47.725	1.9041	1.9088	0.100	515	222	4.8	1.57
47.925	1.8966	1.9013	0.200	534	222	4.9	2.07
52.685	1.7359	1.7402	0.140	829	219	7.7	5.77
57.960	1.5899	1.5938	0.240	37	225	0.3	1.05
58.700	1.5716	1.5754	0.240	69	222	0.6	1.18
59.325	1.5565	1.5603	0.100	292	219	2.7	0.97
63.510	1.4636	1.4672	0.120	106	210	1.0	1.63
67.315	1.3899	1.3933	0.240	48	207	0.4	1.43

File: CU214CV.DI 8-Dec-1996 17:39

Phillips Analytical X-Ray B. V. PC-APD, Diffraction software

Angle [x2i]	d-value 1 []	d-value 2 []	Peak width [x2i]	Peak int [counts]	Back. int [counts]	Rel. int [%]	Signif.
69.310	1.3547	1.3580	0.060	219	204	2.0	1.45
74.020	1.2797	1.2828	0.400	49	199	0.5	1.62
79.020	1.2108	1.2137	0.400	29	199	0.3	0.89
81.985	1.1743	1.1772	0.120	55	193	0.5	1.31
82.540	1.1678	1.1707	0.060	149	193	1.4	1.49
88.870	1.1003	1.1030	0.160	199	190	1.8	1.51
93.205	1.0601	1.0627	0.320	42	182	0.4	0.90
96.355	1.0337	1.0362	0.480	20	182	0.2	1.61
97.880	1.0216	1.0241	0.160	48	180	0.4	0.85
101.685	0.9934	0.9958	0.640	36	180	0.3	1.60
108.155	0.9512	0.9535	0.800	34	177	0.3	1.89
113.295	0.9222	0.9244	0.640	26	166	0.2	1.03
117.860	0.8993	0.9015	0.480	20	166	0.2	0.91

File: CU2C4GYP.DI 8-Dec-1996 17:36

Phillips Analytical X-Ray B. V. PC-APD, Diffraction software

Sample identification: cu2C4gyp
Data measured at: 19-Apr-1996 9:16:00

Diffractometer type: PW3710 BASED
Tube anode: Cu
Generator tension [kV]: 40
Generator current [mA]: 45
Wavelength Alpha1 []: 1.54060
Wavelength Alpha2 []: 1.54439
Intensity ratio (alpha2/alpha1): 0.500
Divergence slit: 1x
Receiving slit: 0.1
Monochromator used: YES

Start angle [x2i]: 10.010
End angle [x2i]: 89.990
Step size [x2i]: 0.020
Maximum intensity: 9120.250
Time per step [s]: 0.800
Type of scan: CONTINUOUS

Minimum peak tip width: 0.00
Maximum peak tip width: 1.00
Peak base width: 2.00
Minimum significance: 0.75
Number of peaks: 42

Angle [x2i]	d-value '1 []	d-value '2 []	Peak width [x2i]	Peak int [counts]	Back. int [counts]	Rel. int [%]	Signif.
11.635	7.5996	7.6183	0.120	42	48	0.5	1.68
20.745	4.2783	4.2889	0.100	64	64	0.7	1.52
22.900	3.8804	3.8899	0.120	85	59	0.9	0.98
25.380	3.5065	3.5152	0.140	9120	55	100.0	47.78
28.525	3.1267	3.1344	0.140	130	42	1.4	4.70
29.115	3.0646	3.0722	0.120	25	41	0.3	1.19
31.300	2.8555	2.8625	0.100	801	32	8.8	5.81
31.925	2.8010	2.8079	0.080	86	30	0.9	0.82
36.250	2.4761	2.4822	0.140	250	21	2.7	5.18
38.605	2.3303	2.3361	0.100	812	18	8.9	6.24
40.775	2.2112	2.2166	0.140	380	18	4.2	6.50
41.280	2.1853	2.1907	0.080	484	18	5.3	2.30
43.255	2.0900	2.0951	0.120	182	18	2.0	3.88
45.380	1.9969	2.0018	0.080	210	17	2.3	1.83
46.790	1.9400	1.9447	0.080	55	17	0.6	0.82
48.620	1.8711	1.8757	0.080	339	17	3.7	1.99
49.105	1.8538	1.8584	0.200	117	16	1.3	3.18
50.310	1.8122	1.8166	0.100	19	16	0.2	1.16
52.135	1.7530	1.7573	0.080	600	16	6.6	1.03
52.245	1.7495	1.7538	0.060	1030	16	11.3	1.70
52.380	1.7453	1.7496	0.040	454	16	5.0	4.53
55.705	1.6488	1.6528	0.140	222	18	2.4	4.20

File: CU204GYP.DI 8-Dec-1996 17:36

Phillips Analytical X-Ray B. V. PC-APD, Diffraction software

Angle [x2i]	d-value '1 []	d-value '2 []	Peak width [x2i]	Peak int [counts]	Back. int [counts]	Rel. int [%]	Signif.
55.835	1.6452	1.6493	0.060	156	18	1.7	0.89
57.720	1.5959	1.5998	0.160	46	18	0.5	1.16
58.945	1.5656	1.5695	0.080	193	17	2.1	1.24
60.645	1.5257	1.5295	0.140	144	17	1.6	4.16
62.180	1.4917	1.4954	0.100	188	16	2.1	3.19
62.410	1.4868	1.4904	0.120	74	16	0.8	1.15
65.395	1.4259	1.4295	0.100	83	15	0.9	1.68
66.915	1.3972	1.4006	0.060	90	15	1.0	1.32
67.110	1.3936	1.3970	0.060	55	15	0.6	1.08
68.725	1.3647	1.3681	0.240	14	15	0.2	1.77
71.335	1.3211	1.3243	0.080	76	14	0.8	1.47
72.810	1.2979	1.3011	0.080	36	14	0.4	2.55
74.130	1.2780	1.2812	0.080	110	14	1.2	0.81
77.025	1.2371	1.2401	0.400	12	14	0.1	1.25
78.560	1.2167	1.2197	0.100	66	14	0.7	1.27
79.840	1.2004	1.2033	0.120	31	14	0.3	0.80
80.045	1.1978	1.2008	0.040	34	14	0.4	0.94
82.725	1.1657	1.1685	0.060	199	14	2.2	1.74
84.240	1.1485	1.1514	0.400	11	14	0.1	1.16
88.325	1.1056	1.1084	0.360	151	17	1.7	8.36

File: CU204A.DI 8-Dec-1996 17:33

Phillips Analytical X-Ray B. V. PC-APD, Diffraction software

Sample identification: cu204a
Data measured at: 28-Mar-1996 16:35:00

Diffractometer type: PW3710 BASED
Tube anode: Cu
Generator tension [kV]: 40
Generator current [mA]: 45
Wavelength Alpha1 []: 1.54060
Wavelength Alpha2 []: 1.54439
Intensity ratio (alpha2/alpha1): 0.500
Divergence slit: 1x
Receiving slit: 0.1
Monochromator used: YES

Start angle [x2i]: 5.010
End angle [x2i]: 99.990
Step size [x2i]: 0.020
Maximum intensity: 9139.360
Time per step [s]: 0.500
Type of scan: CONTINUOUS

Minimum peak tip width: 0.00
Maximum peak tip width: 1.00
Peak base width: 2.00
Minimum significance: 0.75
Number of peaks: 41

Angle [x2i]	d-value '1 []	d-value '2 []	Peak width [x2i]	Peak int [counts]	Back. int [counts]	Rel. int [%]	Signif.
11.625	7.6061	7.6249	0.080	128	30	1.4	1.75
20.890	4.2490	4.2594	0.120	52	46	0.6	0.85
22.945	3.8728	3.8824	0.160	55	42	0.6	1.42
23.385	3.8010	3.8103	0.120	42	42	0.5	2.06
25.430	3.4997	3.5084	0.140	9139	38	100.0	59.49
26.630	3.3447	3.3529	0.060	49	37	0.5	0.81
28.600	3.1186	3.1263	0.140	76	34	0.8	2.72
29.110	3.0651	3.0727	0.120	27	34	0.3	0.82
31.355	2.8506	2.8576	0.120	400	29	4.4	5.78
31.990	2.7955	2.8023	0.120	45	28	0.5	1.71
36.335	2.4705	2.4766	0.160	156	22	1.7	4.54
38.625	2.3292	2.3349	0.080	328	20	3.6	2.36
40.810	2.2094	2.2148	0.100	225	19	2.5	1.69
41.310	2.1838	2.1891	0.060	193	19	2.1	0.79
42.485	2.1260	2.1313	0.120	13	18	0.1	0.82
43.310	2.0874	2.0926	0.120	132	18	1.4	2.31
45.440	1.9944	1.9993	0.060	137	18	1.5	3.47
46.830	1.9384	1.9432	0.160	34	17	0.4	0.89
48.645	1.8702	1.8748	0.120	185	17	2.0	2.85
49.155	1.8520	1.8566	0.200	46	17	0.5	1.62
52.220	1.7503	1.7546	0.100	681	17	7.5	4.72
55.690	1.6492	1.6532	0.140	112	15	1.2	1.88

File: CU204A.DI 8-Dec-1996 17:33

Phillips Analytical X-Ray 8. V.. PC-APD, Diffraction software

Angle [x2i]	d-value '1 []	d-value '2 []	Peak width [x2i]	Peak int [counts]	Back. int [counts]	Rel. int [%]	Signif.
57.750	1.5952	1.5991	0.240	36	15	0.4	2.04
58.935	1.5659	1.5697	0.080	74	15	0.8	0.80
60.645	1.5257	1.5295	0.200	55	14	0.6	2.58
62.215	1.4910	1.4946	0.080	77	14	0.8	1.18
65.445	1.4250	1.4285	0.080	34	15	0.4	0.91
66.930	1.3969	1.4004	0.120	37	15	0.4	1.04
68.395	1.3705	1.3739	0.640	4	14	0.0	1.37
71.415	1.3198	1.3231	0.120	42	14	0.5	0.91
72.895	1.2966	1.2998	0.320	10	14	0.1	0.93
74.140	1.2779	1.2810	0.120	45	14	0.5	1.27
77.090	1.2362	1.2392	0.320	16	13	0.2	1.26
78.615	1.2160	1.2190	0.200	22	12	0.2	0.86
79.825	1.2006	1.2035	0.120	34	12	0.4	1.47
82.575	1.1674	1.1703	0.060	185	12	2.0	0.77
82.840	1.1643	1.1672	0.120	123	12	1.3	0.80
84.200	1.1490	1.1518	0.400	8	12	0.1	0.75
88.365	1.1053	1.1080	0.320	72	11	0.8	4.06
91.125	1.0788	1.0815	0.100	37	9	0.4	1.21
95.570	1.0401	1.0426	0.240	29	12	0.3	1.15

File: CU192DG.DI 8-Dec-1996 17:30

Philips Analytical PC-APD, Diffraction software

Sample identification: cu192dg
Data measured at: 20-Nov-1996 13:59:00

Diffractometer type: PW3710 BASED
Tube anode: Co
Generator tension [kV]: 40
Generator current [mA]: 35
Wavelength Alpha1 []: 1.78896
Wavelength Alpha2 []: 1.79285
Intensity ratio (alpha2/alpha1): 0.500
Divergence slit: 1x
Receiving slit: 0.1
Monochromator used: YES

Start angle [2θ]: 10.010
End angle [2θ]: 119.990
Step size [2θ]: 0.020
Maximum intensity: 198.8100
Time per step [s]: 0.800
Type of scan: CONTINUOUS

Minimum peak tip width: 0.00
Maximum peak tip width: 1.00
Peak base width: 2.00
Minimum significance: 0.75
Number of peaks: 26

Angle [2θ]	d-value θ1 []	d-value θ2 []	Peak width [2θ]	Peak int [counts]	Back. int [counts]	Rel. int [%]	Signif.
13.510	7.6046	7.6211	0.100	161	18	81.1	3.68
14.335	7.1690	7.1846	0.240	12	17	5.8	0.87
20.605	5.0014	5.0123	0.100	121	12	60.9	2.81
24.275	4.2542	4.2634	0.080	37	10	18.7	0.82
27.235	3.7992	3.8075	0.120	22	9	11.1	1.15
29.640	3.4970	3.5046	0.120	14	9	7.3	1.05
31.130	3.3335	3.3407	0.160	199	10	100.0	6.41
32.305	3.2153	3.2223	0.100	50	10	25.4	0.92
33.265	3.1250	3.1318	0.080	151	10	76.1	1.60
33.975	3.0616	3.0682	0.240	16	10	8.0	0.99
37.565	2.7791	2.7841	0.320	12	10	6.2	0.91
38.345	2.7236	2.7296	0.360	44	10	21.9	1.24
41.945	2.4991	2.5045	0.120	14	9	6.9	1.26
43.280	2.4256	2.4308	0.120	7	7	3.4	1.33
53.130	2.0001	2.0045	0.280	40	5	20.0	3.34
54.260	1.9615	1.9658	0.320	20	5	10.2	1.20
55.740	1.9135	1.9176	0.060	182	5	91.7	5.49
57.625	1.8560	1.8600	0.080	149	5	74.9	2.57
57.775	1.8516	1.8556	0.060	76	5	38.1	1.47
61.690	1.7446	1.7484	0.280	3	4	1.3	1.33
64.685	1.6720	1.6756	0.060	14	4	6.9	0.82
66.555	1.6302	1.6337	0.200	14	4	6.9	1.30

File: CU1920G.DI 8-Dec-1996 17:30

Philips Analytical PC-APD, Diffraction software

Angle [x2i]	d-value 1 []	d-value 2 []	Peak width [x2i]	Peak Int [counts]	Back. Int [counts]	Rel. Int [%]	Signif.
82.790	1.3527	1.3557	0.120	11	3	5.5	0.85
90.855	1.2557	1.2584	0.100	27	4	13.6	1.42
92.265	1.2407	1.2434	0.160	11	4	5.5	0.96
108.270	1.1038	1.1062	0.320	10	4	4.8	0.89

File: CU185PY.DI 18-Dec-1996 15:43

Philips Analytical X-Ray B.V. PC-APD, Diffraction software

Sample identification: cu185py
Data measured at: 22-Jul-1995 10:58:00

Diffractometer type: PW3710 BASED
Tube anode: Cu
Generator tension [kV]: 40
Generator current [mA]: 45
Wavelength Alpha1 []: 1.54060
Wavelength Alpha2 []: 1.54439
Intensity ratio (alpha2/alpha1): 0.500
Divergence slit: 1x
Receiving slit: 0.1
Monochromator used: YES

Start angle [x2i]: 10.000
End angle [x2i]: 120.000
Step size [x2i]: 0.020
Maximum intensity: 1713.960
Time per step [s]: 1.000
Type of scan: CONTINUOUS

Minimum peak tip width: 0.00
Maximum peak tip width: 1.00
Peak base width: 2.00
Minimum significance: 0.75
Number of peaks: 38

Angle [x2i]	d-value 'l []	d-value '2 []	Peak width [x2i]	Peak int [counts]	Back. int [counts]	Rel. int [%]	Signif.
27.330	3.2606	3.2686	0.060	58	180	3.4	0.98
28.510	3.1283	3.1360	0.060	286	172	16.7	0.92
33.035	2.7094	2.7160	0.060	1211	129	70.7	3.30
37.080	2.4226	2.4285	0.060	620	85	36.2	1.79
40.755	2.2122	2.2177	0.060	534	69	31.1	2.05
40.870	2.2062	2.2117	0.040	256	67	14.9	5.19
47.420	1.9157	1.9204	0.060	428	59	25.0	2.18
47.550	1.9107	1.9154	0.040	207	59	12.1	7.24
56.265	1.6337	1.6377	0.060	1714	53	100.0	4.92
56.425	1.6294	1.6334	0.060	853	53	49.7	3.25
59.010	1.5641	1.5679	0.060	213	52	12.4	1.54
59.170	1.5602	1.5641	0.060	114	52	6.7	4.15
61.685	1.5025	1.5062	0.080	207	52	12.1	2.91
61.855	1.4988	1.5025	0.080	96	52	5.6	1.37
64.275	1.4481	1.4516	0.080	272	50	15.9	3.45
64.460	1.4444	1.4479	0.060	144	50	8.4	0.98
76.595	1.2429	1.2460	0.060	110	36	6.4	1.30
76.830	1.2397	1.2428	0.060	49	36	2.9	1.23
78.965	1.2115	1.2144	0.060	119	34	6.9	1.05
79.185	1.2086	1.2116	0.080	59	34	3.5	0.82
81.305	1.1824	1.1853	0.060	128	31	7.4	0.95
81.555	1.1794	1.1823	0.080	45	31	2.6	1.30

File: CU18SPY.DI 18-Dec-1996 15:43

Philips Analytical X-Ray B.V. PC-APD, Diffraction software

Angle [x2i]	d-value '1 []	d-value '2 []	Peak width [x2i]	Peak Int [counts]	Back. Int [counts]	Rel. Int [%]	Signif.
83.650	1.1551	1.1580	0.060	59	29	3.5	1.93
83.910	1.1522	1.1550	0.060	44	29	2.5	1.21
88.300	1.1059	1.1086	0.080	142	26	8.3	2.33
88.570	1.1032	1.1059	0.100	48	26	2.8	2.12
95.260	1.0426	1.0452	0.060	552	23	32.2	2.43
95.580	1.0400	1.0425	0.080	219	23	12.8	2.91
99.915	1.0062	1.0087	0.080	128	23	7.4	1.97
100.265	1.0036	1.0061	0.100	49	23	2.9	1.49
102.295	0.9891	0.9916	0.120	77	23	4.5	3.87
102.640	0.9867	0.9892	0.080	45	23	2.6	0.77
107.070	0.9578	0.9602	0.080	121	22	7.1	1.92
107.440	0.9555	0.9579	0.080	59	22	3.5	1.10
114.500	0.9159	0.9181	0.080	32	20	1.9	0.96
117.080	0.9030	0.9053	0.100	112	20	6.6	3.40
117.530	0.9009	0.9031	0.060	45	20	2.6	0.83
119.725	0.8907	0.8929	0.080	38	20	2.2	0.76

File: CU185CV.DI 18-Dec-1996 15:42

Philips Analytical X-Ray B.V. PC-APD, Diffraction software

Sample identification: cu185cv
Data measured at: 23-Jul-1995 11:30:00

Diffractometer type: PW3710 BASED
Tube anode: Cu
Generator tension [kV]: 40
Generator current [mA]: 45
Wavelength Alpha1 []: 1.54060
Wavelength Alpha2 []: 1.54439
Intensity ratio (alpha2/alpha1): 0.500
Divergence slit: 1x
Receiving slit: 0.1
Monochromator used: YES

Start angle [x2i]: 10.000
End angle [x2i]: 120.000
Step size [x2i]: 0.020
Maximum intensity: 5212.840
Time per step [s]: 1.000
Type of scan: CONTINUOUS

Minimum peak tip width: 0.00
Maximum peak tip width: 1.00
Peak base width: 2.00
Minimum significance: 0.75
Number of peaks: 23

Angle [x2i]	d-value '1 []	d-value '2 []	Peak width [x2i]	Peak int [counts]	Back. int [counts]	Rel. int [%]	Signif.
10.815	8.1739	8.1940	0.080	529	128	10.1	4.31
18.735	4.7326	4.7442	0.480	19	225	0.4	0.76
21.730	4.0866	4.0966	0.160	125	286	2.4	1.53
27.695	3.2185	3.2264	0.160	90	289	1.7	0.91
29.270	3.0488	3.0563	0.060	272	269	5.2	0.81
31.815	2.8104	2.8174	0.160	552	243	10.6	4.57
32.840	2.7250	2.7317	0.080	5213	234	100.0	11.52
38.850	2.3162	2.3219	0.320	53	172	1.0	1.64
43.165	2.0941	2.0993	0.480	27	169	0.5	1.46
44.285	2.0437	2.0487	0.080	339	164	6.5	2.72
44.420	2.0378	2.0428	0.060	166	164	3.2	0.93
47.775	1.9022	1.9069	0.200	237	161	4.5	1.86
48.005	1.8937	1.8983	0.120	219	161	4.2	0.77
52.730	1.7346	1.7388	0.060	353	151	6.8	1.42
57.165	1.6101	1.6140	0.400	19	154	0.4	0.94
59.330	1.5564	1.5602	0.160	128	154	2.4	0.82
63.580	1.4622	1.4658	0.320	30	146	0.6	0.95
69.425	1.3527	1.3560	0.320	56	137	1.1	1.42
74.060	1.2791	1.2822	0.640	19	128	0.4	1.09
82.580	1.1674	1.1702	0.160	42	114	0.8	0.84
88.850	1.1005	1.1032	0.160	59	106	1.1	0.87
92.975	1.0622	1.0648	0.640	15	100	0.3	0.89

File: CU185CV.DI 18-Dec-1996 15:42

Philips Analytical X-Ray B.V. PC-APD, Diffraction software

Angle [x2i]	d-value α_1 []	d-value α_2 []	Peak width [x2i]	Peak int [counts]	Back. int [counts]	Rel. int [%]	Signif.
113.060	0.9234	0.9257	0.960	10	86	0.2	0.9

File: CU4538N.DI 18-Dec-1996 15:42

Philips Analytical X-Ray B.V. PC-APD, Diffraction software

Sample identification: cu453bn
Data measured at: 21-Jul-1995 9:24:00

Diffractometer type: PW3710 BASED
Tube anode: Cu
Generator tension [kV]: 40
Generator current [mA]: 45
Wavelength Alpha1 []: 1.54060
Wavelength Alpha2 []: 1.54439
Intensity ratio (alpha2/alpha1): 0.500
Divergence slit: 1x
Receiving slit: 0.1
Monochromator used: YES

Start angle [x2i]: 10.000
End angle [x2i]: 120.000
Step size [x2i]: 0.020
Maximum intensity: 488.4100
Time per step [s]: 1.000
Type of scan: CONTINUOUS

Minimum peak tip width: 0.00
Maximum peak tip width: 1.00
Peak base width: 2.00
Minimum significance: 0.75
Number of peaks: 16

Angle [x2i]	d-value '1 []	d-value '2 []	Peak width [x2i]	Peak int [counts]	Back. int [counts]	Rel. int [%]	Signif.
11.640	7.5964	7.6151	0.100	174	110	35.7	2.54
14.350	6.1673	6.1825	0.240	21	132	4.3	1.19
17.765	4.9887	5.0010	0.080	219	204	44.8	2.23
21.820	4.0699	4.0799	0.960	18	292	3.8	0.76
26.755	3.3294	3.3375	0.100	488	292	100.0	3.78
28.195	3.1625	3.1703	0.100	177	279	36.2	1.41
29.290	3.0467	3.0542	0.640	26	262	5.3	0.77
32.715	2.7352	2.7419	0.240	50	225	10.3	1.69
35.965	2.4951	2.5012	0.160	88	172	18.1	1.05
45.380	1.9969	2.0018	0.080	210	128	43.0	1.77
46.885	1.9363	1.9410	0.240	164	125	33.5	3.39
55.650	1.6503	1.6543	0.960	18	112	3.6	2.06
63.365	1.4666	1.4703	0.480	9	110	1.8	0.87
69.785	1.3466	1.3499	0.560	13	96	2.7	1.52
76.385	1.2458	1.2489	0.480	12	83	2.5	1.03
87.390	1.1151	1.1178	0.960	7	64	1.5	0.85

File: CU453CPY.DI 18-Dec-1996 15:41

Philips Analytical X-Ray B.V. PC-APD, Diffraction software

Sample identification: cu453cpy
Data measured at: 21-Jul-1995 16:00:00

Diffractometer type: PW3710 BASED
Tube anode: Cu
Generator tension [kV]: 40
Generator current [mA]: 45
Wavelength Alpha1 []: 1.54060
Wavelength Alpha2 []: 1.54439
Intensity ratio (alpha2/alpha1): 0.500
Divergence slit: 1x
Receiving slit: 0.1
Monochromator used: YES

Start angle [x2i]: 10.010
End angle [x2i]: 119.990
Step size [x2i]: 0.020
Maximum intensity: 1075.840
Time per step [s]: 1.000
Type of scan: CONTINUOUS

Minimum peak tip width: 0.00
Maximum peak tip width: 1.00
Peak base width: 2.00
Minimum significance: 0.75
Number of peaks: 17

Angle [x2i]	d-value '1 []	d-value '2 []	Peak width [x2i]	Peak int [counts]	Back. int [counts]	Rel. int [%]	Signif.
11.615	7.6127	7.6314	0.080	697	96	64.8	5.65
17.740	4.9957	5.0080	0.120	52	169	4.8	1.05
22.820	3.8938	3.9034	0.100	50	269	4.7	0.77
23.370	3.8034	3.8127	0.120	85	269	7.9	1.07
26.765	3.3281	3.3363	0.080	132	266	12.3	1.11
28.220	3.1598	3.1675	0.240	35	256	3.2	1.20
29.335	3.0421	3.0496	0.140	1076	240	100.0	13.07
33.875	2.6441	2.6506	0.240	34	182	3.1	1.01
45.420	1.9952	2.0002	0.120	45	114	4.2	1.33
46.940	1.9341	1.9389	0.240	40	112	3.7	2.44
48.635	1.8706	1.8752	0.160	83	110	7.7	0.85
49.020	1.8568	1.8614	0.060	174	108	16.2	1.77
57.830	1.5931	1.5971	0.160	98	102	9.1	1.25
58.565	1.5749	1.5788	0.240	21	102	2.0	1.00
71.200	1.3233	1.3265	0.480	12	83	1.1	0.81
91.320	1.0770	1.0797	0.960	8	52	0.8	1.10
98.570	1.0163	1.0188	0.480	11	45	1.0	0.78

File: CU438CPY.DI 18-Dec-1996 15:39

Philips Analytical X-Ray B.V. PC-APD, Diffraction software

Sample identification: cu438cpy
Data measured at: 21-Jul-1995 17:33:00

Diffractometer type: PW3710 BASED
Tube anode: Cu
Generator tension [kV]: 40
Generator current [mA]: 45
Wavelength Alpha1 []: 1.54060
Wavelength Alpha2 []: 1.54439
Intensity ratio (alpha2/alpha1): 0.500
Divergence slit: 1x
Receiving slit: 0.1
Monochromator used: YES

Start angle [x2i]: 10.000
End angle [x2i]: 120.000
Step size [x2i]: 0.020
Maximum intensity: 1428.840
Time per step [s]: 1.000
Type of scan: CONTINUOUS

Minimum peak tip width: 0.00
Maximum peak tip width: 1.00
Peak base width: 2.00
Minimum significance: 0.75
Number of peaks: 13

Angle [x2i]	d-value '1 []	d-value '2 []	Peak width [x2i]	Peak int [counts]	Back. int [counts]	Rel. Int [%]	Signif.
29.360	3.0396	3.0471	0.140	1429	219	100.0	14.87
33.820	2.6483	2.6548	0.200	44	166	3.0	1.22
46.945	1.9339	1.9387	0.240	34	110	2.4	0.83
48.615	1.8713	1.8759	0.100	146	106	10.2	1.04
49.040	1.8561	1.8607	0.080	296	106	20.7	1.29
57.855	1.5925	1.5964	0.240	185	102	12.9	4.37
58.535	1.5756	1.5795	0.160	79	102	5.5	1.14
71.305	1.3216	1.3248	0.240	18	90	1.3	1.04
79.470	1.2050	1.2080	0.120	81	76	5.7	0.85
79.710	1.2020	1.2050	0.060	44	76	3.0	0.84
91.285	1.0774	1.0800	0.480	34	61	2.4	1.65
112.465	0.9266	0.9289	0.800	7	56	0.5	1.22
115.475	0.9109	0.9132	0.480	4	52	0.3	0.81

File: CU453BN.DI 18-Dec-1996 15:40

Philips Analytical X-Ray B.V. PC-APD, Diffraction software

Sample identification: cu453bn
Data measured at: 21-Jul-1995 9:24:00

Diffractometer type: PW3710 BASED
Tube anode: Cu
Generator tension [kV]: 40
Generator current [mA]: 45
Wavelength Alpha1 []: 1.54060
Wavelength Alpha2 []: 1.54439
Intensity ratio (alpha2/alpha1): 0.500
Divergence slit: 1x
Receiving slit: 0.1
Monochromator used: YES

Start angle [x2i]: 10.000
End angle [x2i]: 120.000
Step size [x2i]: 0.020
Maximum intensity: 488.4100
Time per step [s]: 1.000
Type of scan: CONTINUOUS

Minimum peak tip width: 0.00
Maximum peak tip width: 1.00
Peak base width: 2.00
Minimum significance: 0.75
Number of peaks: 16

Angle [x2i]	d-value '1 []	d-value '2 []	Peak width [x2i]	Peak int [counts]	Back. int [counts]	Rel. int [%]	Signif.
11.640	7.5964	7.6151	0.100	174	110	35.7	2.54
14.350	6.1673	6.1825	0.240	21	132	4.3	1.19
17.765	4.9887	5.0010	0.080	219	204	44.8	2.23
21.920	4.0699	4.0799	0.960	18	292	3.8	0.76
26.755	3.3294	3.3375	0.100	488	292	100.0	3.78
28.195	3.1625	3.1703	0.100	177	279	36.2	1.41
29.290	3.0467	3.0542	0.640	26	262	5.3	0.77
32.715	2.7352	2.7419	0.240	50	225	10.3	1.69
35.965	2.4951	2.5012	0.160	88	172	18.1	1.05
45.380	1.9969	2.0018	0.080	210	128	43.0	1.77
46.885	1.9363	1.9410	0.240	164	125	33.5	3.39
55.650	1.6503	1.6543	0.960	18	112	3.6	2.06
63.365	1.4666	1.4703	0.480	9	110	1.8	0.87
69.785	1.3466	1.3499	0.560	13	96	2.7	1.52
76.385	1.2458	1.2489	0.480	12	83	2.5	1.03
87.390	1.1151	1.1178	0.960	7	64	1.5	0.85

File: CU438BN.DI 18-Dec-1996 15:38

Philips Analytical X-Ray B.V. PC-APD, Diffraction software

Sample identification: cu438bn
Data measured at: 21-Jul-1995 14:18:00

Diffractometer type: PW3710 BASED
Tube anode: Cu
Generator tension [kV]: 40
Generator current [mA]: 45
Wavelength Alpha1 []: 1.54060
Wavelength Alpha2 []: 1.54439
Intensity ratio (alpha2/alpha1): 0.500
Divergence slit: 1x
Receiving slit: 0.1
Monochromator used: YES

Start angle [x2i]: 10.000
End angle [x2i]: 120.000
Step size [x2i]: 0.020
Maximum intensity: 778.4100
Time per step [s]: 1.000
Type of scan: CONTINUOUS

Minimum peak tip width: 0.00
Maximum peak tip width: 1.00
Peak base width: 2.00
Minimum significance: 0.75
Number of peaks: 30

Angle [x2i]	d-value 1 []	d-value 2 []	Peak width [x2i]	Peak int [counts]	Back. int [counts]	Rel. int [%]	Signif.
11.670	7.5769	7.5956	0.060	62	142	8.0	0.96
13.995	6.3230	6.3385	0.200	42	159	5.4	0.98
14.350	6.1673	6.1825	0.160	42	164	5.4	0.95
15.980	5.5417	5.5553	0.480	12	180	1.6	0.77
17.750	4.9929	5.0052	0.080	85	204	10.9	0.80
18.505	4.7909	4.8026	0.120	46	219	5.9	1.17
21.855	4.0635	4.0735	0.120	85	279	10.9	2.15
26.775	3.3269	3.3351	0.120	234	286	30.1	0.97
27.005	3.2991	3.3072	0.120	324	286	41.6	1.03
27.310	3.2629	3.2710	0.060	123	286	15.8	0.84
27.555	3.2345	3.2424	0.060	104	286	13.4	0.75
28.195	3.1625	3.1703	0.140	534	286	68.6	6.62
31.875	2.8053	2.8122	0.080	164	240	21.0	1.45
32.685	2.7376	2.7443	0.240	276	234	35.4	6.08
34.045	2.6313	2.6378	0.240	42	219	5.4	0.82
35.710	2.5123	2.5185	0.060	225	202	28.9	1.25
35.980	2.4941	2.5002	0.060	202	196	25.9	1.32
42.960	2.1036	2.1088	0.320	35	169	4.5	1.13
45.435	1.9946	1.9995	0.240	59	161	7.6	0.84
46.910	1.9353	1.9400	0.140	778	159	100.0	3.31
47.075	1.9289	1.9336	0.140	467	159	59.9	1.49
49.160	1.8518	1.8564	0.320	26	154	3.3	0.92

File: CU4388N.DI 18-Dec-1996 15:38

Philips Analytical X-Ray B.V. PC-APD, Diffraction software

Angle [x2i]	d-value '1 []	d-value '2 []	Peak width [x2i]	Peak int [counts]	Back. int [counts]	Rel. int [%]	Signif.
55.635	1.6507	1.6547	0.200	86	137	11.1	1.20
58.190	1.5841	1.5880	0.960	13	137	1.7	1.18
60.365	1.5322	1.5359	0.640	18	139	2.4	0.99
65.430	1.4253	1.4288	0.480	24	132	3.1	2.17
68.415	1.3702	1.3735	0.560	22	123	2.8	1.48
71.915	1.3119	1.3151	0.200	16	114	2.1	0.85
75.260	1.2616	1.2647	0.800	10	112	1.3	0.92
87.120	1.1178	1.1206	0.120	52	90	6.7	0.94

File: CU434MO.DI 18-Dec-1996 15:37

Philips Analytical X-Ray B.V. PC-APD, Diffraction software

Sample identification: cu434mo
Data measured at: 20-Jul-1995 13:03:00

Diffractometer type: PW3710 BASED
Tube anode: Cu
Generator tension [kV]: 40
Generator current [mA]: 45
Wavelength Alpha1 []: 1.54060
Wavelength Alpha2 []: 1.54439
Intensity ratio (alpha2/alpha1): 0.500
Divergence slit: 1x
Receiving slit: 0.1
Monochromator used: YES

Start angle [x2i]: 10.000
End angle [x2i]: 120.000
Step size [x2i]: 0.020
Maximum intensity: 91930.24
Time per step [s]: 1.000
Type of scan: CONTINUOUS

Minimum peak tip width: 0.00
Maximum peak tip width: 1.00
Peak base width: 2.00
Minimum significance: 0.75
Number of peaks: 28

Angle [x2i]	d-value '1 []	d-value '2 []	Peak width [x2i]	Peak int [counts]	Back. int [counts]	Rel. int [%]	Signif.
11.575	7.6389	7.6577	0.140	15	86	0.0	0.88
13.000	6.8046	6.8213	0.080	96	98	0.1	0.95
14.385	6.1524	6.1675	0.100	91930	108	100.0	90.50
17.680	5.0125	5.0248	0.120	31	123	0.0	0.77
20.880	4.2510	4.2614	0.120	44	172	0.0	1.67
26.625	3.3453	3.3535	0.080	240	172	0.3	1.60
29.000	3.0765	3.0841	0.160	2520	156	2.7	32.20
32.685	2.7376	2.7443	0.120	34	125	0.0	0.94
39.550	2.2768	2.2824	0.080	204	72	0.2	1.27
44.130	2.0505	2.0556	0.080	11535	83	12.5	18.40
44.255	2.0450	2.0501	0.060	6545	83	7.1	3.92
49.815	1.8290	1.8335	0.160	154	62	0.2	3.12
56.020	1.6402	1.6443	0.320	26	61	0.0	1.26
58.360	1.5799	1.5838	0.320	35	61	0.0	0.92
60.120	1.5378	1.5416	0.080	9761	61	10.6	15.50
60.290	1.5339	1.5377	0.060	5461	61	5.9	3.72
62.790	1.4787	1.4823	0.240	26	61	0.0	0.94
70.170	1.3401	1.3434	0.120	86	53	0.1	1.84
77.545	1.2301	1.2331	0.100	1096	50	1.2	8.08
77.780	1.2269	1.2299	0.060	655	49	0.7	1.20
86.915	1.1199	1.1227	0.800	13	32	0.0	2.30
88.660	1.1023	1.1050	0.400	24	31	0.0	1.42

File: CU434MC.DI 18-Dec-1996 15:37

Philips Analytical X-Ray B.V. PC-APD, Diffraction software

Angle [x2i]	d-value λ_1 []	d-value λ_2 []	Peak width [x2i]	Peak int [counts]	Back. int [counts]	Rel. int [%]	Signif.
96.140	1.0354	1.0379	0.080	188	32	0.2	0.96
96.500	1.0325	1.0350	0.120	100	32	0.1	1.64
97.435	1.0251	1.0276	0.060	104	32	0.1	1.70
105.045	0.9706	0.9730	0.480	7	27	0.0	0.79
118.955	0.8942	0.8964	0.160	139	32	0.2	1.66
119.470	0.8919	0.8941	0.160	69	32	0.1	0.99

File: CU433MO.DI 18-Dec-1996 15:35

Philips Analytical X-Ray B.V. PC-APD, Diffraction software

Sample identification: cu433mo
Data measured at: 19-Jul-1995 8:55:00

Diffractometer type: PW3710 BASED
Tube anode: Cu
Generator tension [kV]: 40
Generator current [mA]: 45
Wavelength Alpha1 []: 1.54060
Wavelength Alpha2 []: 1.54439
Intensity ratio (alpha2/alpha1): 0.500
Divergence slit: 1x
Receiving slit: 0.1
Monochromator used: YES

Start angle [x2i]: 10.010
End angle [x2i]: 119.990
Step size [x2i]: 0.020
Maximum intensity: 67964.49
Time per step [s]: 1.000
Type of scan: CONTINUOUS

Minimum peak tip width: 0.00
Maximum peak tip width: 1.00
Peak base width: 2.00
Minimum significance: 0.75
Number of peaks: 31

Angle [x2i]	d-value '1 []	d-value '2 []	Peak width [x2i]	Peak int [counts]	Back. int [counts]	Rel. int [%]	Signif.
12.990	6.8098	6.8265	0.120	48	90	0.1	1.45
14.420	6.1375	6.1526	0.100	67964	104	100.0	84.93
22.905	3.8795	3.8891	0.960	10	213	0.0	0.97
26.580	3.3509	3.3591	0.160	50	196	0.1	0.90
29.025	3.0739	3.0815	0.100	1789	177	2.6	9.25
32.695	2.7368	2.7435	0.320	22	139	0.0	1.02
35.900	2.4995	2.5056	0.240	18	100	0.0	0.91
39.565	2.2760	2.2816	0.060	185	79	0.3	1.78
44.150	2.0497	2.0547	0.080	7430	83	10.9	14.31
44.280	2.0439	2.0490	0.060	4651	83	6.8	2.32
49.795	1.8297	1.8342	0.100	142	67	0.2	1.23
56.095	1.6382	1.6423	0.400	26	64	0.0	1.41
58.415	1.5786	1.5825	0.240	27	64	0.0	0.86
60.140	1.5373	1.5411	0.080	6209	64	9.1	11.63
60.310	1.5334	1.5372	0.080	3894	64	5.7	5.71
60.435	1.5305	1.5343	0.040	1815	64	2.7	0.91
60.595	1.5269	1.5306	0.080	697	64	1.0	1.42
62.885	1.4767	1.4803	0.240	20	64	0.0	1.33
70.135	1.3407	1.3440	0.120	81	53	0.1	2.04
73.225	1.2916	1.2948	0.560	3	49	0.0	0.77
77.555	1.2299	1.2330	0.100	713	52	1.0	6.96
77.785	1.2269	1.2299	0.080	433	50	0.6	1.56

File: CU433MC.DI 18-Dec-1996 15:35

Philips Analytical X-Ray B.V. PC-APD, Diffraction software

Angle [x2i]	d-value '1 []	d-value '2 []	Peak width [x2i]	Peak int [counts]	Back. int [counts]	Rel. int [%]	Signif.
86.780	1.1213	1.1241	0.240	18	34	0.0	1.56
88.725	1.1017	1.1044	0.560	35	32	0.1	4.08
96.200	1.0349	1.0375	0.180	207	34	0.3	4.95
96.515	1.0324	1.0349	0.160	104	34	0.2	0.99
97.430	1.0251	1.0276	0.120	41	32	0.1	1.28
100.330	1.0031	1.0056	0.640	7	30	0.0	0.97
105.255	0.9693	0.9717	0.960	10	27	0.0	3.07
118.950	0.8942	0.8964	0.100	139	34	0.2	1.00
119.460	0.8919	0.8941	0.200	71	34	0.1	1.49

File: CU183PY.DI 18-Dec-1996 15:34

Philips Analytical X-Ray B.V. PC-APD, Diffraction software

Sample identification: cu183py
Data measured at: 20-Jul-1995 9:20:00

Diffractometer type: PW3710 BASED
Tube anode: Cu
Generator tension [kV]: 40
Generator current [mA]: 45
Wavelength Alpha1 []: 1.54060
Wavelength Alpha2 []: 1.54439
Intensity ratio (alpha2/alpha1): 0.500
Divergence slit: 1x
Receiving slit: 0.1
Monochromator used: YES

Start angle [x2i]: 10.010
End angle [x2i]: 119.990
Step size [x2i]: 0.020
Maximum intensity: 795.2400
Time per step [s]: 1.000
Type of scan: CONTINUOUS

Minimum peak tip width: 0.00
Maximum peak tip width: 1.00
Peak base width: 2.00
Minimum significance: 0.75
Number of peaks: 31

Angle [x2i]	d-value '1 []	d-value '2 []	Peak width [x2i]	Peak int [counts]	Back. int [counts]	Rel. int [%]	Signif.
11.650	7.5899	7.6086	0.080	98	76	12.3	1.73
27.685	3.2196	3.2275	0.240	23	204	2.9	1.03
28.510	3.1283	3.1360	0.080	296	196	37.2	1.78
33.030	2.7098	2.7164	0.080	795	151	100.0	4.59
37.065	2.4235	2.4295	0.060	454	104	57.1	1.74
40.760	2.2119	2.2174	0.060	396	88	49.8	1.73
47.415	1.9158	1.9206	0.060	279	81	35.1	1.46
47.555	1.9105	1.9152	0.060	139	81	17.5	3.43
49.010	1.8572	1.8617	0.120	32	76	4.1	1.02
56.265	1.6337	1.6377	0.060	630	76	79.2	2.58
56.415	1.6297	1.6337	0.060	331	76	41.7	1.63
59.040	1.5633	1.5672	0.240	29	76	3.7	2.00
61.650	1.5033	1.5070	0.080	98	74	12.3	5.10
61.845	1.4990	1.5027	0.060	45	74	5.6	1.38
64.275	1.4481	1.4516	0.060	279	74	35.1	1.85
64.460	1.4444	1.4479	0.080	106	74	13.3	1.78
76.560	1.2434	1.2465	0.160	29	53	3.7	1.07
78.950	1.2117	1.2146	0.080	50	49	6.3	1.06
81.295	1.1825	1.1854	0.060	34	48	4.2	1.20
88.305	1.1058	1.1086	0.100	15	38	1.9	1.06
95.240	1.0428	1.0454	0.100	125	35	15.8	3.02
95.570	1.0401	1.0426	0.060	64	35	8.0	2.15

File: CU183PY.DI 18-Dec-1996 15:34

Philips Analytical X-Ray B.V. PC-APD, Diffraction software

Angle [x2i]	d-value 'i []	d-value '2 []	Peak width [x2i]	Peak int [counts]	Back. int [counts]	Rel. int [%]	Signif.
96.625	1.0315	1.0340	0.140	10	35	1.2	0.84
99.920	1.0061	1.0086	0.060	76	32	9.5	2.50
100.270	1.0036	1.0060	0.080	21	32	2.7	1.12
102.295	0.9891	0.9916	0.120	22	32	2.8	1.19
102.620	0.9869	0.9893	0.120	18	32	2.2	0.92
107.095	0.9577	0.9600	0.120	37	31	4.7	1.42
110.130	0.9396	0.9419	0.120	15	31	1.9	1.03
117.075	0.9031	0.9053	0.080	44	30	5.5	1.07
119.730	0.8907	0.8929	0.120	13	30	1.6	0.97

File: CU183EN.DI 18-Dec-1996 15:33

Philips Analytical X-Ray B.V. PC-APD. Diffraction software

Sample identification: cu183en
Data measured at: 20-Jul-1995 11:21:00

Diffractometer type: PW3710 BASED
Tube anode: Cu
Generator tension [kV]: 40
Generator current [mA]: 45
Wavelength Alpha1 []: 1.54060
Wavelength Alpha2 []: 1.54439
Intensity ratio (alpha2/alpha1): 0.500
Divergence slit: 1x
Receiving slit: 0.1
Monochromator used: YES

Start angle [x2i]: 10.000
End angle [x2i]: 120.000
Step size [x2i]: 0.020
Maximum intensity: 4816.360
Time per step [s]: 1.000
Type of scan: CONTINUOUS

Minimum peak tip width: 0.00
Maximum peak tip width: 1.00
Peak base width: 2.00
Minimum significance: 0.75
Number of peaks: 33

Angle [x2i]	d-value 1 []	d-value 2 []	Peak width [x2i]	Peak int [counts]	Back. int [counts]	Rel. int [%]	Signif.
11.630	7.6029	7.6216	0.080	182	137	3.8	1.82
13.740	6.4397	6.4556	0.120	69	149	1.4	0.76
18.235	4.8612	4.8731	0.080	222	213	4.6	1.72
26.625	3.3453	3.3535	0.120	59	282	1.2	1.51
27.735	3.2139	3.2218	0.180	4816	279	100.0	50.84
28.970	3.0796	3.0872	0.100	729	269	15.1	5.51
31.365	2.8497	2.8567	0.160	1815	253	37.7	20.83
37.000	2.4276	2.4336	0.200	30	196	0.6	0.89
39.835	2.2612	2.2667	0.240	35	193	0.7	1.12
40.515	2.2248	2.2302	0.120	335	196	7.0	3.06
43.895	2.0610	2.0660	0.160	56	190	1.2	0.96
48.925	1.8602	1.8648	0.060	2830	193	58.8	2.63
49.050	1.8557	1.8603	0.080	4109	193	85.3	4.88
52.825	1.7317	1.7359	0.080	372	190	7.7	0.86
52.965	1.7274	1.7317	0.080	384	190	8.0	0.85
56.250	1.6341	1.6381	0.080	45	177	0.9	0.85
57.315	1.6062	1.6102	0.060	388	174	8.1	4.75
57.875	1.5920	1.5959	0.080	369	174	7.7	1.32
59.190	1.5597	1.5636	0.060	196	174	4.1	1.79
59.360	1.5557	1.5595	0.060	296	174	6.1	1.09
60.785	1.5226	1.5263	0.240	16	172	0.3	0.87
65.485	1.4242	1.4277	0.240	56	169	1.2	0.76

File: CU183EN.DI 18-Dec-1996 15:33

Philips Analytical X-Ray B.V. PC-APD, Diffraction software

Angle [x2i]	d-value 1 []	d-value 2 []	Peak width [x2i]	Peak int [counts]	Back. int [counts]	Rel. int [%]	Signif.
69.740	1.3473	1.3507	0.480	18	159	0.4	1.25
75.015	1.2651	1.2683	0.240	132	154	2.7	2.61
78.620	1.2159	1.2189	0.100	161	149	3.3	0.78
80.430	1.1930	1.1960	0.160	102	149	2.1	1.03
84.195	1.1490	1.1519	0.480	36	139	0.7	2.60
85.860	1.1310	1.1337	0.400	36	135	0.7	0.99
92.010	1.0708	1.0734	0.140	119	130	2.5	1.66
94.910	1.0455	1.0481	0.560	98	125	2.0	5.89
99.220	1.0114	1.0138	0.400	56	123	1.2	2.34
103.945	0.9779	0.9803	0.320	25	119	0.5	0.84
112.105	0.9286	0.9309	0.320	77	112	1.6	1.63

File: CU182EN.DI 18-Dec-1996 15:31

Philips Analytical X-Ray B.V. PC-APD, Diffraction software

Sample identification: cu182en
Data measured at: 18-Jul-1995 12:34:00

Diffractometer type: PW3710 BASED
Tube anode: Cu
Generator tension [kV]: 40
Generator current [mA]: 45
Wavelength Alpha1 []: 1.54060
Wavelength Alpha2 []: 1.54439
Intensity ratio (alpha2/alpha1): 0.500
Divergence slit: 1x
Receiving slit: 0.1
Monochromator used: YES

Start angle [x2i]: 10.010
End angle [x2i]: 119.990
Step size [x2i]: 0.020
Maximum intensity: 6115.240
Time per step [s]: 1.000
Type of scan: CONTINUOUS

Minimum peak tip width: 0.00
Maximum peak tip width: 1.00
Peak base width: 2.00
Minimum significance: 0.75
Number of peaks: 33

Angle [x2i]	d-value '1 []	d-value '2 []	Peak width [x2i]	Peak int [counts]	Back. int [counts]	Rel. int [%]	Signif.
11.595	7.6258	7.6445	0.100	282	142	4.6	3.81
12.340	7.1670	7.1846	0.120	55	149	0.9	1.28
13.705	6.4561	6.4720	0.120	55	156	0.9	1.58
18.235	4.8612	4.8731	0.080	534	190	8.7	3.49
20.720	4.2834	4.2940	0.960	85	196	1.4	1.06
23.380	3.8018	3.8111	0.200	123	202	2.0	0.89
24.815	3.5851	3.5939	0.480	112	204	1.8	0.98
27.750	3.2122	3.2201	0.140	6115	210	100.0	31.35
28.950	3.0817	3.0893	0.060	515	216	8.4	0.98
31.375	2.8488	2.8559	0.140	1325	222	21.7	13.37
40.530	2.2240	2.2294	0.080	161	159	2.6	0.89
42.545	2.1232	2.1284	0.200	21	156	0.3	0.85
43.865	2.0623	2.0674	0.240	29	154	0.5	1.17
49.010	1.8572	1.8617	0.080	3306	146	54.1	6.86
49.145	1.8524	1.8569	0.040	1739	146	28.4	0.89
52.365	1.7305	1.7347	0.100	142	132	2.3	1.13
56.770	1.6203	1.6243	0.120	56	135	0.9	0.99
57.350	1.6053	1.6093	0.100	262	135	4.3	2.79
57.515	1.6011	1.6050	0.060	125	135	2.1	1.09
58.035	1.5880	1.5919	0.080	128	135	2.1	1.16
59.440	1.5538	1.5576	0.080	117	132	1.9	0.97
62.680	1.4810	1.4847	0.640	11	128	0.2	0.77

File: CU182EN.DI 18-Dec-1996 15:31

Philips Analytical X-Ray B.V. PC-APD, Diffraction software

Angle [x2i]	d-value 1 []	d-value 2 []	Peak width [x2i]	Peak int [counts]	Back. int [counts]	Rel. int [%]	Signif.
65.755	1.4190	1.4225	0.560	17	125	0.3	1.91
75.125	1.2636	1.2667	0.100	49	102	0.8	0.75
78.725	1.2146	1.2175	0.080	213	98	3.5	1.37
78.980	1.2113	1.2143	0.060	117	98	1.9	1.70
80.490	1.1923	1.1952	0.120	69	94	1.1	0.82
92.095	1.0700	1.0726	0.060	119	74	1.9	0.79
92.415	1.0671	1.0697	0.060	62	74	1.0	1.28
94.885	1.0458	1.0483	0.200	30	72	0.5	1.05
99.170	1.0117	1.0142	0.640	14	69	0.2	0.89
112.160	0.9283	0.9306	0.120	64	66	1.0	1.01
112.615	0.9258	0.9281	0.080	55	66	0.9	0.77

APPENDIX C

HAND SAMPLE DESCRIPTIONS OF 4500N SAMPLES

DD 2967

cu181, 671.5m: altered quartz-feldspar porphyry with sericite; narrow vein of pink gypsum (late); coating of chlorite on fravture surfaces; < 5% sulphide, disseminated blck-grey tarnished metallic mineral (Fe or Ti-oxide, or possibly mineral of tetrahedrite series).

cu182, 224.76m: quartz and altered (clay?) feldspars; semi-massive to massie veins of pyrite + enargite (lead-grey, metallic, massive and coarse striated crystals); sulphides 15+%, enargite > pyrite (2:1); good separate for sulphur isotopes.

cu183, 225.10m: similar to cu182, 20+% massive veins of enargite + pyrite (probably moderate sphalerite as well, but difficult to determine here); separate for sulphur isotopes.

cu184, 233.04m: beautiful semi-massive to massive pyrite flooded with covellite (occurs interstitially), possibly some chalcopyrite (minor); 30+% sulphides in quartz-feldspar matrix (feldspars altered slightly); no sulphate.

cu185, 234.45m: disseminated fine-grained to medium-grained pyrite + disseminated fine t-medium covellite (isolated euhedral (?) grains); later pyrite + enargite vein < 0.5cm wide; other than the vein, ~5% sulphide in sercitised matrix with blueish sulphate (anhydrite?).

cu186, 314.74m: minor disseminated pyrite +/- covellite, with very narrow (< 1mm) veinlets of covellite-pyrite in quartz vein (1% sulphides or less).

cu187, 316.26m: disseminated covellite (-digenite?) in white flaky sulphate (gypsum) + dissemianted pyrite and pyrite-covellite-digenite; possible separate for suphur isotopes?

cu189, 324.69m: disseminated sulphides (pyrite aggregate with bornite surrounding and interstitial, very fine, rounded grains of bornite +/- pyrite); 1% sulphides in sugary silicate-sulphate matrix with white gypsum.

cu190, 325.20m: < 10% disseminate sulphide, pyrite with digenite-covellite surrounding and interstitial; disseminated digenite-covellite; minor bornite in pyrite assemblage; pyrite-bornite-digenite concentrated along narrow healed fractures in quartz-feldspar porphyry flooded with granular sulphate.

cu191, 325.49m: very altered porphyry, extreme sericitization; abundant disseminated covellite, bornite +/- chalcopyrite, and pyrite; narrow veins of blueish anhydrite contain disseminated covellite-pyrite (?), very fine-grained; 5% sulphides.

cu192, 325.93m: semi-massive to fine-grained disseminated digenite + pyrite (digenite >> pyrite) in highly sericitized rock with pink/orange sugary sulphate (gypsum) + blueish anhydrite; minor occurrences of massive-textured flaky tarnished bornite; 10% sulphides.

cu193, 408.00m: abundant disseminated fine- to medium-grained pyrite + digenite +/- covellite +/- bornite (individual minerals < 0.5mm); 5+% sulphides in highly sericitized porphyry cut by < 1cm milky quartz veins.

cu194, 411.38m: mainly disseminated pyrite-digenite + narrow 1+mm veinlets of pyrite +/- digenite in (mostly) quartz; < 5% sulphides, fine-grained.

cu196, 415.40m: clay-rich altered prophyry with fine-grained disseminated pyrite +/- digenite and vein assemblage pyrite-digenite; 2% sulphides.

cu197, 566.23m: essentially the same as cu196, pyrite > digenite in sericitized rocks.

cu198, 567.48m: minor veinlets of pyrite + digentie; disseminated pyrite and veinlets of massive molybdenite; 2% sulphides in very grungy porphyry.

cu199, 569.42m: fine-grained disseminated pyrite + digenite +/- bornite +/- chalcopyrite; narrow (1mm?) veinlet of covellite (?) + pyrite; 5+% sulphides in quartz-rich rock.

cu200, 574.23m: semi-massive to disseminated pyrite + digenite + chalcopyrite (much less chalcopyrite than pyrite and digenite); narrow veinlets and stringers of pyrite and of digenite + pyrite +/- covellite; 20% sulphides in sercitized quartz porphyry.

cu201, 547.87m: abundant semi-massive to disseminated pyrite + covellite (+/- digenite); minor chalcopyrite; 15% sulphides in moderately sericitized porphyry.

cu202, 575.14m: abundant fine-grained disseminated digenite + pyrite (also occurs with narrow rims of digenite around pyrite), +/- covellite; sericitized (and clay-altered?) feldpars in in porphyry; 5-10% sulphides.

cu203, 576.98m: stringer and disseminated pyrite + covellite, distinct from semi-massive pyrite + digenite +/- covellite assemblage; covellite-digenite-pyrite in blueish anhydrite (?); chalcopyrite sometimes included in this assemblage, or disseminated; 5+% sulphides in sericitized porphyry with sulphate.

cu204, 513.05m: abundant semi-massive to massive pyrite with digenite-covellite surrounding and filling spaces; disseminated pyrite + digenite + covellite, minor chalcopyrite; disseminated pyrite in vein of pinkish-white anhydrite; ~ +/-20% sulphides in sericitized porphyry; good separates for sulphur isotopes.

cu205, 514.90m: vein of pyrite-digenite (?) (steel-grey streak); disseminated pyrite +/- digenite; other than the vein (0.5 to 1cm wide), sample contains 1-3% sulphides in sericitized porphyry

with white gypsum crystals.

cu206, 518.65m: fine stringers of covellite + digenite; disseminated pyrite +/- digenite +/- covellite, and narrow veinlets of pyrite + chalcopyrite; 5+% sulphides in sericitized porphyry with blueish anhydrite and pink gypsum?

cu207, 605.70m: mainly disseminated and fine stringers of pyrite; minor digenite + covellite; bornite seam in sericitized porphyry.

cu208, 607.96m: abundant disseminated to semi-massive pyrite +/- chalcopyrite, + digenite-covellite (bornite?); 5% sulphides, some disseminated in blue anhydrite? in sericitized porphyry; smeared appearance.

cu209, 619.86m: 1-2% disseminated pyrite and covellite in sericitized porphyry.

cu210, 455.90m: disseminated pyrite and chalcopyrite, + covellite, with stringers of chalcopyrite-bornite (very tarnished); <5% sulphides in sericitized rock with pink sulphate - gypsum?

DD 2242

cu431, 38.55m: abundant disseminated chalcopyrite + covellite, covellite > chalcopyrite, looks to be later, filling spaces and veinlets between chalcopyrite; 5% sulphides in sericitized porphyry, no sulphate.

cu432, 40.91m: <0.5cm wide veins of molybdenite; disseminated and narrow stringers of covellite + chalcopyrite; 2% sulphides in sericitized porphyry.

cu433, 56.45m: abundant molybdenite in veins; minor disseminated molybdenite, and chalcopyrite and pyrite + covellite; 5-10% sulphides in dominantly quartz host.

cu434, 95.86m: narrow veinlets of molybdenite, pinching and swelling, and abundant dissemianted covellite and covellite + pyrite; molybdenite dominant sulphide; <5% sulphides in quartz vein host.

cu435, 103.07m: narrow (<0.5cm) veins of ?-pyrite; 5% sulphides in sericitized porphyry with greasy appearance (possibly some gypsum?).

cu436, 103.83m: disseminated chalcopyrite, rounded and envelopped by covellite, and disseminated covellite (minor, <1% for both); abundant disseminated digenite with minor pyrite or chalcopyrite; 5% sulphides in sericitized potassically-altered porphyry with relict pink feldspars.

cu437, 138.24m: mainly disseminated to stringer chalcopyrite with covellite surrounding and filling spaces between chalcopyrite; +/- digenite; 5+% sulphides in quartz and sugary pink gypsum? (soft).

cu438, 139.15m: smeared-out altered porphyry with disseminated to stringer chalcopyrite + bornite +/- covellite, and disseminated covellite; 5% sulphides.

cu439, 141.28m: minor disseminated to stringer chalcopyrite +/- digenite (?); 1% sulphides in sericitized porphyry.

cu440, 142.13m: 4cm * 1mm vein of semi-massive chalcopyrite + minor bornite; narrow stringers of chalcopyrite + bornite; semi-abundant fine-grained disseminated chalcopyrite and covellite (covellite surrounding/replacing chalcopyrite?); 5% sulphides in quartz-rich porphyry.

cu441, 145.32m: fault gouge, very chloritised?; massive area of fine-grained (<1mm) pyrite spheres flooded with digenite; disseminated pyrite + digenite + sphalerite, and chalcopyrite +bornite; 40% sulphides.

cu442, 149.60m: mainly fine stringers of chalcopyrite, semi-massive, with surrounding covellite; disseminated fine to medium-grained (>2mm) aggregates of bornite + covellite and bornite + covellite + chalcopyrite; <5% sulphides in sericitized porphyry with narrow veins (0.5cm) of pink gypsum; minor molybdenite.

cu443, 151.38m: narrow viens and abundant isolated patches of molybdenite; minor molybdenite + pyrite/chalcopyrite; stringers of pyrite + chalcopyrite, minor bornite, minor covellite; disseminated chalcopyrite + bornite; 5+% sulphides in quartz-sericite with later pinkish sulphate (good cleavage)--gypsum? barite?

cu444, 154.42m: abundant stringers of covellite + bornite (+/- digenite) +/- chalcopyrite; disseminated covellite, bornite + chalcopyrite, and minor molybdenite; molybdenite occurs with covellite/bornite +/- chalcopyrite (?); abundant disseminated fine-grained to massive (small patches) of digenite; <10% sulphides in quartz-sericite with pink sulphate - gypsum?

cu445, 153.63m: < 0.5cm wide pyrite veins in 2cm-wide quartz vein in quartz-sericite porphyry; semi-massive pyrite with interstitial digenite-covellite + sphalerite (? silvery to black, some red metallic tarnish, with streak of sphalerite); gives massive sulphides veins with semi-massive pyrite-digenite +/- covellite +/- sphalerite aggregates throughout; 20% sulphides in sample.

cu446, 156.77m: mainly stringers and large (up to 5mm) flaky aggregates of digenite; isseminated rounded chalcopyrite with fine rims of covellite; some digenite-covellite contains euhedral grains of <1mm pyrite; 5% sulphides inmoderately sericitized porphyry,; sulphides occur with feldspars and narrow vein quartz.

cu447, 160.76m: semi-massive to disseminated covellite +/- pyrite; very fine stringers of chalcopyrite + covellite; very fine stringers of covellite; semi-massive covellite occurs in mainly quartz in sericitized porphyry; 5+% sulphides.

cu448, 161.04m: fine stringers and abundant dissemianted digenite-covellite, +/- pyrite; digenite-covellite dissemianted to semi-massive; minor molybdenite?; 5+% sulphides in sericitized porphyry.

cu449, 161.41m: abundant fine stringers of covellite +/- pyrite, and abundant disseminated covellite + digenite t+/- bornite; minor disseminated chalcopyrite +/- rimmed by covellite; 5-10% sulphides in quartz-sericite porphyry.

cu450, 161.98m: abundant fine stringers of covellite with chalcopyrite (covellite >> chalcopyrite, rimming and filling); stringers of bornite +/- chalcopyrite; abundant disseminated covellite, chaclopyrite, bornite; ~ 5% sulphides in sericitized porphyry.

cu451, 164.98m: abundant stringers and disseminated bornite + chalcopyrite; disseminated chalcopyrite with covellite rimming; disseminated covellite + digenite and occasional fine stringers of digenite; veinlet of molybdenite; <5% sulphides in quartz-sericite porphyry; narrow vein of late sulphate with chalcopyrite-bornite stringer concentrated along the boundary.

cu452, 189.86m: very fine stringers and disseminated bornite-chalcopyrite (bornite > chalcopyrite); minor very fine-grained disseminated pyrite; possible minor covellite; < 5% sulphides (mainly bornite-chalcopyrite) in mildly sericitized potassically-altered porphyry.

cu453, 193.10m: abundant disseminated and semi-massive bornite + chalcopyrite; semi-abundant digenite + bornite, minor covellite; < 10% sulphides in (mainly) quartz.

cu454, 193.78m: abundant massive and disseminated (mm size) bornite-chalcopyrite; semi-abundant veinlets of molybdenite; minor fine-grained disseminated covellite; narrow 2-3mm wide vein of sulphate (pink gypsum) + sulphides; 15% sulphides in potassically-altered porphyry with abundant narrow sulphate veins (crossing, diverging, etc.)

cu455, 193.86m: abundant semi-massive to massive chalcopyrite with interstitial covellite; abundant veins of massive bornite-chalcopyrite, 2mm to 1cm wide; 5+% sulphides in quartz (vein?).

cu456, 194.20m: abundant fine stringers and disseminated very fine bornite-chalcopyrite; moderate disseminated covellite + digenite; disseminated sulphides in quartz (veins?) cut by pinkish sulphate veins; 10% sulphides in porphyry.

cu457, 195.76m: abundant veinlets (< 0.5cm wide) of semi-massive to disseminated bornite-chalcopyrite, +/- very fine rims of covellite; disseminated bornite, chalcopyrite and minor covellite throughout; 5+% sulphides in potassically-altered porphyry.

cu458, 196.55m: mainly disseminated minor fine stringers of bornite; disseminated fine-grained covellite +/- digenite, < bornite; possible minor molybdenite; 2% sulphides in potassic and sericitic porphyry (large, cm-scale panels of potassium-feldspar adjacent to quartz-sericite alteration).

cu459, 200.04m: very fine stringers, occassional semi-massive patches, and disseminated chalcopyrite-bornite; disseminated covellite throughout; minor molybdenite; 1-2% sulphides in potassically-altered porphyry.

cu460, 200.75m: abundant narrow (mm scale) undualting pinched veins of semi-massive chalcopyrite-bornite, and covellite +/- digenite; disseminated chalcopyrite, bornite and covellite; < 5% sulphides in potassically-altered porphyry.

cu461, 202.52m: mainly network of 1-3mm wide veinlets of semi-massive to disseminated pyrite + digenite (digenite > pyrite); moderate disseminated to semi-massive bornite; minor disseminated covellite?; 10+% sulphides in mainly quartz.

cu462, 252.55m: sulphides consist mainly of chalcopyrite-bornite disseminated and in fine

stringers; disseminated covellite, < bornite; possible minor molybdenite; 1+% sulphides in potassically-altered porphyry with abundant coarse biotite crystals.

cu463, 257.63m: essentially the same as cu462; 1% sulphides, mainly chalcopyrite-bornite in fine stringers and disseminated throughout potassically-altered porphyry.

cu464, 258.45m: disseminated and stringer bornite-chalcopyrite, with minor covellite rimming chalcopyrite; minor disseminated digenite?; <5% sulphides in potassically-altered porphyry.

cu465, 260.14m: abundant veinlet, stringer, and disseminated chalcopyrite-bornite; disseminated chalcopyrite + pyrite; bornite and/or covellite on late fracture surface; 5% sulphides in potassically-altered porphyry.

cu467, 261.27m: mainly abundant disseminated and fine stringers to a few occurrences of semi-massive pyrite-digenite; one 0.5 to 1cm wide band of massive pyrite + digenite + bornite +/- covellite (vein consists of > 60% sulphide); other than the band of sulphide, sample consists of ~10% sulphide in sericitized porphyry with several narrow (mm scale) veins of white sulphate (gypsum) +/- sulphide.

cu468, 253.23m: mainly veins and disseminated pyrite + chalcopyrite + digenite + covellite, and the assemblage chalcopyrite + bornite; 15% sulphides in sericitized porphyry.

cu469, 263.66m: some fine stringers and abundant very fine-grained disseminated chalcopyrite + pyrite +/- covellite +/- bornite; abundant disseminated covellite-digenite (?); 1-2% sulphides in quartz-rich veins with minor sericite cutting potassically-altered porphyry.

cu470, 264.53m: minor very fine-grained stringers and disseminated chalcopyrite + covellite, with covellite disseminated on its own or as fine rims around chcalcopyrite; < 1% sulphides in potassically-altered porphyry.

cu471, 264.98m: narrow (1-2mm) bands of sulphide, 3cm apart, pyrite + digenite + covellite, with possible bornite; fine-grained disseminated pyrite and digenite-covellite throughout; 1% sulphides in moderately sericitized potassically-altered porphyry; abundant coarse biotite crystals.

cu472, 265.60m: mainly very fine-grained disssemianted to stringer chalcopyrite +/- bornite with covellite surrounding and disseminated on its own; 1% sulphides in sericitized potassically-altered porphyry with abundant large biotite crystals.

cu473, 284.39m: minor sulphides, consisting mainly of very fine stringers and some disseminated chalcopyrite +/- pyrite, with minor bornite; 1+% sulphides in potassically-altered porphyry with abundant large biotite crystals.

cu474, 286.75m: narrow veinlet of digenite bordered by covellite (up to 1.5mm wide); abundant very fine-grained disseminated covellite-digenite; rounded chalcopyrite with covellite rims; 2% sulphides in potassically-altered porphyry.

cu475, 282.04m: dissemianted, stringer, and fine stockwork veins of chalcopyrite, rimmed and sometimes invaded by covellite; stockwork and disseminated chalcopyrite + bornite; < 5% sulphides in potassically-altered porphyry.

cu476, 288.10m: abundant fine stringers of chalcopyrite (+/- minor bornite) with covellite rimming and/or replacing (?); stringers are cut in some places by narrow pinching and swelling veins of pyrite-digenite-covellite; abundant disseminated chalcopyrite (+/- bornite) wtih covellite, and covellite on its own; 5% sulphides in potassically-altered porphyry.

cu477, 288.65m: veins of semi-massive to massive chalcopyrite with very minor bornite and minor bordering covellite; disseminated chalcopyrite with covellite rims throughout; possible minor sphalerite?; 5+% sulphides in moderately sericitized porphyry (chalcopyrite veins with quartz-sericite halos cutting through potassically-altered porphyry.

cu478, 288.95m: very fine stringer to disseminated covellite (+ digenite?); minor chalcopyrite stringers wtih rims of covellite; abundant large crystals of biotite, some associated with sulphides; 1-2% sulphides in potassically-altered porphyry.

DD 2234

cu479, 294.20m: patches of massive pyrite with minor digenite rimming small rounded grains or aggregates of pyrite; some massive digenite in assemblage pyrite-digenite; 5+% sulphides in potassically-altered porphyry with minor sulphate.

cu480, 295.55m: abundant disseminated to semi-massive patches and veins (narrow, < 3mm wide) of pyrite + digenite, with covellite rimming massive digenite; dissemianted pyrite and digenite-covellite; 5% sulphides in potassically-altered porphyry.

cu481, 295.98m: criss-crossing veinlets and 1-3mm wide bands of pyrite + digenite, possible minor covellite; semi-abundant disseminated digenite +/- covellite throughout porphyry and in pink sulphate (gypsum) veins; 5-7% sulphides in potassically-altered porphyry with sulphate.

cu482, 297.53m: very well-defined vein of pyrite + covellite + chalcopyrite, 1+mm wide in 1cm wide quartz vein, cutting potassically-altered porphyry; very fine-grained disseminated chalcopyrite with rims of covellite; 1+% sulphides.

cu483, 297.89m: very fine-grained chalcopyrite +/- bornite dissemianted throughout quartz veins, wtih covellite rimming chalcopyrite; narrow undualting veinlet of chalcopyrite +/- bornite +/- pyrite cutting through slightly sericitized porphyry; 1% sulphides.

cu484, 298.65m: disseminated and stockwork veins of chalcopyrite, + very minor pyrite; 1-2% sulphides in quartz-rich potassically-altered porphyry.

cu485, 299.82m: vein of chalcopyrite + pyrite (chalcopyrite > pyirite) with very minor fine-

grained digenite? covellite?; very fine-grained dissemianted chalcopyrite wtih rims of covellite; 2% sulphides in potassically-altered porphyry.

cu486, 301.37m: disseminated chalcopyrite, chalcopyrite + bornite, and bornite with possible minor covellite; veinlet of chalcopyrite; 1+% sulphides disseminated in quartz and feldspar in potassically-altered porphyry.

cu487, 301.95m: disseminated chalcopyrite + bornite, bornite, and minor covellite; locally covellite borders semi-massive chalcopyrite; 2-3% sulphides in potassically-altered porphyry with some sericitization.

cu488, 302.69m: abundant disseminated fine-grained chalcopyrite-bornite, where bornite is not always in massive form, and occurs locally with chalcopyrite as octahedra and/or cubes; dissemianted chalcopyrite and bornite; minor lead-grey massive mineral--possibly enargite?; 1+% sulphides in sericitized potassically-altered porphyry wtih narrow pink veins of sulphate (gypsum); abundant coarse disseminated crystals of biotite.

cu489, 305.73m: one 5mm wide vein of pyrite + digenite, and abundant disseminated pyrite + digenite +/- covellite; 2% sulphides in potassically-altered porphyry.

cu490, 307.95m: abundant disseminated to semi-massive chalcopyrite + bornite +/- covellite, strung into veinlets; disseminated covellite, +/- rimming chalcopyrite; 7% sulphides in quartz-veined potassically-altered porphyry with some sericitization.

cu491, 306.79m: mostly disseminated digenite-covellite, and minor stringeres; minor chalcopyrite-bornite, and disseminated bornite +/- digenite (?); 3+% sulphides in quartz-rich porphyry veined wtih sulphates (white gypsum?).

cu492, 308.20m: 1-2mm wide pinched veins of pyrite-digenite with minor covellite bordering;

minor disseminated digenite +/- covellite; 1% sulphides in large quartz vein.

cu493, 216.30m: mainly semi-massive and disseminated chalcopyrite + pyrite (pyrite later?); 5% sulphides in pink sulphate (gypsum) veins in sericitized porphyry.

cu494, 219.84m: moderate disseminated chalcopyrite + bornite +/- covellite; minor bornite + covellite; possible digenite; abundant biotite, typical sample of potassic alteration; 2% sulphides in potassically-altered porphyry.

cu495, 221.49m: abundant semi-massive pyrite + chalcopyrite, with interstitial covellite; 15-29% sulphides in sericitized porphyry (sericite-anhydrite rock).

cu496, 244.40m: minor disseminated chalcopyrite +/- bornite; < 1% sulphide in potassically-altered porphyry with abundant coarse biotite crystals.

cu497, 245.49m: very minor disseminated chalcopyrite and pyrite; < 1% sulphides in potassically-altered porphyry with abundant biotite.

cu498, 245.68m: similar to cu497, minor disseminated chalcopyrite and minro pyrite; abundant coarse biotite in potassically-altered porphyry with < 1% sulphides.

cu499, 249.15m: semi-massive pyrite aggregate with interstitial covellite + digenite; minor disseminated bornite in pyrite aggregate; 10% sulphides in slightly sericitized porphyry with gypsum veins wtih anhydrite cores.

cu500, 250.00m: massive sulphide, mainly pyrite with interstitial digenite-covellite; dissmeinated copper-sulphides in flaky white gypsum; 40% sulphides with massive sulphate.

cu501, 250.70m: semi-massive patches and disseminated pyrite + digenite; 10% sulphides in

sericitized porphyry with sulphate.

cu502, 252.15m: mainly semi-massive patches and disseminated pyrite + digenite + cvoellite; 5-10% sulphides in sericitized porphyry with abundant sulphate (blueish anhydrite).

cu503, 253.27m: abundant semi-massive chalcopyrite (+/- pyrite?) + bornite, wtih cvoellite rims; semi-massive patches of covellite; 10+% sulphides in extremely sericitized porphyry.

cu504, 107.86m: narrow veinlets of chalcopyrite + bornite +/- covellite rims; 1 veinlet of bornite +/- covellite rim; abundant disseminated pyrite; 2-3% sulphides in quartz veins and disseminated through sericitized potassically-altered porphyry.

cu505, 108.32m: minor disseminated chalcopryite, chalcopyrite with covellite rims, and disseminated covellite; minor fine stringers of chalcopyrite with massive interstitial covellite; 1% sulphides in quartz-veined potassically-altered porphyry with abundant coarse biotite crystals.

cu506, 111.09m: minor disseminated chalcopyrite +/- bornite, and chalcopyrite with covellite rims; 1% sulphides or less in potassically-altered porphyry with abundant biotite.

cu507, 113.65m: vein of chalcopyrite-bornite with covellite rim, 1-3 mm wide in quartz-sericite vein; abundant disseminated chalcopyrite, bornite, and covellite in sericitized vein in potassically-altered porphyry; 7+% sulphides.

cu508, 114.71m: fine-grained stringer to disseminated chalcopyrite +/- bornite with fine covellite rims; minor disseminated enargite?; 1-2% sulphides in sericitized potassically-altered porhyry with coarse biotite crystals.

cu509, 115.80m: mainly disseminated chalcopyrite + covellite +/- sphalerite (?); 2-3% sulphides in potassically-altered porphyry with <1cm-wide gypsum vein cutting potassic alteration assemblage.

REFERENCES

Alvarez, O. and Flores, R. 1985. Alteracion y mineralizacion hipogena en el yacimiento de Chuquicamata, Chile. Actas, 4th Chilean Geol.Congress, Antofagasta. 23, pp. 78-100.

Ambrus, J. 1978. Chuquicamata deposit. *in* International Molybdenum Encyclopedia 1778-1978, Vol. 1. Resources and Production (ed. A. Sutolov). Intermet, Santiago de Chile, pp. 87-93.

Amcoff, O. 1988. Experimental replacement of chalcopyrite by bornite: textural and chemical changes during a solid-state process. Mineral. Deposita. 23 (4), pp. 286-292.

Amosse, J. 1978. Variation in wolframite composition according to temperature at Borralha, Portugal, and Enguyales, France. Econ. Geol. 73 (6), pp. 1170-1175.

Barton, P.B. Jr. 1973. Solid solutions in the system Cu-Fe-S. Part I: The Cu-S and Cu-Fe-S joins. Econ. Geol. 68, pp. 455-465.

Barton, P.B. Jr. 1970. Sulfide petrology. Mineral. Soc. America, Special Paper 3, pp. 187-198.

Barton. P.B. Jr., Bethke, P.M. and Toulmin, P. III. 1963. Equilibrium in ore deposits. Mineral. Soc. America, Special Paper 1, pp. 171-185.

Barton, P.B. Jr. and Skinner, B.J. 1979. Sulfide mineral stabilities. *in* Geochemistry of Hydrothermal Ore Deposits, 2nd Ed. (ed. H.L. Barnes). Wiley, New York. Pp. 236-333.

Barton, P.B. Jr. and Toulmin, P. III. 1966. Phase relations involving sphalerite in the Fe-Zn-S system. Econ. Geol. 61 (5), pp. 815-849.

Bateman, A.M. and Lasky, S.G. 1932. Covellite-chalcocite solid solution and exsolution. Econ. Geol. 27 (1), pp. 52-86.

Beaudoin, G., Taylor, B.E., Rumble, D., and Thiemens, M. 1994. Variations in the sulfur isotope composition of troilite from the Canon Diablo iron meteorite. Geochim. Et Cosmochim. Acta. 58 (19), pp. 4253-4255.

Brett, R. 1964. Experimental data from the system Cu-Fe-S and their bearing on exsolution textures in ores. Econ. Geol. 59, pp. 1241-1269.

Brimhall, G.H. Jr. and Ghiorso, M.S. 1983. Origin and ore-forming consequences of the advanced argillic alteration process in hypogene environments by magmatic gas contamination of meteoric fluids. Econ. Geol. 78 (1), pp. 73-90.

Cabri, L.J. 1973. New data on phase relations in the Cu-Fe-S system. Econ. Geol. 68, pp. 443-454.

Clark, A.H. 1993. Are outsize porphyry copper deposits either anatomically or environmentally distinctive? *in* Giant Ore Deposits (eds. B.H. Whiting, C.J. Hodgson and R. Mason), Society of Economic Geologists, Special Publication 2, pp. 213-283.

Cook, R.B. 1978. Famous mineral localities: Chuquicamata, Chile. Mineralogical Record, October, 1978, pp. 321-333.

Craig, J.R. and Kullerud, G. 1973. The Cu-Zn-S system. Mineral. Deposita. 8 (1), pp. 81-91.

Craig, J.R. and Scott, S.D. 1974. Sulfide phase equilibria. *in* Sulfide Mineralogy (ed. P.H. Ribbe), Reviews in Mineralogy, 2.

Deer, W.A., Howie, R.A., and Zussman, J. 1962. Rock-Forming Minerals, Vol. 5, Non-Silicates. John Wiley and Sons, New York. 371p.

Economou, M.I. 1981. A second occurrence of the copper sulfides geerite and spionkopite in Eretria, central Greece. Neues Jahrb. Mineral.,-Monatsh. 11, pp. 489-494.

Evans, H.T. Jr. and Konnert, J.A. 1976. Crystal structure refinement of covellite. American Mineralogist. 61 (9-10), pp. 996-1000.

Faure, G. 1991. Chemical weathering of mineral deposits *in* Principles and Application of Inorganic Geochemicstry. Macmillan Publishing Company. pp. 473-499.

Field, C.W. and Gustafson, L.B., 1976. Sulfur isotopes at El Salvador, Chile. Economic Geology. 71 (8), pp. 1533-1548.

Friedman, I. and O'Neil, J., 1977. Chapter KK. Compilation of stable isotope fractionation factors of geochemical interest *in* Data of Geochemistry (ed. M. Fleischer), Geological Survey Professional Paper 440-KK.

Garrels, R.M. 1954. Mineral species as fundtions of pH and oxidation-reduction potentials, with special reference to the zone of oxidation and secondary enrichment of sulphide ore deposits. Geochim. Cosmochim. Acta. 5, pp. 153-168.

Goble, R.J. 1981. The leaching of copper from anilite and the production of a metastable copper sulfide structure. Canadian Min. 19, pp. 583-591.

Goble, R.J. 1980. Copper sulfides from Alberta; yarrowite Cu_9S_8 and spionkopite $Cu_{39}S_{28}$. Canadian Min. 18 (4), pp. 511-518.

Gustafson, J.M. and Hunt, J.P. 1975. The porphyry copper seposit at El Salvador, Chile. Econ. Geol. 70, pp. 857-912.

Haynes, F.M. 1984. A geochemical model for sulfide paragenesis and zoning in the Cu-Fe-As-S system (Tsumeb, South West Africa/ Namibia). Chemical Geology. 47 (3-4), pp. 183-190.

Hoefs, J., 1987. Stable Isotope Geochemistry, 3rd Edition, Springer-Verlag, 241 p.

Holland, H.D. 1965. Some applications of thermochemical data to problems of ore deposits II: Mineral assemblages and the composition of ore-forming fluids. Econ. Geol. 60 (6), pp. 1101-1166.

Hubberton, H.W. 1980. Sulfur isotope fractionations in the Pb-S, Cu-S and Ag-S systems. Geochem. Journal. 14 (4), pp. 177-184.

Jaffe, H.W. 1988. The crystal chemistry of the covalent bond *in* Principles of Crystal Chemistry and Refractivity, Cambridge University Press, pp. 27-41.

Kajiwara, Y. and Krouse, H.R. 1971. Sulfur isotope partitioning in metallic sulfide systems. Can. J. Earth Sci. 8, pp. 1397-1408.

Klein, C. and Hurlbut, C. Jr. (after James D. Dana). 1977. Manual of Mineralogy (20th Ed.). John Wiley and Sons. 530 p.

Kostov, I. and Minceva-Stefanova, J. 1981. Sulfide Minerals: Crystal Chemistry, Paragenesis and Systematics. Bulgarian Academy of Sciences.

Lindsay, D., Zentilli, M., and Ossandon, G.C. 1995. Evolution of permeability in an active ductile to brittle shear system controlling the mineralization at the Chuquicamata porphyry copper deposit, Chile. *in* Proceedings, GIANT ORE DEPOSITS II (ed. A.H. Clark), Controls on the Scale of Orogenic Magmatic-Hydrothermal Mineralization, Queen's University, Kingston, Canada, April 25-27, 1995, pp. 57-85.

Lopez, V.M. 1939. The primary mineralization at Chuquicamata, Chile. Econ. Geol. 34, pp. 674-711.

Lowell, J.D. and Guilbert, J.M. 1970. Lateral and vertical alteration-mineralization zoning in porphyry ore deposits. Econ. Geol. 65 (4), pp. 373-408.

MacInnis, I.N. 1993. Literature Review of the Cu-S and Related Systems Pertaining to Porphyry Copper Deposits. *Report by Cuesta Research Limited, Canada, for Contract No 519307-021 with Division Chuquicamata, CODELCO, December 1993.*

Maske, S. and Skinner, B.J. 1971. Studies of the sulfosalts of copper, I: phases and phase relations in the system Cu-As-S. Econ. Geol. 66, pp. 901-918.

Matsuhisa, Y., Nakagawa, S., Kusakabe, M., and Ojeda, J.M. 1984. Stable isotope study of El Teniente porphyry copper deposit, Chile, *in* Report of Research and Development Cooperation ITIT Projects no. 7911: Reasearch on calc-alkaline magmatism and related mineralisation in Chile. Geological Survey of Japan, March 1984, pp. 34-47.

Meyer, C. and Hemley, J.J. 1967. Wall Rock Alteration. *in* Geochemistry of Hydrothermal Ore Deposits, 2nd Ed. (ed. H.L. Barnes). Wiley, New York, pp. 166-235.

Moh, Gunter H. 1971. Blue remaining covellite and its relations to phases in the sulfur rich portion of the copper-sulfur system at low temperatures. Mineral. Soc. Japan., Special Paper No. 1, pp. 226-232.

Morimoto, N. 1963. On the transition of bornite. Mineral. Soc. America, Special Paper 1, pp. 153-156.

Morimoto, N. and Koto, K. 1970. Phase relations of the Cu-S system at low temperatures: stability of anilite. Amer. Mineral. 55 (1-2), pp. 106-117.

Mumme, W.G., Sparrow, G.J. and Walker, G.S. 1988. Roxbyite, a new copper sulphide mineral from the Olympic Dam deposit, Roxby Downs, South Australia. Mineral. Magazine. 52, pp. 223-230.

Neilsen, H. 1979. Sulfur isotopes *in* Lectures in Isotope Geology (eds. E. Jager and J.C. Hunziker), Springer-Verlag, pp. 283-312.

Nekrasov, I.Y., Sorokin, V.I. and Osadchiy, Y.G. 1981. Causes of increased tin capacity of sphalerite. Int. Geol. Review. 23 (2), pp. 173-178.

Ohmoto, H., 1986. Stable isotope geochemistry of ore deposits *in* Stable Isotopes in High Temperature Geological Processes (eds. J.W. Valley, H.Pp. Taylor and J.R. O'Neil), Reviews in Mineralogy Volume 16, Mineralogical Society of America, pp.491-555.

Ohmoto, H., 1972. Systematics of sulfur and carbon isotopes in hydrothermal ore deposits. Economic Geology. 67, pp. 551-578.

Ohmoto, H, and Lasaga, A.C. 1982. Kinetics of reactions between aqueous sulfates and sulfides in hydrothermal systems. Geochim. Cosmochim. Acta. 46, pp. 1727-1745.
Orlandi, P., Merlino, S., Duchi, G., and Vezzalini, G. 1981. Colusite: a new occurrence and crystal chemistry. Canadian Min. 19, pp. 423-427.

Orlandi, P., Merlino, S., Duchi, G., and Vezzalini, G. Colusite: a new occurrence and crystal chemistry. Canadian Min. 19 (3), pp. 423-427.

Pirajno, F. 1992. Hydrothermal Mineral Deposits. Springer-Verlag. 695 p.

Potter, R.W. II. 1977. An electrochemical investigation of the system copper-sulfur. Econ. Geol. 72, pp. 1524-1542.

Potter, R.W.II. and Evans, H.T. Jr. 1976. Definitive X-ray powder data for covellite, anilite, djurleite, and chalcocite. Journal of Research U.S.G.S. 4 (2), pp. 205-212.

Putnis, A., Grace, J. and Cameron, W.E. 1977. Blaubleibender covellite and its relationship to normal covellite. Contrib. Mineral. Petrol. 60 (2), pp. 209-217.

Ramdohr, P. 1980. The Ore Minerals and their Intergrowths. 2nd Ed., in two volumes. Pergamon Press, 1200 p.

Ravenhurst, C., Reynolds, P., Zentilli, M., and Lindsay, D. High-precision $^{40}Ar/^{39}Ar$ dating of two consecutive hydrothermal events in the Chuquicamata porphyry copper system, Chile. *submitted to* Isotope Geoscience, Oct. 1996.

Reutter, K.J., Chong, G. and Scheuber, E. 1993. The 'West Fissure' and the Precordilleran fault system of northern Chile, *in* Andean Geodynamics, ISAG 93, ORSTROM/ Oxford University Press, pp. 237-240.

Rickard, D.T. 1972. Covellite formation in low temperature aqueous solutions. Mineralium Deposita. 7 (2), pp. 180-188.

Rimstitd, J.D., Chermak, J.A. and Newcomb, W.D. 1986. The oxidation of sulfide minerals. *in* Extended Abstracts, Fifth International Symposium on Water-Rock Interaction (ed. B. Hitchon), 5, pp. 471-474.

Romberger, S.B. and Barnes, H.L. 1970. Ore solution chemistry III: solubility of CuS in sulfide solutions. Econ.Geol. 65 (8), pp. 901-919.

Roseboom, E.H. Jr. 1966. An investigation of the system Cu-S and some natural copper sulfides between 25° and 700°C. Econ. Geol. 61 (4), pp. 641-672.

Rye, R.O. and Ohmoto, H. 1974. Sulfur and carbon isotopes and ore genesis: a review. Econ. Geol. 69, pp. 826-842.

Sakai, H. 1968. Isotopic properties of sulfur compounds in hydrothermal processes. Geochem. Journal. 2, pp. 29-49.

Sasaki, A., Ulriksen, C., Sato, K., and Ishihara, S. 1984. Sulfur isotope reconnaissance of porphyry copper and manto-type deposits in Chile, *in* Report of Research and Development Cooperation ITIT Projects no. 7911: Reasearch on calc-alkaline magmatism and related mineralisation in Chile. Geological Survey of Japan, March 1984, pp. 48-56.

Schneeberg, E.P. 1973. Sulfur fugacity measurements with the electrochemical cell $Ag|AgI|Ag_{2+X}S,f_{S2}$. Econ. Geol. 68, pp. 507-517.

Schwartz, G.M. and Park, C.F. Jr. 1930. Pseudo-eutectic textures. Econ. Geol. 25 (6), pp. 658-663.

Scott, S.D. and Barnes, H.L. 1972. Sphalerite-wurtzite equilibria and stoichiometry. Geochim. Cosmochim. Acta. 36 (11), pp. 1275-1295.

Sillitoe, R.H. 1988. Epochs of intrusion-related copper mineralisation in the Andes. J. South Am. Earth Sci. 1, 89-108.

Sillitoe, R.H. 1973. The tops and bottoms of porphyry copper deposits. Econ. Geol. 68, pp. 799-815.

Sillitoe, R.H. and Clark, A.H. 1969. Copper and copper-iron sulfides as the initial products of supergene oxidation, Copiapo mining district, northern Chile. Amer. Miner. 54 (11-12), pp. 1684-1710.

Sillitoe, R.H. and McKee, E.H. 1996. Age of supergene oxidation and enrichment in the Chilean porphyry copper province. Econ. Geol. 91, pp. 164-179.

Skinner, B.J., Luce, F.D. and Makovicky, E. 1972. Studies of the sulfosalts of copper, III: phases and phase relations in the system Cu-Sb-S. Econ. Geol. 67, pp. 924-938.

Spiridonov, E.M., Chvileva, T.N. and Badalov, A.S. 1984. Antimony-bearing colusite Cu26 V2 As2 Sb2 Sn2 S32, of the Kairagach deposit and on the varieties of colusite. Int. Geol. Review. 26 (5), pp. 534-539.

Stroitelev, A.D. and Babinskiy, M.D. 1969. On the possibility of using sphalerite as a geological thermometer. Geochem. International. 6 (Suppl.), pp. 289-293.

Soto, H.M. 1979. Alteracion y mineralizacion primeria en Chuquicamata. Unpublished Ph.D. Thesis, Universidad de Salamanca, Spain, 233 p.

Taylor, B.E. 1987. Stable isotope geochemistry of ore-froming fluids *in* Short Course in Stable Isotope Geochemistry of Low Temperature Fluids (ed. T.K. Kyser), Mineralogical Association of Canada Volume 13, pp. 337-445.

Tobey, E. Preliminary Report on the Alteration and Sulfide Mineral Zoning at Chuquicamata, Chile. Inernal Report for CODELCO, July, 1971. 18 p.

Vaughan, D.J. and Craig, J.R. 1978. Mineral Chemistry of Metal Sulfides. Cambridge University Press, New York.

Voyevodin, V.N. 1981. The relationship between chemical composition of wolframites and the geological conditions of their formation. Int. Geol. Review. 23 (5), pp. 561-570.

Walsh, C.A. and Rimstitd, J.D. 1986. Rates of reaction of covellite and blaubleibender covellite with ferric iron at pH 2.0. The Canadian Mineralogist. 24 (1), pp. 35-44.

York, D. 1969. Least-squares fitting of a straight line with correlated errors. Earth Planet. Sci. Lett. 5, pp. 320-324.

Yund, R.A. and Kullerud, G. 1966. Thermal stability of assemblages in the Cu-Fe-S system. J. Petrology. 7 (3), pp. 454-488.

Zentilli, M., Graves, M., Lindsay, D., Ossandon, G., and Camus, F. 1995. Recurrent mineralization in the Chuquicamata porphyry copper system: Restrictions on genesis from mineralogical, geochronological and isotopic studies, *in* Proceedings, GIANT ORE DEPOSITS II (ed. A.H. Clark), Controls on the Scale of Orogenic Magmatic-Hydrothermal Mineralization, Queen's Unversity, Kingston, Canada, April 25-27, 1995, pp. 86-100K.

Zentilli, M., Leiva, G., Rojas, J., and Graves, M. 1994. The Chuquicamata system revisited. Actas, VII Congresso Geologico Chileno, Concepcion. 2, pp. 1647-1651.

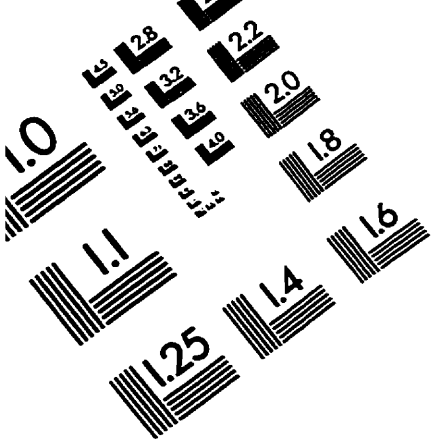

TEST TARGET (QA-3)

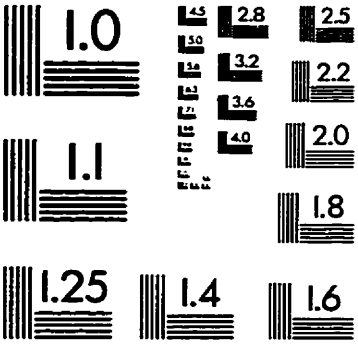

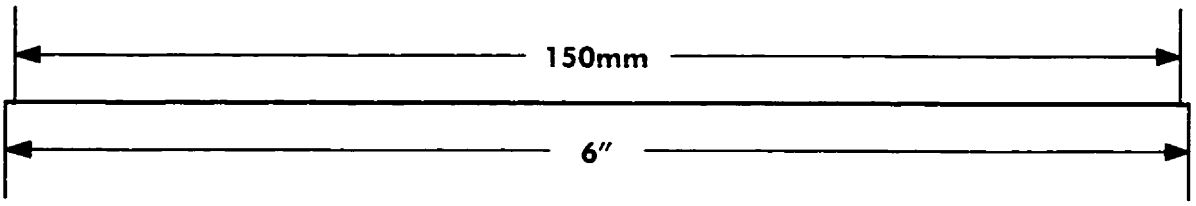

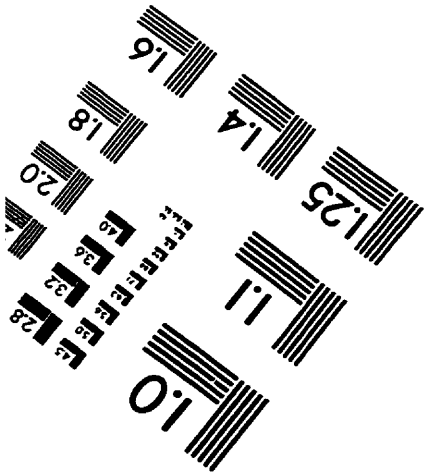

APPLIED IMAGE, Inc
1653 East Main Street
Rochester, NY 14609 USA
Phone: 716/482-0300
Fax: 716/288-5989